

NASA CR-114649

## **AIRCRAFT NOISE SOURCE AND CONTOUR ESTIMATION**

By D. G. Dunn and N. A. Peart

D6-60233  
July 1973

Available to the public

(NASA-CR-114649) AIRCRAFT NOISE SOURCE  
AND CONTOUR ESTIMATION (Boeing Commercial  
Airplane Co., Seattle) 233 p HC \$13.75

N73-31945

CSCL 20A

Unclas

G3/2 18163

Prepared under contract NAS2-6969 by

Boeing Commercial Airplane Company  
P.O. Box 3707  
Seattle, Washington 98124

for

Ames Research Center  
NATIONAL AERONAUTICS AND SPACE ADMINISTRATION

1. Report No. <b>NASA CR-114649</b>		2. Government Accession No.		3. Recipient's Catalog No.	
4. Title and Subtitle <b>AIRCRAFT NOISE SOURCE AND CONTOUR ESTIMATION</b>				5. Report Date <b>July 1973</b>	
				6. Performing Organization Code	
7. Author(s) <b>D. G. Dunn and N. A. Peart</b>				8. Performing Organization Report No. <b>D6-60233</b>	
9. Performing Organization Name and Address <b>Boeing Commercial Airplane Company P.O. Box 3707 Seattle, Washington 98124</b>				10. Work Unit No.	
				11. Contract or Grant No. <b>NAS2-6969</b>	
12. Sponsoring Agency Name and Address <b>National Aeronautics and Space Administration Washington, D.C. 20546</b>				13. Type of Report and Period Covered <b>Contractor Report</b>	
				14. Sponsoring Agency Code	
15. Supplementary Notes <div style="display: flex; justify-content: space-between;"> <div> Project Manager, D. H. Hickey  NASA-Ames Research Center  Moffett Field, California 94035 </div> <div> Computer programs may be obtained from  COSMIC, Computer Software Management Information Center  112 Barrow Hall, University of Georgia  Athens, Georgia 30601 </div> </div>					
16. Abstract <p>Calculation procedures are presented for predicting the noise-time histories and noise contours (footprints) of five basic types of aircraft: turbojet, turbofan, turboprop, V/STOL, and helicopter. The procedures have been computerized to facilitate prediction of the noise characteristics during takeoffs, flyovers, and/or landing operations. The user's guide for the computer programs is provided in a companion report, NASA CR-114650</p>					
17. Key Words (Suggested by Author(s)) Aircraft noise prediction Noise suppression Acoustic lining				18. Distribution Statement <b>Unclassified--unlimited</b>	
19. Security Classif. (of this report) <b>Unclassified</b>		20. Security Classif. (of this page) <b>Unclassified</b>		21. No. of Pages <b>241</b>	
				22. Price* <b>\$3.00</b>	

# CONTENTS

	Page
1.0 SUMMARY . . . . .	1
2.0 INTRODUCTION . . . . .	3
3.0 CONCLUSIONS . . . . .	6
4.0 RECOMMENDATION . . . . .	6
5.0 DISCUSSION . . . . .	7
5.1 Macroscopic View of the Problem . . . . .	7
5.1.1 Definitions/Limitations/Assumptions . . . . .	12
5.1.2 Geometry Solution . . . . .	16
5.1.3 Noise Extrapolation . . . . .	21
5.1.4 Lining Treatment . . . . .	27
5.1.5 Configuration Corrections . . . . .	35
5.1.6 Summation of Component Noise . . . . .	35
5.1.7 Output for Noise Contour Estimation . . . . .	38
5.2 Noise Source Estimation . . . . .	38
5.2.1 Measured Noise Data . . . . .	40
5.2.2 Jet Noise . . . . .	42
5.2.3 Core and Turbine Noise . . . . .	108
5.2.4 Compressor or Fan Noise . . . . .	122
5.2.5 Propeller, Helicopter, and Tilt Rotor Noise . . . . .	148
5.3 Noise Contour Estimation . . . . .	175
5.3.1 Acoustic Data . . . . .	178
5.3.2 Aero/Propulsion Data . . . . .	178
5.3.3 Noise Contour Calculation . . . . .	179
5.3.4 Area Calculation . . . . .	181
5.3.5 Noise Estimate on Sideline . . . . .	182
APPENDIX A--Theoretical Ground Reflection Prediction Procedure . . . . .	183
APPENDIX B--Theoretical Ejector Performance . . . . .	191
REFERENCES . . . . .	227

# **AIRCRAFT NOISE SOURCE AND CONTOUR ESTIMATION**

**By D. G. Dunn and N. A. Peart  
Boeing Commercial Airplane Company**

## **1.0 SUMMARY**

Reflecting the need for analyzing and, if possible, reducing the community noise resulting from aircraft operations, the Boeing Commercial Airplane Company, under contract to NASA-Ames, has developed a computer program for predicting the noise generated by five basic types of aircraft: turbojet, turbofan, turboprop, V/STOL, and helicopter. A second program has been developed which calculates contours of equal noise level (footprints) and the area within the contours for an airplane during takeoff and approach operations. The footprint program is compatible with the NASA-Ames flight simulator. The flight simulator provides aerodynamic and engine performance data, and the footprint program calculates contours for equal noise level, thereby providing an estimate of the noise exposure produced by an aircraft operation. Typical results from the computer programs are shown in figure 1. These computer programs are intended to assist aircraft designers by identifying the noise characteristics of various aircraft and engine configurations. These noise levels can then be compared to community noise goals.

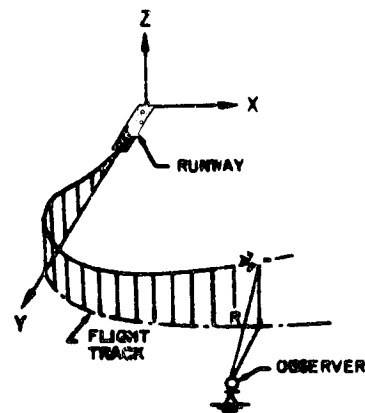
Aircraft noise prediction techniques used within the aviation community are usually based on empirical data and the resulting procedures vary. These differences arise in numerous ways; e.g., (1) the same acoustic data can be formulated into prediction procedures with varying degrees of sophistication and complexity, (2) differences in noise measurements do occur in similar tests when some of the important variables can not be controlled, and (3) the complexities in noise generation and propagation have fostered more than one theoretical view of the phenomena involved.

The source noise prediction and extrapolation techniques presented in this report represent the state of the art during the contract time period. The procedures are primarily empirical. Some parts of the procedures were obtained from published literature and in some instances unpublished methods used within the Boeing Commercial Airplane Company were employed. The selection of techniques were made to provide a base for comparisons among aircraft design choices and for evaluation of aircraft operations. However, results from these procedures can not be expected to agree exactly with absolute noise levels calculated by other schemes. In many instances, an engine/airframe configuration has its own peculiarities. These peculiarities may require corrections



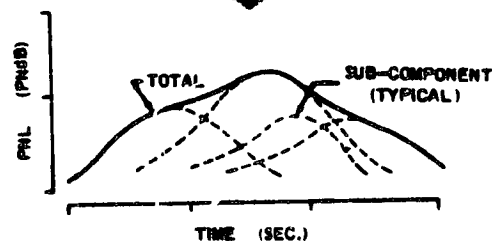
### 1 NOISE SOURCE ESTIMATION PROGRAM RESULTS

- SOUND PRESSURE LEVEL (SPL) SPECTRA vs. TIME
- PERCEIVED NOISE LEVEL (PNL) vs. TIME
- EFFECTIVE PERCEIVED NOISE LEVEL (EPNL)



### 2 NOISE CONTOUR ESTIMATION PROGRAM RESULTS

- EPNL OR MAXIMUM PNL CONTOUR POINTS
- AREA WITHIN EACH CONTOUR
- NOISE ESTIMATES (EPNL or MAX. PNL) ON SIDELINES FROM FLIGHT TRACK



1 RESULTS GIVEN FOR EACH NOISE COMPONENT AT EACH OBSERVER / FLIGHT PATH SEGMENT DEFINED BY THE USER.

2 REQUIRES NOISE SOURCE PREDICTIONS OR MEASUREMENTS AT A SERIES OF POINTS AS DISCUSSED IN SECTION 5.3.

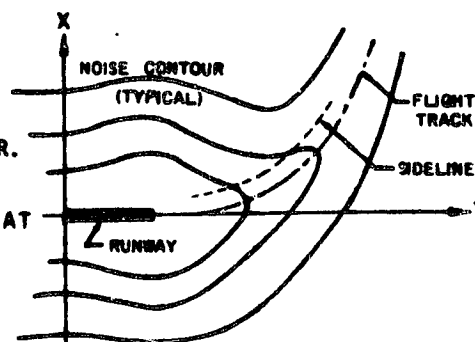


FIGURE 1.—RESULTS FROM NOISE SOURCE AND CONTOUR COMPUTER PROGRAMS

to be applied to the predicted levels for a particular noise source component or changes in one or more of the various calculation methods offered in this report.

It is extremely difficult to assess the accuracy of noise prediction procedures. This difficulty results from insufficient data for known sources (individual component sources which combine to give the total noise of the system), anomalies in measured data, and the small number of different engine/source configurations. Comparisons of predicted with measured noise levels (Effective Perceived Noise Levels, EPNdB) for current airplanes have shown that the tolerance for these methods is generally  $\pm 5$  EPNdB. It should be recognized that noise levels are logarithmic quantities, and an error in a noise estimate can result in a large error in a contour estimate such as area. Hence, the tolerance for the contour estimation procedure largely depends on the confidence level associated with the acoustic data that is used.

A description of how to use the computer programs is contained in a companion report (ref. 1). This portion of the report contains the engineering description of the noise prediction procedures embodied in the computer programs.

## 2.0 INTRODUCTION

The increase in commercial aviation in the last decade has been accompanied by increased complaints from communities directly exposed to the higher noise levels associated with aircraft operations. Initial attempts to reduce the community noise exposure have included changes in takeoff and approach procedures, development of acoustically treated inlets and mounting jet noise suppressors on the exhaust nozzles. Also, Federal noise regulations (ref. 2) have established noise limits for new airplanes that are significantly lower than first generation jet operation levels. This recent emphasis on reducing airplane noise has resulted in considerable acoustics-related research and development activities. These activities have been primarily directed toward defining the noise generating mechanisms of aircraft engines and defining ways of reducing noise at its source through design innovations and suppression devices.

The implementation of noise reduction technology in engine, nacelle, and acoustic lining design has resulted in a generation of quieter airplanes, e.g., the Boeing 747, Douglas DC-10, Lockheed L-1011, and Cessna Citation. Numerous other programs are currently under way, each with the objective of either reducing the noise of current airplanes or developing noise technology for application to future aircraft. Throughout these research programs, there has been only minimal effort devoted to developing the methodology required for predicting the total community noise performance of new airplanes. This report represents the state of the art calculation procedure for aircraft community noise prediction.

The current contract, NAS2-6969, has been completed in two parts—Phases A and B (ref. 3). Phase A (ref. 4) consisted of providing relatively "crude" computerized procedures applying to noise source estimation of conventional turbojets or turbofans. Also, part of the Phase A effort was the development of computerized procedures for noise contour estimation adaptable to "real-time" flight simulation. The computer programs were designed to operate on the IBM System 360/67 with the additional requirement that the noise contour program would operate on the Xerox Sigma VII and VIII computers in conjunction with the NASA-Ames flight simulator. Phase B consisted of supplying more advanced computerized procedures for noise source prediction. The computer program for this purpose has been written to provide 1/3 octave band noise estimates for such configurations as advanced technology "quiet" engines, lift fans, lift/cruise fans, ejector/suppressor, blown-flap, propeller, helicopter, and tilt rotor aircraft, etc., in addition to that for conventional jet aircraft. Also, the contour program has been updated to be applicable for the more generalized requirements.

The discussion section of this report has been divided into three parts. The first deals with the overall view of the noise prediction procedures. The second deals with the description of the various computer modules for noise source estimation. Table 1 lists the computer modules included.

In each of the computer modules, the user has the option to specify reductions on a spectral basis when suppression devices are employed. For these situations where lining is installed, a calculation procedure applicable to optimized, single or double layer linings is available. These procedures are included in the noise source estimation program for those items noted in the list for the noise source computer modules in table 1.

After the individual noise source spectra are computed for a datum condition (free-field, 1 meter from source), extrapolation techniques are then used to adjust the datum spectra to correspond to the noise observed as the aircraft flies by an observer. The spectra obtained are functions of time and permit the calculation of the effective perceived noise level during takeoff and/or landing.

The third part of the discussion deals with the procedures used to calculate noise contours. At the discretion of the user, an additional output of the noise source program can be a set of tabular data on IBM cards to define an acoustic data routine for the noise contour program. The acoustic function can be either peak perceived noise level or effective perceived noise level versus some engine performance parameter, range at the closest point of approach, and elevation angle. This function is then used for calculating noise contours as described in section 5.3. The computer programs for this task are designed to run in "real time" on the Xerox Sigma VII or VIII computers for flight simulations and in "batch mode" on the IBM System 360/67.

**TABLE 1.—NOISE SOURCE ESTIMATION COMPUTER MODULES**

	<u>No. of Modules</u>
● Measured Data	1
● Jet Noise	5
a. Single exhaust nozzle	
b. Co-annular exhaust nozzles	
c. Ejector/suppressor*	
d. Slot nozzle with augmentor flap*	
e. Externally-blown flap	
● Noise Generated Inside Primary Duct	2
a. Core*	
b. Turbine*	
● Compressor or Fan Noise	3
a. Inlet compressor or fan*	
b. Discharge fan*	
c. Lift-fans*	
● Propeller, Helicopter and Tilt Rotor	2
a. Empirical propeller procedure	
b. Theoretical propeller/rotor procedures	
<b>Total</b>	<b>13</b>

\*Denotes optional use of lining

### 3.0 CONCLUSIONS

This is the final report for contract NAS2-6969. It describes the results for the Phase B portion of the contract. Empirical procedures are described which represent the state of the art and are the best approaches readily at hand for estimating the community noise levels for the five basic types of aircraft mentioned in the summary. At the present time, comprehensive theoretical procedures do not exist for noise prediction for all the aircraft mentioned. In some cases, theoretical methods can be computerized, but they are computationally expensive, require more detailed information than is readily available, and do not provide significantly more accurate *absolute* levels than that obtained by empirical means.

Past experience has shown that when suppression devices are used to reduce the acoustic levels of major noise source(s); new noise sources always appear. New prediction procedures must be continually developed to reflect the noise contribution of the new sources. Also, the existing procedures must be continually refined to reflect the change in engine design and the demand for increased accuracy.

### 4.0 RECOMMENDATION

In general, aircraft noise prediction methods will change as technology improves; therefore, it is recommended that these procedures and the corresponding computer programs be periodically reviewed and updated. To provide guidance on future developments and to gain a better understanding of the mechanisms involved, a theoretical analysis should accompany any revisions of the empirical procedures presented herein.

## 5.0 DISCUSSION

### 5.1 MACROSCOPIC VIEW OF THE PROBLEM

Noise prediction procedures have been developed for five basic types of aircraft: turbojet; turbofan; turboprop; V/STOL; and helicopter. Figure 2 shows these propulsion systems and the types of noise sources associated with each type. Of the five basic types of airplanes, the V/STOL aircraft is the most complicated because of the different high-lift configurations presently being considered—blown-flap, augmentor-wing, lift fan/jet and tilt rotor. In addition, the V/STOL configurations may have more than one type of powerplant, i.e., conventional turbofan wing mounting with lift fans in the wing or lift jets attached to the airplane's fuselage.

In order to provide the flexibility required in predicting the noise from the several source contributors for a given aircraft, the approach shown in figure 3 is used. The prediction consists of four steps:

1) **Solution of the Flight Path/Observer Geometry:**

In this step the airplane is assumed to move along a straight line, i.e., constant climb gradient. At angular increments of  $10^\circ$ ,  $20^\circ$ , . . .  $170^\circ$  between the flight path and a line to the observer, sampling points for the aircraft's position are taken which correspond to a set of observation times during the flight when the noise is heard. At each aircraft position, all geometrical terms required to extrapolate the noise from the source to the observer are determined. After the airplane/observer geometry is defined, the next step considers the orientation\* of the noise sources.

2) **Calculation and Summation of the Sound Levels for Each Source:**

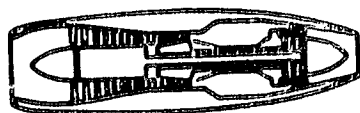
For each point along the flight path segment, spherical coordinate angles relative to the noise source reference axis are calculated. See  $(\psi, \psi_0, \beta_0)$  in figure 4. These angles describe the location on a sphere about a source where the noise is to be determined. Thus, non-axial-symmetric\*\* radiation patterns can be considered.

---

\*The angular orientation of the gross thrust vector for a powerplant about the aircraft's lateral axis with respect to the horizon.

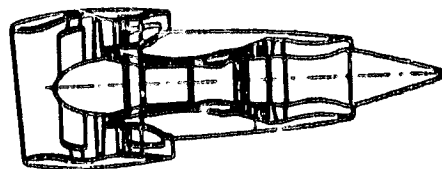
\*\*Except for conventional single engine aircraft, the radiation patterns will be non-axial-symmetric.

### TURBOJET



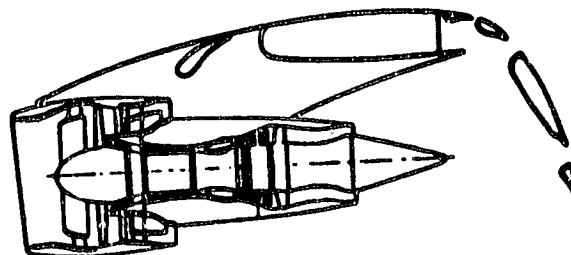
1. PRIMARY JET
2. CORE & TURBINE
3. COMPRESSOR (INLET)

### TURBOFAN



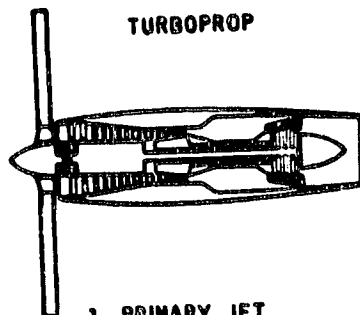
1. PRIMARY & SECONDARY
2. CORE & TURBINE
3. FAN (INLET & EXIT)

### STOL (BLOWN FLAP) — TURBOFAN



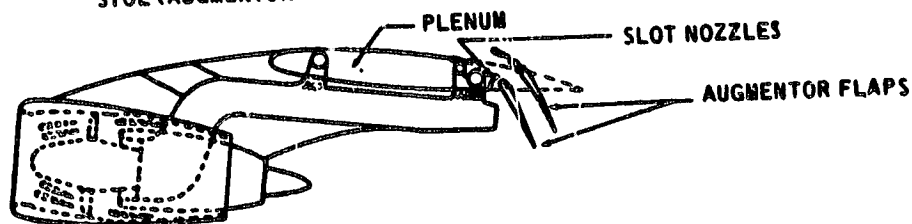
1. PRIMARY & SECONDARY JET MODIFIED FOR BLOWN FLAP
2. CORE & TURBINE
3. FAN (INLET & EXIT)

### TURBOPROP



1. PRIMARY JET
2. CORE & TURBINE
3. COMPRESSOR (INLET)
4. PROPELLER

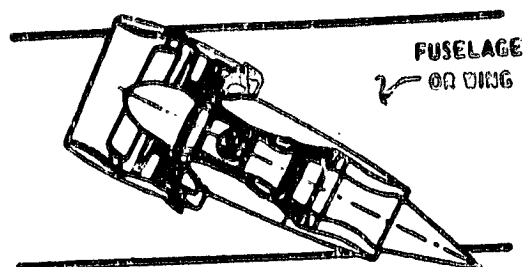
### STOL (AUGMENTOR-WING) — TURBOFAN



1. PRIMARY & SECONDARY JET MODIFIED FOR AUGMENTOR WING
2. CORE & TURBINE
3. FAN (INLET & EXIT)

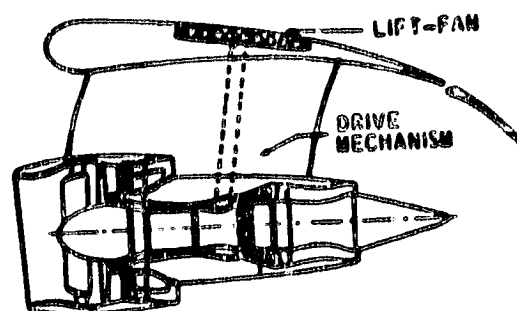
FIGURE 2.—REPRESENTATIVE PROPULSION SYSTEMS AND NOISE SOURCES

# V/STOL (LIFT FAN/JET) — TURBOFAN

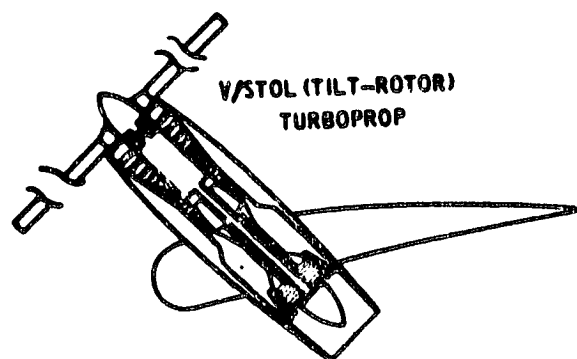


1. PRIMARY & SECONDARY JET
2. CORE & TURBINE
3. FAN (INLET & EXIT)

# STOL (LIFT FAN) — TURBOFAN

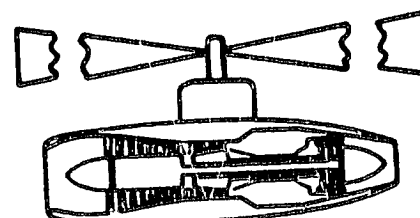


1. PRIMARY & SECONDARY JET
2. CORE & TURBINE
3. FAN (INLET & EXIT)
4. LIFT FAN



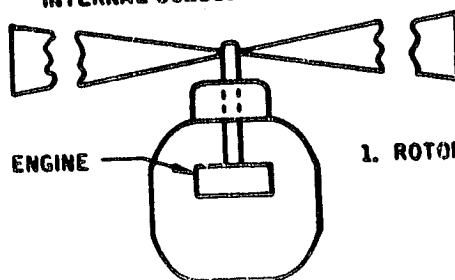
1. ROTOR NOISE
2. PRIMARY JET NOISE
3. CORE & TURBINE
4. COMPRESSOR (INLET)

# HELICOPTER — TURBINE-DRIVEN



1. ROTOR NOISE
2. PRIMARY JET NOISE
3. CORE & TURBINE
4. COMPRESSOR (INLET)

# HELICOPTER INTERNAL COMBUSTION ENGINE



1. ROTOR NOISE

FIGURE 2.—CONCLUDED



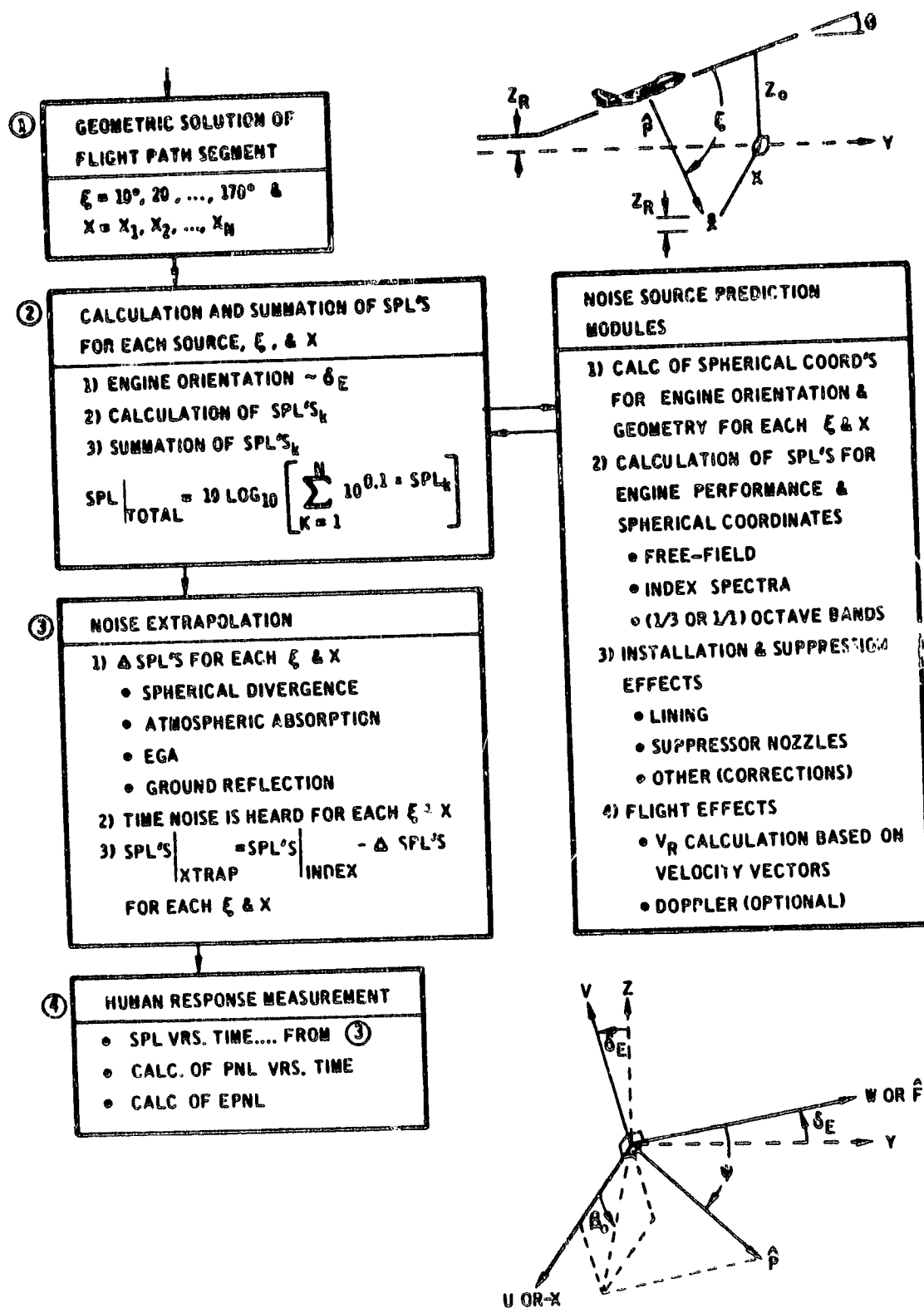


FIGURE 3.—COMPUTATION SEQUENCE

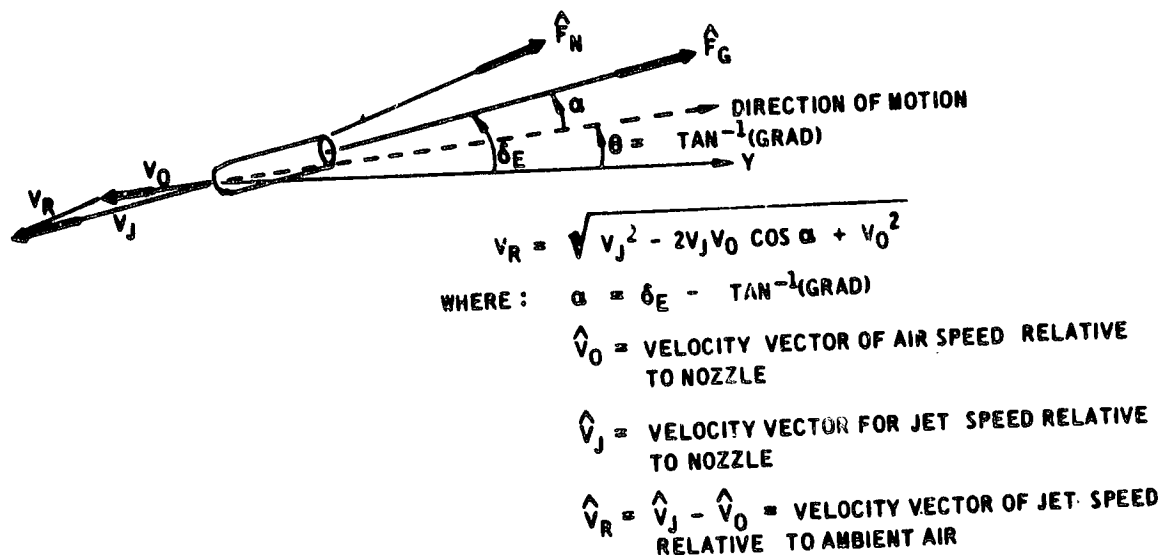
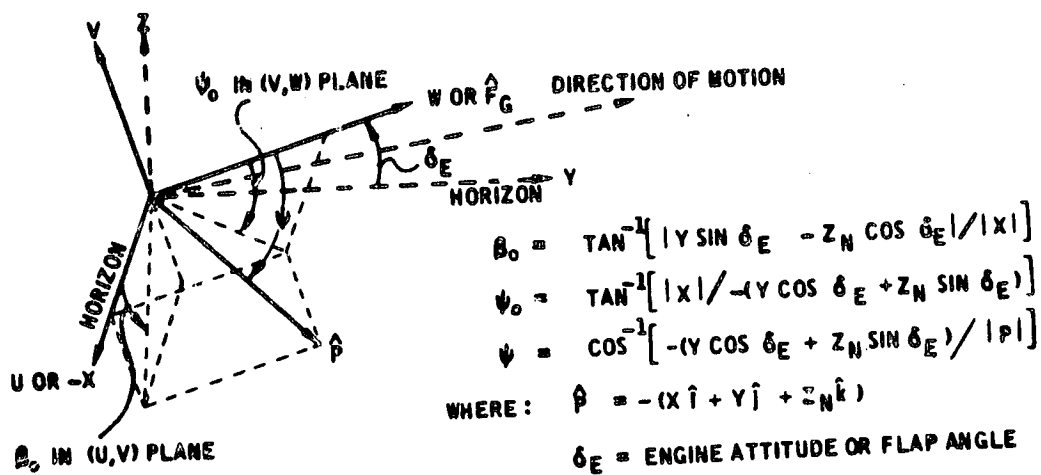


FIGURE 4.—ENGINE ORIENTATION AND FLIGHT CONSIDERATIONS

The noise attributed to each source is then calculated and summed to form a total of all the sound sources at each aircraft position. The noise levels thus formed represent free-field, index (1/3 or 1/1) octave band spectra, on a sphere (radius = 1 meter) radiating toward the observer at each position considered along the flight path segment.

3) **Extrapolation of the Index Noise Spectra:**

In this step, sound attenuation due to spherical divergence, atmospheric absorption, and extra-ground-attenuation is considered (refs. 5 through 8). In addition, the interference phenomena of ground reflection is included as an option (section 5.1.3.2 and appendix A). The results from this step represent the total (1/3 or 1/1) octave band spectra versus time received by the observer as the aircraft passes by.

4) **Human Response Measures:**

The extrapolated spectra are used to calculate the human response measures; Perceived Noise Level (PNL), tone-corrected PNL, and Effective Perceived Noise Level (EPNL). The EPNL is determined by integrating the antilogarithm (Base 10) of the tone-corrected PNL with respect to time (refs. 2 and 9), not from a transfer curve as was done during Phase A of the current contract (ref. 4). Since there is some question regarding the validity of the tone-correction procedure, an estimate of the effective perceived noise level EPNL is provided, based on the regular PNL-time history. Occasionally, the procedure gives a tone-correction when in fact no tones can be observed in the 1/3-octave or narrow-band spectra. This estimate is denoted in the computer output by an asterisk beside the EPNL label. The omission of a tone penalty also solves the problem of obtaining an EPNL estimate when only full octave band spectra are available and tone-corrected PNL's can not be calculated. Further detail on each step mentioned above is presented in the following sections.

### **5.1.1 Definitions/Limitations/Assumptions**

#### **5.1.1.1 Flight and Weather Conditions**

The noise prediction procedures defined herein are limited to flight operations, where the airplane speeds are less than Mach 0.35. The SAE procedures (refs. 5 through 8) that are used for noise extrapolation are limited to the following weather conditions:

Temperature	-1° to 32°C (30° to 90° F)
Relative humidity	30% to 100%
Downwind	0 to 16 km per hr (10 mph)

Figure 5 shows the "weather windows" that are currently recommended by the SAE for acoustic testing and by the FAA for noise certification of new aircraft.

#### 5.1.1.2 Index/Free-Field Spectra

The far-field noise data used to develop the prediction methods in this report contained atmospheric and ground effects that are inherent in most acoustic test data. These effects have been estimated and removed from the data, i.e., the data was corrected to free-field conditions (no reflecting ground plane) and extrapolated back to a distance of 1 meter from the source (assumed a point) in order to remove atmospheric absorption. The resulting spectra are given the term "Index/Free-Field Spectra." They do not represent the levels which would be observed at one meter from an engine, but rather far-field levels artificially synthesized in order to remove the effects mentioned above.

#### 5.1.1.3 Far-Field/Point Source(s)

The acoustic far-field is defined as those distances greater than or equal to ten times the acoustic wavelength of interest, or ten times the characteristic source dimension. At these distances, the noise observed may be considered to have originated at a point. Thus, the spacing between engines, etc., can be considered negligible, as the observer is sufficiently far away from the airplane such that the noise appears to be emitting from a single point.

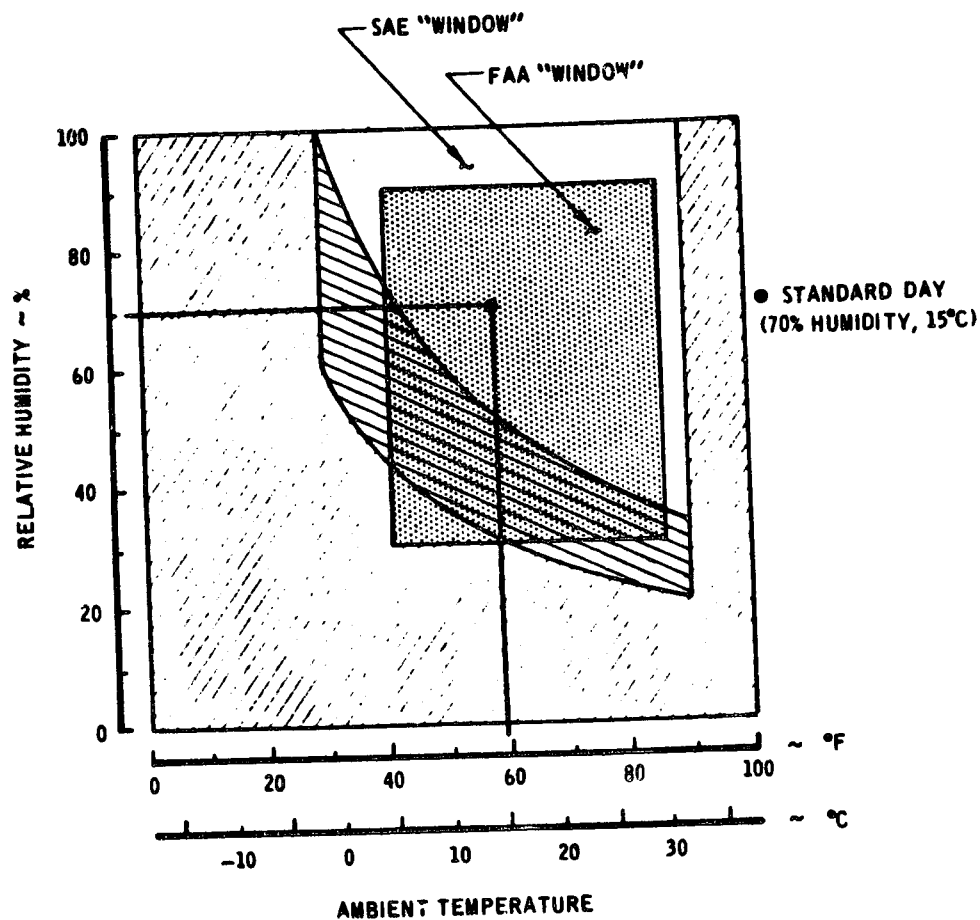
#### 5.1.1.4 Noise Extrapolation

SAE procedures (ref. 5 through 8) are used for extrapolating the datum spectra (Index, Free-Field) to other positions in the acoustic field. The extrapolation procedures consider the attenuation of sound due to spherical divergence, atmospheric absorption, and the turbulent boundary layer near the ground.

If the acoustic impedance of the ground is known, the interference phenomena due to ground reflection can be estimated (sec. 5.1.3.2 and app. A). Otherwise, it is assumed that the observed noise levels will be typically free-field plus 3 dB—the nominal effect of ground reflection.

#### 5.1.1.5 Scaling

For each noise component, it is assumed that the noise and the thrust from different powerplants can be scaled for comparisons, if the powerplants pass equivalent mass flows when operating at the same gasdynamic conditions. The scale factor is determined from mass flow measurements:



#### LEGEND





-  ACOUSTIC TESTING WEATHER: CORRECTIONS TO STANDARD DAY CONDITIONS ARE SMALL (REF. 6)
-  ACOUSTIC TESTING DONE DURING THESE CONDITIONS MAY REQUIRE ATMOSPHERIC ABSORPTION CORRECTIONS (REF. 6 )
-  DO NOT MAKE ACOUSTIC TESTS: DATA CAN NOT BE ADEQUATELY CORRECTED TO STANDARD DAY CONDITIONS (REF. 6 )
-  NOISE CERTIFICATION FLIGHT TESTS MAY BE CONDUCTED UNDER THESE CONDITIONS (REF. 2 )

FIGURE 5.—WEATHER "WINDOWS" FOR ACOUSTIC TESTING

$$\text{Scale Factor} = \sqrt{\dot{m}_1 / \dot{m}_2} \quad (1)$$

where ( $\dot{m}_1, \dot{m}_2$ ) are the mass flows of two different powerplants operating at identical gasdynamics, i.e., Mach number and temperature. Thus, the acoustic and performance data for engine two can be scaled to engine one by multiplying *all linear* dimensions, including *acoustic wavelength*, by the scale factor. Note that acoustic frequency is inversely proportional to wavelength. Since thrust is proportional to area, it scales with the square of the scale factor.

#### 5.1.1.6 Multiple Engines

For multiple engine aircraft, an increase in noise is observed over that predicted for a single engine. If  $N$  identical sources are present with no interference, the increase is

$$\Delta \text{dB} \approx 10 \log_{10}(N) \quad (2A)$$

However, it has been found (refs. 7 and 10) that the increase in noise predicted by equation (2A) is too high for sound which propagates near a jet exhaust of an adjacent engine in order to reach the observer. An empirical relationship has been developed (ref. 10) for predicting the changes in aircraft-generated sound attributed to the attenuation/scattering/refraction effects caused by jet effluxes. This effect is expressed as a function of the number of identical engines  $N$ , azimuth angle  $\psi_0$ , and elevation angle  $\beta_0$  shown in figure 4. The formula is

$$\Delta \text{dB} \approx \left\{ 10 - \frac{20}{N} \left[ \frac{\cos^8 (90^\circ - [\beta_0/90^\circ]^{0.8})}{1 + (1 + \cot^2 \psi_0)^2} \right] \right\} \log_{10}(N) \quad (2B)$$

This assumes that the engines have co-planar exits and that their centerlines lie on a common plane. Scant information is available for establishing the influence of fuselage/wing shielding. For conventional jet transports; i.e., engines mounted under the wings, the effects have not been observed. Other types of engine mountings require additional tests.

#### 5.1.1.7 Flight Effects

The effect of aircraft motion for jet noise is accomplished by the use of the jet velocity relative to the ambient air (ref. 7) as the key parameter, instead of the jet velocity relative to the nozzle. However, an exception to this rule occurs when predicting the jet noise for an augmentor-wing (sec. 5.2.2.4). The overall sound pressure level data for this noise source (ref. 11) is normalized with respect to total temperature and nozzle pressure ratio. The effect of airplane speed on this component is at present unknown, because part of the jet noise is generated inside the augmentor

flap and part is generated outside. In order to determine the effects of motion, a flight or wind tunnel test is required and the resultant acoustic measurements should be compared to that for an equivalent static test, i.e., free-stream velocity equals zero.

The other noise component (core, turbine, fan, rotors, etc.) procedures account for the motion of the source by utilizing the results from theory (refs. 12 and 13). The sound pressure level spectra are Doppler-shifted, and a level correction,  $10 \log_{10} (1 - M_0 \cos \xi)^n$ , is applied. The value for the exponent,  $n$ , varies with the type of source being considered. Additional detail on the corrections for flight are presented in section 5.2.

### 5.1.2 Geometry Solution

The first step in the procedure is the geometric solution for the aircraft/source position versus time. This is required for extrapolating the index/free-field spectra to the observer and for computing the non-axial-symmetric noise characteristics of each source. The analysis for this solution is shown below:

Required Data (see fig. 6)

GRAD	Climb gradient, i.e., $\tan \theta$ for $Z \geq Z_R$
X	Sideline distance
$Z_0$	Airplane height above the ground when at $Y = 0$
$Z_R$	Observer height above the ground
$\xi$	Angle between the flight path and sound propagation path
$C_A$	Average speed of sound over the propagation path. This value is approximated by $C_A \approx 0.5 (C_{Z0} + C_{ZR})$ where $C_{Z0}$ and $C_{ZR}$ are the local speeds of sound at altitude $Z_0$ and $Z_R$ , respectively
$C_Z$	Speed of sound at aircraft altitude, $Z$ . This value is approximated by $C_Z \approx C_{Z0}$
$M_0$	Aircraft Mach number

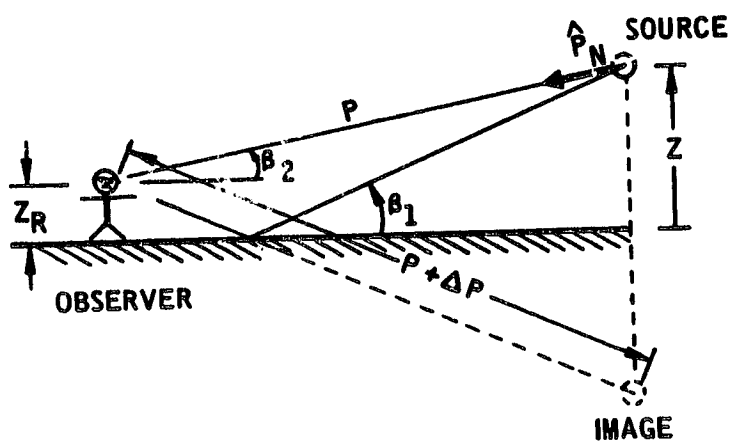
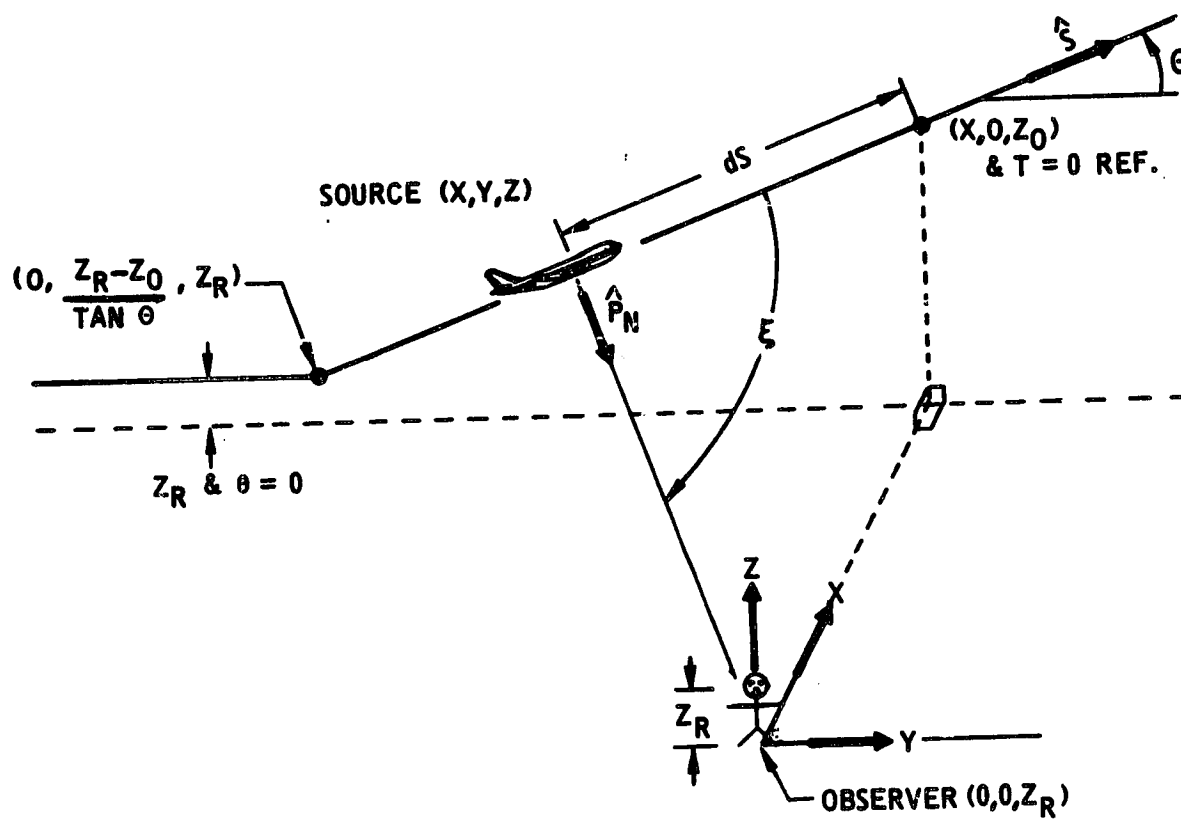


FIGURE 6.—FLIGHT PATH SEGMENT GEOMETRY



# Results (see fig. 6)

$(Y, Z)$	Aircraft coordinates
$P$	Sound propagation path distance
$\Delta P/P$	Relative increase in path length for ground reflected signal
$\beta_1$	Angle of incidence for ground reflected signal relative to grazing incidence
$\beta_2$	Elevation angle used in extra-ground-attenuation formula
$\tau$	Retarded time when sound is generated relative to the visual overhead reference; i.e., aircraft is at $Y = 0$
$t$	Time the observer hears the acoustic signal relative to the visual overhead reference

## Unit Vectors

$(\hat{i}, \hat{j}, \hat{k})$	$(X, Y, Z)$ coordinate system
$\hat{S}$	Direction of flight $\hat{S} = \cos \theta \hat{j} + \sin \theta \hat{k}$
$\hat{P}_N$	Direction of sound propagated $\hat{P}_N = -(X \hat{i} + Y \hat{j} + Z_N \hat{k})/P$ with $Z_N = Z - Z_R$

The basic approach in obtaining a solution for the flight path geometry is to solve the three governing equations below for the distance  $Y$ , which yields a value of  $Z$  greater than or equal to  $Z_R$ . If the solution for  $Y$  yields a value of  $Z$  less than  $Z_R$ , it is assumed that the climb gradient is zero, corresponding to the noise source being at the observer height.

$$P \cos \xi = P \hat{P}_N \cdot \hat{S} = -[Y \cos \theta + (Z - Z_R) \sin \theta] \quad (3A)$$

$$P^2 = X^2 + Y^2 + (Z - Z_R)^2 \quad (3B)$$

$$Z = Z_0 + Y \tan \theta \quad (3C)$$

A value for Y is obtained by forming the quadratic equation (4), from the substitution of equations (3B) and (3C) into the square of equation (3A). Simplification yields

$$a Y^2 - b Y + c = 0 \quad (4)$$

where

$$a = (\sin \xi / \cos \theta)^2$$

$$b = -2 Z_{no} \tan \theta \sin^2 \xi$$

$$c = Z_{no}^2 \sin^2 \theta - (X^2 + Z_{no}^2) \cos^2 \xi$$

$$Z_{no} = Z_o - Z_R$$

The roots of equation (4) are then given by

$$Y = Q_1 \pm Q_2$$

with

$$Q_1 = b/(2a) = -0.5 Z_{no} \sin (2 \theta)$$

$$Q_2 = \sqrt{Q_1^2 - \frac{c}{a}}$$

$$Q_2 = \cos \theta \sqrt{X^2 + (Z_{no} \cos \theta)^2 / \tan^2 \xi}$$

Substitution of both roots into equation (3A) eliminates the erroneous  $(Q_1 + Q_2)$  root and gives the solution

$$Y = Q_1 - Q_2 \quad (5)$$

After Y is determined, Z and P are computed using equations (3C) and (3B) respectively. The increase in path length for the ground reflected signal is computed by

$$\Delta P / P = \sqrt{r + 1} - 1 \quad \text{for } |r| \geq \epsilon \quad (6A)$$

$$= \lim_{N \rightarrow \infty} \sum_{K=1}^N B_K \quad \text{for } |r| < \epsilon \quad (6B)$$

where

$$\begin{aligned} \epsilon &= \pi / 45 \\ r &= 4 Z Z_R / P^2 \\ B_1 &= 0.5 r \\ B_{k+1} &= -r B_k \left( \frac{2K-1}{2K} \right) \end{aligned}$$

Once the distances are determined, the angles used in the extrapolation formulas are defined by

$$\beta_1 = \tan^{-1} [ |Z_N^*| / \sqrt{P^2 - (Z_N^*)^2} ] \quad (7)$$

$$\text{with } Z_N^* = Z + Z_R$$

$$\beta_2 = \sin^{-1} [ Z_N / P ] \quad (8)$$

Next, the time that the sound is generated and observed is computed relative to the aircraft reference position (X, O, Z<sub>O</sub>), shown in figure 6. The resulting formulas are as follows; i.e., let

$$dS^2 = Y^2 + (Z - Z_O)^2 \quad (9A)$$

$$dS = [\text{sign of } Y] \sqrt{dS^2}$$

$$\tau = dS / (M_O C_Z) \quad (9B)$$

$$t = \tau + (P / C_A)$$

This completes the geometry analysis required for noise extrapolation. If the orientation angle ( $\delta_E$ ) of the noise source reference system is given, (see fig. 4), the complete geometry for noise ~~prediction~~ <sup>prediction</sup> is determined using

$$\begin{aligned} \psi &= \text{directivity angle} \\ &= \cos^{-1} [ -(Y \cos \delta_E + Z_N \sin \delta_E) / |P| ] \end{aligned} \quad (10A)$$

$$\begin{aligned}\psi_o &= \text{azimuth angle} \\ &= \tan^{-1} [ |X| / - (Y \cos \delta_E + Z_N \sin \delta_E) ]\end{aligned}\quad (10B)$$

$$\begin{aligned}\beta_o &= \text{elevation angle} \\ &= \tan^{-1} [ |Y \sin \delta_E - Z_N \cos \delta_E| / |X| ]\end{aligned}\quad (10C)$$

\*NOTE\*  $90^\circ < \psi_o \leq 180^\circ$  when  $(Y \cos \delta_E + Z_N \sin \delta_E)$  is positive.

### 5.1.3 Noise Extrapolation

The predicted noise components are treated as free-field (index) spectra at a reference distance of one meter. The techniques for extrapolating from the source to the observer are basically the same as those used during Phase A of the contract (ref. 4) with the exceptions listed below.

- 1) Extra-ground-attenuation (refs. 7 and 8)
- 2) Multiple-engine effect (sec. 5.1.1.6)
- 3) Ground reflection (refs. 14 through 19)

A revision of the extra-ground-attenuation methods was made to reflect information obtained from recent JT8D flight test data (unpublished) and to match the standards (refs. 7 and 8) more closely.

The multiple-engine effect can cause non-axial-symmetric radiation patterns; therefore, it was removed from the extrapolation step and included as part of the prediction methods for each noise component (sec. 5.2).

A theoretical ground reflection procedure has been included as a user option (sec. 5.1.3.2). If the impedance of the reflecting ground plane is known, the user of the noise source prediction computer program can estimate the effects of this interference phenomena instead of using a 3 dB addition to the free-field spectra.

Thus, the noise extrapolation procedures contain the following four items (see fig. 6).

- 1) Spherical divergence (ref. 7)  $20 \log_{10}(P/P_o)$   
     where  $P_o = 1$  meter

- 2) Atmospheric absorption where  $\bar{\alpha}(f)$  is the average loss coefficient (dB/KM) over the propagation path. This parameter is a function of frequency, ambient temperature, and humidity (ref. 5).  $\bar{\alpha}(f) [P/1000]$
- 3) Extra-ground-attenuation  $EGA(f, P, \beta_2)$
- 4) Ground reflection  $GR\left(f, P, \frac{\Delta P}{P}, \beta_1, \frac{Z_1}{Z_0}, \frac{K_1}{K_0}\right)$   
where  $(Z_1/Z_0)$  and  $(K_1/K_0)$  are the normalized impedance and wave number respectively for the ground.

References 5 and 7 provide all necessary detail on spherical divergence and atmospheric absorption, respectively. Hence these items are omitted from further discussion here.

#### 5.1.3.1 Extra-Ground-Attenuation (EGA)

The best available standard, in a form useful for prediction, is contained in reference 8. This report (based on an average of a large number of measurements) provides a procedure for calculating extra-ground-attenuation as a function of distance, frequency, elevation angle, and wind direction. This attenuation is thought to be due to a combination of two effects: refraction due to wind and temperature gradients; and dispersion due to the turbulent boundary layer. The latter is nearly always present; however, the former dominates for upwind propagation. Unfortunately, the reference defines the EGA for only a single wind velocity -10 mph. In addition, the phenomenon is defined only at source/observer heights of 1.73 meters (6 ft.) for up-wind propagation. According to reference 8 the attenuation is essentially constant in the downwind sector (cone angles greater than  $120^\circ$ ). Because of the limitations, it has been common industry practice to use downwind propagation for wind speed of 10 mph as a standard.

Using this standard, EGA is a function of distance, frequency, and elevation angle. Data are shown in reference 8 at elevation angles of  $0-2^\circ$ ,  $10^\circ$ , and  $20^\circ$ . During Phase A of the contract, this data was represented by a function of the following form:

$$EGA(f, P, \beta_2) = EGA(f, P, 0^\circ) \exp [-K(f) \sqrt{\tan \beta_2}]$$

where

$EGA(f, P, 0^\circ)$	=	EGA at $0-2^\circ$ elevation angle
$f$	=	frequency
$P$	=	distance
$\beta_2$	=	elevation angle
$K(f)$	=	is chosen to fit the data at $10^\circ$ and $20^\circ$

This function was modified during the Phase B effort because it predicted substantial amounts of EGA at high elevation angles, a phenomenon not observed during flight tests; e.g., nearly 2 PNdB at  $\beta_2 = 30^\circ$  for 0.25 N.Mi. sideline noise estimates. During the JT8D Retrofit Feasibility Study for DOT/FAA, a large number of noise measurements were made at various altitudes from 122 M to 2750 M and at several thrust values. A minimum of three flights were made at each altitude and thrust. From a preliminary analysis of the data, it appears that EGA approaches zero at elevation angles greater than  $45^\circ$ . In view of the above, a third formula, which goes to zero at  $45^\circ$  and linearly connects the data in reference 8 was chosen until better data becomes available. The formula is

$$EGA(f, P, \beta_2) = EGA(f, P, 0^\circ) F(\beta_2, f) \quad (11)$$

where  $EGA(f, P, 0^\circ)$  is obtained by linear interpolation with respect to  $\log(P)$  and  $\log(f)$  on the data given in table 2. The function  $F(\beta_2, f)$  is shown in figure 7 and is tabulated in table 3.

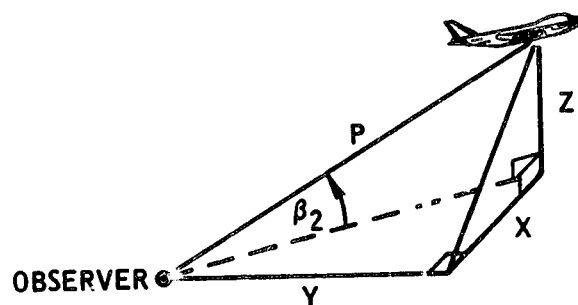
#### 5.1.3.2 Ground Reflection

The particular model considered is a point source, homogeneous media (air and ground), and a smooth/infinite/reflecting plane with complex acoustic wave impedance based on the acoustic analog to that in electromagnetic theory (refs. 14 through 19). From this model, it has been found that the reflection effects are quite sensitive to the aircraft/observer geometry, the source frequency, and wave number ratio ( $K_1/K_0$ ), and the normal impedance ( $Z_1/Z_0$ ) of the ground. Complication arises because the values of these last two parameters are not common knowledge for various types of terrain. If the parameters  $Z_1/Z_0$  and  $K_1/K_0$  are not known but only guessed, the predicted ground reflection effect can make the Effective Perceived Noise Level more in error than that obtained by simply adding 3 dB to free-field data. However, this phenomena does deserve study because its spectral effects are significant. A detailed analysis for the optional ground reflection procedure incorporated in the computer program is provided in appendix A.

**TABLE 2.—TABULATION OF DATA FOR COMPUTING EXTRA GROUND ATTENUATION AT  
0° ELEVATION ANGLE—EGA (I, P, 0°) in DB**

Reference: Figure 3 of SAE AIR 876

Distance P in (ft)	Log <sub>10</sub> (P)	Log <sub>10</sub> (f)					
		1.7245	2.0256	2.3266	2.6276	2.9287	3.2297 thru 3.8318
≤ 1	0.0	0	0	0	0	0	0
100	2.0	0.2	0.3	0.5	0.6	0.7	0.8
140	2.1761	0.3	0.5	0.6	0.8	1.0	1.1
200	2.301	0.5	0.7	1.0	1.2	1.5	1.7
300	2.4771	0.7	1.1	1.4	1.8	2.2	2.4
400	2.6021	0.8	1.5	1.9	2.4	2.7	3.1
600	2.7781	1.1	2.1	2.6	3.2	3.6	4.4
800	2.9031	1.5	2.5	3.2	4.0	4.8	5.8
1000	3.0	2.0	3.0	4.0	5.0	6.0	7.2
1400	3.1461	3.0	4.3	5.6	7.1	8.5	10.1
2000	3.3010	4.2	6.0	7.7	9.7	11.1	13.0
3000	3.4771	5.0	7.0	9.1	11.2	13.1	14.7
4000	3.6021	5.0	7.1	9.7	11.8	14.0	15.4
6000	3.7781	5.0	7.2	9.9	12.0	14.6	15.9
≥ 8000	≥ 3.9031	5.0	7.2	10.0	12.0	14.8	16.0
		37.5/75	75/150	150/300	300/600	600/1200	1200/2400 thru 4800/9600
OCTAVE BAND LIMITS - (Hz)							



$$EGA(f, P, \beta_2) \approx EGA(f, P, 0^\circ) \quad F(\beta_2, f)$$

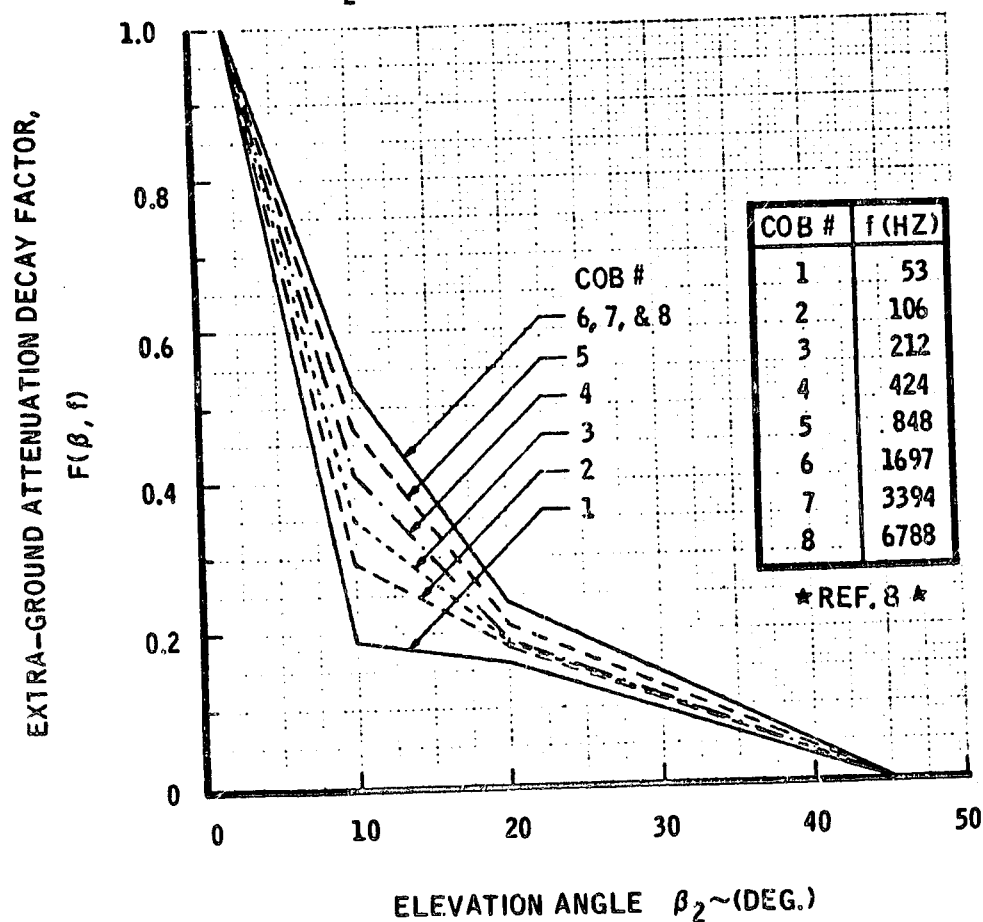


FIGURE 7.—DECAY FACTORS FOR COMPUTING EXTRA-GROUND ATTENUATION  
(COMMERCIAL OCTAVES)



TABLE 3.—DATA POINTS FOR EGA DECAY FACTOR

ELEV. $\theta_2$ in DEG	EGA DECAY FACTORS, $F(\theta_2, f)$					
0	1.0	1.0	1.0	1.0	1.0	1.0
2	1.0	1.0	1.0	1.0	1.0	1.0
10	.186	.297	.352	.406	.468	.534
20	.163	.183	.188	.198	.214	.235
45	0.	0.	0.	0.	0.	0.
90	0.	0.	0.	0.	0.	0.
	1	2	3	4	5	6,7,8
	COMMERCIAL OCTAVE BAND NUMBER					

\*NOTE\* Values in Table above were obtained from Figure 4 (Appendix 2) of SAE AIR 923. The  $\Delta$ dB error was minimized by using

$$F = \sum \Delta dB \times \Delta dB|_{MAX} / \sum \Delta dB|^2_{MAX}$$

for ranges P = 250, 350, 500, 700, 1000, 1-00, 2000, 2800, 4000 feet.

#### 5.1.4 Lining Treatment

Current technology in predicting the attenuation of acoustic linings incorporates a combination of experimental correlation and theoretical analysis. The acoustic wave attenuation analysis is based on a rectangular duct with mean flow and boundary layer effects. Equivalent duct heights for non-rectangular duct geometries are obtained by equating flow areas, treated areas, and duct lengths. Far-field attenuation directivity corrections have been obtained from engine ground test data.

In the application of this technology, three types of prediction procedures of different detail and complexity can be identified. These three types are (1) prediction of the attenuation spectrum for a given lining design, (2) prediction of the lining parameters for a given duct configuration where the attenuation of a noise spectrum is maximized, and (3) prediction of the attenuation spectrum for a given duct with lining parameters unspecified, but assumed to be chosen such that the attenuation of a given noise spectrum is maximized.

The first kind of prediction (1) can be made relatively inexpensive by the solution of the equations governing wave propagation in a lined duct of somewhat idealized geometry, leading to solutions which compare reasonably well with data. To accomplish the second kind of prediction requires an optimization program. The optimization program iterates the procedures contained in the first kind of prediction (1) resulting in the optimum lining parameters that maximize the attenuation of a noise spectrum. Although optimization programs exist, they are too costly to run, except in final design of a lined duct configuration.

The greatest need for predictions are of the third kind, which arise in trade studies, where the effects of such parameters as inlet length, number of splitter rings, and engine choice are investigated. For these cases, a simplified procedure which uses attenuation spectra corresponding to optimized linings is used. These attenuation spectra are somewhat idealized, i.e., made to conform to a standard shape in order to avoid the expense of an exact calculation. Experience with this approach, though approximate, shows good correlation with results from detailed predictions for perceived noise level reductions. This approach has been incorporated into the computer program. The following discussion pertains to the type 3 prediction procedure.

This procedure encompasses two types of optimized linings: single-layer and double-layer. The single-layer procedure gives the user two options. The first option considers only a single design point; i.e., fixed engine conditions. The second option considers multiple-design-points; i.e., the engine conditions vary over a limited range. A compromise between peak attenuation and bandwidth is made because the lining is expected to attenuate tones that track with the engines' shaft speed (rpm).

For double-layer linings, an increase in bandwidth can be realized with the same peak attenuation as that given by single-layer linings. Thus, double-layer linings can be used for the multiple-design-point option described above, to provide the same perceived noise level reduction for a slightly less amount of lining area.

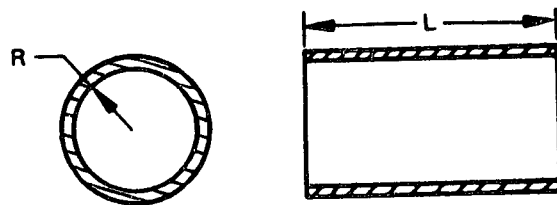
The source noise computer program contains lining attenuation calculation procedures as an option for lining treatment of the following noise components:

- 1) Compressor and inlet fan
- 2) Discharge fan
- 3) Lift fan
- 4) Core and turbine
- 5) Ejector-suppressor jet noise
- 6) Slot nozzle with augmentor-flap jet noise

Within these procedures, there are several methods available for calculating the lining attenuation spectra. These methods are as follows:

- 1) For each target frequency, the user defines the magnitude of maximum attenuation and the percentage of the total area that is treated. The program then determines the spectrum shape.
- 2) The user defines the effective duct height, the ratio of apparent treatment length to effective duct height, and the percentage of the total area that is treated for each target frequency. The program then determines the spectrum shape.
- 3) The user defines the geometry of the lining in terms of the length and radii of cylindrical walls, and the percentage of the total area that is treated for each target frequency. The program then determines the spectrum shape.

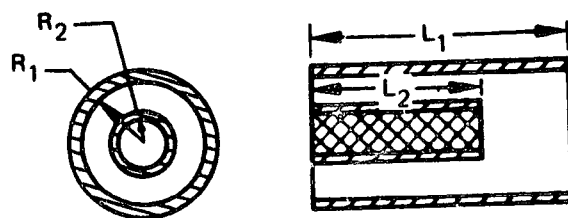
The user is limited to the configurations shown in figure 8 when defining the linings geometrically.



a) CIRCULAR DUCT

(Number of walls = 1)

( $H = R$ )

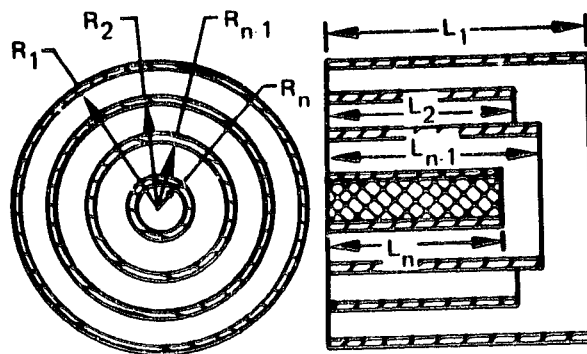


b) ANNULAR DUCT

(Number of walls = 2)

Innermost and outermost walls are lined on one side.

( $H = R_1 - R_2$ )



c) "n" CONCENTRIC WALLS

(Number of walls = n)

Innermost and outermost walls are lined on one side, interior walls are lined on both sides.

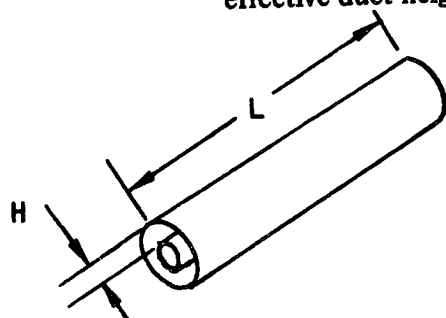
( $H_{n-1} = R_{n-1} - R_n$ )

FIGURE 8.—LINING GEOMETRY

The lining attenuation prediction procedure involves the successive use of five figures. These curves consider duct geometry, treatment area, target frequency, speed of sound, duct Mach number, attenuation over a range of power settings, attenuation spectrum shape, and directivity angle. Depending on user requirements, any or all of the procedures may be used. The use of each figure is explained in detail below.

Figure 9 is an estimate of the peak attenuation obtainable for an optimum single-layer lining at a single power setting and a zero Mach number. The required data are:

- 1)  $L/H$  One half the ratio of actual treatment area to duct cross sectional flow area. Actual treatment area is typically about 65% of that which would be calculated from a nacelle half-section drawing.  $L$  is the apparent treatment length.  $H$  is the effective duct height. See sketch for example.



Inside of outer cylinder is lined  
Outside of inner cylinder is lined

- 2)  $f_t H/c$  Non-dimensional target frequency, where  $f_t$  is the target frequency for peak attenuation, and  $c$  is the speed of sound.

Figure 10 shows the variation of the single-design-point peak attenuation with the duct Mach number. However, it should be remembered that these curves represent optimum linings at the same frequency and different Mach numbers; not the same lining at a different Mach number, as is the case in typical duct data and theoretical analysis.

Figure 11 shows the compromise when a lining is designed to operate effectively over a range of power settings—the usual case. The correction factors cause a reduction  $K$  in peak attenuation, but an increase in bandwidth by an amount  $(1/K)$  or  $(1/K')$  respectively for single or double layer linings. The inlet mode attenuation is compromised more than the exhaust mode because, as the power setting is changed, the engine blade passage frequencies and the peak lining attenuation frequency shift in opposite directions for the inlet mode, and in the same direction for the exhaust mode.

Figure 12 gives the attenuation spectrum shape. This is used to obtain the attenuation of sound at frequencies other than the target frequency. It is considered representative of an average single-layer-lining case: the reasonable compromise between the maximum obtainable attenuation at

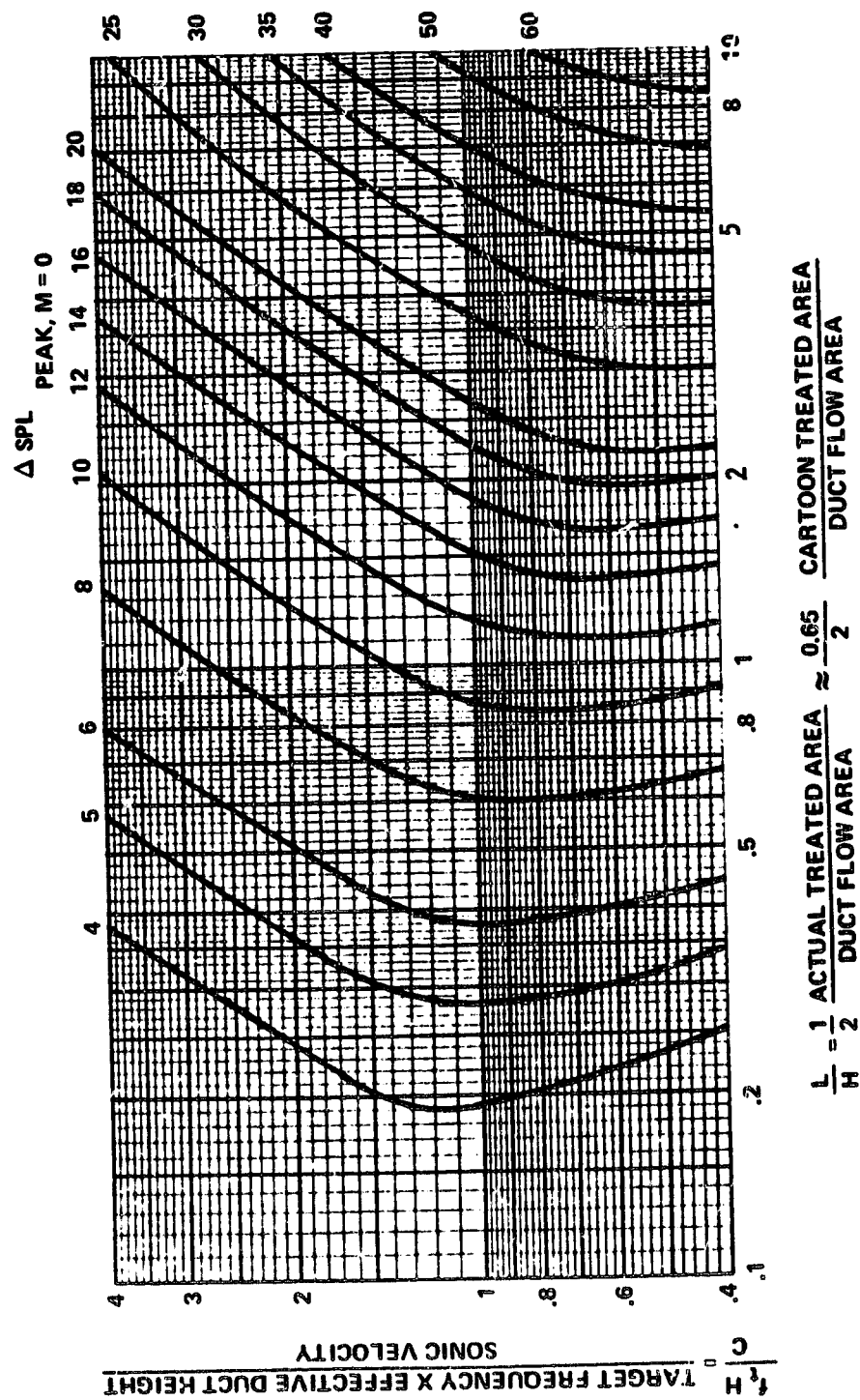


FIGURE 9.—EFFECT OF DUCT GEOMETRY, TREATED AREA, TARGET FREQUENCY, AND SPEED OF SOUND ON REALIZABLE LINING ATTENUATION

$M$  = MACH NUMBER  
 $(\Delta dB)_M$  = REALIZABLE ATTENUATION @  $M$   
 $(\Delta dB)_0$  = REALIZABLE ATTENUATION @  $M = 0$   
 $(\Delta dB)_M = (\Delta dB)_0 \left[ (\Delta dB)_M / (\Delta dB)_0 \right] \times K$   
 $K$  = MULTIPLE DESIGN POINT CORRECTION (FIGURE 11)

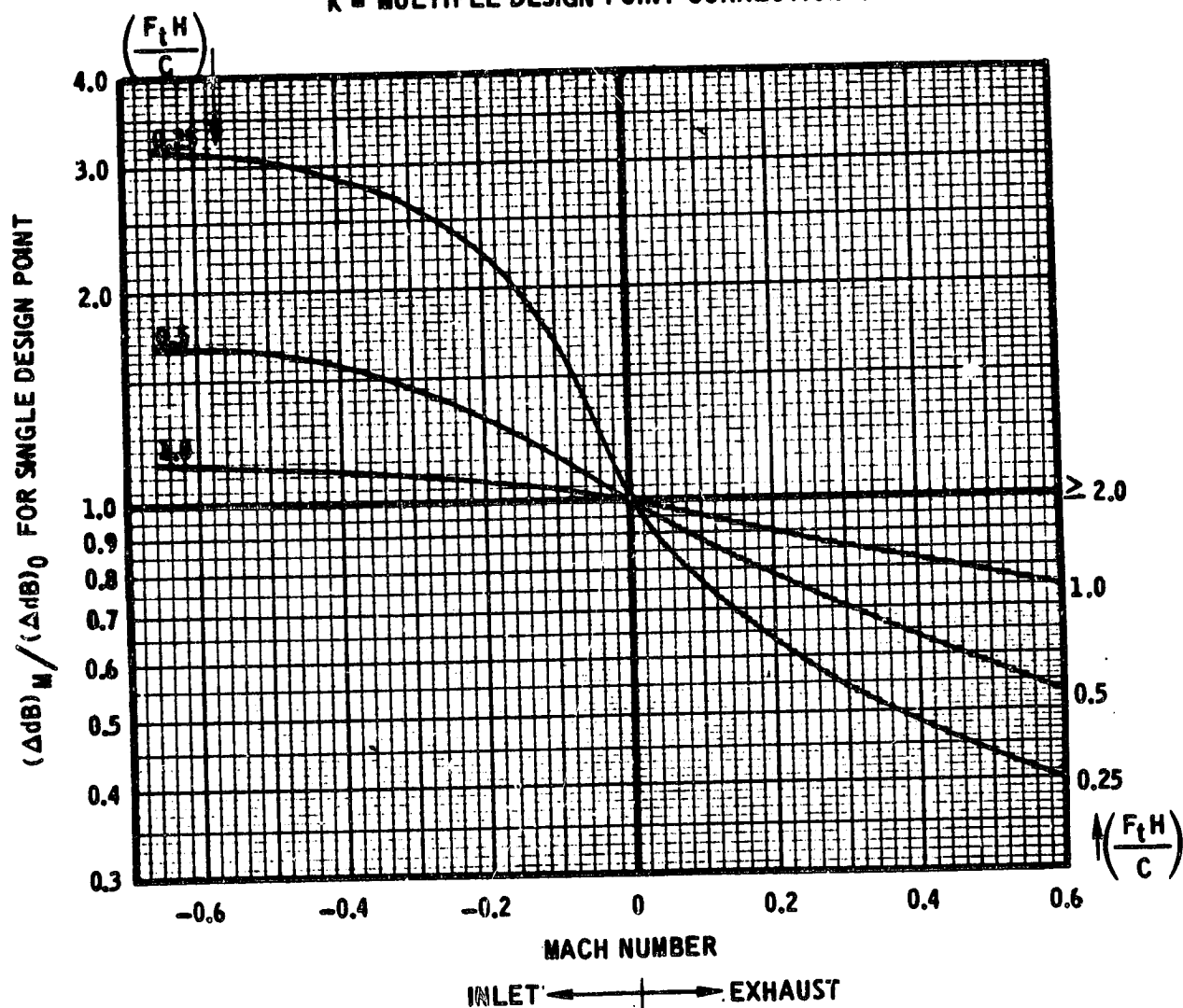


FIGURE 10.—ATTENUATION CORRECTION FOR MACH NUMBER EFFECT

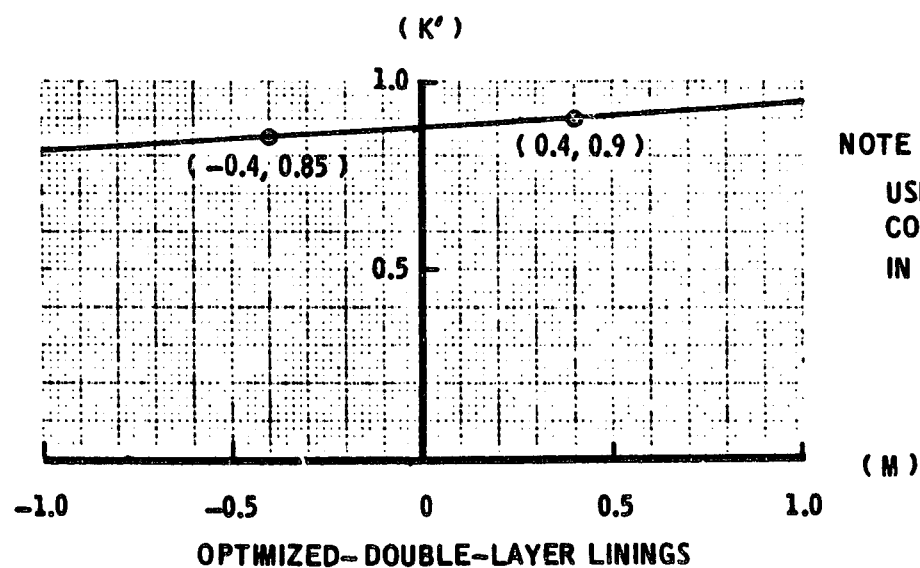
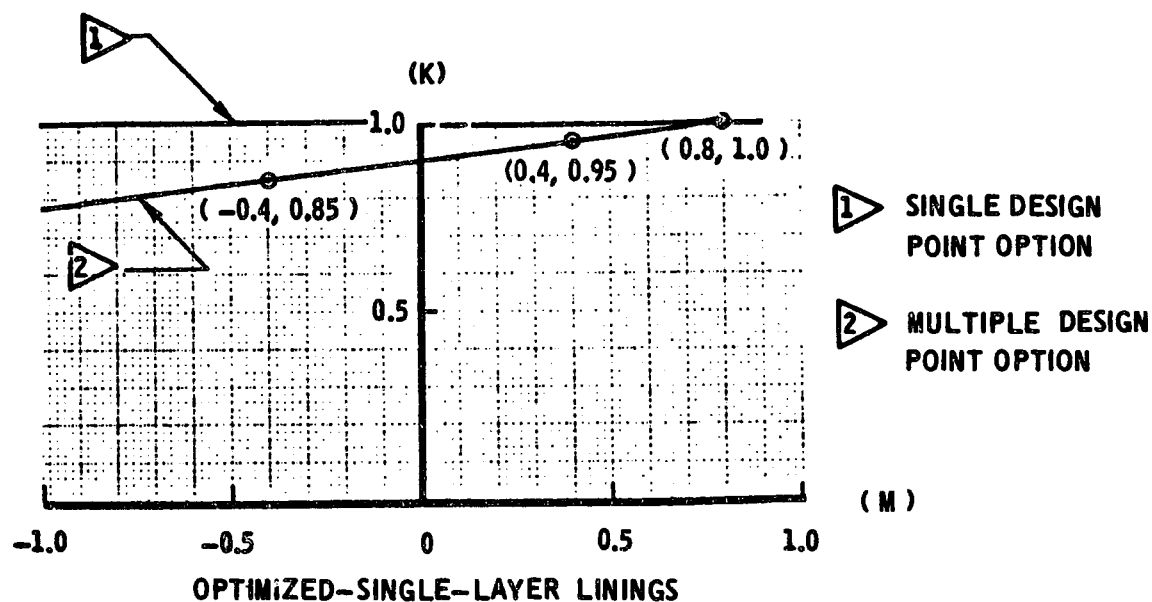


FIGURE 11.—BANDWIDTH CORRECTION FACTORS



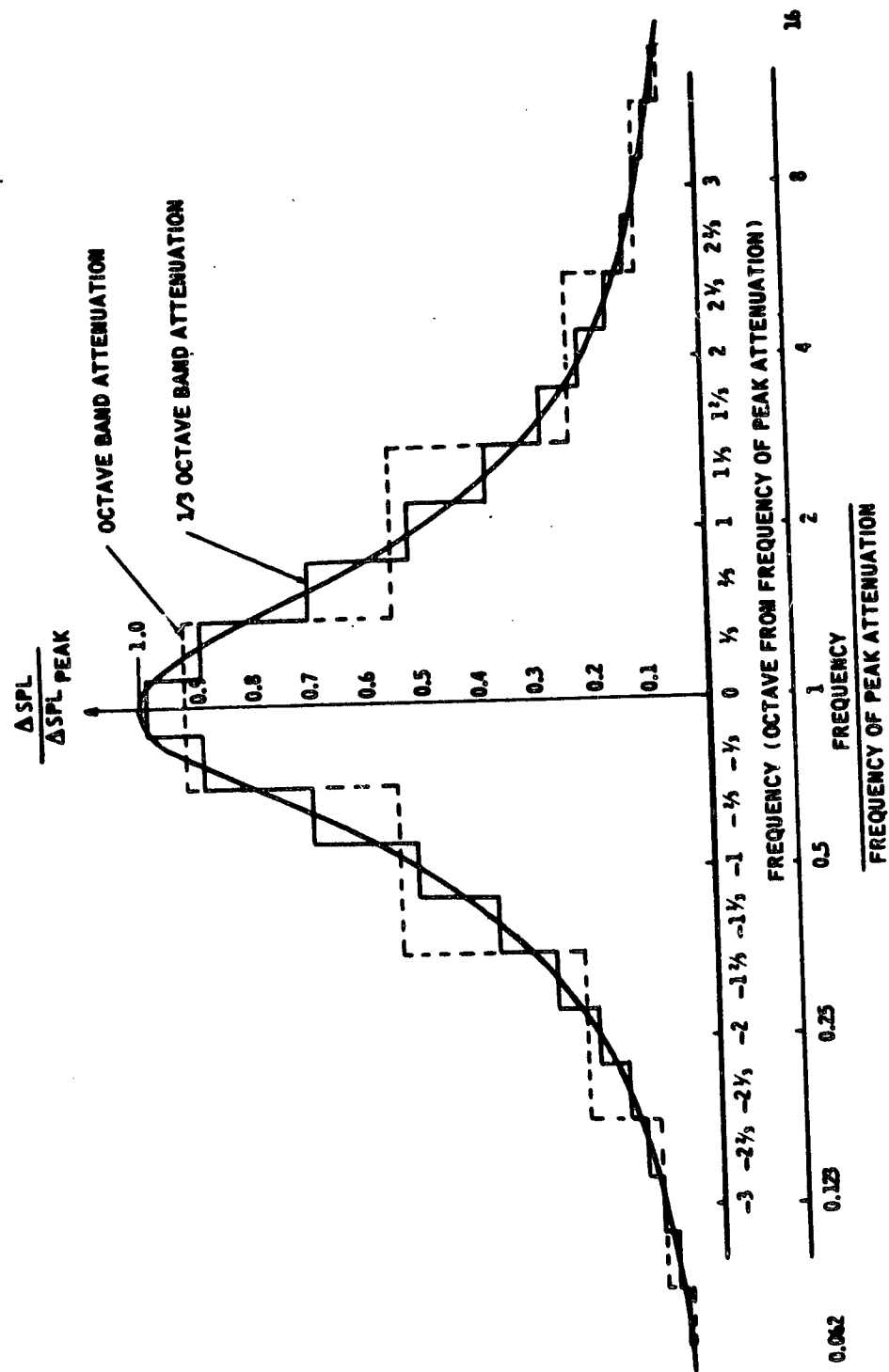


FIGURE 12.—TYPICAL SHAPE OF LINING ATTENUATION SPECTRA

the target frequency and the requirement for attenuation bandwidth using the single-design-point option. To approximate the use of the multiple-design-point option or the use of double layer linings, the bandwidth is increased by multiplying the argument in octaves,  $\log_2(f/f_T)$ , by the factor (K or K'), shown in figure 11.

Figure 13 gives the far field directivity correction to apply to the attenuation spectrum. Figure 14 shows a comparison between the predicted attenuation and the experimental data.

### 5.1.5 Configuration Corrections

The effects of fuselage/wing shielding and reflection have not been defined due to the scarcity of information on the influence of engine placement and, furthermore, it is expected that these effects are small for conventional jet transports. However, any radical change in engine location, e.g., over-the-wing-mounting, or use of suppression devices, etc., could result in a substantial change in noise level and require corrections to be employed. Since there is no way to anticipate the changes in airplane/engine configurations, the approach taken here is to let the user of the program define corrections for each noise component.

The corrections prescribed by the user for each noise component can be used for: (1) a  $\Delta$  dB to be subtracted from the overall sound pressure level or (2)  $\Delta$  dB's to be subtracted from the noise spectrum. The program permits the corrections to vary with the directivity angle,  $\psi$ . If the Doppler-shift option is selected in predicting a noise component, the program assumes the corrections are representative of that obtained from a static test and it will Doppler-shift the prescribed correction spectra.

### 5.1.6 Summation of Component Noise

The problem is structured to permit the calculation of the datum spectra for each noise component on a common reference sphere at angles  $10^\circ, 20^\circ, \dots, 170^\circ$  relative to the flight path. Thus, individual noise components are added together in the usual manner for logarithmic quantities. As each noise component is determined, the total noise for all the sources is accumulated using equation (12) below. The result represents the total sound radiating toward the observer at each aircraft position considered. Further detail on the prediction of the component noise for each source is given in section 5.2.

$$\text{SPL}_{\text{TOTAL}} = 10 \log_{10} \left[ \sum_{k=1}^M 10^{0.1 \text{ SPL}_k} \right] \quad (12)$$

EACH  
COMP.

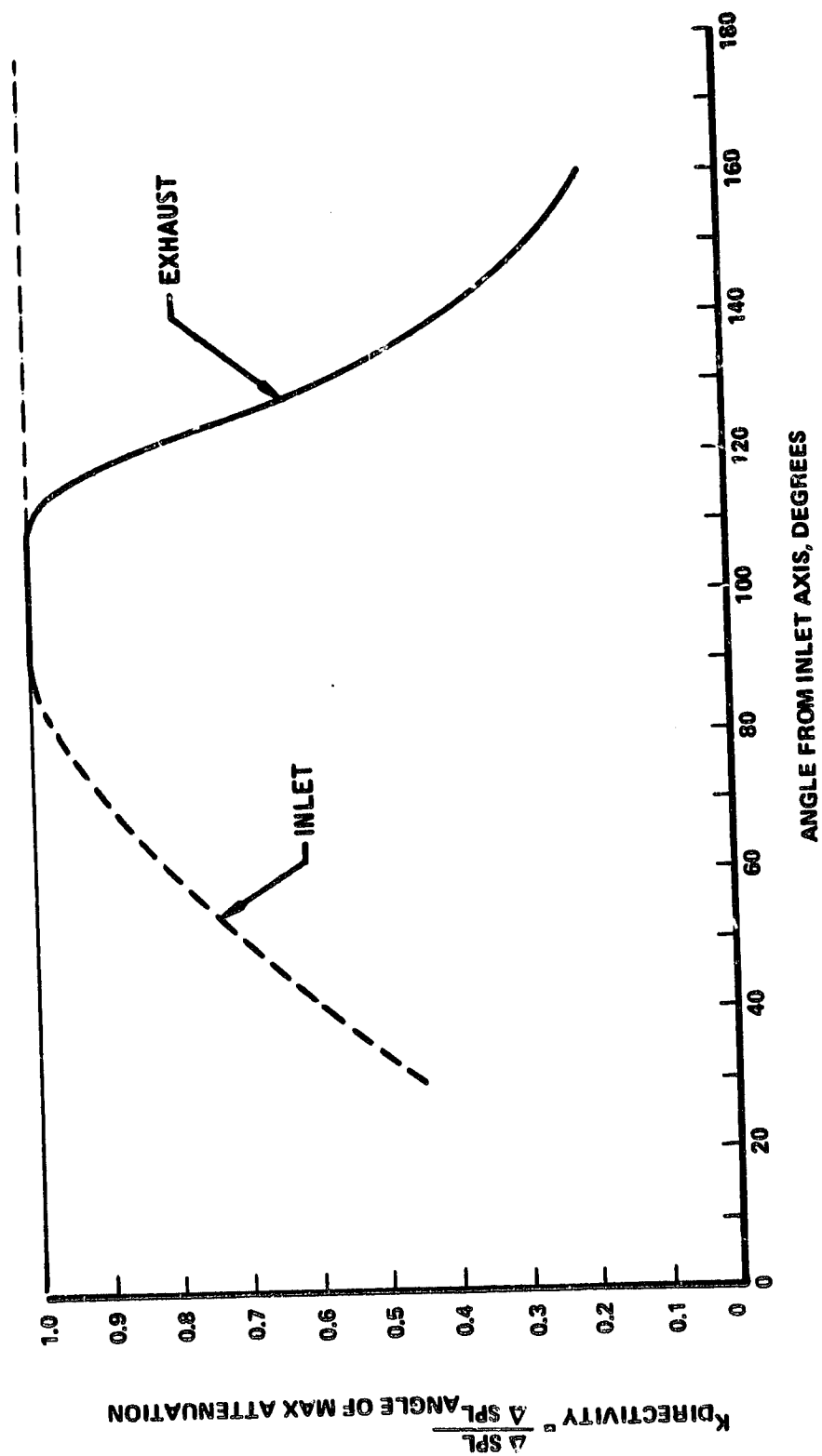


FIGURE 13.—DIRECTIVITY OF LINING ATTENUATION

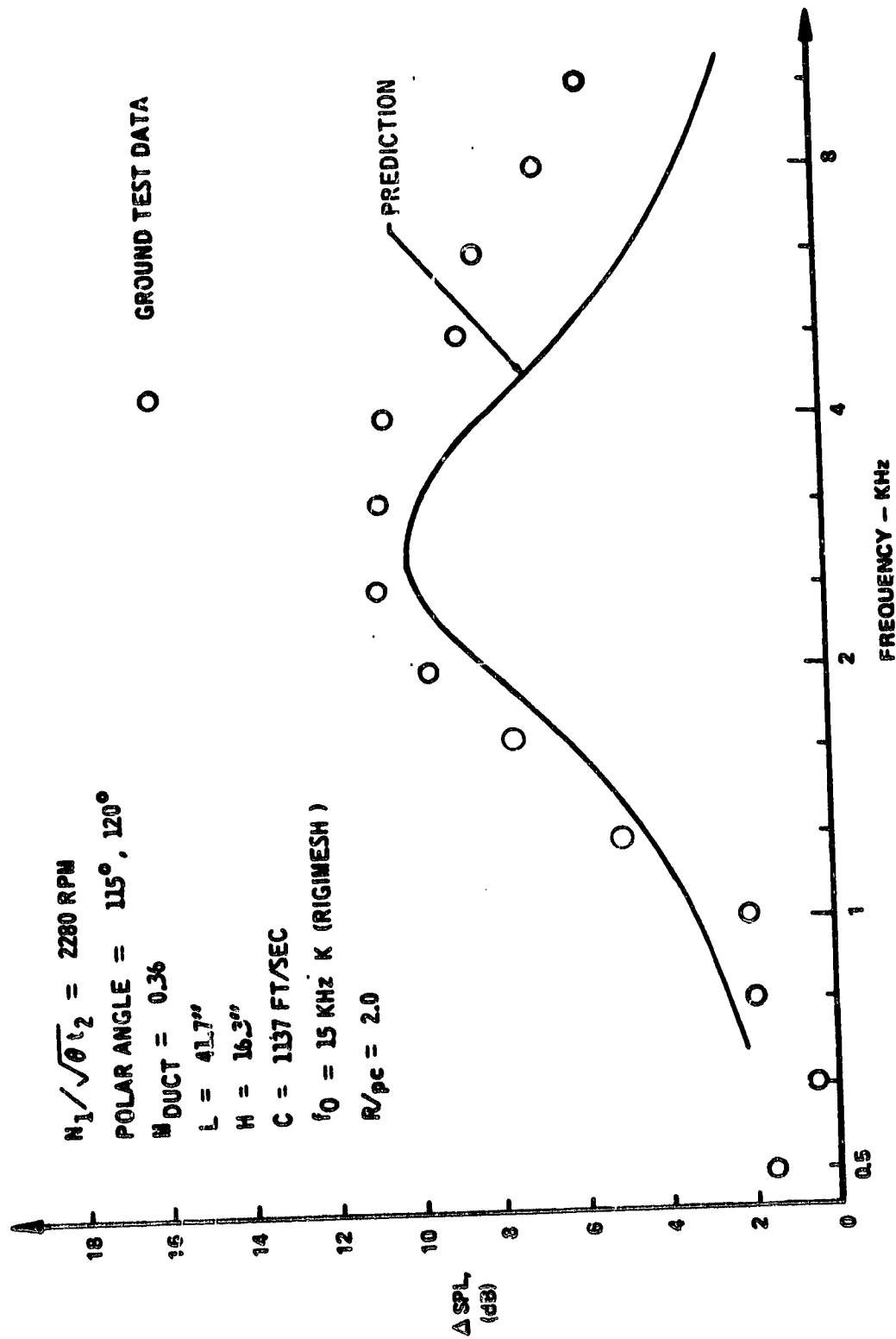


FIGURE 14.—COMPARISON OF PREDICTED AND ACTUAL ATTENUATION

### 5.1.7 Output for Noise Contour Estimation

One of the requirements of the noise prediction computer program is the linkage of its output, a data table, with the noise contour program. The output variables for the data table are listed below and illustrated in figure 15. The format used for the output file is (1PE12.3, 3E12.3).

NL Noise level (EPNL or PNL maximum) corresponding to each district combination of values for EPP,  $\alpha$ , LR.

EPP Engine performance parameter. This variable is to be specified by the user as a correlation parameter for noise and may correspond to engine pressure ratio, jet velocity, engine speed (rpm), etc. During Phase A of the contract, this parameter was engine pressure ratio (ref. 4).

$\alpha$  Elevation angle in degrees (ref. 4). It is computed as  $[\alpha = \cos^{-1}(X/P)]$  where P is the range at the closest point of approach (fig. 6).

LR Logarithm (base 10) of the range at the closest point of approach (CPA). It is computed as  $\log_{10}(P)$  when  $\xi$  is equal to  $90^\circ$  (fig. 6).

## 5.2 NOISE SOURCE ESTIMATION

The computer program has been generalized to accommodate several different types of noise sources associated with current and future aircraft. The following list describes the types of noise source prediction modules that have been included in the "Noise Source Computer Program."

### Reference

#### 1) Measured Data

#### 2) Jet Noise

- |  |                |
|--|----------------|
| a) Single exhaust nozzle                   | 7, 20, and 21  |
| b) Co-annular exhaust nozzles              | 22             |
| c) Ejector/Suppressor nozzle (JT8D design) | 23, 24, and 25 |
| d) Slot nozzle with augmentor flap (STOL)  | 11, 26, and 27 |
| e) Externally-blown flap (STOL)            | 28 and 29      |

#### 3) Core and Turbine Noise (Turbojets/Turbofans)

# VARIABLES

- 1) NL A THREE-DIMENSIONAL DATA ARRAY OF NOISE LEVEL AS A FUNCTION OF (EPP, LR,  $\alpha$ ). THE NOISE LEVEL VALUES REPRESENT EPNL OR PEAK PNL, ETC.
  - 2) EPP A ONE-DIMENSIONAL DATA ARRAY OF ENGINE PERFORMANCE PARAMETER VALUES FOR THE (NL) ARRAY.
  - 3) LR A ONE-DIMENSIONAL DATA ARRAY OF  $\log_{10}$  (RANGE AT CPA) VALUES FOR THE (NL) ARRAY.
  - 4)  $\alpha$  A ONE-DIMENSIONAL DATA ARRAY OF ELEVATION ANGLES FOR THE (NL) ARRAY.
- ★NOTE★ DATA ARRAYS (NL, EPP, LR,  $\alpha$ ) DEFINE THE THREE-DIMENSIONAL TABULAR FUNCTION,  $NL = f_1(EPP, LR, \alpha)$  THE DATA CORRESPONDS TO LEVEL FLIGHT AT A NOMINAL AIRCRAFT VELOCITY, AND DIRECTIVITY ANGLE  $\psi$  OF PEAK NOISE RADIATION.

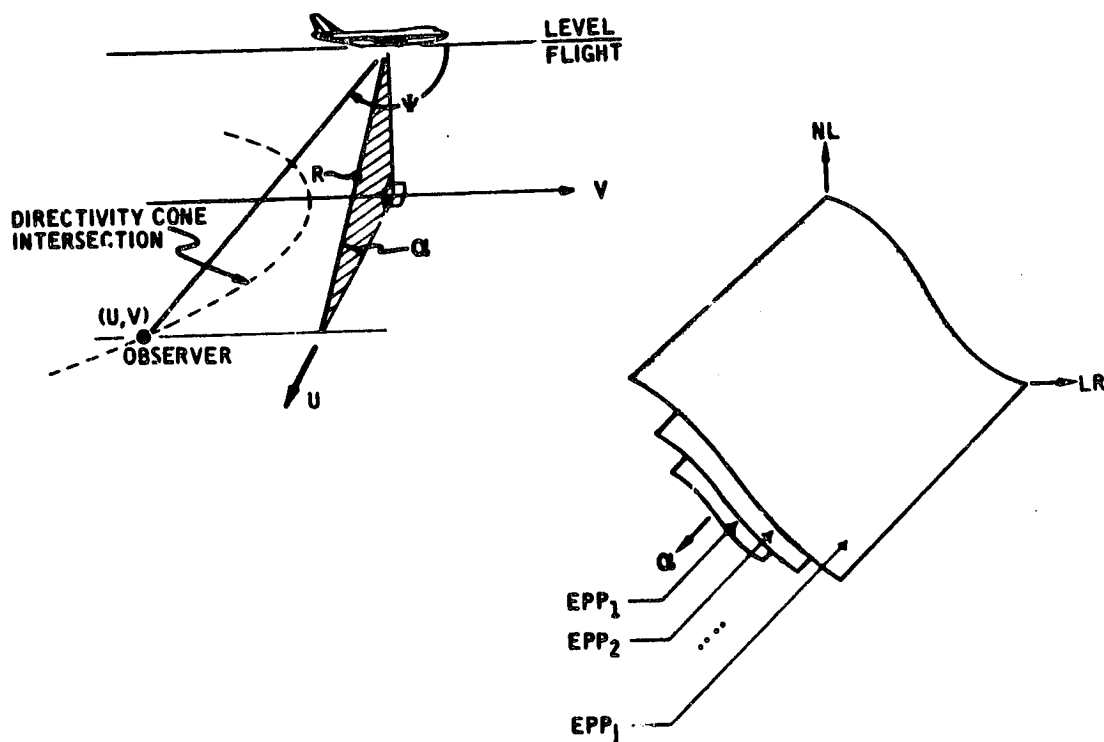


FIGURE 15.-ACOUSTIC DATA FOR NOISE CONTOUR COMPUTER PROGRAM

- 4) Compressor and Fan Noise
  - a) Conventional turbojets/turbofans 30 and 31
  - b) Lift-fans
  
- 5) Propeller, Helicopter and Tilt Rotor Noise
  - a) Empirical propeller procedures 32
  - b) Theoretical propeller/rotor procedures 33 through 38

All, or any subset, of the modules available can be used for noise prediction. Each module may be called up to a maximum of three times, corresponding to an aircraft having three different types of engines mounted on it. This restriction does not apply to the number of engines of the same type and orientation angle,  $\delta_E$ .

In each noise prediction module, the known non-axial-symmetric characteristics in the radiation patterns are considered in the calculation of the datum spectra (free-field, index); e.g., the multiple-engine correction formula equation (2B) in section 5.1.1.6. This also includes any user specified installation effects (sec. 5.1.4 and 5.1.5) on the radiation patterns. Other factors considered are flight versus static conditions; relative velocity, Doppler-shift, etc., (sec. 5.1.1.7 and fig. 4). The optional use of lining as a suppression device can be included in the modules; 2c, 2d, 3, and 4 listed above.

As evident from the options available, the user of the program can predict the noise for almost any aircraft presently flying, and some which have not been built yet. However, empirical procedures have their limits and failure is anticipated. (The complexity of the types of aircraft presently being studied could also be the limit.) For these cases, a module has been included to accept measured data to provide more accurate results when one or more of the models presented are considered inadequate.

#### 5.2.1 Measured Noise Data

Since measured data is generally more reliable than that obtained from current prediction procedures, the capability of including measured data in the computer program is available. The measured noise is assumed to be sound pressure level spectra, SPLS, given in dB re  $20 \mu\text{N/M}^2$  as a function of three or four variables for axial-symmetric or non-axial-symmetric type sources, respectively. The independent variables are frequency (eight preferred 1/1 octave bands or twenty-four 1/3 octave bands defined in table 4), some prescribed engine performance parameter, directivity angle ( $\psi$ ), and elevation angle ( $\beta_0$ ). Prescribed spectra are assumed to represent far-field noise extrapolated back to a free-field, index condition. Thus, the levels can be treated as independent of local ambient conditions.

**TABLE 4.—FILTER BAND DEFINITION AND ATMOSPHERIC ABSORPTION  
AT 45.7 m (150 FT) FROM A SOUND SOURCE**

TYPE OF ANALYSIS	BAND NO.	CENTER FREQUENCY $f$ (Hz)	FILTER LIMITS (Hz)	ABSORPTION COEFFICIENT $\bar{\alpha}(f)$ (dB/KM)	ATMOSPHERIC ABSORPTION $\Delta d\beta$ (dB)
1. PREFERRED FULL OCTAVES	17-19	63.1	44.7/89.1	0.2	0.
	20-22	126.	89.1/178	0.6	0.
	23-25	251.	178/355	1.2	0.
	26-28	501.	355/708	2.4	0.1
	29-31	1000	708/1410	4.9	0.2
	32-34	2000	1410/2820	10.2	0.5
	35-37	3980	2820/5620	25.7	1.2
	38-40	7940	5620/11200	47.3	2.2
2. PREFERRED (1/3) OCTAVES	17	50.1	44.7/56.2	0.2	0.
	18	63.1	56.2/70.8	0.3	0.
	19	79.4	70.8/89.1	0.4	0.
	20	100.	89.1/112	0.5	0.
	21	126.	112/141	0.6	0.
	22	158.	141/178	0.8	0.
	23	200.	178/224	1.0	0.
	24	251.	224/282	1.2	0.1
	25	316.	282/355	1.5	0.1
	26	398.	355/447	1.9	0.1
	27	501.	447/562	2.4	0.1
	28	631.	562/708	3.0	0.1
	29	794.	708/891	3.9	0.2
	30	1000	891/1120	4.9	0.2
	31	1260	1120/1410	6.2	0.3
	32	1580	1410/1780	7.9	0.4
	33	2000	1780/2240	10.2	0.5
	34	2510	2240/2820	13.5	0.6
	35	3160	2820/3550	18.4	0.8
	36	3980	3550/4470	25.7	1.2
	37	5010	4470/5620	30.5	1.4
	38	6310	5620/7080	43.2	2.0
	39	7940	7080/8910	63.8	2.9
	40	10000	8910/11200	91.8	4.2

1 15°C, 70% Relative Humidity

2  $\bar{\alpha}(f) \times 0.0457$  KM

3 frequencies listed are exact to three significant digits. Often conventional listings round to two significant digits for convenience (ASA S1.11-1966).



The computer program's function is to interpolate on these data at specified aircraft operating conditions and extrapolate the spectra to the observer. No effort is made to scale, correct for aircraft speed, etc., because no information is known about the type of sound source the noise represents or the measurement conditions in which the data were obtained.

### 5.2.2 Jet Noise

For the procedures presented in this report, jet noise is defined as the noise generated by jet flows as they exhaust into the atmosphere. The actual noise generation is thought to take place in the flow regions where the jet flow interacts with the atmosphere. The noise generated upstream inside the engine is discussed in sections 5.2.3 through 5.2.4,

In the case of a single jet, the noise producing regions are shown shown in figure 16. In the past, the noise produced by this jet was correlated with three parameters—density, area, and velocity relative to the ambient air, yielding considerable success in predicting maximum passby noise of turbojet engines (refs. 4 and 7).

However, turbofan engines have replaced the turbojet engines as the most common power plant for today's air transport fleet. The new turbofan engines are considerably quieter than the turbojets and the jet noise produced by the newer engines has been observed to differ from that predicted by the SAE procedure (ref. 7). Clearly, a revised procedure was necessary. During Phase A of the current contract, a relatively "crude" revision was made (ref. 4), but the subject demanded better precision for estimating time-integrated subjective measures, as prescribed for the Phase B part of the contract. This required prediction of noise at several angular positions relative to the inlet centerline, instead of just at that angle where the maximum noise occurs. For the case of lift jets attached to an aircraft's fuselage, it was of particular importance to calculate the relative jet velocity vectorially as shown in figure 4, section 5.1 because an increase in jet noise occurs with crossflow imposed on the jet, i.e., the relative jet velocity is greater than that without crossflow. The procedures presented here for jet noise are empirical and represent the state-of-art in solving this problem.

Before the noise prediction procedure for a single jet is presented, it is worth noting some technological developments (ref. 39 through 41) that are taking place at this time which could result in a more comprehensive prediction procedure. Figure 16 shows the noise producing shear regions in a single jet and the corresponding relative acoustic power level as a function of distance from the nozzle exit plane. This distribution of energy can be further broken down with respect to frequency  $f/f_0$  and position  $X/X_0$  as was done in references 39 and 40. Hence the noise producing regions appear to be structured and not random as previously believed. Thus, it may be possible that a one-dimensional source distribution model can be developed for predicting the noise in a far-field.

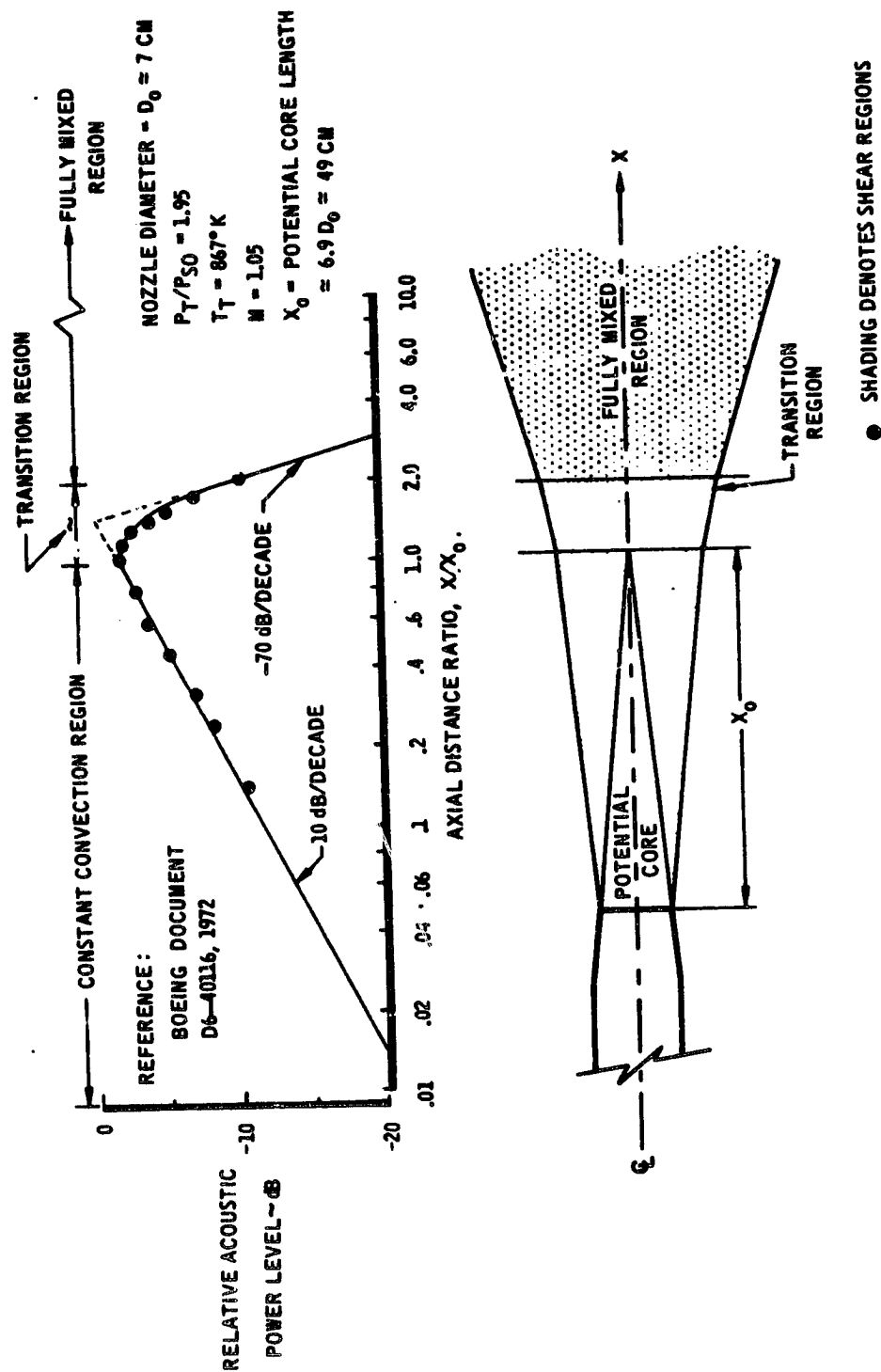


FIGURE 16.—JET OF A SINGLE NOZZLE

This math model could then be used to correct ground static noise data to a point source, and eliminate the parallax errors that occur in extrapolating the data to other positions in the acoustic field. The model could also be used to simulate flight conditions from ground static tests by accounting for the change in potential core, velocity, etc., that cause a spectrum shift with flight speed. The present SAE practice (ref. 7) gives two spectrum shape curves for flight and ground static predictions when in theory there should only be one.

In addition to the above, a better normalization of jet noise results when the acoustic power is related to the mechanical power, convection Mach number, density and temperature ratios as outlined below in equation form and illustrated in figure 17.

Total acoustic power,

$$W_A \sim W_O \left( \frac{\rho}{\rho_O} \right) \left( \frac{T_S}{T_{SO}} \right)^4 M_c^m \quad (13)$$

where the one-dimensional jet flow parameters are

$$W_O = \text{mechanical power} = \left( \frac{\dot{m}}{2g} \right) |\hat{V}_J - \hat{V}_O|^2$$

$$\frac{\rho}{\rho_O} = \text{mean density ratio}$$

$$\frac{T_S}{T_{SO}} = \text{mean static temperature ratio}$$

$$M_c = \text{mean convection Mach number} \\ \approx 0.5 |\hat{V}_J - \hat{V}_O| / C_J$$

$$m = 5 \text{ for quadrupole sources}$$

$$\hat{V}_J = \text{jet velocity vector relative to the nozzle}$$

$$\hat{V}_O = \text{nozzle velocity vector relative to ambient air}$$

$$C_J = \text{mean speed of sound in the jet}$$

$$\dot{m} = \text{mass flow} = \rho A |\hat{V}_J|$$

$$A = \text{discharge area}$$

DATA FROM FIGURE 5C OF REFERENCE 20

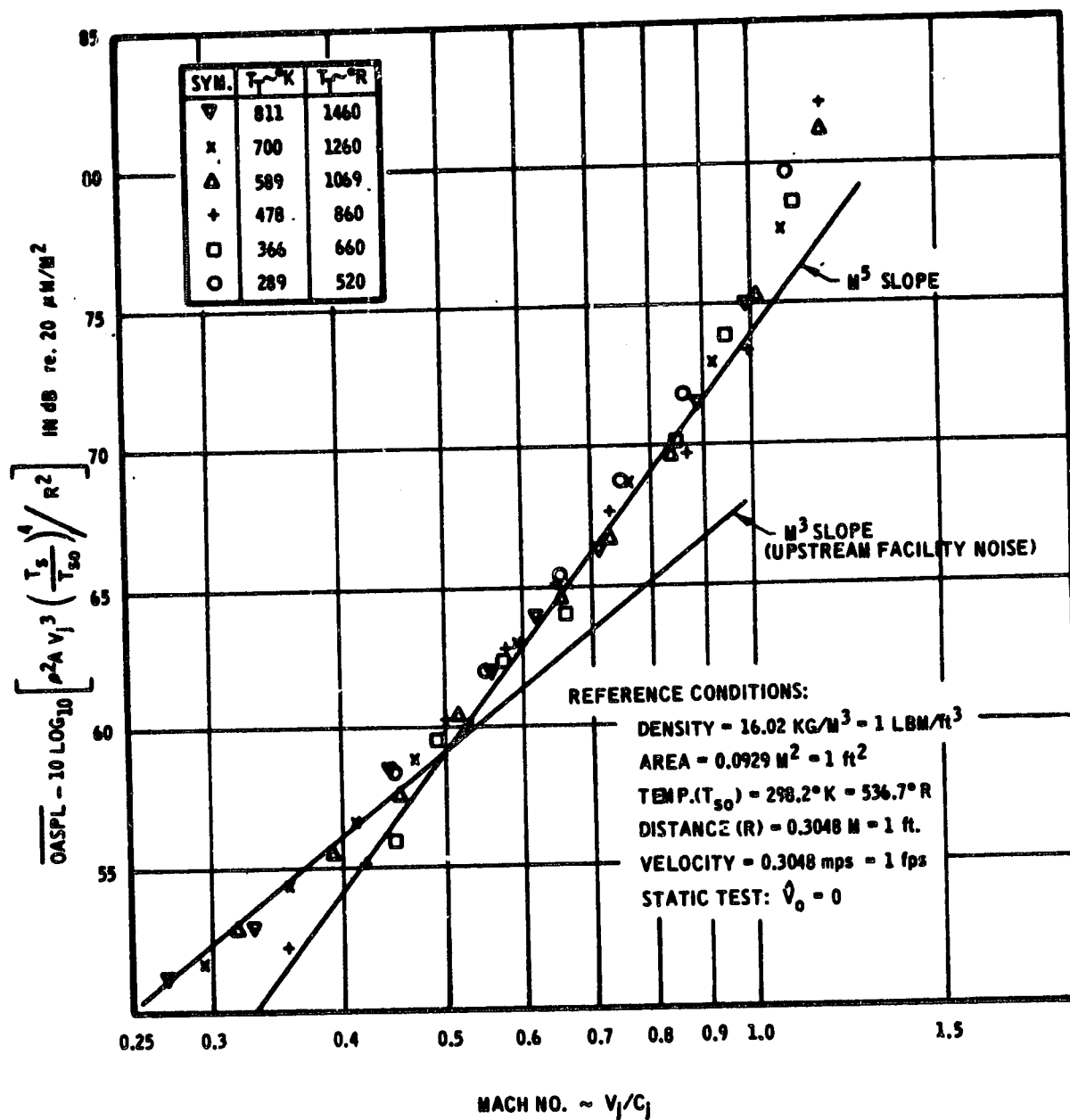


FIGURE 17.—SPACE-AVERAGED OVERALL SOUND PRESSURE LEVEL AS A FUNCTION OF MACH NUMBER

Equivalent forms of equation (13) are:

$$W_A \sim W_o \left( \frac{\rho}{\rho_o} \right) \left( \frac{T_s}{T_{so}} \right)^{1.5} \left| \frac{\hat{V}_J - \hat{V}_O}{c_o} \right|^5 \text{ OR}$$

$$\sim W_o \left( \frac{\rho c_J}{\rho_o c_o} \right) \left( \frac{T_s}{T_{so}} \right) \left| \frac{\hat{V}_J - \hat{V}_O}{c_o} \right|^5$$

The above suggestions are preliminary and further work is required prior to incorporation into the empirical procedures currently used. This should not be interpreted to imply that the methods now used are inadequate and cause gross errors; but it does suggest that they will require additional refinement to increase the range of application.

#### 5.2.2.1 Single Exhaust Nozzle

In the present procedure (ref. 20), the noise produced by the jet of a single nozzle has been correlated with relative jet velocity  $(\hat{V}_J - \hat{V}_O)$  as shown in figure 18. This curve was developed from the data given in reference 20 for a 2.54 cm diameter nozzle and was extended to match the predicted results of reference 7 for velocities greater than 760 mps (2500 fps). In formula form, the space-average, overall sound pressure level is

$$\overline{OASPL} \sim F(V_R) + 10 \log_{10} \left[ \left( \frac{\rho}{\rho_R} \right)^n \frac{A}{A_R} \right] \quad (14)$$

where

$\rho$  is the jet density and the reference density,  $\rho_R$ , is 16.02 KG/M<sup>3</sup> (1 lbm/ft<sup>3</sup>)

$A$  is the fully-expanded discharge area and the reference area,  $A_R$ , is 0.0929 M<sup>2</sup> (1 ft<sup>2</sup>)

$V_R$  is the magnitude of  $(\hat{V}_J - \hat{V}_O)$

$n$  varies with  $V_R$  as shown in figure 19

Previous definitions (ref. 7) for the overall SPL used a  $\rho^2$  normalization instead of a  $\rho^n$  term used here. The value of  $n$  was determined by "force-fitting" the formula to experimental data (ref. 20) so that the term,  $F(V_R)$ , was approximately proportional to  $V_R^8$  for velocities less than 760 mps.

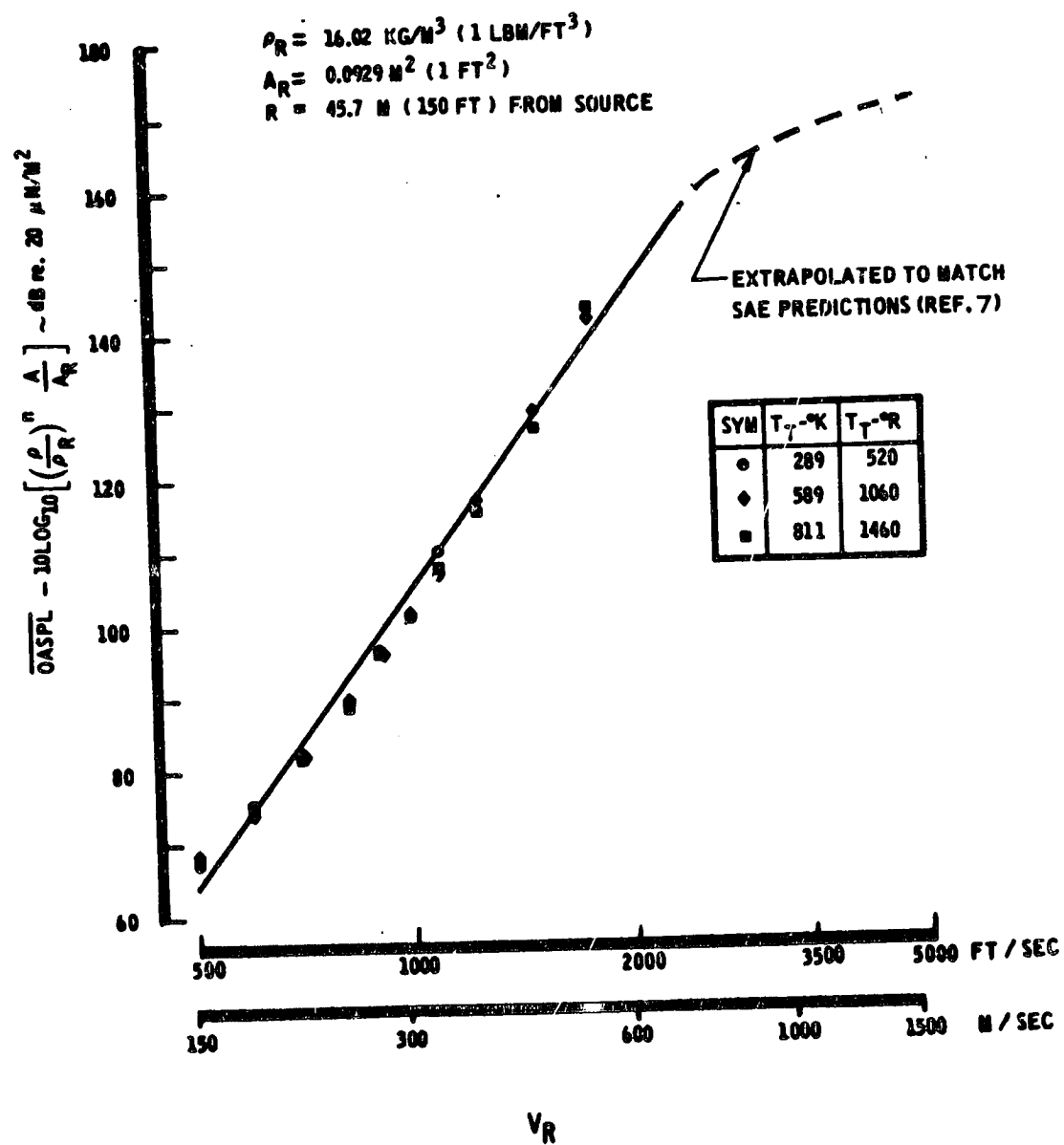


FIGURE 18.— $\overline{\text{OASPL}}$ , SPACE-AVERAGED OVERALL SOUND PRESSURE LEVEL  
 VERSUS RELATIVE JET VELOCITY

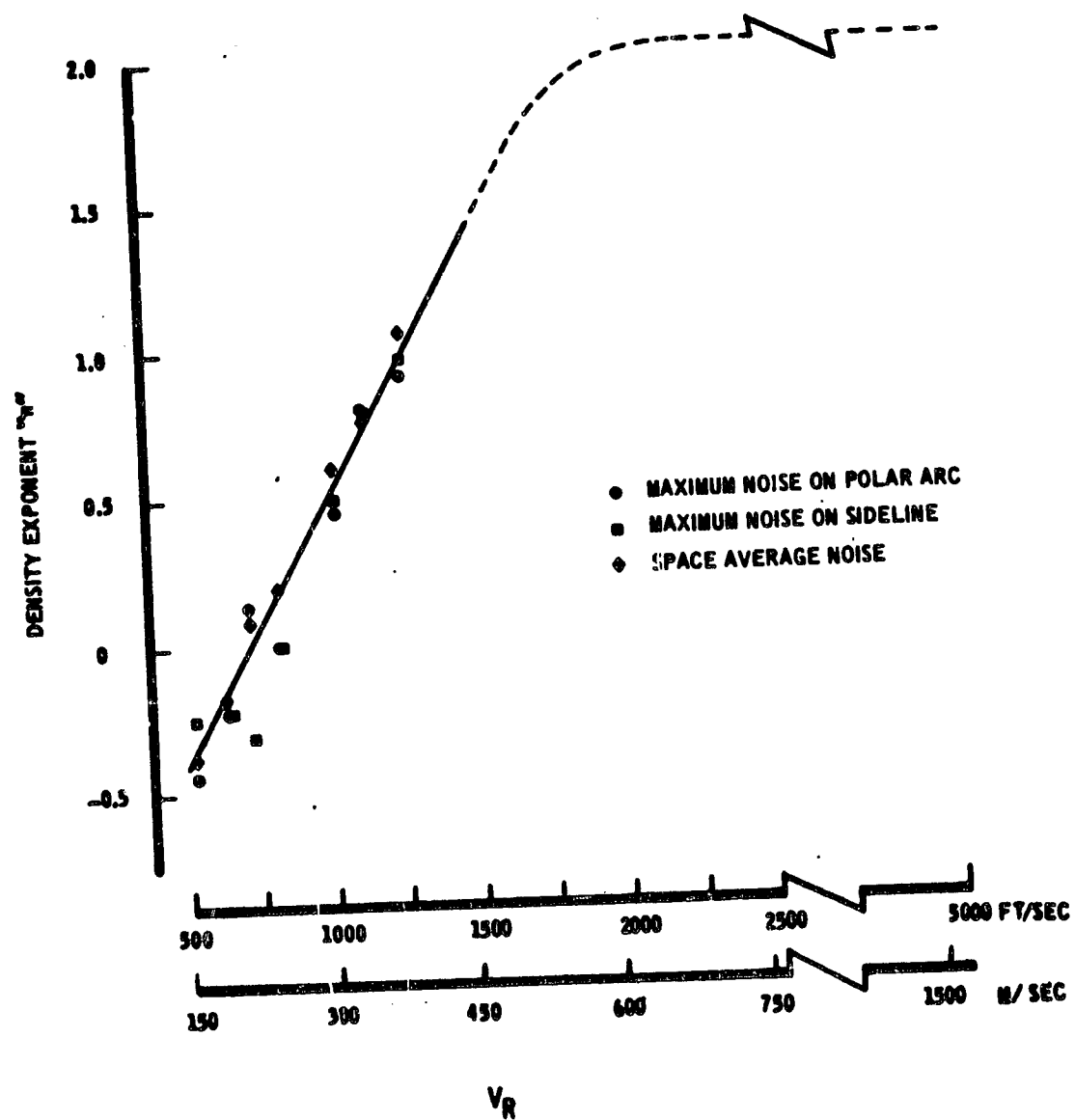


FIGURE 19.—DENSITY EXPONENT ( $n$ ) VERSUS RELATIVE JET VELOCITY

The free-field, space-average,  $\overline{\text{SPL}}$  spectrum for (1/3) octaves is determined from figure 20 as a function of Strouhal Number.

$$\overline{\text{SPL}}(f) = \overline{\text{OASPL}} + F(\text{SN}) \quad (15)$$

where

$f$  = geometric-mean frequency for a pass band

$\text{SN} = f/f_0$

$f_0$  = characteristic frequency =  $V_R/D_0$

$D_0^2 = \left(\frac{4}{\pi}\right) A$

Two spectrum shaping curves have been provided in figure 20 corresponding to the flight and ground curves given by SAE (ref. 7).

Next, the SPL spectrum at a particular directivity angle ( $\psi$ ) is obtained by interpolating from the data shown in table 5. This table was developed from data given in reference 21 and provides a correction to add to the space-average SPL for the desired spectrum.

$$\text{SPL}(f) = \overline{\text{SPL}}(f) + F(S, V_R, \psi) \quad (16)$$

where

$S$  = an effective Strouhal number to enter the table  
 $= f D_0/U_0$

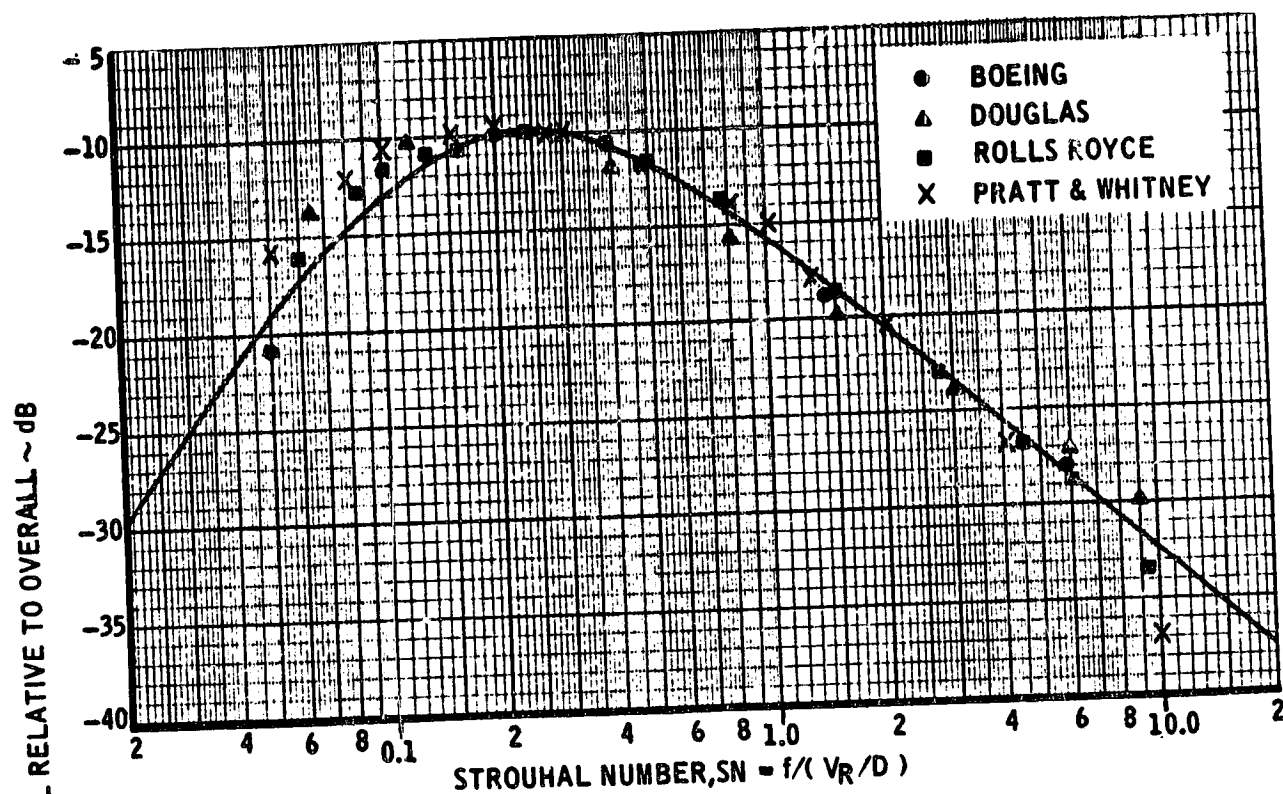
$U_0 = 304.8 \text{ m/s} = 1000 \text{ fps}$

The results from equation (16) represent the free-field levels for a single engine at 45.7 M (150 ft) from the source. The spectrum is corrected to the datum condition ( $P = 1 \text{ M}$ ) through use of table 4.

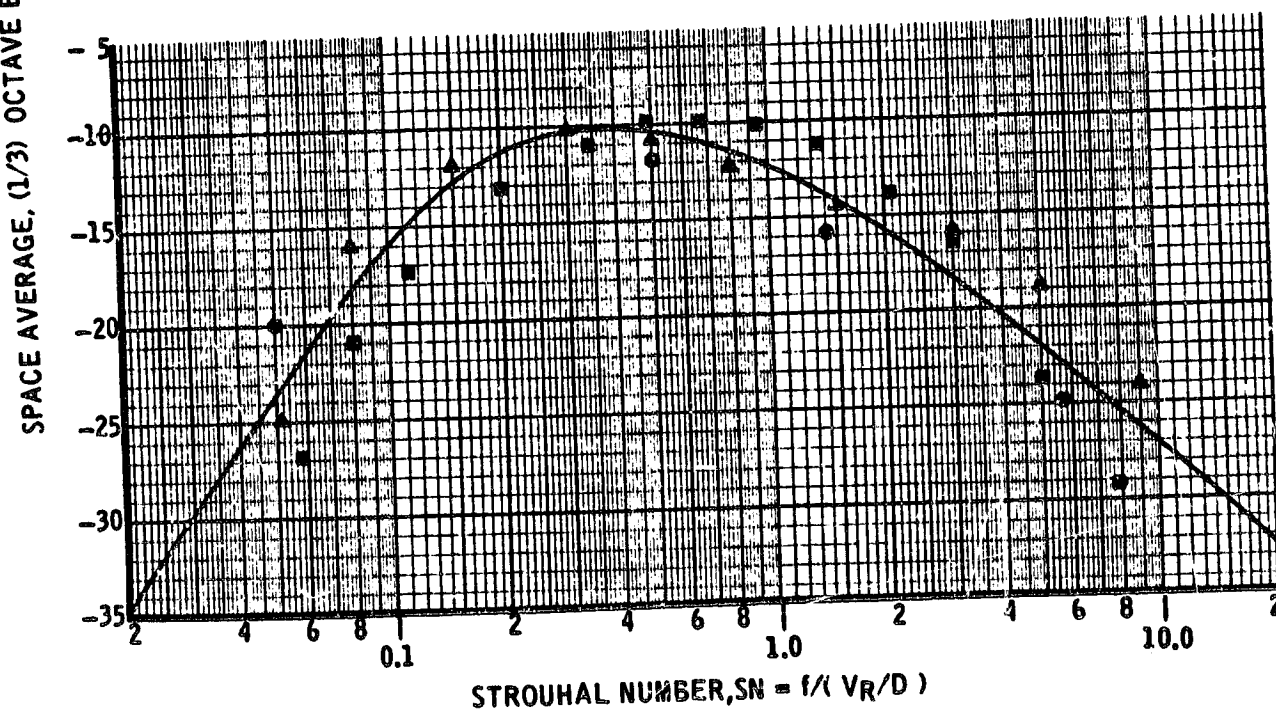
$$\left. \text{SPL}(f) \right|_{1 \text{ M}} = \left. \text{SPL}(f) \right|_{45.7 \text{ M}} + 33.2 + \Delta \text{dB}(f) \quad (17)$$

The effect of multiple engines of the same type and orientation is accomplished by adding the correction (eq. (2B), sec. 5.1.1.6) to the result given by equation (17). This completes the prediction of jet noise for a single nozzle.





a) GROUND SPECTRUM



b) FLIGHT SPECTRUM

FIGURE 20.-SAE-AIR 876 SPECTRUM SHAPES

**TABLE 5.—JET NOISE DIRECTIVITY CORRECTION IN DECIBELS**

[illegible]

$\text{SMA } 20 \div 300.5 = \text{SMA } 20.75 \div 1.52 = \text{MA } 13.65$

REFLECTIVITY ANGLE, PSI. IN DEG

EF 6.14dL	0.	10.	20.	30.	40.	50.	60.	70.	80.	90.	100.	110.	120.	130.	140.	150.	160.	170.	180.
5.1	-5.1	-5.3	-7.5	-7.8	-8.0	-7.9	-7.7	-8.5	-5.1	-4.8	-2.3	-0	.6	2.4	4.1	5.9	5.7	5.5	-18.5
5.2	-5.2	-6.4	-7.6	-8.1	-8.3	-8.2	-7.3	-5.9	-5.6	-6.2	-2.7	-1.1	.6	2.3	4.1	5.9	6.0	6.3	-18.0
5.3	-7.4	-7.5	-7.7	-8.4	-8.6	-8.2	-8.2	-7.3	-6.1	-4.6	-4.1	-1.4	.6	2.2	4.1	5.9	6.3	6.5	-13.4
5.4	-3.1	-4.0	-7.3	-7.6	-8.0	-8.3	-8.0	-7.8	-6.5	-5.1	-3.4	-1.6	.1	2.0	4.1	6.0	6.7	7.3	-12.7
5.5	-3.1	-3.6	-8.1	-8.4	-8.2	-8.3	-8.2	-8.2	-7.6	-5.5	-4.8	-1.9	-1.1	1.9	4.1	6.0	7.0	8.2	-13.8
5.6	-3.1	-3.1	-8.1	-8.9	-9.1	-9.1	-9.5	-7.6	-6.4	-4.9	-3.2	-1.3	.5	2.3	4.1	5.0	5.0	5.0	-15.0
5.7	-7.3	-3.1	-3.3	-3.8	-6.4	-8.6	-4.1	-7.1	-5.8	-4.2	-2.8	-1.7	1.2	3.8	4.0	4.1	3.0	1.8	-18.1
5.8	-7.2	-7.0	-7.4	-7.6	-8.6	-8.3	-7.6	-6.5	-5.2	-3.6	-2.0	-1.1	1.8	3.2	4.0	3.1	1.0	-1.1	-21.1
5.9	-8.1	-8.7	-7.3	-7.1	-7.7	-7.2	-8.6	-5.6	-4.5	-3.1	-1.6	.3	2.3	3.5	3.7	2.6	.5	-1.5	-21.5
6.0	-5.1	-5.0	-5.2	-5.5	-6.5	-6.2	-7.5	-4.7	-3.7	-2.7	-1.1	.6	2.9	3.7	3.3	2.0	0.0	-1.8	-17.7
6.1	-5.1	-5.0	-5.2	-5.5	-6.5	-6.2	-7.5	-4.7	-3.7	-2.7	-1.1	.6	2.9	3.6	4.0	3.0	1.5	-5.5	-22.3
6.2	-5.1	-5.0	-5.2	-5.5	-6.5	-6.2	-7.5	-4.7	-3.7	-2.7	-1.1	.6	2.9	3.5	2.7	1.5	.3	-1.6	-22.8
6.3	-5.1	-5.0	-5.2	-5.5	-6.5	-6.2	-7.5	-4.7	-3.7	-2.7	-1.1	.6	2.9	3.1	1.4	0.0	-0	-1.5	-22.2
6.4	-5.1	-5.0	-5.2	-5.5	-6.5	-6.2	-7.5	-4.7	-3.7	-2.7	-1.1	.6	2.9	3.0	.1	-1.5	-2.0	-2.0	-22.0
6.5	-5.1	-5.0	-5.2	-5.5	-6.5	-6.2	-7.5	-4.7	-3.7	-2.7	-1.1	.6	2.9	3.0	-1	-1.5	-2.0	-2.1	-22.0
6.6	-5.1	-5.0	-5.2	-5.5	-6.5	-6.2	-7.5	-4.7	-3.7	-2.7	-1.1	.6	2.9	3.0	.5	-1.5	-2.0	-1.3	-22.0
6.7	-5.1	-5.0	-5.2	-5.5	-6.5	-6.2	-7.5	-4.7	-3.7	-2.7	-1.1	.6	2.9	3.0	.5	-1.5	-2.0	-2.3	-22.0
6.8	-5.1	-5.0	-5.2	-5.5	-6.5	-6.2	-7.5	-4.7	-3.7	-2.7	-1.1	.6	2.9	3.3	.3	-1.1	-1.7	-0	-21.7
6.9	-5.1	-5.0	-5.2	-5.5	-6.5	-6.2	-7.5	-4.7	-3.7	-2.7	-1.1	.6	2.9	3.7	1.1	-0	-1.3	-7	-21.3
7.0	-5.1	-5.0	-5.2	-5.5	-6.5	-6.2	-7.5	-4.7	-3.7	-2.7	-1.1	.6	2.9	3.0	1.9	-4	-1.0	-5	-21.0
7.1	-5.1	-5.0	-5.2	-5.5	-6.5	-6.2	-7.5	-4.7	-3.7	-2.7	-1.1	.6	2.9	2.7	.6	-1.6	-2.2	-2.0	-22.1
7.2	-5.1	-5.0	-5.2	-5.5	-6.5	-6.2	-7.5	-4.7	-3.7	-2.7	-1.1	.6	2.9	2.4	1.3	-0	-2.7	-3.5	-23.6
7.3	-5.1	-5.0	-5.2	-5.5	-6.5	-6.2	-7.5	-4.7	-3.7	-2.7	-1.1	.6	2.9	2.0	0.0	-3.9	-4.6	-5.0	-25.9
7.4	-5.1	-5.0	-5.2	-5.5	-6.5	-6.2	-7.5	-4.7	-3.7	-2.7	-1.1	.6	2.9	1.6	-1.3	-5.1	-5.8	-6.5	-27.2
7.5	-5.1	-5.0	-5.2	-5.5	-6.5	-6.2	-7.5	-4.7	-3.7	-2.7	-1.1	.6	2.9	1.3	-2.1	-5.8	-6.5	-7.2	-27.2

IMMEDIATELY ANGLE, P&L, IN DEG.

RELATIVE JET VELOCITY,  $v_0 = 5.55 \pm 0.2$  M/S =  $1.00 \pm 0.3$  FPS

**TABLE 5.—Continued**

EFFECTIVE STANDARD		DIRECTIONAL ANGLE, PS IN DEG.																		
STANDARD		0.	10.	20.	30.	40.	50.	60.	70.	80.	90.	100.	110.	120.	130.	140.	150.	160.	170.	180.
1.00E-01	1.00E-01	-15.5	-16.2	-15.9	-15.6	-15.2	-14.3	-14.3	-13.5	-12.6	-11.3	-9.7	-7.9	-4.3	-2	5.1	7.3	7.2	7.1	-13.0
1.00E-01	1.00E-01	-16.5	-16.3	-15.1	-15.8	-15.4	-14.5	-14.3	-13.5	-12.5	-11.2	-9.5	-7.5	-4.0	2	5.4	7.6	7.2	6.8	-13.2
1.00E-01	1.00E-01	-16.5	-16.4	-16.3	-15.0	-15.0	-13.9	-13.5	-12.4	-11.1	-9.1	-7.1	-5.1	-3.7	6	5.7	7.9	7.2	6.5	-13.5
1.00E-01	1.00E-01	-16.5	-16.4	-16.3	-15.0	-15.0	-13.9	-13.5	-12.4	-11.1	-9.1	-7.1	-5.1	-3.7	6	5.7	7.9	7.2	6.5	-13.5
2.00E-01	2.00E-01	-15.4	-16.5	-16.4	-16.2	-15.6	-15.7	-14.4	-13.5	-12.4	-10.9	-9.1	-6.8	-3.3	1.1	6.1	8.1	7.2	6.2	-13.0
2.00E-01	2.00E-01	-15.7	-16.0	-16.0	-15.4	-15.4	-14.4	-13.4	-12.4	-11.4	-9.4	-7.4	-5.4	-3.0	1.5	6.4	8.4	7.2	6.1	-14.0
2.00E-01	2.00E-01	-15.7	-15.2	-15.2	-14.9	-14.5	-13.9	-13.0	-12.1	-10.9	-9.4	-7.5	-5.0	-1.5	2.5	6.1	7.2	6.1	5.1	-14.0
4.00E-01	4.00E-01	-15.3	-15.0	-14.7	-13.5	-13.1	-12.4	-11.7	-10.7	-9.6	-8.1	-6.1	-3.5	0	3.5	5.7	6.0	4.9	3.0	-16.2
5.00E-01	5.00E-01	-12.7	-12.4	-12.3	-12.0	-11.6	-11.3	-10.3	-9.3	-8.2	-6.7	-4.7	-2.1	1.5	4.5	5.4	4.0	3.0	2.8	-17.2
6.00E-01	6.00E-01	-11.3	-11.8	-11.7	-11.0	-11.1	-10.4	-9.7	-8.7	-7.5	-6.0	-4.0	-1.5	1.9	4.5	5.2	4.4	2.5	0.9	-19.2
8.00E-01	8.00E-01	-11.3	-11.3	-11.1	-10.9	-11.5	-9.3	-8.3	-6.8	-5.2	-3.2	-0.5	2.4	4.5	5.0	3.9	1.4	1.4	-1.1	-21.1
1.00E-01	1.00E-01	-11.5	-10.5	-10.5	-10.4	-10.6	-9.3	-8.4	-7.4	-6.1	-4.5	-2.5	0.3	2.8	4.5	4.0	3.5	0.2	-1.1	-23.1
1.00E-01	1.00E-01	-11.5	-10.5	-10.5	-10.4	-10.6	-9.3	-8.4	-7.4	-6.1	-4.5	-2.5	0.3	2.8	4.5	4.0	3.5	0.2	-1.1	-23.1
1.00E-01	1.00E-01	-11.5	-10.5	-10.5	-10.4	-10.6	-9.3	-8.4	-7.4	-6.1	-4.5	-2.5	0.3	2.8	4.5	4.0	3.5	0.2	-1.1	-23.1
1.00E-01	1.00E-01	-11.5	-10.5	-10.5	-10.4	-10.6	-9.3	-8.4	-7.4	-6.1	-4.5	-2.5	0.3	2.8	4.5	4.0	3.5	0.2	-1.1	-23.1
1.00E-01	1.00E-01	-11.5	-10.5	-10.5	-10.4	-10.6	-9.3	-8.4	-7.4	-6.1	-4.5	-2.5	0.3	2.8	4.5	4.0	3.5	0.2	-1.1	-23.1
1.00E-01	1.00E-01	-11.5	-10.5	-10.5	-10.4	-10.6	-9.3	-8.4	-7.4	-6.1	-4.5	-2.5	0.3	2.8	4.5	4.0	3.5	0.2	-1.1	-23.1
1.00E-01	1.00E-01	-11.5	-10.5	-10.5	-10.4	-10.6	-9.3	-8.4	-7.4	-6.1	-4.5	-2.5	0.3	2.8	4.5	4.0	3.5	0.2	-1.1	-23.1
1.00E-01	1.00E-01	-11.5	-10.5	-10.5	-10.4	-10.6	-9.3	-8.4	-7.4	-6.1	-4.5	-2.5	0.3	2.8	4.5	4.0	3.5	0.2	-1.1	-23.1
1.00E-01	1.00E-01	-11.5	-10.5	-10.5	-10.4	-10.6	-9.3	-8.4	-7.4	-6.1	-4.5	-2.5	0.3	2.8	4.5	4.0	3.5	0.2	-1.1	-23.1
1.00E-01	1.00E-01	-11.5	-10.5	-10.5	-10.4	-10.6	-9.3	-8.4	-7.4	-6.1	-4.5	-2.5	0.3	2.8	4.5	4.0	3.5	0.2	-1.1	-23.1
1.00E-01	1.00E-01	-11.5	-10.5	-10.5	-10.4	-10.6	-9.3	-8.4	-7.4	-6.1	-4.5	-2.5	0.3	2.8	4.5	4.0	3.5	0.2	-1.1	-23.1
1.00E-01	1.00E-01	-11.5	-10.5	-10.5	-10.4	-10.6	-9.3	-8.4	-7.4	-6.1	-4.5	-2.5	0.3	2.8	4.5	4.0	3.5	0.2	-1.1	-23.1
1.00E-01	1.00E-01	-11.5	-10.5	-10.5	-10.4	-10.6	-9.3	-8.4	-7.4	-6.1	-4.5	-2.5	0.3	2.8	4.5	4.0	3.5	0.2	-1.1	-23.1
1.00E-01	1.00E-01	-11.5	-10.5	-10.5	-10.4	-10.6	-9.3	-8.4	-7.4	-6.1	-4.5	-2.5	0.3	2.8	4.5	4.0	3.5	0.2	-1.1	-23.1
1.00E-01	1.00E-01	-11.5	-10.5	-10.5	-10.4	-10.6	-9.3	-8.4	-7.4	-6.1	-4.5	-2.5	0.3	2.8	4.5	4.0	3.5	0.2	-1.1	-23.1
1.00E-01	1.00E-01	-11.5	-10.5	-10.5	-10.4	-10.6	-9.3	-8.4	-7.4	-6.1	-4.5	-2.5	0.3	2.8	4.5	4.0	3.5	0.2	-1.1	-23.1
1.00E-01	1.00E-01	-11.5	-10.5	-10.5	-10.4	-10.6	-9.3	-8.4	-7.4	-6.1	-4.5	-2.5	0.3	2.8	4.5	4.0	3.5	0.2	-1.1	-23.1
1.00E-01	1.00E-01	-11.5	-10.5	-10.5	-10.4	-10.6	-9.3	-8.4	-7.4	-6.1	-4.5	-2.5	0.3	2.8	4.5	4.0	3.5	0.2	-1.1	-23.1
1.00E-01	1.00E-01	-11.5	-10.5	-10.5	-10.4	-10.6	-9.3	-8.4	-7.4	-6.1	-4.5	-2.5	0.3	2.8	4.5	4.0	3.5	0.2	-1.1	-23.1
1.00E-01	1.00E-01	-11.5	-10.5	-10.5	-10.4	-10.6	-9.3	-8.4	-7.4	-6.1	-4.5	-2.5	0.3	2.8	4.5	4.0	3.5	0.2	-1.1	-23.1
1.00E-01	1.00E-01	-11.5	-10.5	-10.5	-10.4	-10.6	-9.3	-8.4	-7.4	-6.1	-4.5	-2.5	0.3	2.8	4.5	4.0	3.5	0.2	-1.1	-23.1
1.00E-01	1.00E-01	-11.5	-10.5	-10.5	-10.4	-10.6	-9.3	-8.4	-7.4	-6.1	-4.5	-2.5	0.3	2.8	4.5	4.0	3.5	0.2	-1.1	-23.1
1.00E-01	1.00E-01	-11.5	-10.5	-10.5	-10.4	-10.6	-9.3	-8.4	-7.4	-6.1	-4.5	-2.5	0.3	2.8	4.5	4.0	3.5	0.2	-1.1	-23.1
1.00E-01	1.00E-01	-11.5	-10.5	-10.5	-10.4	-10.6	-9.3	-8.4	-7.4	-6.1	-4.5	-2.5	0.3	2.8	4.5	4.0	3.5	0.2	-1.1	-23.1
1.00E-01	1.00E-01	-11.5	-10.5	-10.5	-10.4	-10.6	-9.3	-8.4	-7.4	-6.1	-4.5	-2.5	0.3	2.8	4.5	4.0	3.5	0.2	-1.1	-23.1
1.00E-01	1.00E-01	-11.5	-10.5	-10.5	-10.4	-10.6	-9.3	-8.4	-7.4	-6.1	-4.5	-2.5	0.3	2.8	4.5	4.0	3.5	0.2	-1.1	-23.1
1.00E-01	1.00E-01	-11.5	-10.5	-10.5	-10.4	-10.6	-9.3	-8.4	-7.4	-6.1	-4.5	-2.5	0.3	2.8	4.5	4.0	3.5	0.2	-1.1	-23.1
1.00E-01	1.00E-01	-11.5	-10.5	-10.5	-10.4	-10.6	-9.3	-8.4	-7.4	-6.1	-4.5	-2.5	0.3	2.8	4.5	4.0	3.5	0.2	-1.1	-23.1
1.00E-01	1.00E-01	-11.5	-10.5	-10.5	-10.4	-10.6	-9.3	-8.4	-7.4	-6.1	-4.5	-2.5	0.3	2.8	4.5	4.0	3.5	0.2	-1.1	-23.1
1.00E-01	1.00E-01	-11.5	-10.5	-10.5	-10.4	-10.6	-9.3	-8.4	-7.4	-6.1	-4.5	-2.5	0.3	2.8	4.5	4.0	3.5	0.2	-1.1	-23.1
1.00E-01	1.00E-01	-11.5	-10.5	-10.5	-10.4	-10.6	-9.3	-8.4	-7.4	-6.1	-4.5	-2.5	0.3	2.8	4.5	4.0	3.5	0.2	-1.1	-23.1
1.00E-01	1.00E-01	-11.5	-10.5	-10.5	-10.4	-10.6	-9.3	-8.4	-7.4	-6.1	-4.5	-2.5	0.3	2.8	4.5	4.0	3.5	0.2	-1.1	-23.1
1.00E-01	1.00E-01	-11.5	-10.5	-10.5	-10.4	-10.6	-9.3	-8.4	-7.4	-6.1	-4.5	-2.5	0.3	2.8	4.5	4.0	3.5	0.2	-1.1	-23.1
1.00E-01	1.00E-01	-11.5	-10.5	-10.5	-10.4	-10.6	-9.3	-8.4	-7.4	-6.1	-4.5	-2.5	0.3	2.8	4.5	4.0	3.5	0.2	-1.1	-23.1
1.00E-01	1.00E-01	-11.5	-10.5	-10.5	-10.4	-10.6	-9.3	-8.4	-7.4	-6.1	-4.5	-2.5	0.3	2.8	4.5	4.0	3.5	0.2	-1.1	-23.1
1.00E-01	1.00E-01	-11.5	-10.5	-10.5	-10.4	-10.6	-9.3	-8.4	-7.4	-6.1	-4.5	-2.5	0.3	2.8	4.5	4.0	3.5	0.2	-1.1	-23.1
1.00E-01	1.00E-01	-11.5	-10.5	-10.5	-10.4	-10.6	-9.3	-8.4	-7.4	-6.1	-4.5	-2.5	0.3	2.8	4.5	4.0	3.5	0.2	-1.1	-23.1
1.00E-01	1.00E-01	-11.5	-10.5	-10.5	-10.4	-10.6	-9.3	-8.4	-7.4	-6.1	-4.5	-2.5	0.3	2.8	4.5	4.0	3.5	0.2	-1.1	-23.1
1.00E-01	1.00E-01	-11.5	-10.5	-10.5	-10.4	-10.6	-9.3	-8.4	-7.4	-6.1	-4.5	-2.5	0.3	2.8	4.5	4.0	3.5	0.2	-1.1	-23.1
1.00E-01	1.00E-01	-11.5	-10.5	-10.5	-10.4	-10.6	-9.3	-8.4	-7.4	-6.1	-4.5	-2.5	0.3	2.8	4.5	4.0	3.5	0.2	-1.1	-23.1
1.00E-01	1.00E-01	-11.5	-10.5	-10.5	-10.4	-10.6	-9.3	-8.4	-7.4	-6.1	-4.5	-2.5	0.3	2.8	4.5	4.0	3.5	0.2	-1.1	-23.1
1.00E-01	1.00E-01	-11.5	-10.5	-10.5	-10.4	-10.6	-9.3	-8.4	-7.4	-6.1	-4.5	-2.5	0.3	2.8	4.5	4.0	3.5	0.2	-1.1	-23.1
1.00E-01	1.00E-01	-11.5	-10.5	-10.5	-10.4	-10.6	-9.3	-8.4	-7.4	-6.1	-4.5	-2.5	0.3	2.8	4.5	4.0	3.5	0.2	-1.1	-23.1
1.00E-01	1.00E-01	-11.5	-10.5	-10.5	-10.4	-10.6	-9.3	-8.4	-7.4	-6.1	-4.5	-2.5	0.3	2.8	4.5	4.0	3.5	0.2	-1.1	-23.1
1.00E-01	1.00E-01	-11.5	-10.5	-10.5	-10.4	-10.6	-9.3	-8.4	-7.4	-6.1	-4.5	-2.5	0.3	2.8	4.5	4.0	3.5	0.2	-1.1	-23.1
1.00E-01	1.00E-01	-11.5	-10.5	-10.5	-10.4	-10.6	-9.3	-8.4	-7.4	-6.1	-4.5	-2.5	0.3	2.8	4.5	4.0	3.5	0.2	-1.1	-23.1
1.00E-01	1.00E-01	-11.5	-10.5	-10.5	-10.4	-10.6	-9.3	-8.4	-7.4	-6.1	-4.5	-2.5	0.3	2.8	4.5	4.0	3.5	0.2	-1.1	-23.1
1.00E-01	1.00E-01	-11.5	-10.5	-10.5	-10.4	-10.6	-9.3	-8.4	-7.4	-6.1	-4.5	-2.5	0.3	2.8	4.5	4.0	3.5	0.2	-1.1	-23.1
1.00E-01	1.00E-01	-11.5	-10.5	-10.5	-10.4	-10.6	-9.3	-8.4	-7.4	-6.1	-4.5	-2.5	0.3	2.8	4.5	4.0	3.5	0.2	-1.1	-23.1
1.00E-01	1.00E-01	-11.5	-10.5	-10.5	-10.4	-10.6	-9.3	-8.4	-7.4	-6.1	-4.5	-2.5	0.3	2.8	4.5	4.0	3.5	0.2	-1.1	-23.1
1.00E-01	1.00E-01	-11.5	-10.5	-10.5	-10.4	-10.6	-9.3	-8.4	-7.4	-6.1	-4.5	-2.5	0.3	2.8	4.5	4.0	3.5	0.2	-1.1	-23.1
1.00E-01	1.00E-01	-11.5	-10.5	-10.5	-10.4	-10.6	-9.3	-8.4	-7.4	-6.1	-4.5	-2.5	0.3	2.8	4.5	4.0	3.5	0.2	-1.1	-23.1
1.00E-01	1.00E-01	-11.5	-10.5	-10.5	-10.4	-10.6	-9.3	-8.4	-7.4	-6.1	-4.5	-2.5	0.3	2.8	4.5	4.0	3.5	0.2	-1.1	-23.1
1.00E-01	1.00E-01	-11.5	-10.5	-10.5	-10.4	-10.6	-9.3	-8.4	-7.4	-6.1	-4.5	-2.5	0.3							

RELATIVE JET VELOCITY,  $V_4 = 3.61E+02$  M/S =  $1.25E+03$  FPS

DIFFRACTIVITY ANGLE, PSI, IN DEG-

RELATIVE JET EFFICIENCY,  $\eta_{\text{jet}}$  =  $0.57 \pm 0.02$  M+S =  $0.50 \pm 0.03$  PFS

TIME JET VELOCITY, V<sub>J</sub> = 3.30 ± 0.02 M<sub>S</sub> = 1.75E+03 FPS

# TARI E 5.—Continued

EFFECTIVE STATIONAL NUMBER		DIRECTIONALITY ANGLE, PSALAN DEG																		
		5.	10.	20.	30.	40.	50.	60.	70.	80.	90.	100.	110.	120.	130.	140.	150.	160.	170.	180.
1.00	-1	-19.7	-10.7	-18.7	-18.7	-16.7	-18.4	-17.7	-16.8	-15.4	-13.9	-12.1	-9.5	-6.3	1.1	5.7	8.2	7.0	5.8	-14.3
	1	-19.3	-19.0	-19.0	-19.0	-18.0	-18.1	-17.2	-15.6	-14.1	-12.1	-9.1	-6.0	1.5	6.0	8.0	8.0	6.0	4.0	-18.0
	1	-13.3	-19.3	-19.3	-19.3	-13.2	-18.5	-17.6	-16.2	-14.4	-12.1	-8.7	-3.7	1.9	6.3	7.8	5.0	2.4	17.6	
2.00	-1	-19.7	-19.7	-19.7	-19.7	-15.7	-19.5	-19.0	-18.1	-16.7	-14.6	-12.0	-8.4	-4.3	2.2	6.7	7.7	4.0	1.4	-19.7
	1	-20.1	-21.0	-21.0	-21.0	-20.4	-19.9	-19.3	-18.5	-17.1	-15.1	-12.0	-8.0	-3.9	2.9	7.0	7.5	3.0	1.6	-21.6
	1	-19.2	-19.2	-19.2	-19.2	-19.2	-19.1	-18.7	-18.0	-16.7	-14.6	-11.7	-9.7	-2.5	3.4	7.3	7.3	3.7	1.3	-19.7
3.00	-1	-19.3	-19.3	-19.3	-19.3	-18.3	-18.3	-18.1	-17.5	-16.4	-14.0	-11.3	-7.3	-2.0	4.2	7.7	7.2	4.3	1.4	-18.6
	1	-17.5	-17.5	-17.5	-17.5	-17.4	-17.4	-17.0	-16.0	-13.5	-11.0	-7.0	-1.5	5.0	8.0	7.0	5.0	2.9	2.9	-17.1
	1	-19.3	-19.3	-19.3	-19.3	-15.0	-15.0	-14.3	-14.7	-13.5	-12.0	-10.0	-6.5	-1.3	5.0	7.7	6.7	3.7	1.4	-19.6
4.00	-1	-17.5	-17.5	-17.5	-17.5	-12.5	-12.5	-12.3	-11.9	-10.5	-9.0	-6.0	-3.0	-1.2	5.0	7.3	6.3	2.3	1.6	-21.6
	1	-17.1	-17.1	-17.1	-17.1	-10.0	-10.0	-10.0	-9.8	-9.0	-8.0	-7.1	-5.9	-3.5	1.0	7.0	7.8	6.3	1.0	-23.8
	1	-17.2	-17.2	-17.2	-17.2	-9.4	-9.4	-9.8	-8.5	-8.0	-7.1	-5.9	-3.5	1.0	5.0	6.3	5.0	1.0	1.0	-26.6
5.00	-1	-17.1	-17.1	-17.1	-17.1	-8.6	-8.6	-7.5	-6.9	-6.2	-5.1	-3.9	-1.8	1.7	5.0	5.7	4.0	2.3	1.0	-28.8
	1	-17.1	-17.1	-17.1	-17.1	-8.2	-8.2	-7.3	-6.3	-5.4	-4.2	-3.0	-1.8	1.1	3.0	5.0	5.0	3.0	1.0	-31.2
	1	-11.3	-11.0	-10.3	-9.5	-8.6	-7.0	-6.6	-5.6	-4.5	-3.1	-1.5	1.5	3.2	5.0	5.0	2.0	1.0	1.0	-30.9
6.00	-1	-17.1	-17.1	-17.1	-17.1	-8.9	-8.9	-8.8	-8.7	-8.5	-8.1	-7.3	-6.0	3.3	5.0	5.0	2.5	1.0	1.0	-31.3
	1	-17.1	-17.1	-17.1	-17.1	-9.3	-8.3	-7.1	-5.9	-4.6	-3.0	-1.0	1.2	3.5	5.0	5.0	2.3	1.0	1.0	-31.5
	1	-10.3	-9.7	-9.5	-9.3	-8.4	-7.0	-6.6	-5.6	-4.4	-2.7	-1.7	1.6	3.7	5.0	4.7	2.0	1.0	1.0	-34.5
7.00	-1	-17.1	-17.1	-17.1	-17.1	-7.5	-6.9	-6.1	-5.3	-4.2	-2.5	-1.3	1.1	3.8	5.0	4.3	1.8	1.0	1.0	-37.8
	1	-17.1	-17.1	-17.1	-17.1	-6.6	-6.2	-5.6	-5.0	-4.0	-2.0	0.0	2.5	4.0	5.0	4.0	1.5	1.0	1.0	-41.6
	1	-17.1	-17.1	-17.1	-17.1	-6.6	-6.1	-5.5	-4.7	-3.6	-1.7	1.3	2.9	4.3	5.0	4.2	1.7	1.0	1.0	-48.1
8.00	-1	-17.1	-17.1	-17.1	-17.1	-6.6	-6.1	-5.3	-4.4	-3.2	-1.3	1.7	3.4	4.5	5.0	4.3	1.8	1.0	1.0	-48.7
	1	-17.1	-17.1	-17.1	-17.1	-6.6	-6.1	-5.3	-4.4	-3.2	-1.3	1.7	3.4	4.5	5.0	4.3	1.8	1.0	1.0	-48.7
	1	-17.1	-17.1	-17.1	-17.1	-6.6	-6.1	-5.3	-4.4	-3.2	-1.3	1.7	3.4	4.5	5.0	4.3	1.8	1.0	1.0	-48.7
9.00	-1	-17.1	-17.1	-17.1	-17.1	-6.6	-6.1	-5.3	-4.4	-3.2	-1.3	1.7	3.4	4.5	5.0	4.3	1.8	1.0	1.0	-48.7
	1	-17.1	-17.1	-17.1	-17.1	-6.6	-6.1	-5.3	-4.4	-3.2	-1.3	1.7	3.4	4.5	5.0	4.3	1.8	1.0	1.0	-48.7
	1	-17.1	-17.1	-17.1	-17.1	-6.6	-6.1	-5.3	-4.4	-3.2	-1.3	1.7	3.4	4.5	5.0	4.3	1.8	1.0	1.0	-48.7
10.00	-1	-17.1	-17.1	-17.1	-17.1	-6.6	-6.1	-5.3	-4.4	-3.2	-1.3	1.7	3.4	4.5	5.0	4.3	1.8	1.0	1.0	-48.7
	1	-17.1	-17.1	-17.1	-17.1	-6.6	-6.1	-5.3	-4.4	-3.2	-1.3	1.7	3.4	4.5	5.0	4.3	1.8	1.0	1.0	-48.7
	1	-17.1	-17.1	-17.1	-17.1	-6.6	-6.1	-5.3	-4.4	-3.2	-1.3	1.7	3.4	4.5	5.0	4.3	1.8	1.0	1.0	-48.7

RELATIVE JET VELOCITY, VR = 5.10E+12 M/S = 2.00E+03 FPS



**TABLE 5.—Concluded**

EFFECTIVE SPECTRUM		DIRECTIONALITY ANGLE, ES. IN DEG																	
U.	10.	20.	30.	40.	50.	60.	70.	80.	90.	100.	110.	120.	130.	140.	150.	160.	170.	180.	
1.0000-01	19.3	19.4	19.5	19.7	19.8	19.9	20.0	20.1	20.2	20.3	20.4	20.5	20.6	20.7	20.8	20.9	21.0	21.1	
1.0000-02	19.3	19.4	19.5	19.7	19.8	19.9	20.0	20.1	20.2	20.3	20.4	20.5	20.6	20.7	20.8	20.9	21.0	21.1	
1.0000-03	19.3	19.4	19.5	19.7	19.8	19.9	20.0	20.1	20.2	20.3	20.4	20.5	20.6	20.7	20.8	20.9	21.0	21.1	
1.0000-04	19.3	19.4	19.5	19.7	19.8	19.9	20.0	20.1	20.2	20.3	20.4	20.5	20.6	20.7	20.8	20.9	21.0	21.1	
1.0000-05	19.3	19.4	19.5	19.7	19.8	19.9	20.0	20.1	20.2	20.3	20.4	20.5	20.6	20.7	20.8	20.9	21.0	21.1	
1.0000-06	19.3	19.4	19.5	19.7	19.8	19.9	20.0	20.1	20.2	20.3	20.4	20.5	20.6	20.7	20.8	20.9	21.0	21.1	
1.0000-07	19.3	19.4	19.5	19.7	19.8	19.9	20.0	20.1	20.2	20.3	20.4	20.5	20.6	20.7	20.8	20.9	21.0	21.1	
1.0000-08	19.3	19.4	19.5	19.7	19.8	19.9	20.0	20.1	20.2	20.3	20.4	20.5	20.6	20.7	20.8	20.9	21.0	21.1	
1.0000-09	19.3	19.4	19.5	19.7	19.8	19.9	20.0	20.1	20.2	20.3	20.4	20.5	20.6	20.7	20.8	20.9	21.0	21.1	
1.0000-10	19.3	19.4	19.5	19.7	19.8	19.9	20.0	20.1	20.2	20.3	20.4	20.5	20.6	20.7	20.8	20.9	21.0	21.1	
1.0000-11	19.3	19.4	19.5	19.7	19.8	19.9	20.0	20.1	20.2	20.3	20.4	20.5	20.6	20.7	20.8	20.9	21.0	21.1	
1.0000-12	19.3	19.4	19.5	19.7	19.8	19.9	20.0	20.1	20.2	20.3	20.4	20.5	20.6	20.7	20.8	20.9	21.0	21.1	
1.0000-13	19.3	19.4	19.5	19.7	19.8	19.9	20.0	20.1	20.2	20.3	20.4	20.5	20.6	20.7	20.8	20.9	21.0	21.1	
1.0000-14	19.3	19.4	19.5	19.7	19.8	19.9	20.0	20.1	20.2	20.3	20.4	20.5	20.6	20.7	20.8	20.9	21.0	21.1	
1.0000-15	19.3	19.4	19.5	19.7	19.8	19.9	20.0	20.1	20.2	20.3	20.4	20.5	20.6	20.7	20.8	20.9	21.0	21.1	
1.0000-16	19.3	19.4	19.5	19.7	19.8	19.9	20.0	20.1	20.2	20.3	20.4	20.5	20.6	20.7	20.8	20.9	21.0	21.1	
1.0000-17	19.3	19.4	19.5	19.7	19.8	19.9	20.0	20.1	20.2	20.3	20.4	20.5	20.6	20.7	20.8	20.9	21.0	21.1	
1.0000-18	19.3	19.4	19.5	19.7	19.8	19.9	20.0	20.1	20.2	20.3	20.4	20.5	20.6	20.7	20.8	20.9	21.0	21.1	
1.0000-19	19.3	19.4	19.5	19.7	19.8	19.9	20.0	20.1	20.2	20.3	20.4	20.5	20.6	20.7	20.8	20.9	21.0	21.1	
1.0000-20	19.3	19.4	19.5	19.7	19.8	19.9	20.0	20.1	20.2	20.3	20.4	20.5	20.6	20.7	20.8	20.9	21.0	21.1	
1.0000-21	19.3	19.4	19.5	19.7	19.8	19.9	20.0	20.1	20.2	20.3	20.4	20.5	20.6	20.7	20.8	20.9	21.0	21.1	
1.0000-22	19.3	19.4	19.5	19.7	19.8	19.9	20.0	20.1	20.2	20.3	20.4	20.5	20.6	20.7	20.8	20.9	21.0	21.1	
1.0000-23	19.3	19.4	19.5	19.7	19.8	19.9	20.0	20.1	20.2	20.3	20.4	20.5	20.6	20.7	20.8	20.9	21.0	21.1	
1.0000-24	19.3	19.4	19.5	19.7	19.8	19.9	20.0	20.1	20.2	20.3	20.4	20.5	20.6	20.7	20.8	20.9	21.0	21.1	
1.0000-25	19.3	19.4	19.5	19.7	19.8	19.9	20.0	20.1	20.2	20.3	20.4	20.5	20.6	20.7	20.8	20.9	21.0	21.1	
1.0000-26	19.3	19.4	19.5	19.7	19.8	19.9	20.0	20.1	20.2	20.3	20.4	20.5	20.6	20.7	20.8	20.9	21.0	21.1	
1.0000-27	19.3	19.4	19.5	19.7	19.8	19.9	20.0	20.1	20.2	20.3	20.4	20.5	20.6	20.7	20.8	20.9	21.0	21.1	
1.0000-28	19.3	19.4	19.5	19.7	19.8	19.9	20.0	20.1	20.2	20.3	20.4	20.5	20.6	20.7	20.8	20.9	21.0	21.1	
1.0000-29	19.3	19.4	19.5	19.7	19.8	19.9	20.0	20.1	20.2	20.3	20.4	20.5	20.6	20.7	20.8	20.9	21.0	21.1	
1.0000-30	19.3	19.4	19.5	19.7	19.8	19.9	20.0	20.1	20.2	20.3	20.4	20.5	20.6	20.7	20.8	20.9	21.0	21.1	
1.0000-31	19.3	19.4	19.5	19.7	19.8	19.9	20.0	20.1	20.2	20.3	20.4	20.5	20.6	20.7	20.8	20.9	21.0	21.1	
1.0000-32	19.3	19.4	19.5	19.7	19.8	19.9	20.0	20.1	20.2	20.3	20.4	20.5	20.6	20.7	20.8	20.9	21.0	21.1	
1.0000-33	19.3	19.4	19.5	19.7	19.8	19.9	20.0	20.1	20.2	20.3	20.4	20.5	20.6	20.7	20.8	20.9	21.0	21.1	
1.0000-34	19.3	19.4	19.5	19.7	19.8	19.9	20.0	20.1	20.2	20.3	20.4	20.5	20.6	20.7	20.8	20.9	21.0	21.1	
1.0000-35	19.3	19.4	19.5	19.7	19.8	19.9	20.0	20.1	20.2	20.3	20.4	20.5	20.6	20.7	20.8	20.9	21.0	21.1	
1.0000-36	19.3	19.4	19.5	19.7	19.8	19.9	20.0	20.1	20.2	20.3	20.4	20.5	20.6	20.7	20.8	20.9	21.0	21.1	
1.0000-37	19.3	19.4	19.5	19.7	19.8	19.9	20.0	20.1	20.2	20.3	20.4	20.5	20.6	20.7	20.8	20.9	21.0	21.1	
1.0000-38	19.3	19.4	19.5	19.7	19.8	19.9	20.0	20.1	20.2	20.3	20.4	20.5	20.6	20.7	20.8	20.9	21.0	21.1	
1.0000-39	19.3	19.4	19.5	19.7	19.8	19.9	20.0	20.1	20.2	20.3	20.4	20.5	20.6	20.7	20.8	20.9	21.0	21.1	
1.0000-40	19.3	19.4	19.5	19.7	19.8	19.9	20.0	20.1	20.2	20.3	20.4	20.5	20.6	20.7	20.8	20.9	21.0	21.1	
1.0000-41	19.3	19.4	19.5	19.7	19.8	19.9	20.0	20.1	20.2	20.3	20.4	20.5	20.6	20.7	20.8	20.9	21.0	21.1	
1.0000-42	19.3	19.4	19.5	19.7	19.8	19.9	20.0	20.1	20.2	20.3	20.4	20.5	20.6	20.7	20.8	20.9	21.0	21.1	
1.0000-43	19.3	19.4	19.5	19.7	19.8	19.9	20.0	20.1	20.2	20.3	20.4	20.5	20.6	20.7	20.8	20.9	21.0	21.1	
1.0000-44	19.3	19.4	19.5	19.7	19.8	19.9	20.0	20.1	20.2	20.3	20.4	20.5	20.6	20.7	20.8	20.9	21.0	21.1	
1.0000-45	19.3	19.4	19.5	19.7	19.8	19.9	20.0	20.1	20.2	20.3	20.4	20.5	20.6	20.7	20.8	20.9	21.0	21.1	
1.0000-46	19.3	19.4	19.5	19.7	19.8	19.9	20.0	20.1	20.2	20.3	20.4	20.5	20.6	20.7	20.8	20.9	21.0	21.1	
1.0000-47	19.3	19.4	19.5	19.7	19.8	19.9	20.0	20.1	20.2	20.3	20.4	20.5	20.6	20.7	20.8	20.9	21.0	21.1	
1.0000-48	19.3	19.4	19.5	19.7	19.8	19.9	20.0	20.1	20.2	20.3	20.4	20.5	20.6	20.7	20.8	20.9	21.0	21.1	
1.0000-49	19.3	19.4	19.5	19.7	19.8	19.9	20.0	20.1	20.2	20.3	20.4	20.5	20.6	20.7	20.8	20.9	21.0	21.1	
1.0000-50	19.3	19.4	19.5	19.7	19.8	19.9	20.0	20.1	20.2	20.3	20.4	20.5	20.6	20.7	20.8	20.9	21.0	21.1	
1.0000-51	19.3	19.4	19.5	19.7	19.8	19.9	20.0	20.1	20.2	20.3	20.4	20.5	20.6	20.7	20.8	20.9	21.0	21.1	
1.0000-52	19.3	19.4	19.5	19.7	19.8	19.9	20.0	20.1	20.2	20.3	20.4	20.5	20.6	20.7	20.8	20.9	21.0	21.1	
1.0000-53	19.3	19.4	19.5	19.7	19.8	19.9	20.0	20.1	20.2	20.3	20.4	20.5	20.6	20.7	20.8	20.9	21.0	21.1	
1.0000-54	19.3	19.4	19.5	19.7	19.8	19.9	20.0	20.1	20.2	20.3	20.4	20.5	20.6	20.7	20.8	20.9	21.0	21.1	
1.0000-55	19.3	19.4	19.5	19.7	19.8	19.9	20.0	20.1	20.2	20.3	20.4	20.5	20.6	20.7	20.8	20.9	21.0	21.1	
1.0000-56	19.3	19.4	19.5	19.7	19.8	19.9	20.0	20.1	20.2	20.3	20.4	20.5	20.6	20.7	20.8	20.9	21.0	21.1	
1.0000-57	19.3	19.4	19.5	19.7	19.8	19.9	20.0	20.1	20.2	20.3	20.4	20.5	20.6	20.7	20.8	20.9	21.0	21.1	
1.0000-58	19.3	19.4	19.5	19.7	19.8	19.9	20.0	20.1	20.2	20.3	20.4	20.5	20.6	20.7	20.8	20.9	21.0	21.1	
1.0000-59	19.3	19.4	19.5	19.7	19.8	19.9	20.0	20.1	20.2	20.3	20.4	20.5	20.6	20.7	20.8	20.9	21.0	21.1	
1.0000-60	19.3	19.4	19.5	19.7	19.8	19.9	20.0	20.1	20.2	20.3	20.4	20.5	20.6	20.7	20.8	20.9	21.0	21.1	
1.0000-61	19.3	19.4	19.5	19.7	19.8	19.9	20.0	20.1	20.2	20.3	20.4	20.5	20.6	20.7	20.8	20.9	21.0	21.1	
1.0000-62	19.3	19.4	19.5	19.7	19.8	19.9	20.0	20.1	20.2	20.3	20.4	20.5	20.6	20.7	20.8	20.9	21.0	21.1	
1.0000-63	19.3	19.4	19.5	19.7	19.8	19.9	20.0	20.1	20.2	20.3	20.4	20.5	20.6	20.7	20.8	20.9	21.0	21.1	
1.0000-64	19.3	19.4	19.5	19.7	19.8	19.9	20.0	20.1	20.2	20.3	20.4	20.5	20.6	20.7	20.8	20.9	21.0	21.1	
1.0000-65	19.3	19.4	19.5	19.7	19.8	19.9	20.0	20.1	20.2	20.3	20.4	20.5	20.6	20.7	20.8	20.9	21.0	21.1	
1.0000-66	19.3	19.4	19.5	19.7	19.8	19.9	20.0	20.1	20.2	20.3	20.4	20.5	20.6	20.7	20.8	20.9	21.0	21.1	
1.0000-67	19.3	19.4	19.5	19.7	19.8	19.9	20.0	20.1	20.2	20.3	20.4	20.5	20.6	20.7	20.8	20.9	21.0	21.1	
1.0000-68	19.3	19.4	19.5	19.7	19.8	19.9	20.0	20.1	20.2	20.3	20.4	20.5	20.6	2					

RELATIVE JET VELOCITY,  $V_{rel} = 9.14 \pm 0.2 \text{ M/S} = 3.06 \pm 0.5 \text{ FPS}$

### 5.2.2.2 Co-Annular Exhaust Nozzles

For a co-annular jet, i.e., a jet with both primary and secondary flows, the noise producing regions are shown in figure 21 and are defined as: (1) the inner shear layer, which is due to the interaction between the primary and secondary flows; (2) the outer shear layer, which is due to the interaction of the secondary with the surrounding air; and (3) the mixed flow region where the combined jet flows have become fully developed turbulence.

For noise prediction purposes, the co-annular jet is considered to have the noise generating characteristics of two independent single jet flows; one represented by the inner shear layer and the second represented by the summation of the outer shear layer and the mixed flow region.

The noise characteristics of the inner shear layer alone are predicted first as though the secondary flow was absent, i.e., the same as in section 5.2.2.1, except that the levels are then adjusted to account for the presence of the secondary flow surrounding the primary flow. To predict the noise of the outer shear layer and mixed flow region, it is necessary to calculate the *acoustical* equivalent flow parameters for the secondary stream of the co-annular flow system. This is a phenomenological, force-fit approach and it has no physical implications to the mean one-dimensional flow parameters for the flow region being considered. These calculated parameters are then used to predict the secondary flow jet noise as though it was a single jet. The predicted noise of the total co-annular jet is the energy sum of that produced by the two flows mentioned above (ref. 22).

*Noise prediction for inner shear layer.*—The noise from the inner shear layer is predicted in the same manner as that described in the previous section 5.2.2.1 with the following exception. In the step where the space-averaged  $\overline{\text{SPL}}$  spectrum is calculated, (eq. 15), a correction term is inserted

$$\overline{\text{SPL}}(f) = \overline{\text{SPL}}(f) + \Delta dB(f) \quad (18)$$

where

$$\Delta dB(f) = 10 \log_{10} \left| \frac{V_{J1} - V_{J2}}{V_{J1}} \right|^m$$

$$m = \text{experimentally determined exponent (ref. 22) shown in figure 22}$$

$$= F(A_2/A_1, f/f_1)$$

$$V_{J1}, V_{J2} = \text{primary/secondary velocities relative to the nozzle}$$

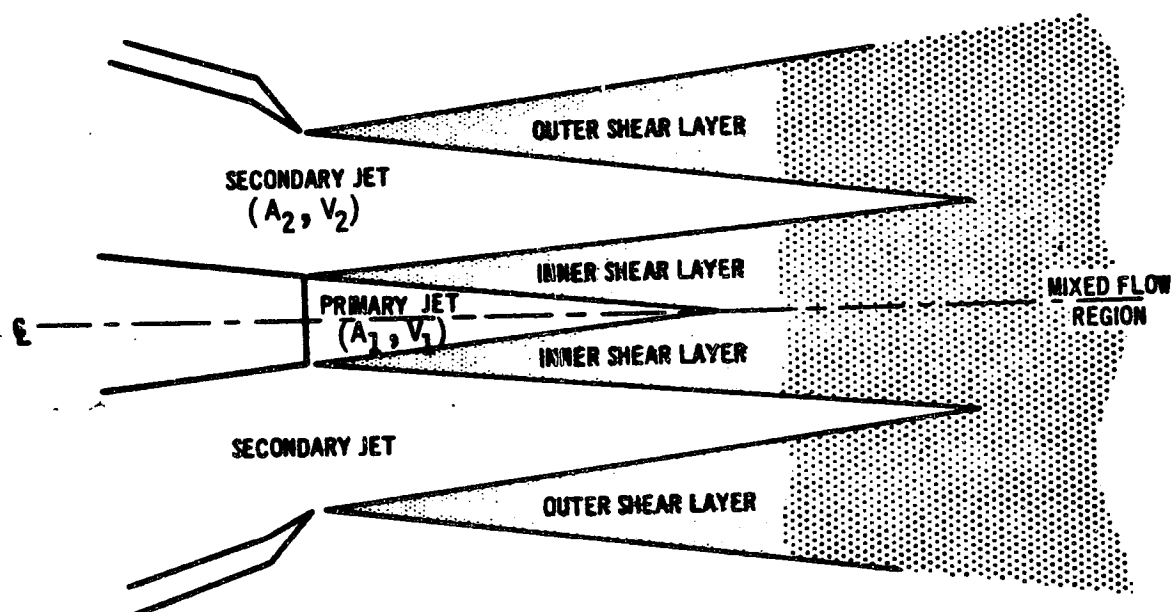


FIGURE 21.—IDEALIZED NOISE SOURCE REGIONS FOR CO-ANNULAR JETS

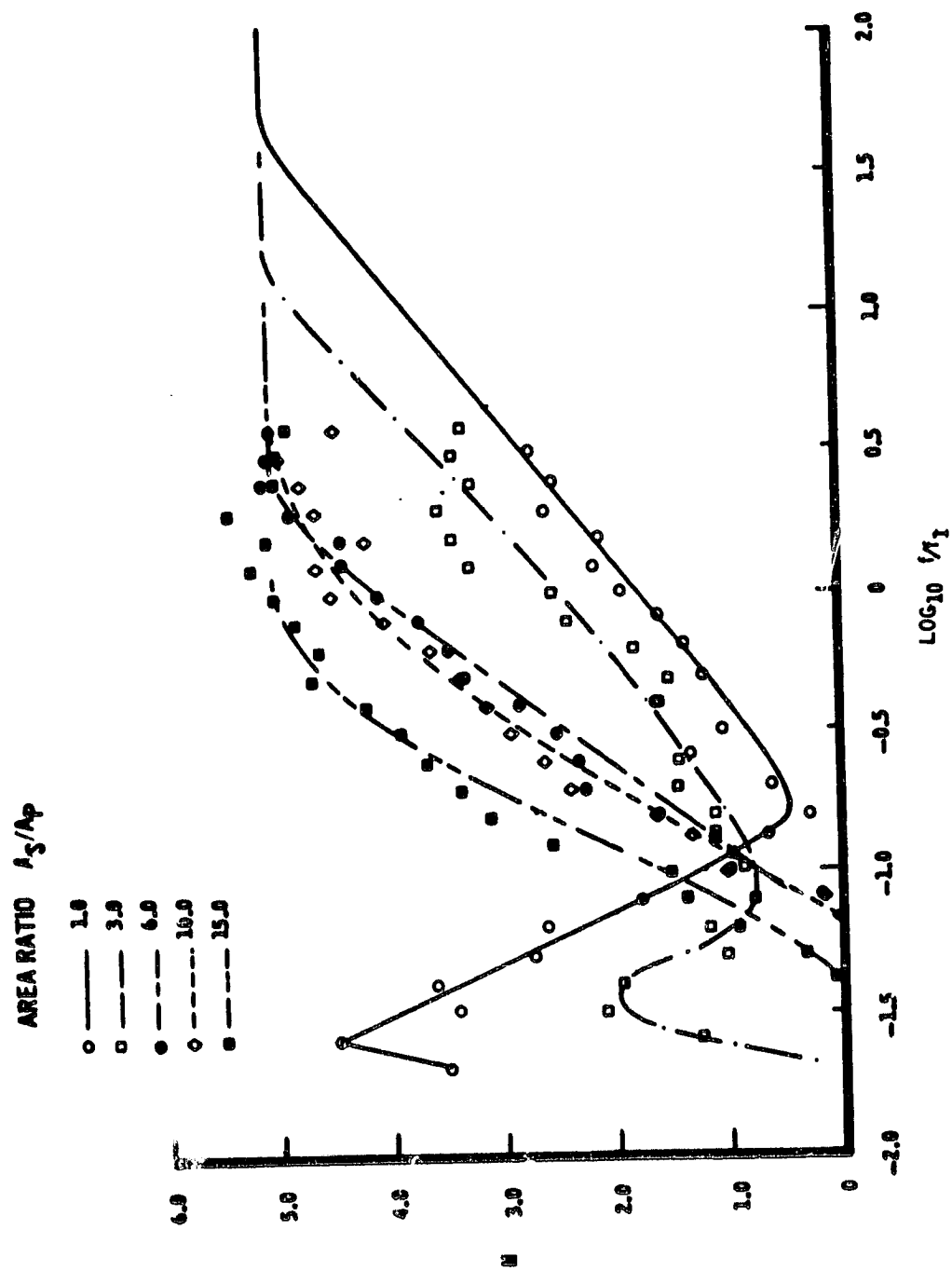


FIGURE 22.— $M$  VS STROUHAL NUMBER,  $f/H_1$

$A_1, A_2$  = primary/secondary discharge areas

$f_1$  =  $V_{J1}/D_1$

$D_1^2$  =  $\frac{4}{\pi}A_1$

Note: A singularity exists whenever  $V_{J2}$  approaches  $V_{J1}$ . In the program whenever  $|(V_{J1} - V_{J2})/V_{J1}|$  is less than 0.1, the inner shear layer is assumed to vanish and hence produces no noise. Further, the above procedure has not been verified for the case of  $V_{J2} > V_{J1}$ , but the computer program still considers this a valid case.

*Noise prediction for outer shear layer and mixed flow region.*—In this step, the noise is predicted in the same manner as that described for a single exhaust, section 5.2.2.1, except the parameters ( $\rho, A, V_R$ ) are the acoustical equivalent terms defined below.

$\rho$  = mean one-dimensional flow density of secondary discharge

$A$  =  $A_1 + A_2$

$$V_J^2 = V_{J1}^2 \left[ \frac{1 + \left(\frac{A_2}{A_1}\right) \left(\frac{V_{J2}}{V_{J1}}\right)^2}{1 + \left(\frac{A_2}{A_1}\right)} \right]$$

$$V_R^2 = V_J^2 - 2 V_J V_O \cos \alpha + V_O^2$$

$\alpha$  = angle between gross thrust vector and the direction of motion

### 5.2.2.3 Ejector/Suppressor Nozzles

A multi-element suppressor nozzle is shown in figure 23. This modification (lobe or tubular nozzles) of the exit hardware of jet engines can yield a considerable amount of noise suppression when compared to a conventional circular discharge nozzle. The suppression is believed to result from the change in turbulent mixing—an alternation of the turbulence scale and a reduction in the mean relative jet velocity gradients (ref. 24), since an increase in induced secondary air is observed. This implies an integration over the total volume of the jet. However, this is just a gross observation of a very complicated phenomena. In fact, the processes are so complicated that they defy theoretical analysis. Only empirical methods have yielded feasible designs (ref. 25).

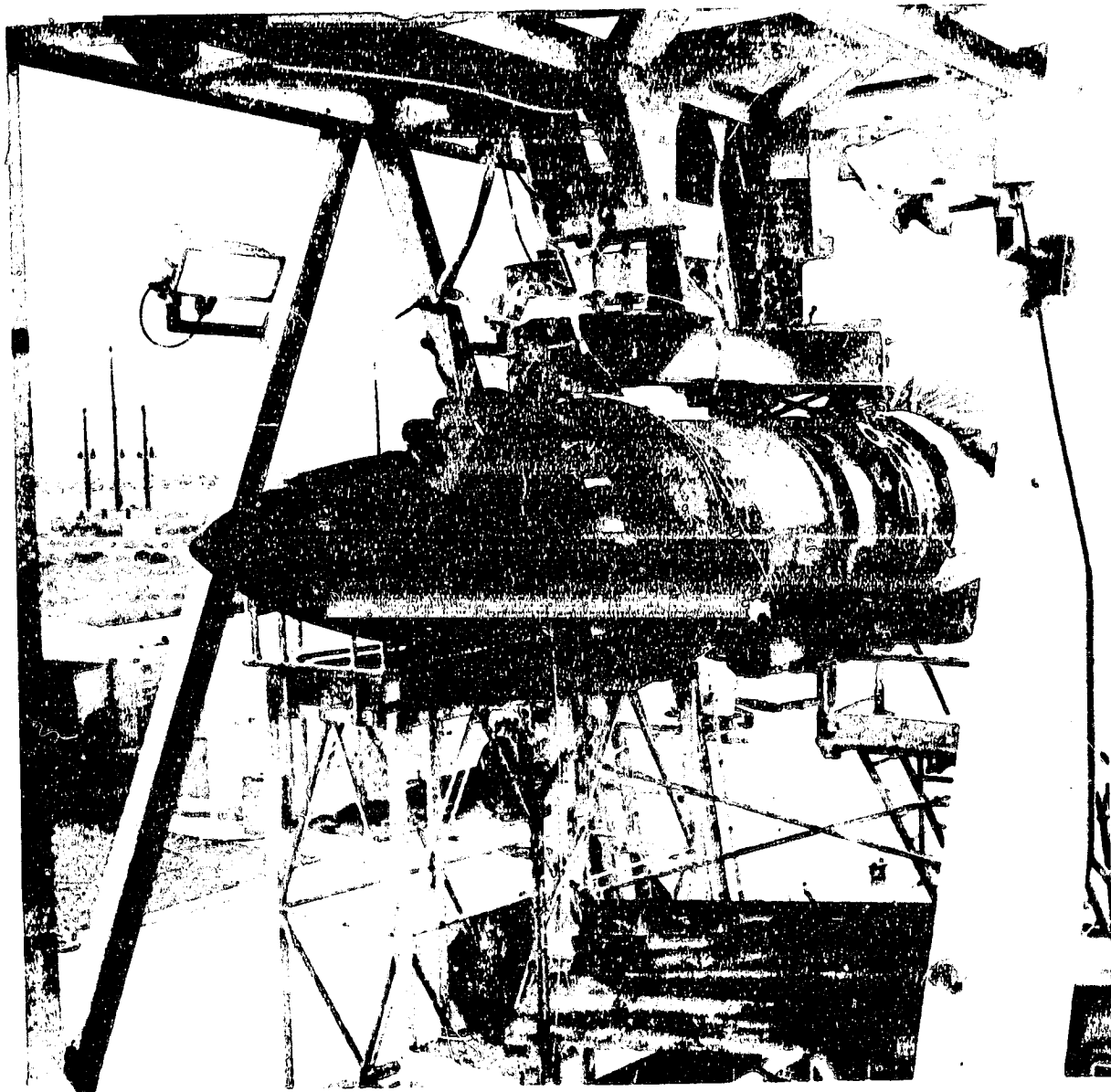


*FIGURE 23.—MULTI-ELEMENT SUPPRESSOR ON TEST STAND*

For the purpose of jet noise prediction, the noise from a multi-element nozzle can be considered to consist of two parts—(1) premerging noise and (2) postmerging noise. The pre-merging noise is generated in the region close to the nozzle where the structure of the individual jets can be identified. The postmerging noise is generated in a region downstream from the nozzle, after the individual jets and induced secondary air has merged into a single "uniform" jet of lower bulk velocity. The high-frequency portion of the resultant total jet noise spectrum is usually dominated by the premerging noise, while that of the low-frequency portion is associated with the postmerging noise. The noise for each component is predicted in a manner similar to that of a round nozzle. The total jet noise is then obtained by summing, on an energy basis, the spectra for premerging and postmerging noise.

When a shroud, commonly called an ejector, is added to the multi-element suppressor, an increase in suppression can occur, provided that the shroud length to diameter ratio,  $L/D$ , is large. However, long ejectors have considerable weight, and losses in flight associated with them; hence, they have not been studied in depth as a noise suppression item. Another approach (ref. 25) uses a shorter ejector which incorporates lining to achieve the same result. Even this approach has its limits because all the premerging noise does not propagate normal to the ejector walls, and only part of the noise is intercepted by the lining. Further, only limited types of lining materials can be used due to the thermal environment of the exhaust.

For short shrouds,  $L/D$  less than 2.5, without lining, no significant reduction in premerging noise has been observed when compared to that of a "bare" suppressor configuration. This leads to the assumption that the noise from a short, hardwall ejector/suppressor can be predicted in a manner similar to that for a "bare" suppressor. This requires knowledge of the ejector performance, however, because the presence of a shroud (ejector) imposes a constraint on the boundaries of the premerging and postmerging regions. Ejector performance can be obtained by use of a theoretical, one-dimensional, flow analysis if one assumes 100% mixing inside the shroud. Appendix B contains an example of the parametric curves that can be obtained from the configuration shown in figure 24, taking this approach.

The present noise prediction procedure is essentially empirical. It is based on the analysis of an extensive amount of round nozzle and suppressor noise data from the following types of tests:

- 1) Full scale JT8D, JT3C, JT4/J75 and JT12 static engine tests.
- 2) Model scale hot flow test ( $A = 45.6 \text{ cm}^2$ ).
- 3) Flight test for the 707, 727, and 737 airplanes.

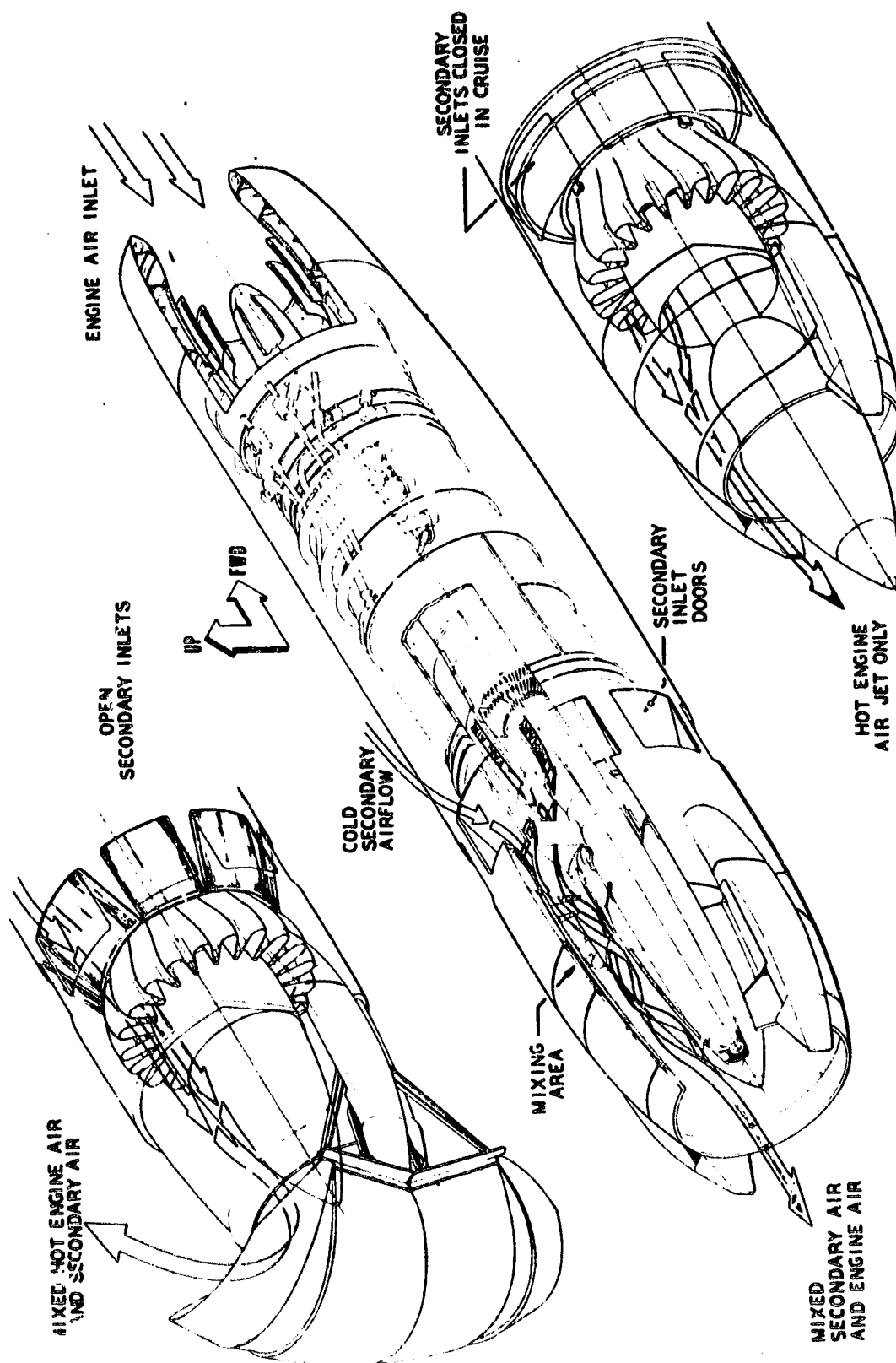


FIGURE 24.—SCHEMATIC OF 727 PHASE 2 NACELLE



The results of the procedure are 1/3 octave band spectra at the free-field, index condition described in section 5.1.1.2. The overall accuracy of the procedure is dependent upon the ability to predict the premerging noise spectrum. This, in turn, depends upon the configuration of study. For turbofan engines, e.g., the JT8D, the procedure predicts this component low by approximately 5 dB. Apparently there is a velocity defect upstream from the suppressor nozzle exit which increases the turbulence in the jet for the JT8D configuration and hence increases the premerging noise. The list in table 6 represent the tolerances in PNdB based on observations from ground static tests, that can be expected for the procedure, provided that the area ratio for the suppressor is between 1.5 and 4.5. The area ratio is defined as total flow area (primary plus induced secondary) divided by the primary discharge area at the suppressor exit plane.

Figure 25 shows a comparison of a sample prediction with measured data.

*Postmerging noise prediction.*—Consider the ejector/suppressor configuration shown in figure 24. The postmerging noise for the ejector exhaust is assumed to be similar to that of a conventional circular jet. The techniques described in section 5.2.2.1 could be applied; however, a slightly different approach is taken here. The overall sound pressure level for a single engine is related to the relative jet velocity, density of the exhaust, static temperature and discharge area. The relation is

$$\text{OASPL}(\psi) = F_1(V_R, \psi) + 10 \log_{10} \left[ \left( \frac{\rho}{\rho_R} \right)^2 \left( \frac{T_S}{T_{SR}} \right)^{1.5} \left( \frac{A}{A_R} \right) \right] \quad (19)$$

where

$F_1(V_R, \psi)$  is obtained from figure 26.

$V_R$  = relative jet velocity =  $|\hat{V}_J - \hat{V}_O|$

$V_J$  = mean one-dimensional flow velocity for the ejector exhaust

$\rho$  = mean one-dimensional flow density for the ejector exhaust

$\rho_R$  = reference density = 16.02 KG/M<sup>3</sup> (1 lbm/ft<sup>3</sup>)

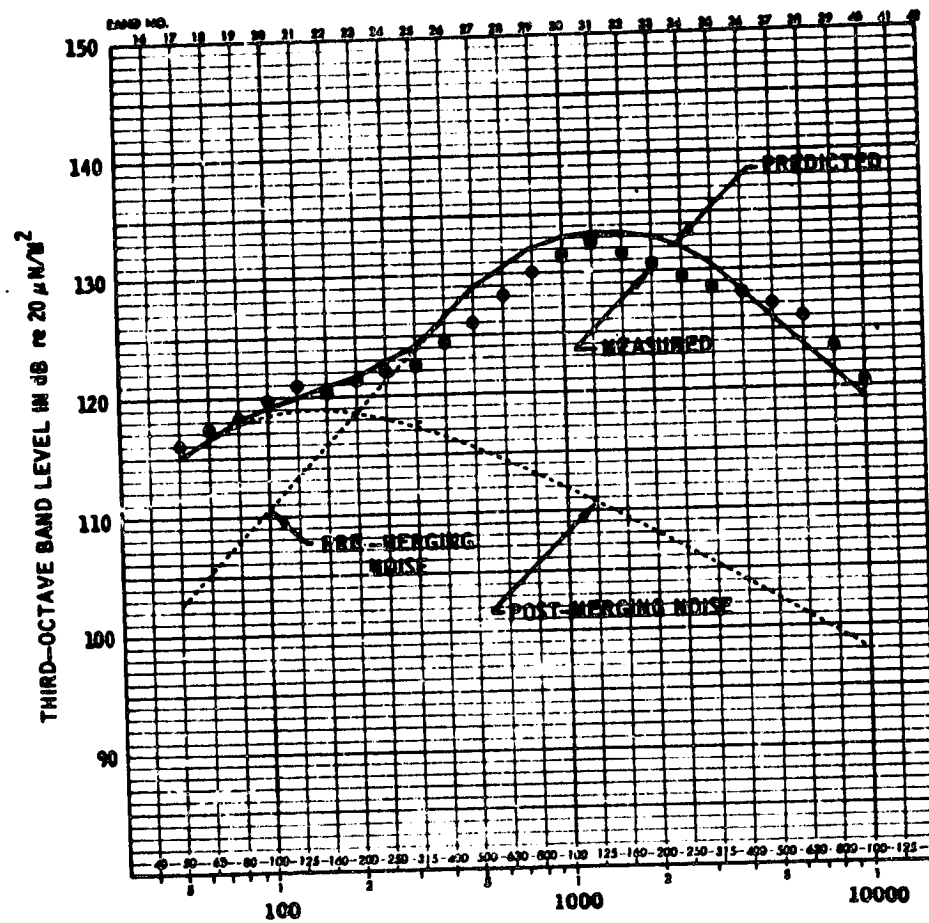
$T_S$  = mean one-dimensional flow static temperature

$T_{SR}$  = reference temperature from figure 27

**TABLE 6.—TOLERANCES**

Engine type	Configuration	
	Bare suppressor	Ejector/suppressor <sup>a</sup>
Turbojet	$\pm 2$ PNdB	$\pm 3$ PNdB
Turbofans	$-5 \pm 2$ PNdB	$-2 \pm 3$ PNdB

<sup>a</sup>Short, hardwall shrouds:  $L/D \leq 2.5$ .



FREQUENCY IN HERTZ			
NUMBER OF TUBES	37	TOTAL TEMPERATURE	703° K (1265° R)
AREA RATIO	3.3	AREA	0.352 M <sup>2</sup> (3.78 FT <sup>2</sup> )
AIRPLANE SPEED	0	ENGINE PRESSURE RATIO	2.04
DIRECTIVITY ANGLE	120°	ENGINE	YJ75

FIGURE 25.—FREE-FIELD SOUND PRESSURE LEVEL SPECTRA NORMALIZED TO 1 METER RADIUS

# REFERENCE CONDITIONS

• DISTANCE R = 1 METER

•  $\rho_R = 16.02 \text{ KG/M}^3$  (1 LBM/FT<sup>3</sup>)

•  $A_R = 0.0929 \text{ M}^2$  (1 FT<sup>2</sup>)

• FREE-FIELD

•  $T_{SR}$  - REFERENCE TEMP  
(FIGURE 27)

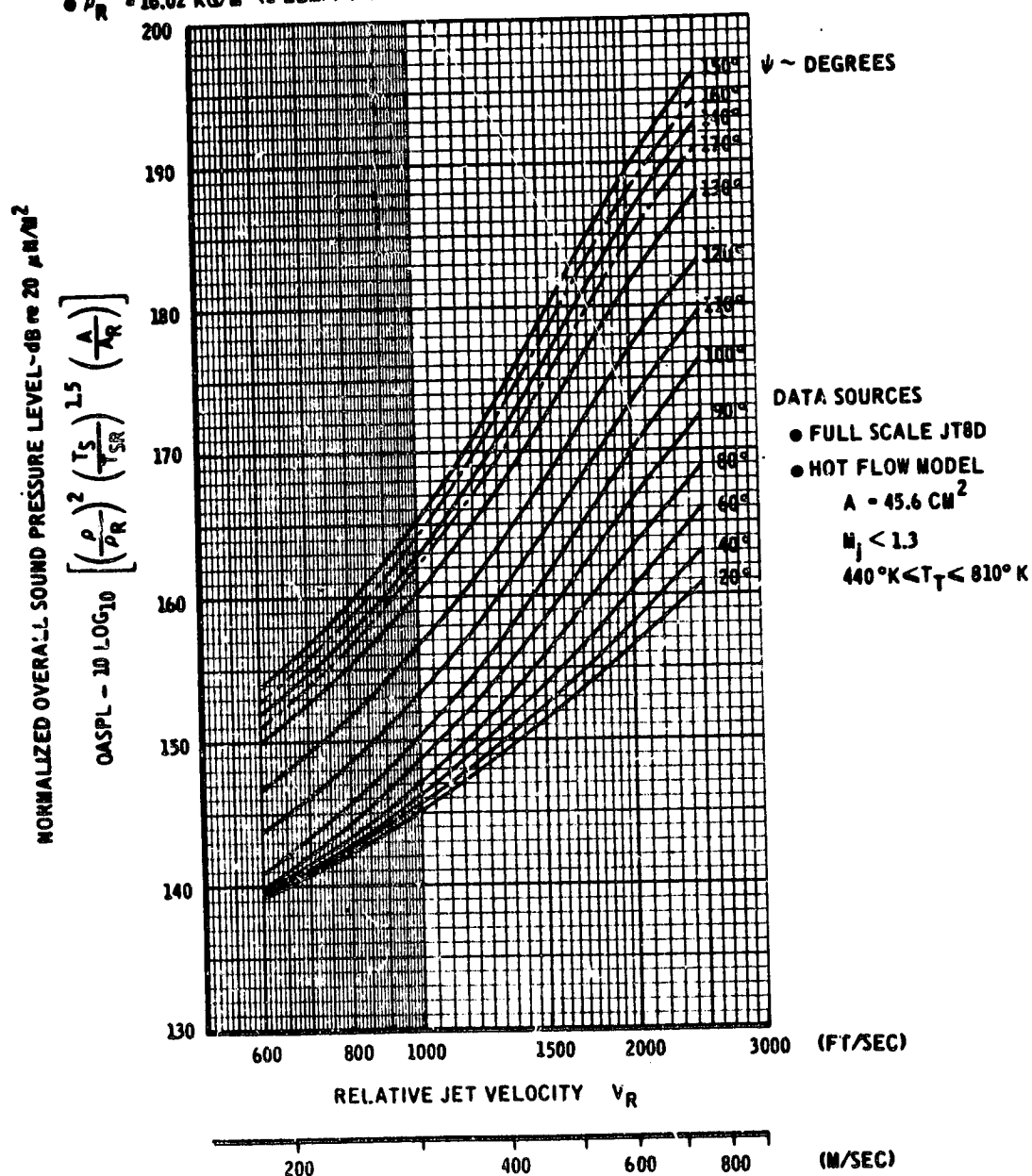


FIGURE 26.—NORMALIZED OVERALL SOUND PRESSURE LEVEL VS. RELATIVE JET VELOCITY

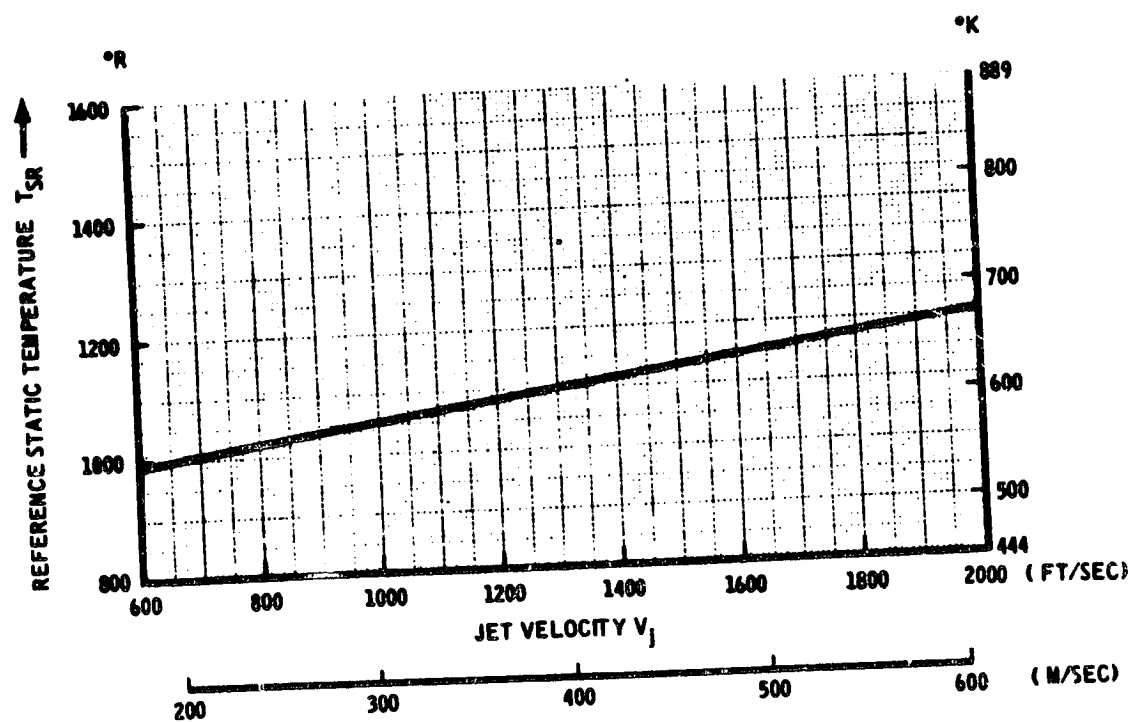


FIGURE 27.—REFERENCE STATIC TEMPERATURE VS JET VELOCITY

$A$  = discharge area of the ejector

$A_R$  = reference area =  $0.0929 \text{ M}^2$  ( $1 \text{ ft}^2$ )

The 1/3 octave band SPL spectrum is calculated by adding the following corrections to the OASPL, i.e.,

$$\text{SPL}(f, \psi) = \text{OASPL}(\psi) + F_2(f/f_0) + F_3(f/f_0, \psi) \quad (20)$$

where

$F_2(f/f_0)$  is obtained from figure 28

$F_3(f/f_0, \psi)$  is obtained from figure 29

$f_0$  = characteristic frequency

$$= \left( \frac{V_J^2}{V_{RD}} \right) F_4(V_R, \psi) \text{ from figure 30.}$$

$$D = \text{ejector exit diameter} = \sqrt{\frac{4}{\pi}} A$$

When the shroud is removed, the one-dimensional flow parameters for the postmerging noise region are difficult to define. This problem has been avoided through use of the one-dimensional flow parameters for the suppressor exhaust. This approach resulted in an empirical correction term being added to equation (19). The correction term is defined as a function of area ratio, AR, and relative velocity, i.e.,

$$\Delta \text{dB} = 0.34 \sqrt{\text{AR} - 1} F_5(V_R)$$

from figure 31, and the "effective" one-dimensional flow parameters to use in equations (19) and (20) above are:

$V_J$  = velocity for the suppressor exhaust

$\rho$  = density for the suppressor exhaust

$T_S$  = static temperature for the suppressor exhaust

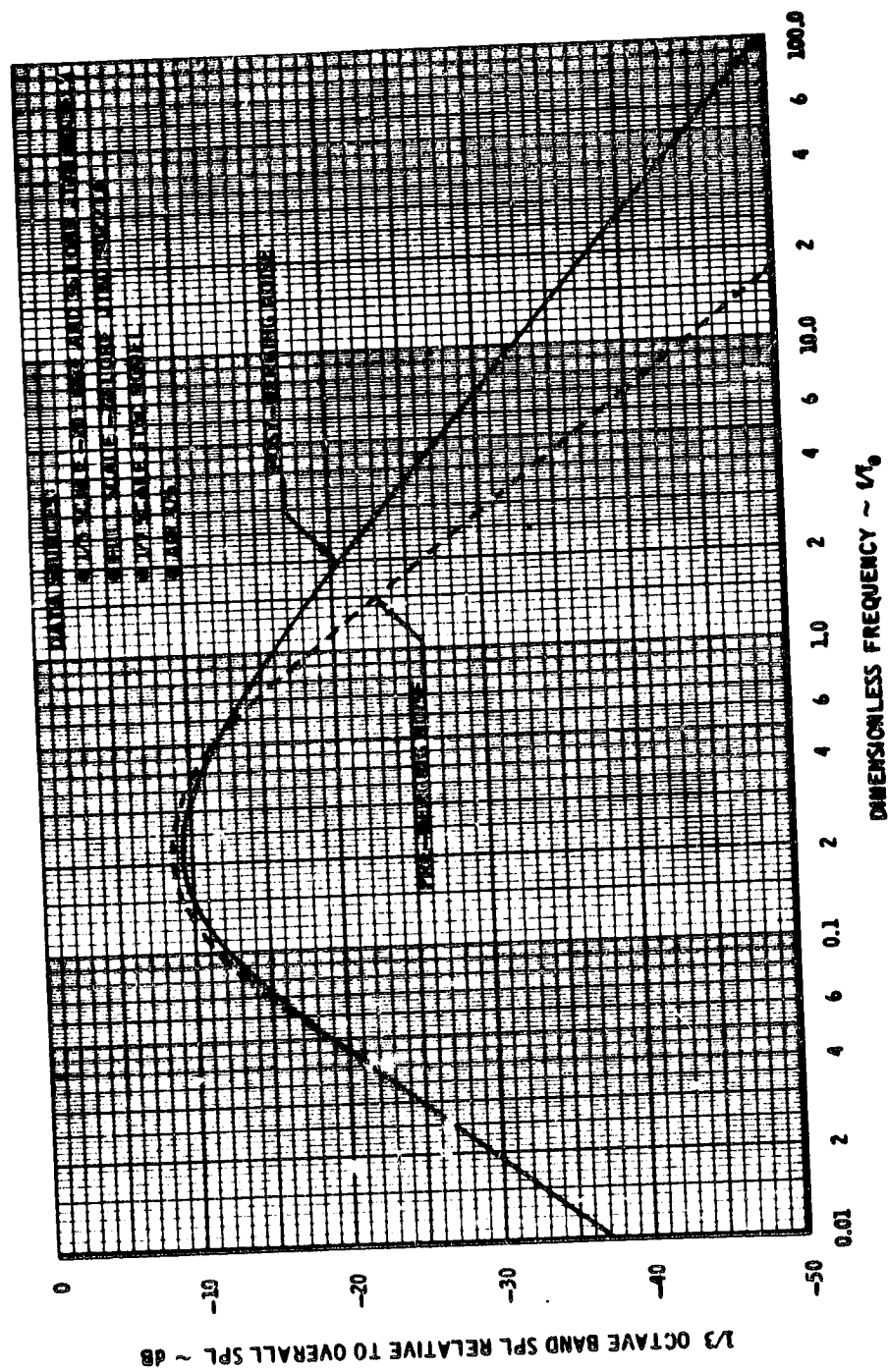


FIGURE 28.—INDEX SPECTRUM SHAPE

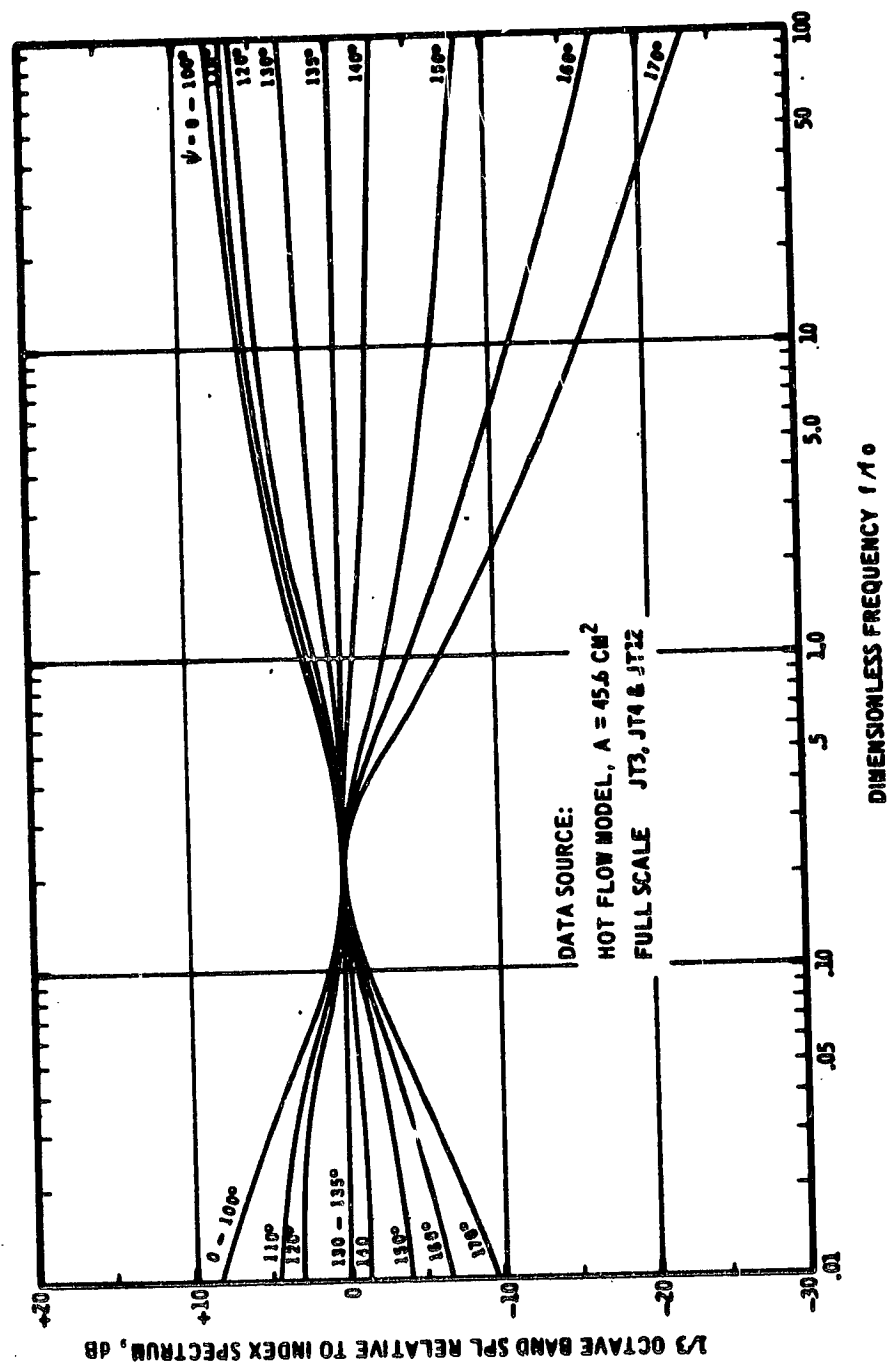


FIGURE 29.—SPECTRUM DIRECTIVITY CORRECTIONS



DATA SOURCE:

HOT FLOW MODEL

$A = 45.6 \text{ CM}^2$

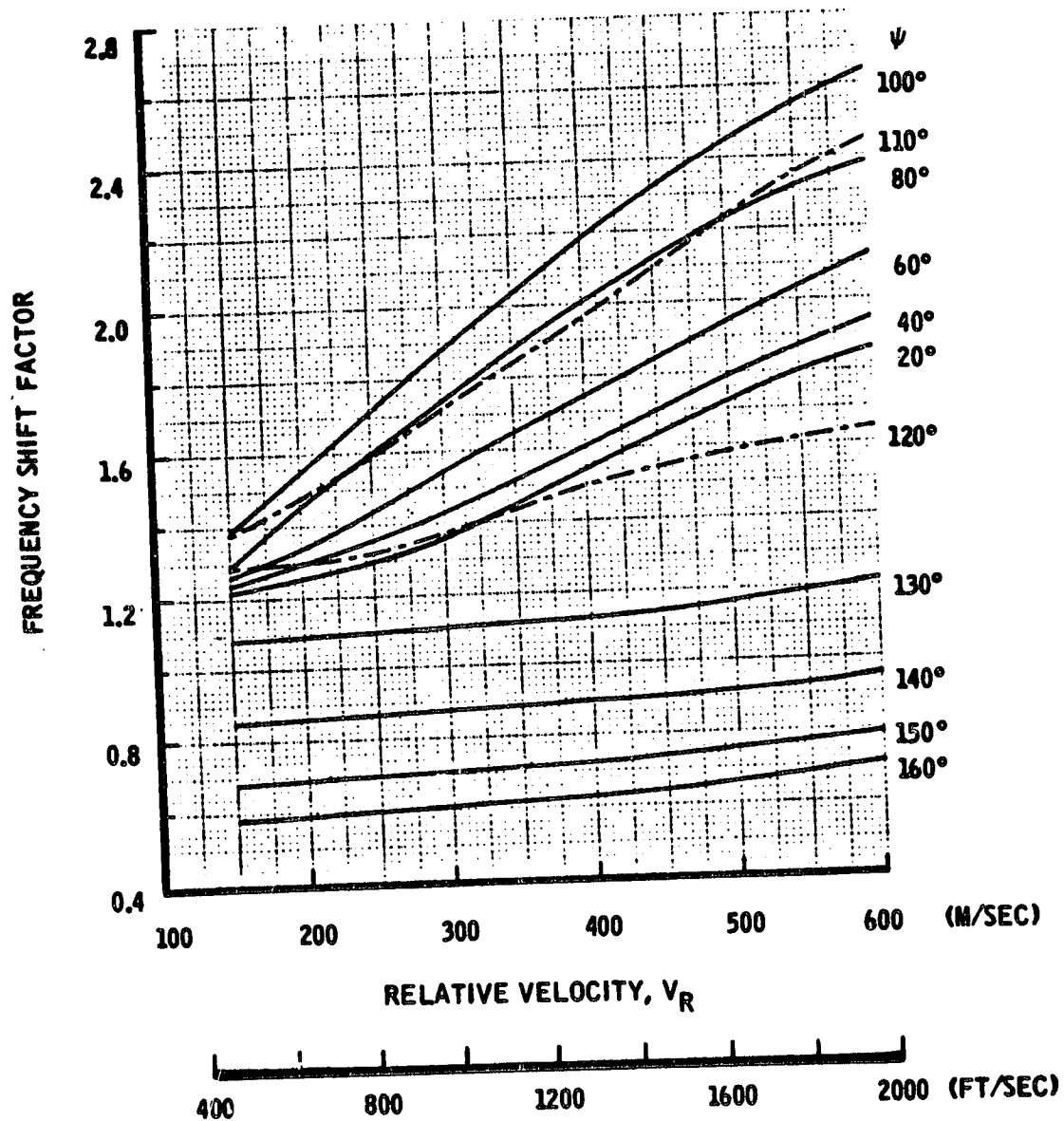


FIGURE 30.—FREQUENCY SHIFT DUE TO CONVECTION

DATA SOURCE	PR	$T_T$ -°K	$T_T$ -°R
MAE-62 1/7 th SCALE JT3C	2.2	868	1560
FULL SCALE JT8D	1.8	750	1350
FULL SCALE J75	2.0	695	1250

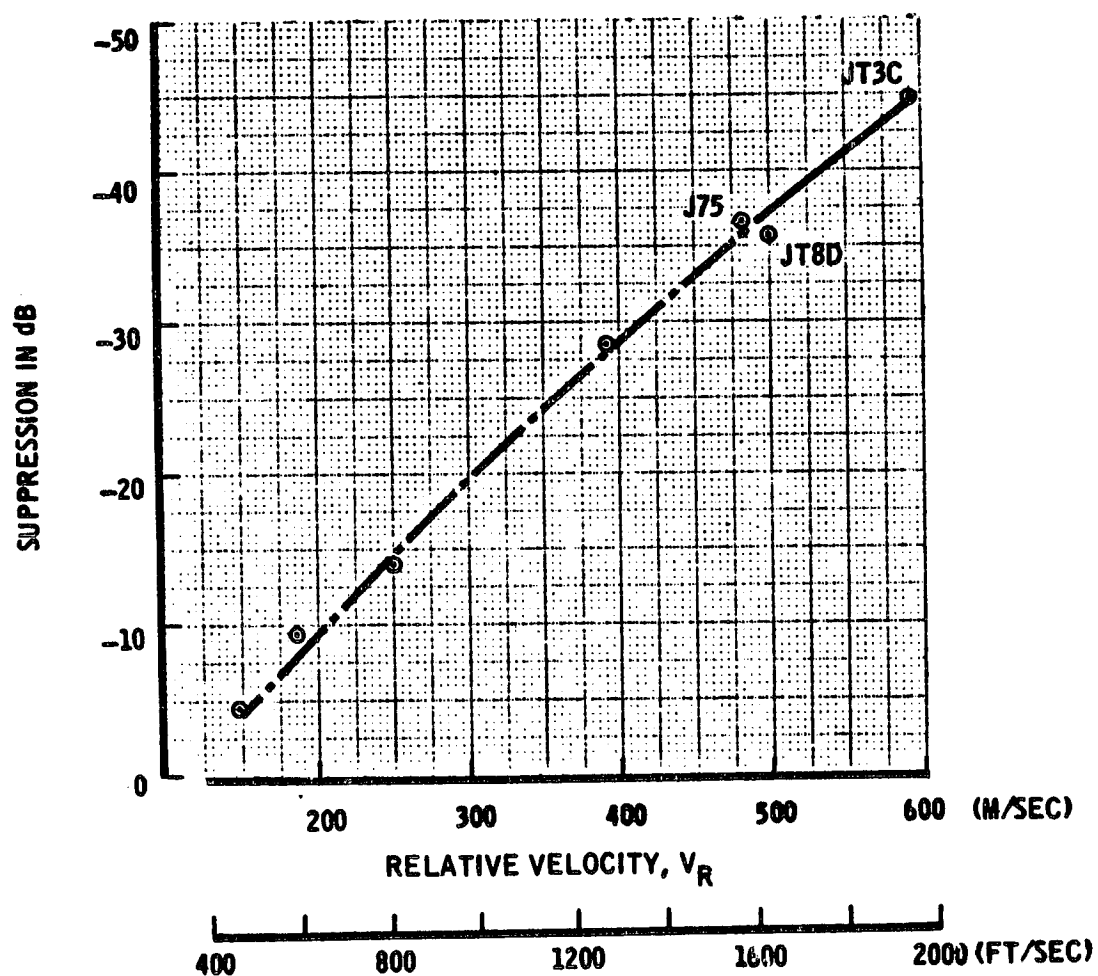


FIGURE 31.—POST-MERGING NOISE SUPPRESSION VERSUS RELATIVE VELOCITY  
FOR BARE SUPPRESSOR CONFIGURATION

A = discharge area of suppressor

$$D = \sqrt{\left(\frac{4}{\pi}\right) A AR}$$

**Premerging noise prediction.**—Consider the “bare” suppressor configuration shown in figure 23. The premerging noise of a single element, tube or lobe, etc., is assumed to be similar to that of a conventional circular jet of the same discharge area. However, the individual jets for the multi-element suppressor interfere with each other and alter the turbulent structure (ref. 24). By dimensional analysis, the effects of the interferring jets have been related to the number of elements and the area ratio for the suppressor. From this analysis the space average, overall sound pressure level for this component is defined empirically as

$$\begin{aligned} \overline{OASPL} \approx & F_1(V_R, 120^\circ) + 10 \log_{10} \left[ \left( \frac{\rho}{\rho_R} \right)^2 \left( \frac{T_s}{T_{SR}} \right)^{1.5} \left( \frac{A}{A_R} \right) \right] \\ & + F_6(N) + F_7(AR) \end{aligned} \quad (21)$$

where

$F_1(V_R, 120^\circ)$  is obtained from figure 26

$F_6(N)$  is obtained from figure 32

$F_7(AR)$  is obtained from figure 33

$$V_R \approx V_J - (V_S - 0.2 C_O)$$

$V_S$  = induced secondary velocity

$$\approx \frac{.4}{.42} C_O \text{ ground static}$$

$$\approx \frac{.46}{.42} C_O \text{ in flight}$$

$C_O$  = ambient speed of sound

$N$  = number of elements

$AR$  = area ratio: (primary + induced secondary)/primary

DATA SOURCE:  
 $M_AE = 63$   $PR = 2.2$   $T_T = 868^\circ K (1560^\circ R)$   
 $AR = 5.7$   $M_j < 1.3$

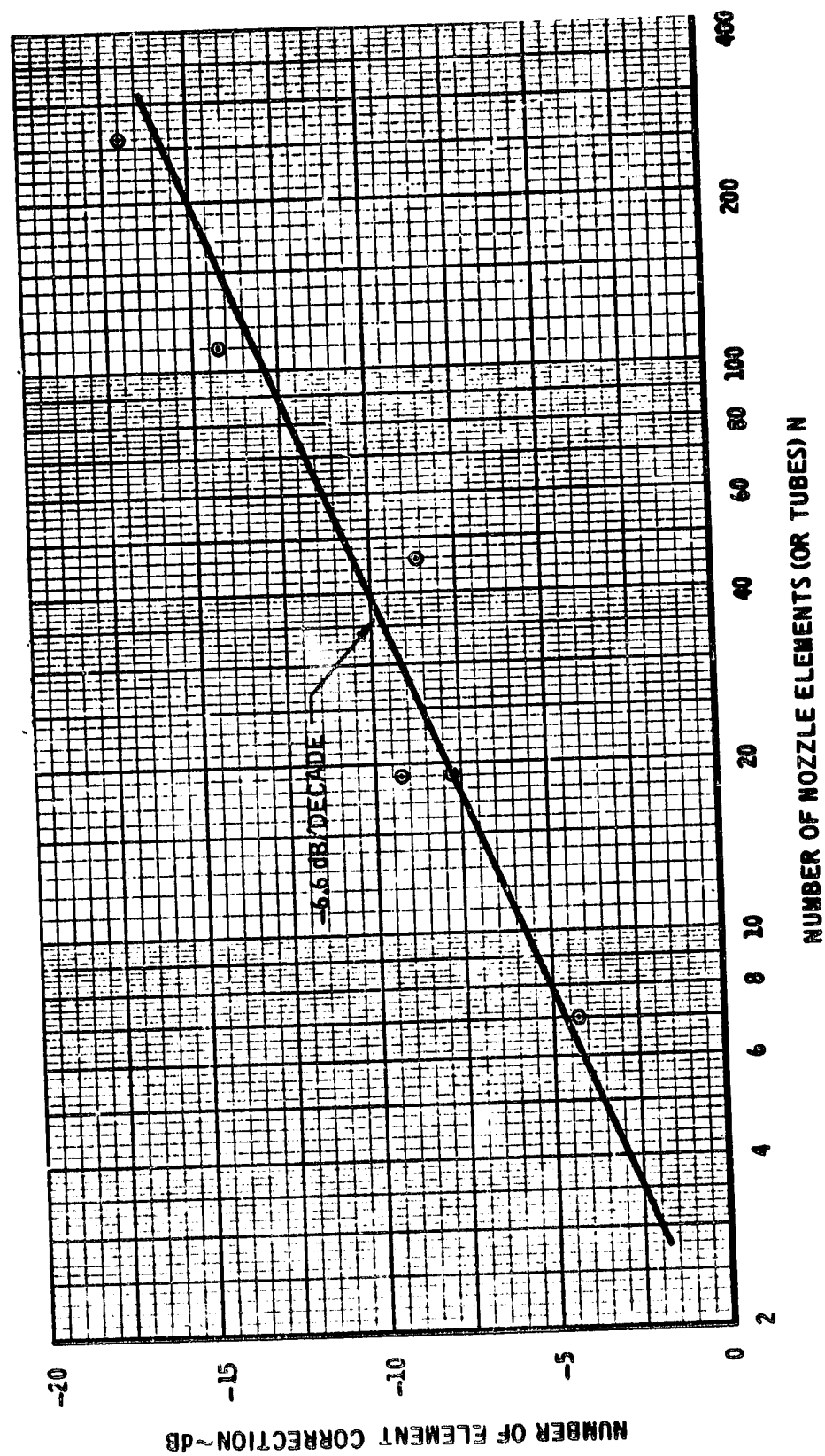


FIGURE 32.—EFFECT OF NUMBER OF ELEMENTS

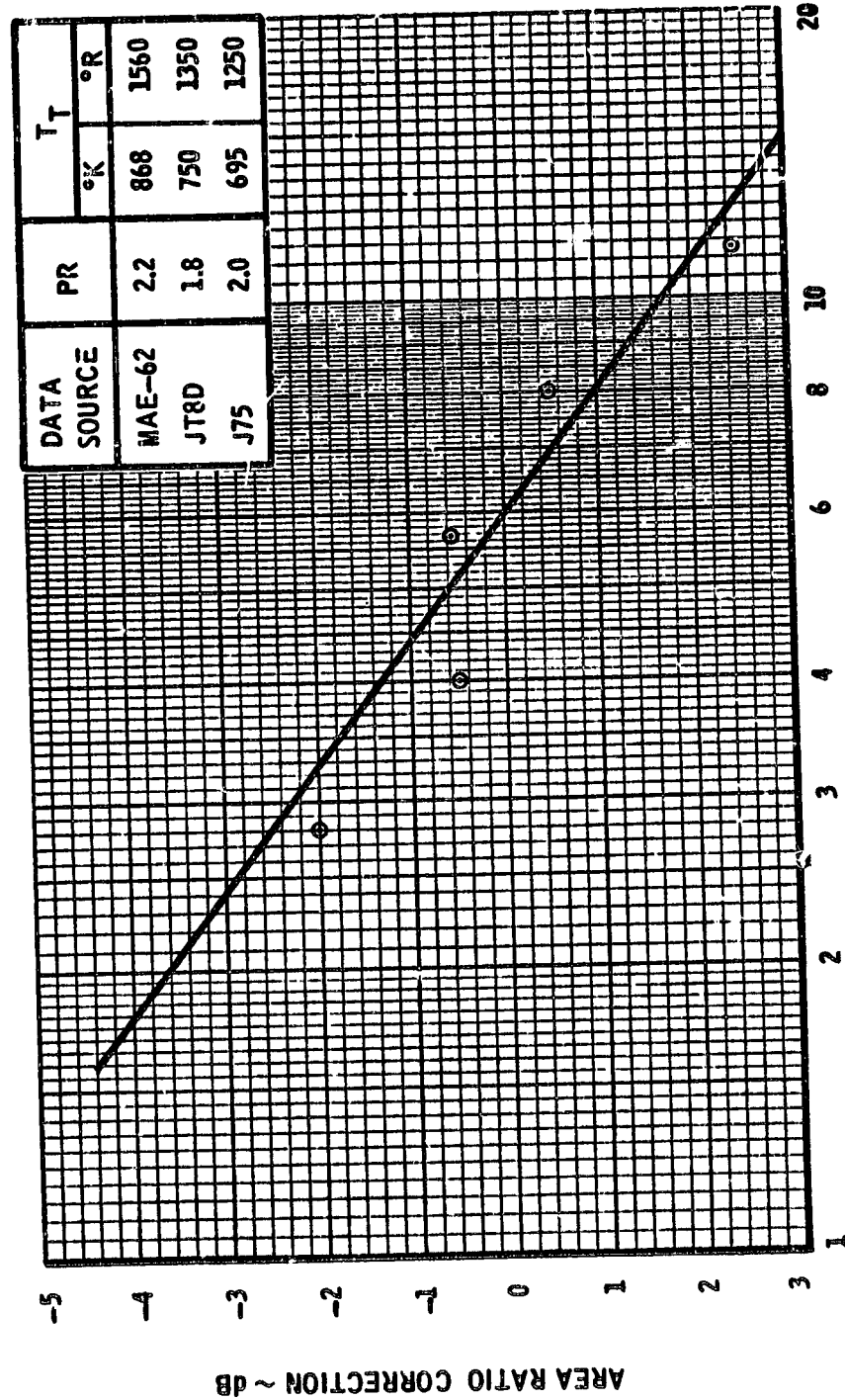


FIGURE 33.—EFFECT OF AREA RATIO

and the mean one-dimensional flow parameters  $V_J$ ,  $\rho$ ,  $T_S$ ,  $A$  represent velocity, density, static temperature, and discharge area for the suppressor, respectively.

The overall SPL varies with the directivity angle,  $\psi$ , and is defined by

$$OASPL(\psi) = \overline{OASPL} + F_8(\psi) \quad (22)$$

where  $F_8(\psi)$  is obtained from figure 34.

Finally, the 1/3 octave band SPL spectrum is obtained in a manner similar to that for the postmerging noise, except that the characteristic frequency,  $f_o$ , is typically higher and an apparent shift  $10^\circ$  relative to the postmerging noise must be added to the directivity angle. That is

$$SPL(f, \psi) = OASPL(\psi) + F_2(f/f_o) + F_3(f/f_o, \psi + 10^\circ) \quad (23)$$

where

$F_2(f/f_o)$  is obtained from figure 28.

$F_3(f/f_o, \psi + 10^\circ)$  is obtained from figure 29

$$f_o = \left( \frac{V_J^2}{V_R D} \right) F_4(V_R, \psi) F_9(M_J)$$

$$D = \text{effective element diameter} = \sqrt{\frac{4}{\pi}} A/N$$

$F_4(V_R, \psi)$  is obtained from figure 30

$F_9(M_J)$  is obtained from figure 35

$M_J =$  Mach number of the suppressor exhaust.

When a hardwall shroud,  $L/D$  less than 2.5, is placed on the exhaust system, the performance of the configuration changes and the induced secondary Mach number increases and typically varies between 0.4 and 0.6 for the configuration studied in appendix B. For this short shroud, no apparent shielding takes place and the premerging noise level has not been observed to change significantly. However, this will not be the case when the shroud is lined (see sec. 5.1.4).

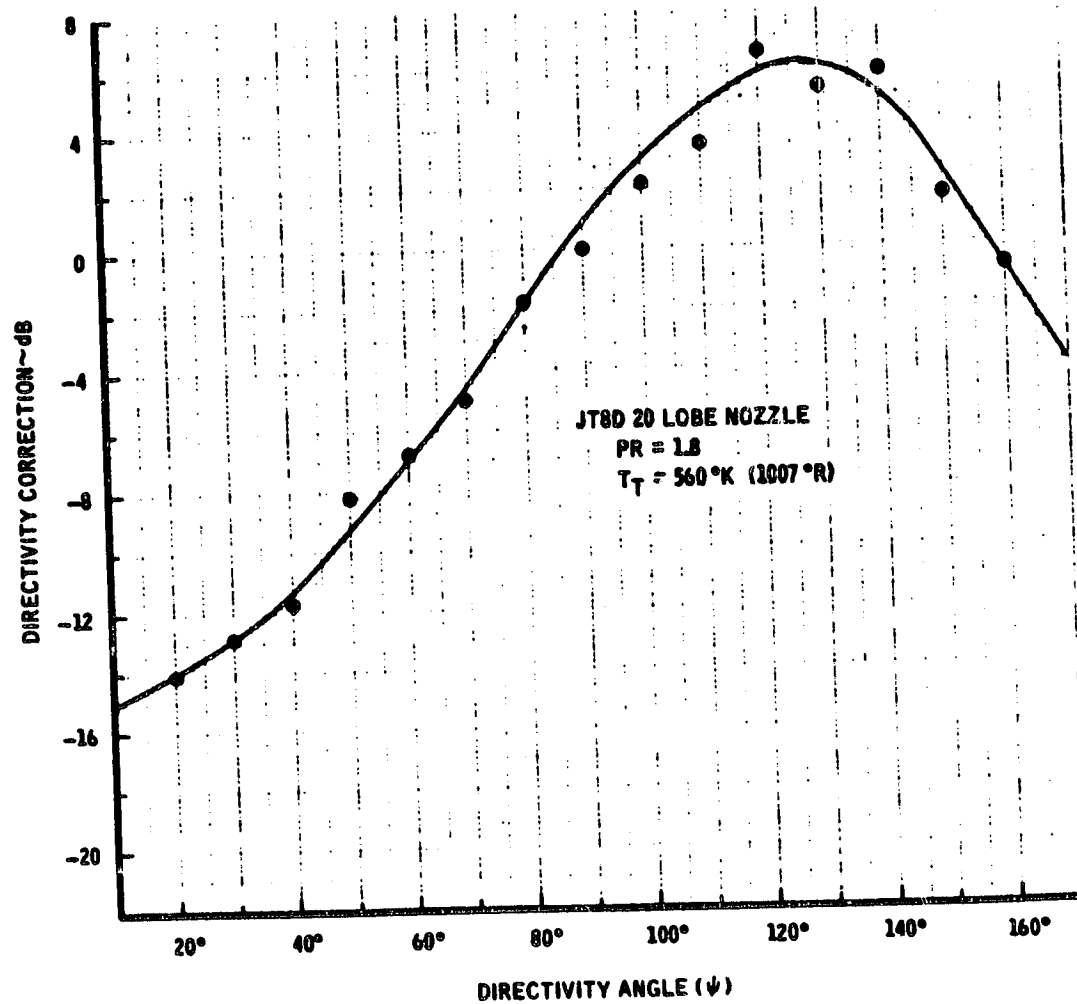


FIGURE 34.—PRE-MERGING NOISE DIRECTIVITY CORRECTION

TEST DATA:

- 2.54 CM DIAMETER MODEL (BSRL)
- ▲ JT8D FULL SCALE ENGINE
- J93 ENGINE

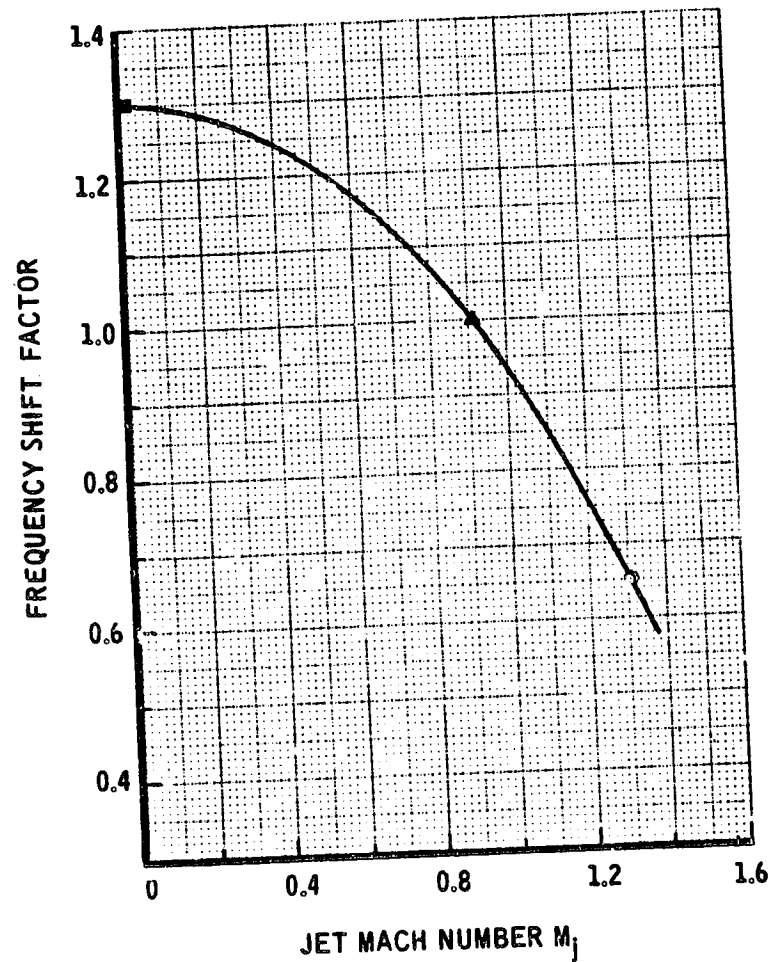


FIGURE 35.—FREQUENCY SHIFT DUE TO REFRACTION AND POTENTIAL CORE CHANGE



The total noise level for the "bare" suppressor, or the ejector/suppressor configuration is the energy sum of the spectra for the premerging and postmerging noise components. The effect of multiple engines with this type of exhaust hardware is estimated by use of equation (2B) in section 5.1.1.6.

#### 5.2.2.4 Slot Nozzle With an Augmentor Flap

An empirical noise prediction procedure has been developed for a typical slot nozzle/augmentor flap configuration shown in figure 36. The augmentor flap is unlined, but its geometry is considered representative of that which would be used on an augmentor-wing STOL aircraft. The procedure is based on the data obtained from model tests (ref. 11) conducted under NASA contract NAS2-6344.

Unfortunately, during the time this procedure was being developed, the recommended nozzle configuration for an augmentor-wing aircraft changed (ref. 26). This new nozzle was still a slot, but incorporated a series of screech shields in the flow. The corresponding acoustic data was not available for analysis during the present contract period and, therefore, the application of the procedure given here is limited. It should serve as a baseline for further development in noise prediction procedures for an augmentor-wing aircraft.

The current procedure is based on a static test program where the model was a 100 to 1 slot nozzle with an augmentor flap positioned at a corresponding flap angle of 35° during takeoff. Table 7 gives the particular range of test conditions considered and also includes that of a full-scale equivalent augmentor wing configuration.

The full scale equivalent acoustic data was extrapolated to the index condition ( $R = 1$  M) and 3 dB was subtracted to approximate free-field levels. The validity of the test data corresponding to elevation angles,  $\beta_0 = 30^\circ$ , and  $60^\circ$ , was doubtful. For these data, an average between the levels measured on each side of the model was used to approximate the free-field plus 3 dB condition. The overall sound pressure level data were then normalized with respect to total temperature ratio, nozzle pressure ratio, and nozzle discharge area for each value of the directivity angle ( $\psi$ ) and elevation angle ( $\beta_0$ ).

This normalization yielded a series of straight line plots with respect to the logarithms of the independent variables:  $P_T/P_{S0}$ ,  $T_T/T_{T0}$ , and area. Hence, a simple relation for the overall sound pressure level was obtained by a least-squares-fit to the data with an R-M-S error of 1.7 dB. The relation is

$$\text{OASPL}(\psi, \beta_0) = a_0 + 10 \log_{10} \left[ \left( \frac{T_T}{T_{T0}} \right)^{a_1} \left( \frac{P_T}{P_{S0}} \right)^{a_2} \left( \frac{A}{A_R} \right) \right] \quad (24)$$

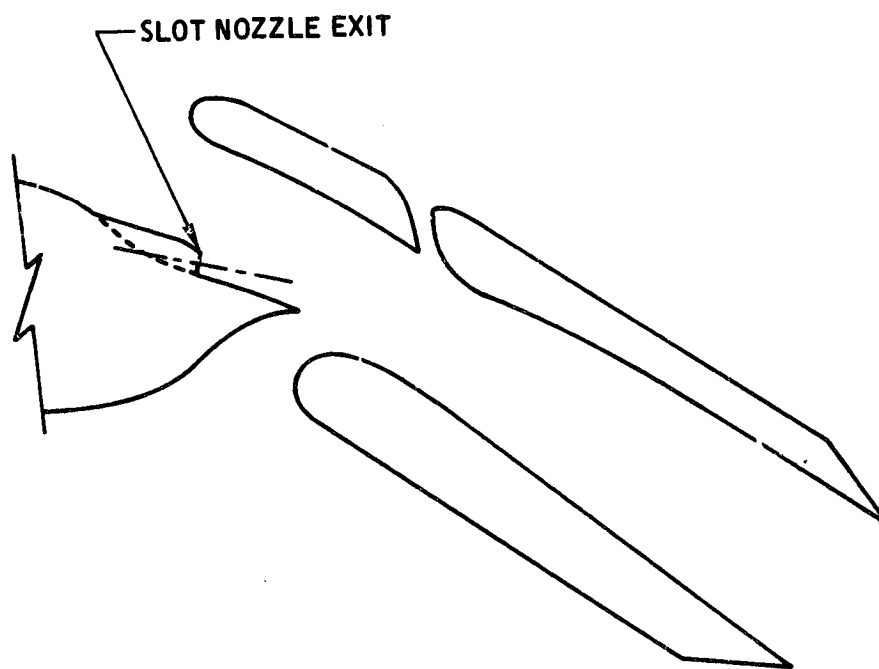


**FIGURE 36.—SLOT NOZZLE WITH AUGMENTOR FLAP**

**TABLE 7.—RANGE OF TEST CONDITIONS**

Test Condition	Model	Full-Scale Eq. (Scale Factor=6.4)
a. Nozzle Pressure Ratio( $P_T/P_{S0}$ )	1.6 to 3.0	Same
b. Total Temperature Ratio ( $T_T/T_{T0}$ )	1.0 to 1.43	Same
c. Nozzle Discharge Area (A)	120.6 cm <sup>2</sup> (18.7 in <sup>2</sup> )	0.494 M <sup>2</sup> (5.32 ft <sup>2</sup> )
d. Microphone Radius (R)	15.2 M (50 ft)	97.5 M (320 ft)
e. Geometric-Mean Frequency (f)	315 Hz to 64 KHz	50 Hz to 10 KHz

\*NOTE\*  $P_{S0} \approx 1.0$  S. ATM. = 2116 psfa

$T_{T0} \approx 296$  °K = 532 °R

with the parameters:

$a_0$  = function of  $\psi$  and  $\beta_0$  from table 8

$a_1$  = function of  $\psi$  from table 8

$a_2$  = function of  $\psi$  and  $\beta_0$  from table 8

$A_R$  = reference area =  $0.494 \text{ M}^2$  ( $5.32 \text{ ft}^2$ )

This relation is shown in figure 37 along with the corresponding data used to develop it. The nozzle configuration upon which this analyses is based produced screech at nozzle pressure ratios exceeding two. No correction was made to the OASPL to eliminate the effects of screech. However, the irregularities it produced in the spectra were "smoothed" in the development of a spectrum shape formula.

The 1/3 octave band, spectrum shape formula was obtained by plotting (SPL - OASPL) versus Strouhal number (ref. 7). The characteristic dimension of the slot that was used to calculate the Strouhal number corresponded to the hydraulic diameter for the flow. However, a temperature stratification was observed between the hot,  $T_T/T_{TO} = 1.43$ , and the cold,  $T_T/T_{TO} = 1.0$ , flow data. To further collapse the data, a modified Strouhal number was used which included the total temperature ratio as a factor. That is

$$\text{SPL}(f, \psi, \beta_0) = \text{OASPL}(\psi, \beta_0) + F(S) \quad (25)$$

where

$F(S)$  = spectrum shape curve shown in figure 38

$S$  = modified Strouhal number =  $f/f_0$

$f_0$  = characteristic frequency =  $\left(\frac{V_R}{D}\right)\left(\frac{T_T}{T_{TO}}\right)^{-1}$

$D$  = hydraulic diameter =  $4 A/\text{Perimeter}$   
 $= 2 H/(1 + H/L)$

$(H, L)$  = slot height and length, respectively

TABLE 8.—FORMULA CONSTANTS

$\psi$ (deg)	$\beta$ (deg)	$a_0$ (dB)	$a_1$	$a_2$
100	90	118.9	<u>1.57</u>	6.38
	60	120.4	↓	6.16
	30	121.4		5.22
	0	117.1	↓	5.13
110	90	119.9	<u>1.93</u>	6.48
	60	122.3	↓	5.80
	30	122.0		5.25
	0	117.2	↓	5.31
120	90	121.1	<u>2.95</u>	6.49
	60	124.1	↓	5.52
	30	122.3		5.07
	0	118.6	↓	5.04
130	90	120.9	<u>3.43</u>	6.17
	60	123.8	↓	5.67
	30	120.7		5.23
	0	118.7	↓	5.34
140	90	128.6	<u>2.53</u>	4.83
	60	127.6	↓	4.88
	30	126.1		4.62
	0	122.9	↓	4.60
150	90	122.8	<u>2.11</u>	4.95
	60	123.4	↓	4.73
	30	122.4		4.63
	0	118.8	↓	5.15
160	90	119.5	<u>2.05</u>	5.18
	60	119.8	↓	5.17
	30	121.4		4.54
	0	118.2	↓	5.33

NOTES:

•  $\Phi$  = CORRELATION PARAMETER =  $\left[ \left( \frac{T_T}{T_{T0}} \right)^{a_1} \left( \frac{P_T}{P_{S0}} \right)^{a_2} \left( \frac{A}{A_R} \right) \right]$

WHERE ( $a_0, a_1, a_2$ ) = LEAST-SQUARES-FIT CONSTANTS FROM TABLE 8

• REFERENCE CONDITIONS:

$T_{T0} = 296^\circ \text{ K } (532^\circ \text{ R})$

$P_{S0} = \text{STANDARD ATMOSPHERE (2116 psfa)}$

$A_R = 0.494 \text{ M}^2 (5.32 \text{ FT}^2)$

• FREE-FIELD, INDEX ( $R = 1 \text{ M}$ )

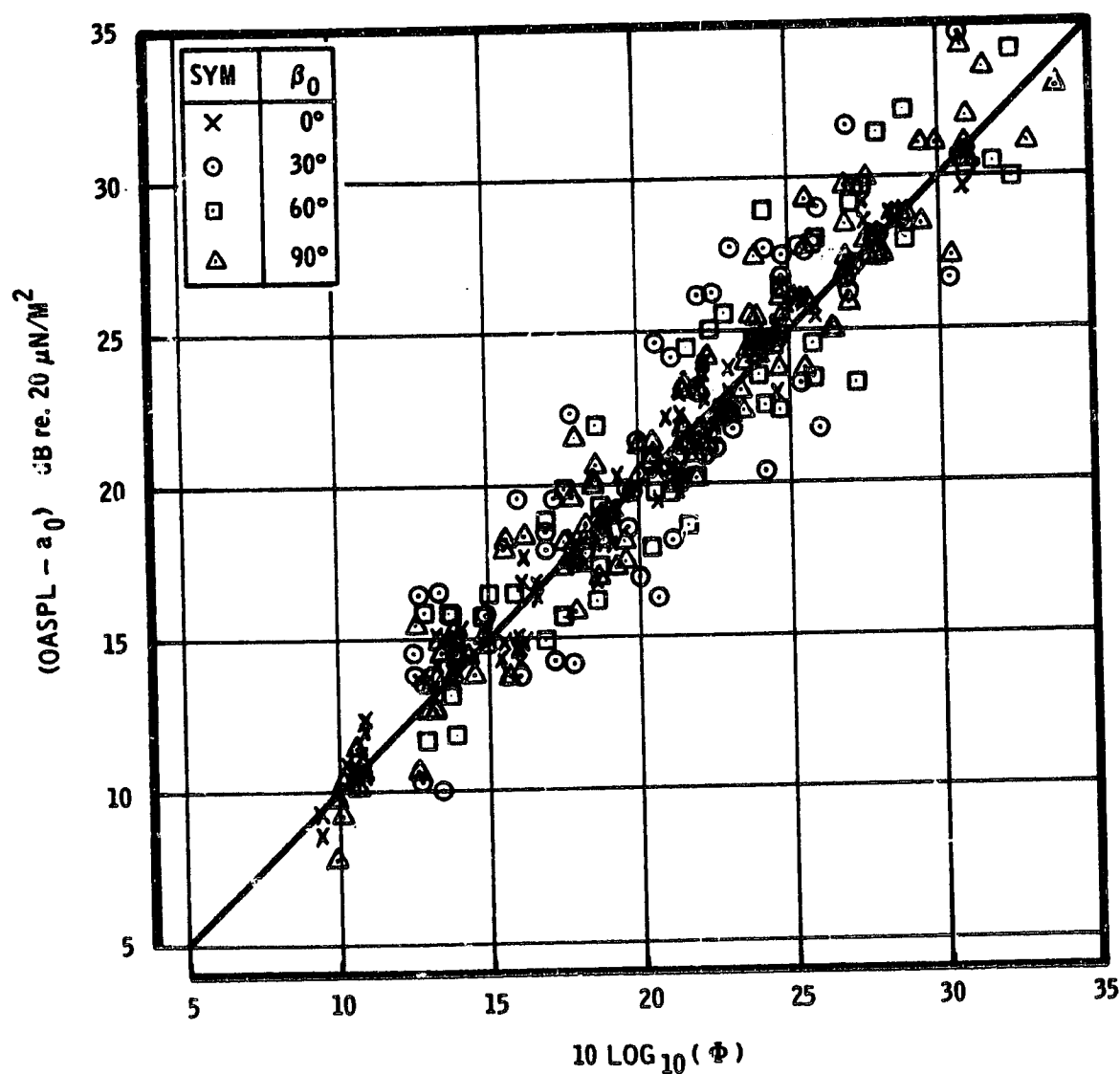


FIGURE 37.—OVERALL SOUND PRESSURE LEVEL CORRELATION

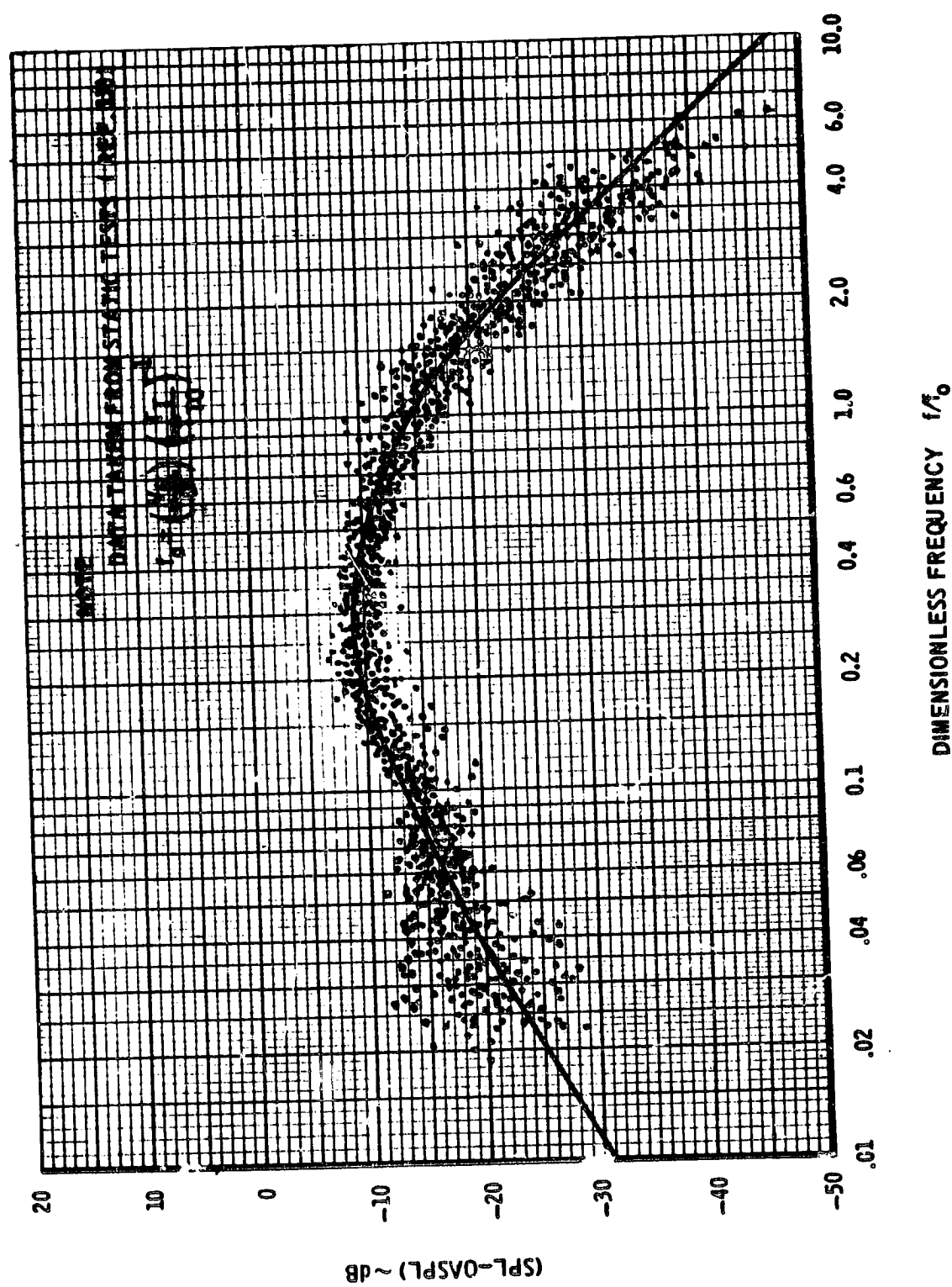


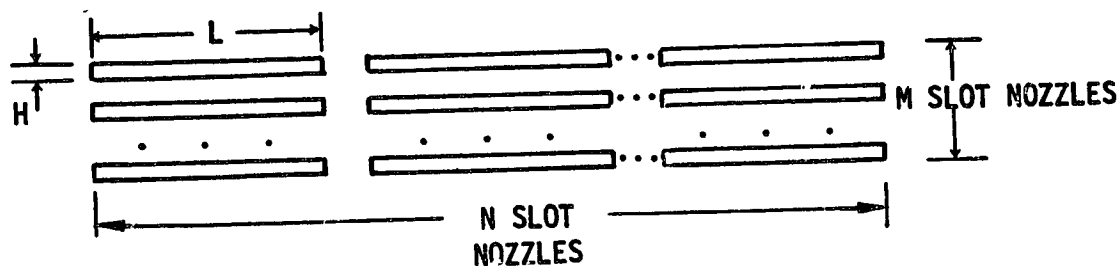
FIGURE 38.—1/3 OCTAVE BAND SPECTRUM SHAPE

$$V_R = |\hat{V}_J - \hat{V}_O|$$

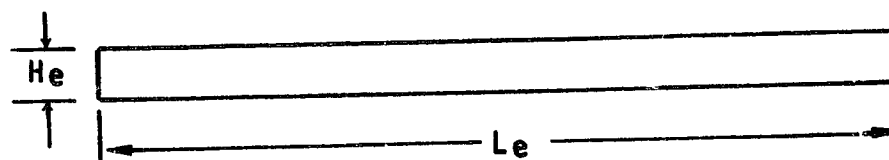
$\hat{V}_J$  = jet velocity relative to the nozzle

Although figure 38 shows a certain amount of data scatter, the scatter is largely due to ground reflection and to screech for pressure ratios greater than two. The dependence with respect to variations in the angles,  $\Psi$ , and  $\beta_0$  is weak. Hence, the use of a single curve is not expected to cause serious error in human response estimates, such as perceived noise level.

*Multiple slot/flap configurations.*—The use of multiple slot/flap configurations by STOL aircraft can be broken down into a single “acoustic equivalent” slot/flap configuration, provided the spacing between the slots is small compared to the slot dimensions, i.e., less than 10%. The sketch below illustrates how this can be done.



“Acoustically” this is approximately equivalent to



where

$$H_e = M H$$

$$L_e = N L$$

Thus, the use of multiple slot/flap configurations requires the change of only two input variables in the basic prediction defined previously, that is

$$A = M N H L$$

$$D = 2 M H / [1 + (M H) / (N L)]$$



where  $H$  is the typical slot height, and  $L$  is the typical slot length.

*Required additional work.*—Reflecting on some of the recent developments mentioned in section 5.2.2.1, it is believed that a better formulation could result through use of different independent variables than nozzle pressure ratio ( $P_T/P_{SO}$ ) and total temperature ratio ( $T_T/T_{TO}$ ) used in equations (24) and (25) above—namely static temperature ratio and convection Mach number. The present procedure has not been validated for predicting the noise of an aircraft in flight. These new variables would give more insight as to how the effects of flight could be predicted. Further work is recommended using this approach in the analysis of the data obtained from the tests described in references 11 and 27.

#### 5.2.2.5 Externally Blown-Flap Configuration

A model of an externally blown-flap configuration is shown in figures 39 and 40. The engine exhaust is redirected by the flap(s) and an increase in lift occurs. This lift-augmentation makes the device desirable for STOL aircraft. However, the blown flap has a penalty—more noise is produced than that from a conventional wing mounting such as that on the current commercial airplane fleet (ref. 29).

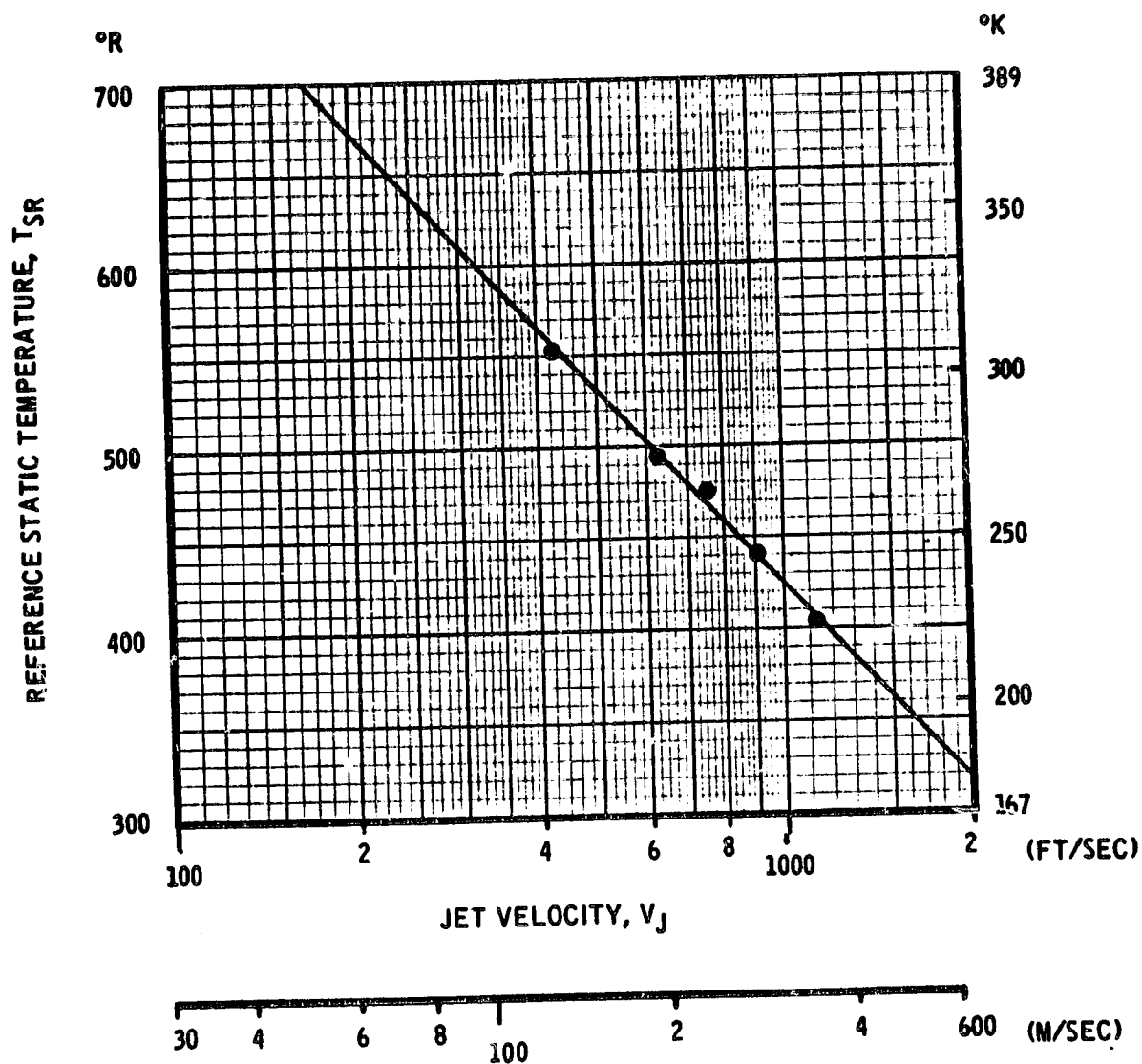
The increase in noise can be attributed to two items. The first is the presence of an additional noise source, impingement of the turbulent jet producing a fluctuating force on the flap(s), which has "dipole" characteristics. This force is the source for the dipole component and has been given the term "impingement noise" in reference 28 and this terminology will be used here. The second item causing an increase in noise is due to a change in the jet structure. This results from the presence of the flap which alters the radiation pattern of jet noise. Also, the jet velocity gradients at the trailing edge of the flap can produce more noise than that for a free jet. However, when the flaps are extended, the impingement noise usually dominates in the far-field. Therefore this report deals with the noise prediction for this case. When the flap(s) are retracted, the jet noise component dominates over the impingement noise, but the additional noise produced at the trailing edge of the flap(s) is assumed to be insignificant, i.e., it is convected and refracted aft and does not contribute to the noise observed below the aircraft. Thus, the techniques presented for single and co-annular exhaust nozzles in sections 5.2.2.1 and 5.2.2.2, can be applied to the exhaust as though it were a free jet.

The acoustic data used to develop the noise prediction procedure for the blown-flap configuration were obtained from reference 28. The conditions for the static test were as listed in table 9, and shown in figure 41.



**TABLE 9.—TEST CONDITIONS (REFER TO FIGS. 39 AND 40)**

Item	Sym.	Condition
a. Static temperature	$T_s$	Figure 41
b. Jet velocity	$V_j$	150 to 350 M/S
c. Nozzle diameter	D	5.2 cm (2.05 in.)
d. Relative nozzle position	H/D	0.2 to 1.5
when $\alpha_N = 45^\circ$	$L_L/D$	-3.9 to 1.2
	L/D	3.3 to 7.1
e. Nominal Flap Angle	$\alpha_N$	$0^\circ$ to $45^\circ$
f. Directivity Angle	$\psi$	$10^\circ$ to $180^\circ$
g. Elevation Angle	$\beta_o$	$0^\circ$ to $90^\circ$
h. Microphone Radius	R	3.05 M (10 ft)
i. Geometric-mean-frequencies	f	0.2 to 20 KHz



NOTE:  
DATA WERE CALCULATED USING PRESSURE RATIO  
AND VELOCITY DATA GIVEN IN REF, 28

FIGURE 41.—REFERENCE STATIC TEMPERATURE VS. JET VELOCITY

In order to extend the range of application to hot flows, a static temperature ratio term has been included (see sec. 5.2.2). Noise levels for flight conditions are estimated by relating the overall sound pressure level to the impingement velocity on the flaps and applying the Doppler correction for a random dipole source. Figure 42 shows the variation in the overall sound pressure level with the impingement velocity and flap angle. The approximate 5th to 6th power slope with respect to velocity implies the dominance of the dipole source for the reference configuration, i.e.,  $L/D = 7.1$ ,  $H/D = 1.5$ . At higher jet velocities and/or larger values of  $L/D$  and  $H/D$ , the jet noise component may dominate over the impingement noise. But for the reported test configuration, the impingement noise exceeds the jet noise by 10 to 7 dB for a jet velocity range, 150 to 325 M/S. Hence, the jet noise emitted from a STOL aircraft using the blown-flap during takeoff will contribute typically less than 0.5 dB to the total noise observed in the far field.

In equation form, the overall sound pressure level at the datum condition (free-field, index:  $R = 1 \text{ M}$ ) is given by

$$\begin{aligned} \text{OASPL} = & [F_1(V_F, 90^\circ) + 10 \log_{10} \{ (a + \sin^2 \alpha_N) / b \} ] \\ & + 10 \log_{10} \left[ \left( \frac{T_S}{T_{SR}} \right)^{1.5} \left( \frac{\rho}{\rho_R} \right)^2 \left( \frac{A}{A_R} \right) (1 - M_0 \cos \theta)^{-3} \right] \\ & + F_3(\psi, \alpha_N, V_j) + F_4(\beta, \psi, \alpha_N) + F_5(X_N, \psi) F_6(\alpha_N) \quad (26) \end{aligned}$$

where

$$\begin{aligned} V_F &= \text{flap impingement velocity} \\ &\approx \left| (\hat{V}_J - \hat{V}_O) F_2(L/D) + \hat{V}_O \right| \end{aligned}$$

$F_1$  through  $F_6$  represent the empirical curves shown in figures 42 through 47, respectively

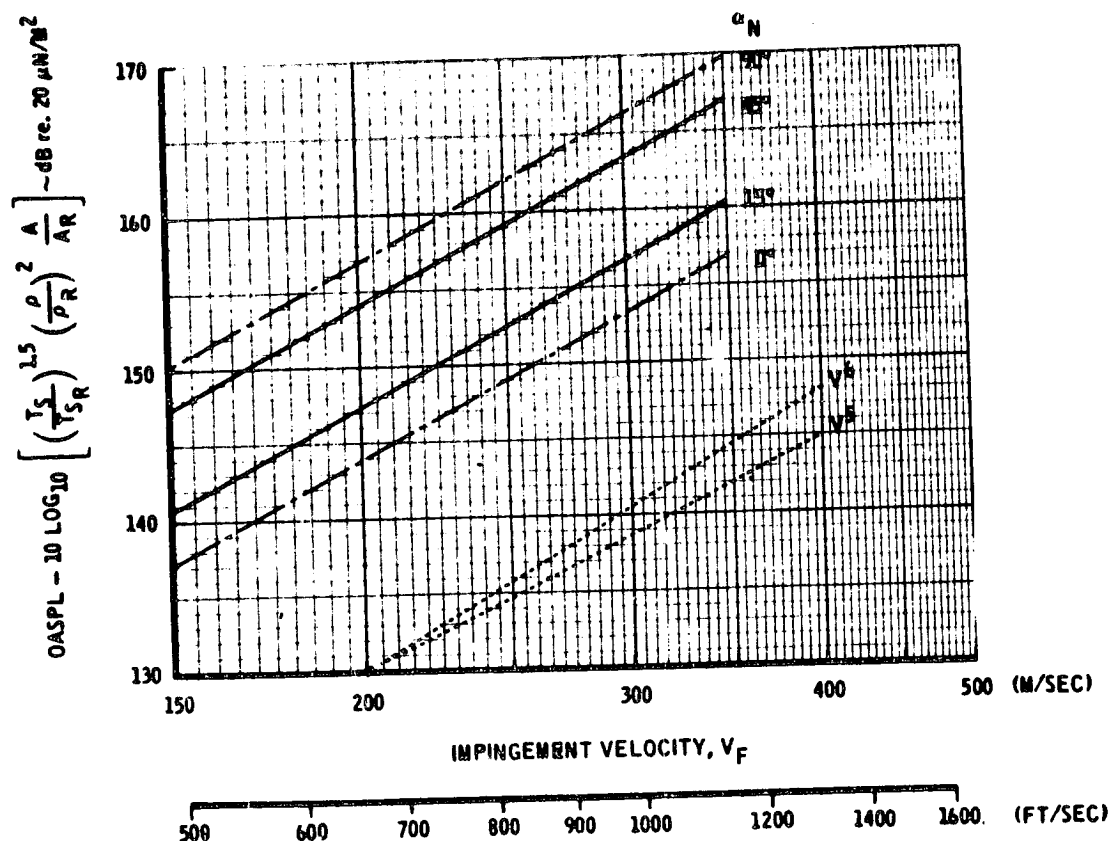
$$\hat{V}_J = \text{centerline jet velocity vector at the nozzle exit}$$

$$\hat{V}_O = \text{velocity vector of the ambient air relative to the nozzle and flap(s)}$$

$$\alpha_N = \text{nominal flap angle (fig. 40)}$$

$$(a, b) = \text{empirical constants (0.0526, 1.0526) chosen to fit the data in figure 42}$$

$$T_S = \text{static temperature of the jet (absolute units)}$$



REFERENCE CONDITIONS:

FREE-FIELD, INDEX ( $R = 1 \text{ M}$ )

STATIC TEST,  $M_0 = 0$

$T_{SR}$  - REF. STATIC TEMPERATURE FROM FIGURE 41.

$\rho_R$  - REFERENCE DENSITY -  $16.02 \text{ KG/M}^3$  ( $1 \text{ LBM/FT}^3$ )

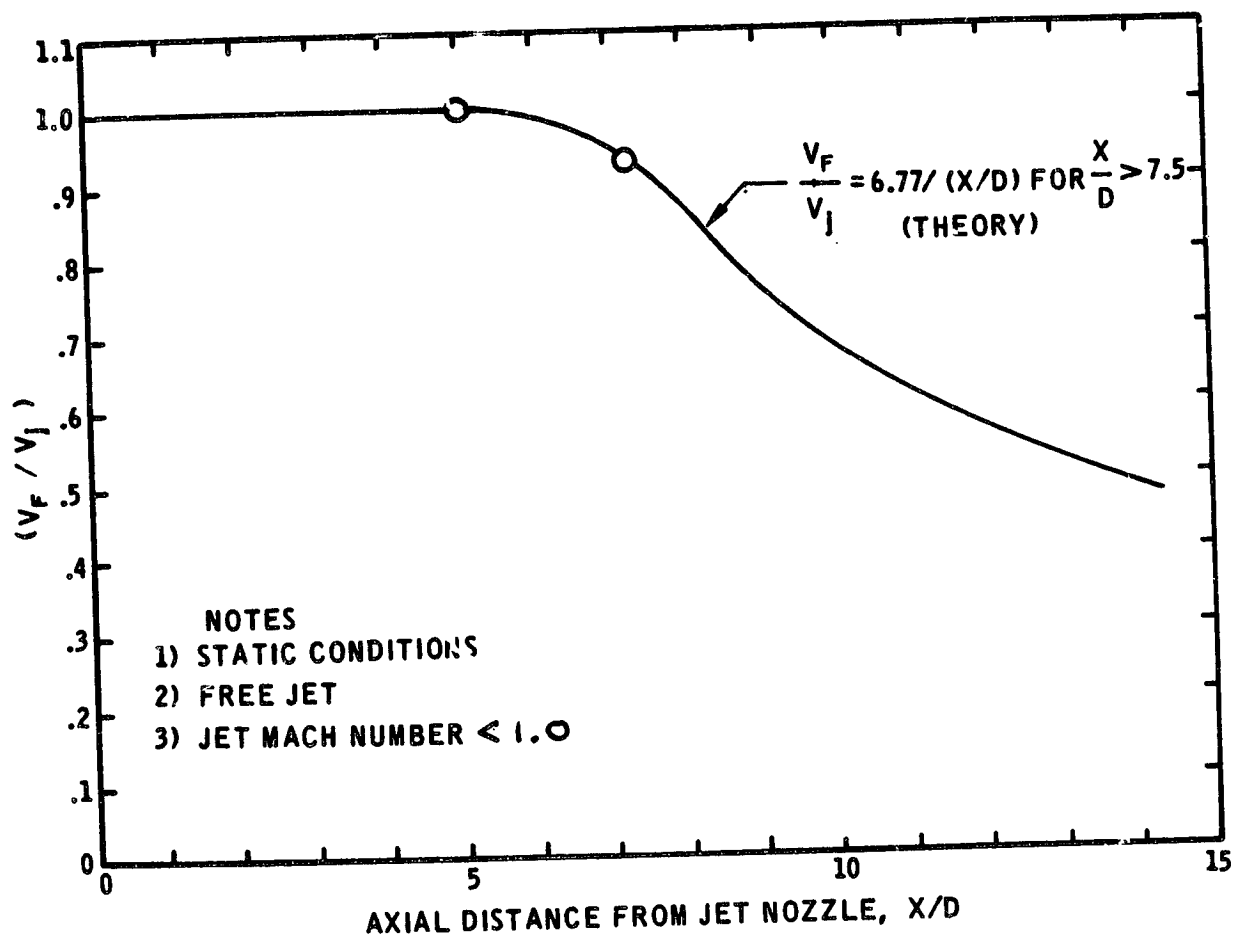
$A_R$  - REFERENCE AREA -  $0.0929 \text{ M}^2$  ( $1 \text{ FT}^2$ )

$\psi = 80^\circ$

$\beta_0 = 90^\circ$

$(L/D) (H/D) = 10.65$

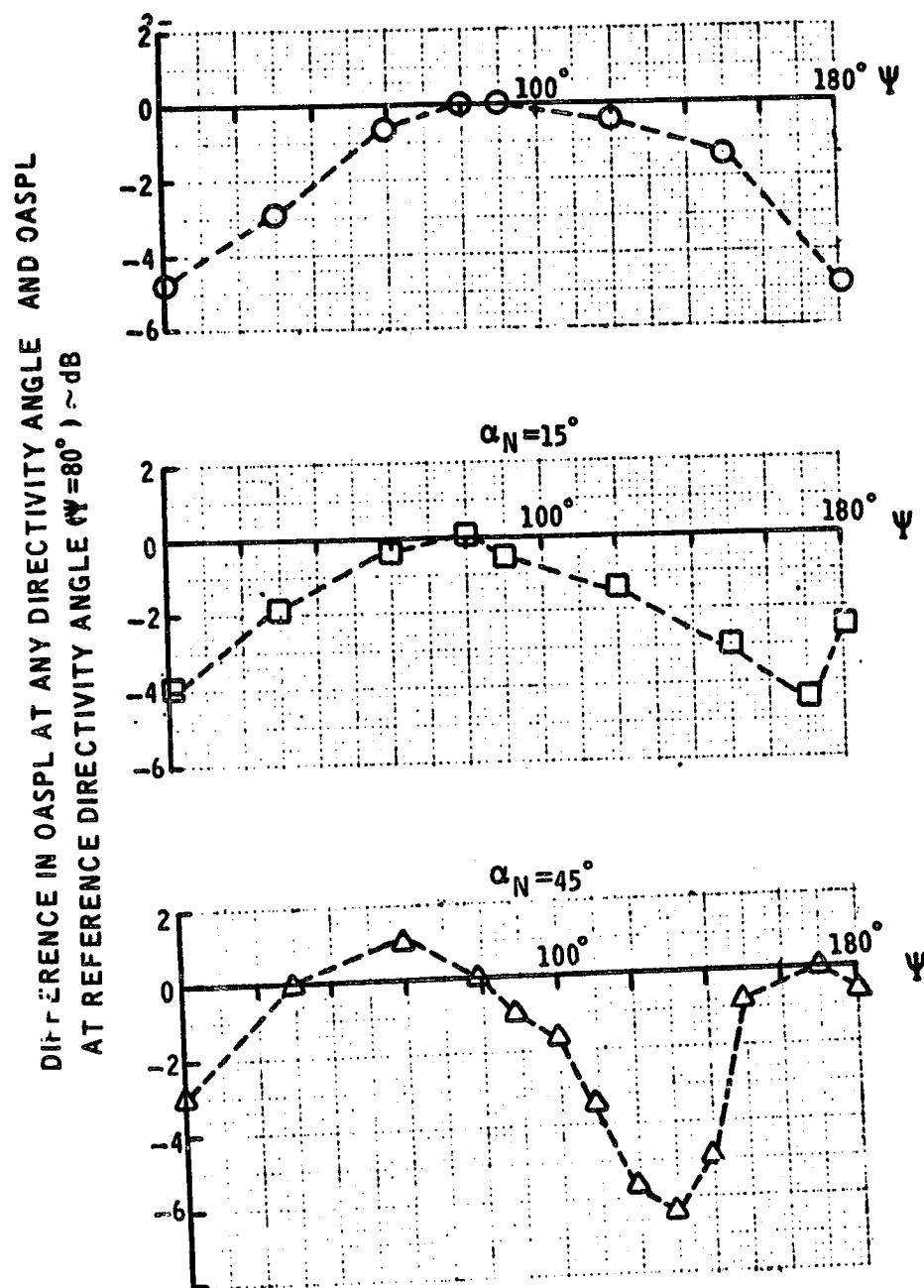
FIGURE 42.-OVERALL SOUND PRESSURE LEVEL VERSUS IMPINGEMENT VELOCITY



$V_F$  = CENTERLINE VELOCITY AT AXIAL DISTANCE (X) FROM NOZZLE EXIT  
 $V_J$  = CENTERLINE VELOCITY AT NOZZLE EXIT  
 $D$  = NOZZLE DIAMETER

FIGURE 43.—VARIATION OF EXHAUST JET VELOCITY WITH AXIAL DISTANCE FROM NOZZLE EXIT

NOMINAL FLAP ANGLE  $\alpha_N = 0^\circ$



a)  $V_j = 190$  M/S (624 FPS)

FIGURE 44.—CHANGE IN OVERALL SPL WITH DIRECTIVITY ANGLE RELATIVE TO  $\psi = 80^\circ$



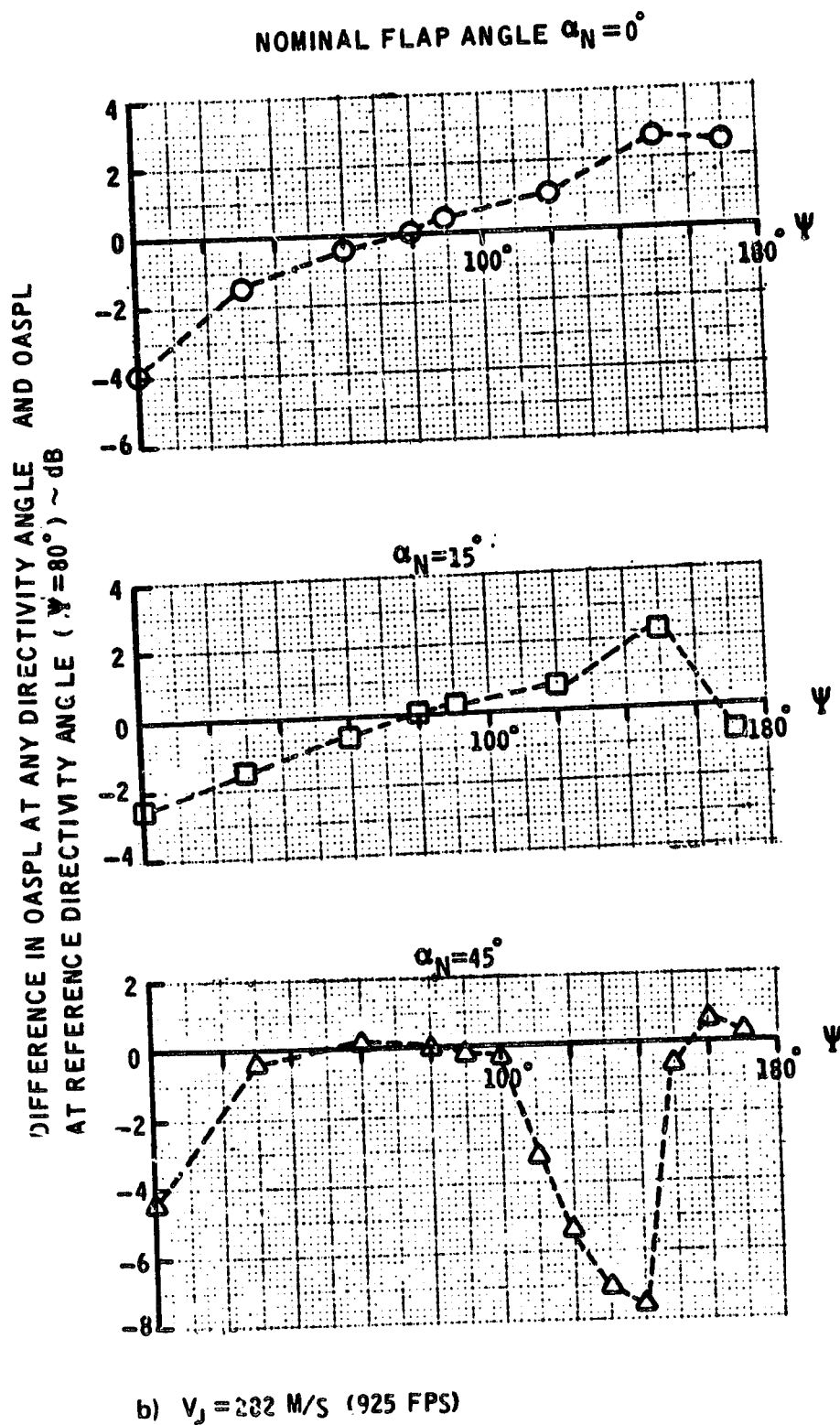
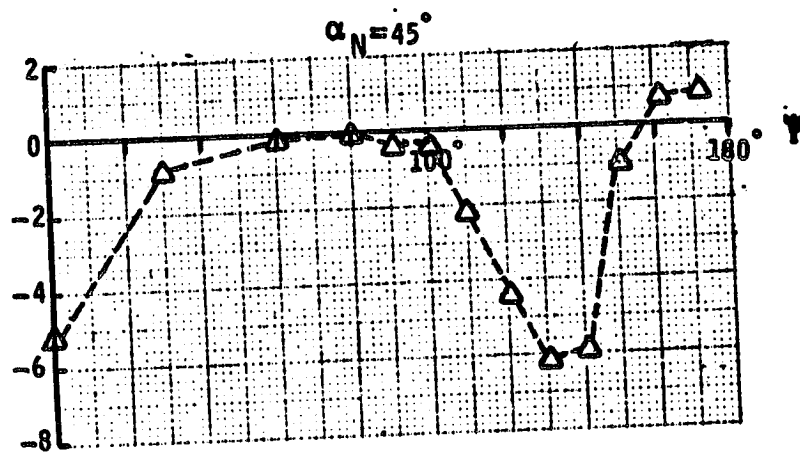
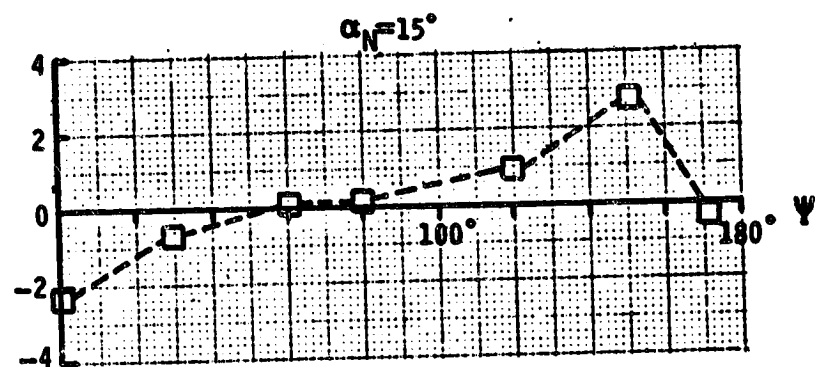
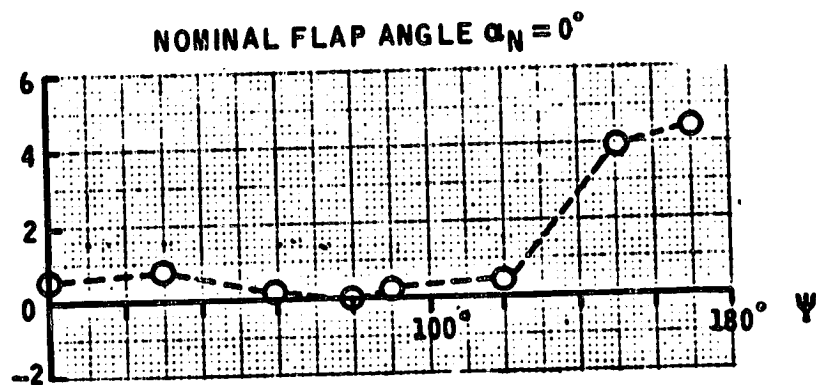


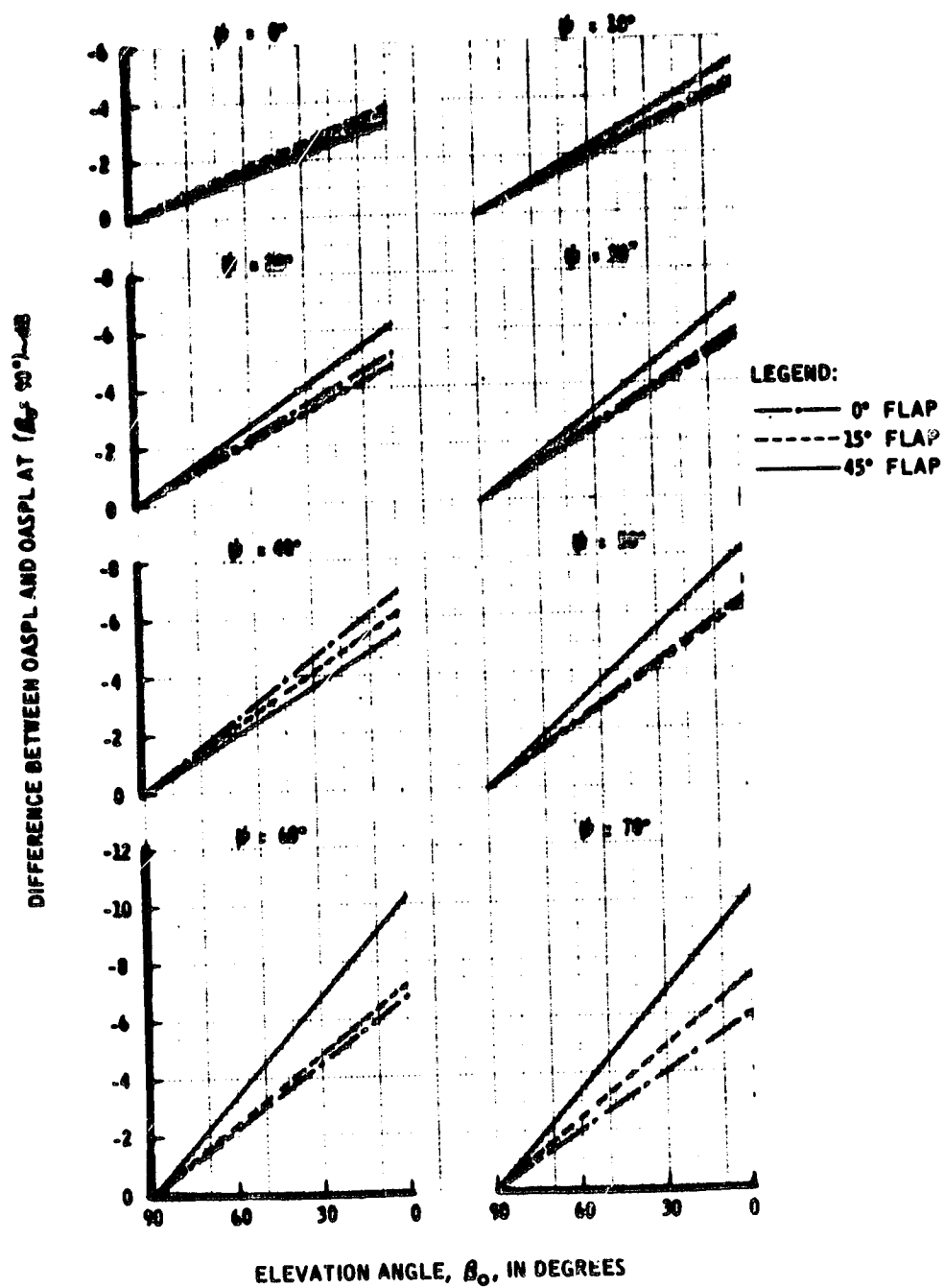
FIGURE 44.—CONTINUED

DIFFERENCE IN OASPL AT ANY DIRECTIONAL ANGLE  
AT REFERENCE DIRECTIONAL ANGLE ( $\Psi = 80^\circ$ ) ~dB



c)  $V_j = 343 \text{ M/S}$  (1125 FPS)

FIGURE 44.-CONCLUDED



a)  $\psi$  = DIRECTIVITY ANGLE RE, INLET =  $0^\circ$  TO  $70^\circ$

FIGURE 45.—VARIATION IN OASPL WITH ELEVATION ANGLE

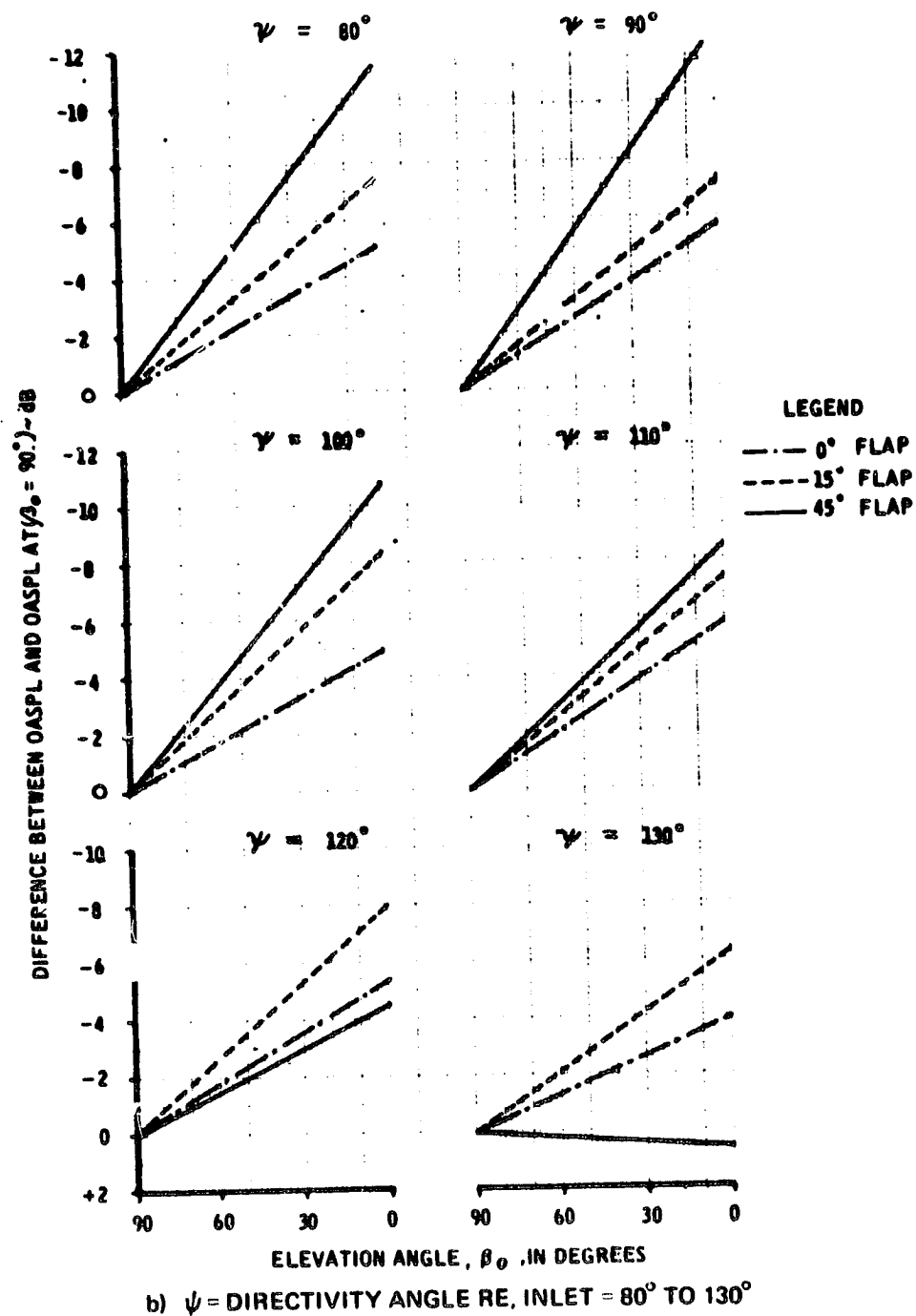
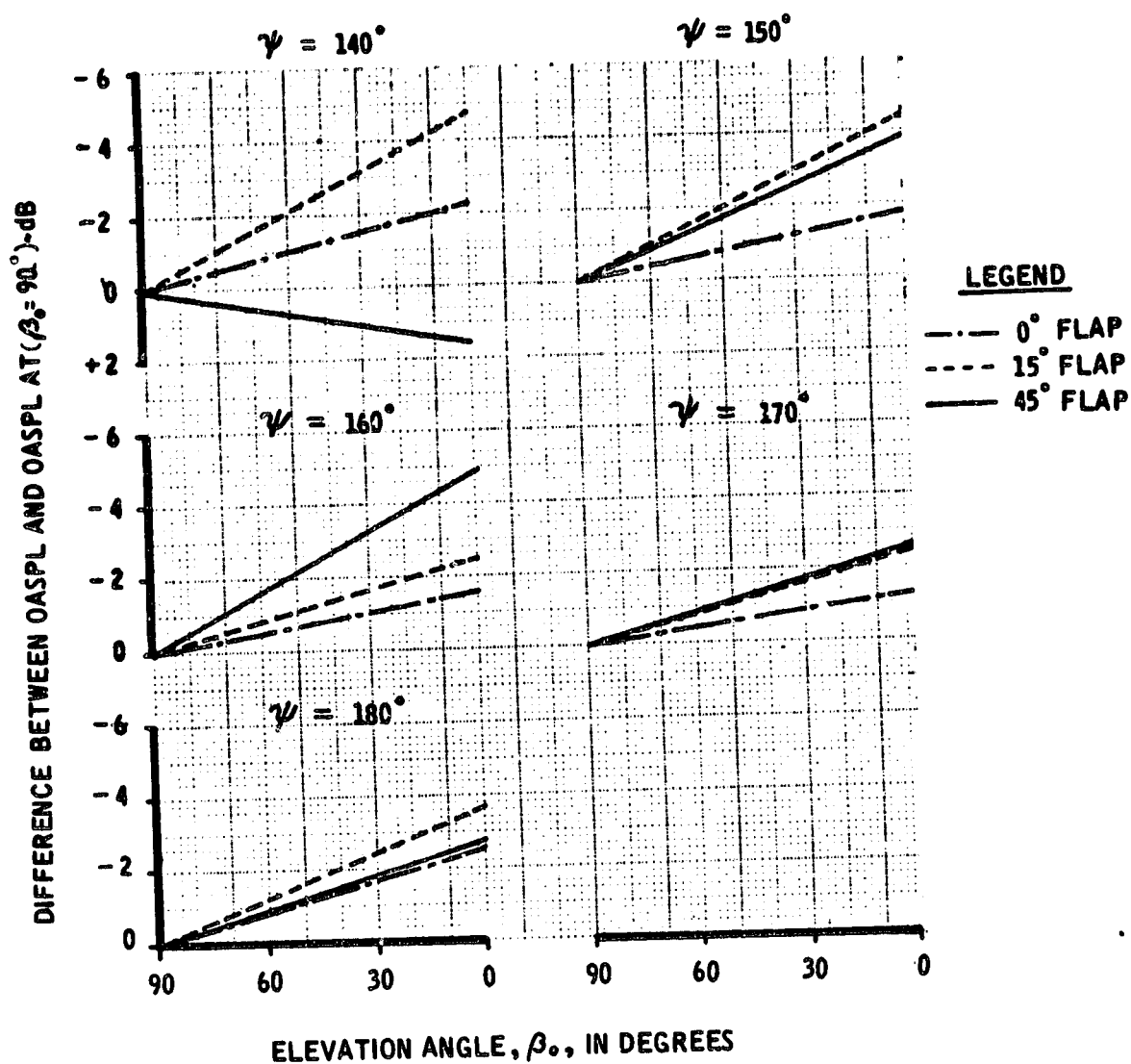


FIGURE 45.—CONTINUED



c)  $\psi$  = DIRECTIVITY ANGLE RE, INLET =  $140^\circ$  TO  $180^\circ$

FIGURE 45.—CONCLUDED

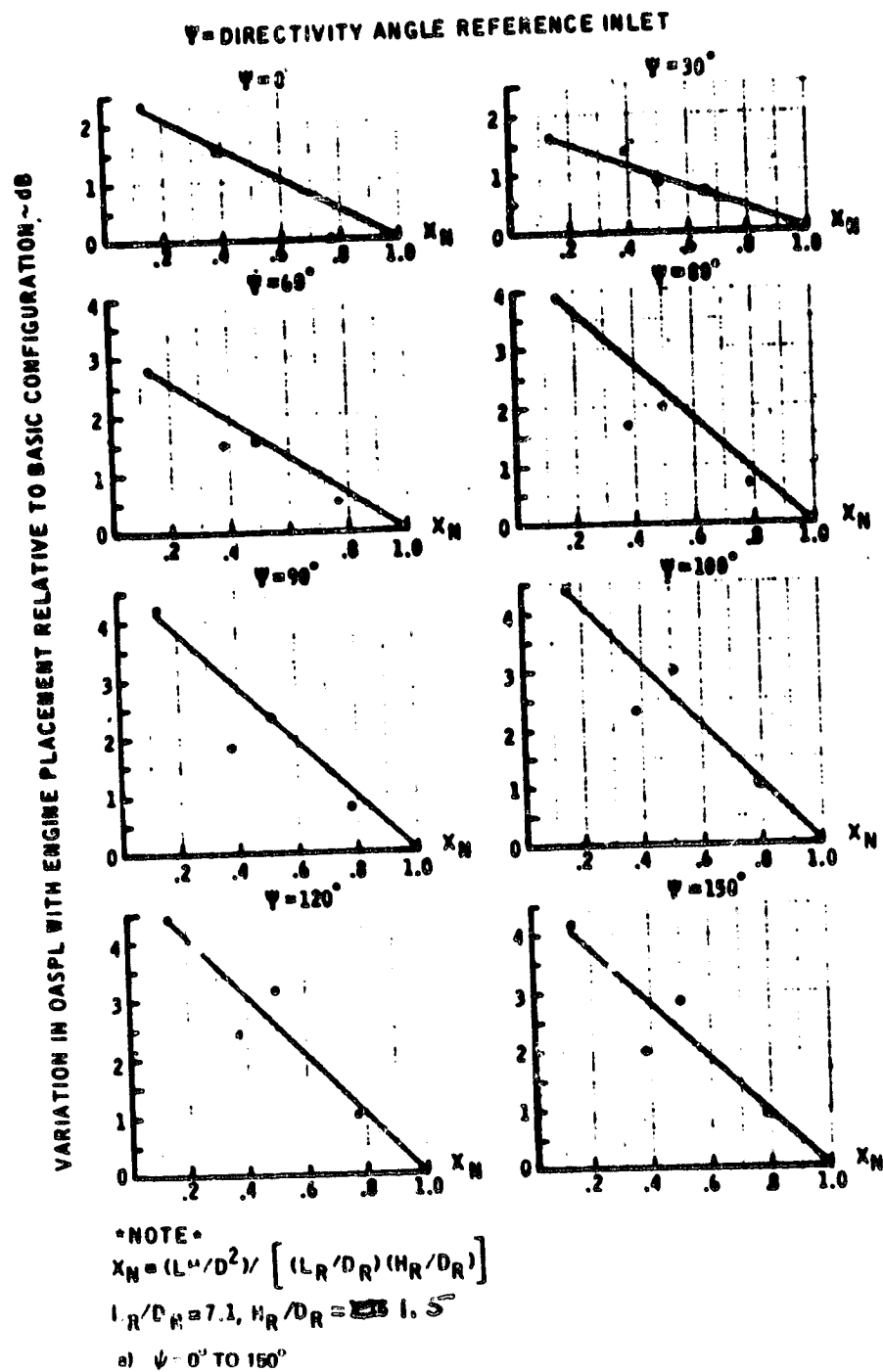
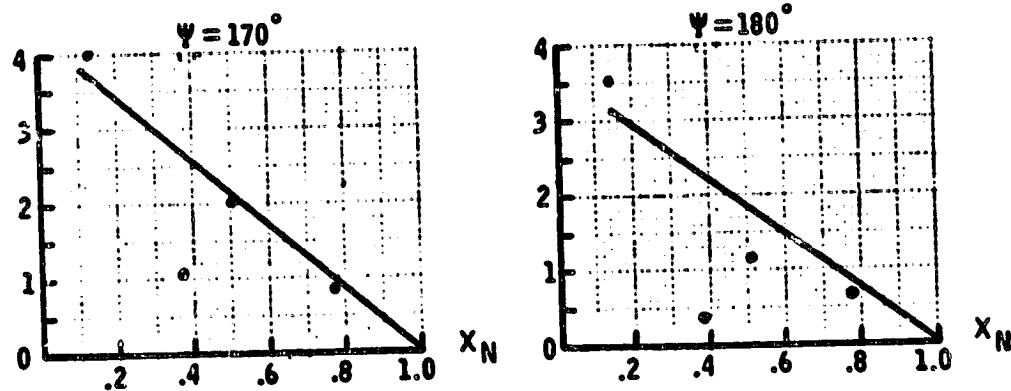


FIGURE 46.—CHANGE IN OVERALL SPL RELATIVE TO BASIC CONFIGURATION  
FOR NOMINAL FLAP CONDITION  $\alpha_N = 45^\circ$

VARIATION IN OASPL WITH ENGINE PLACEMENT  
RELATIVE TO BASIC CONFIGURATION ~dB



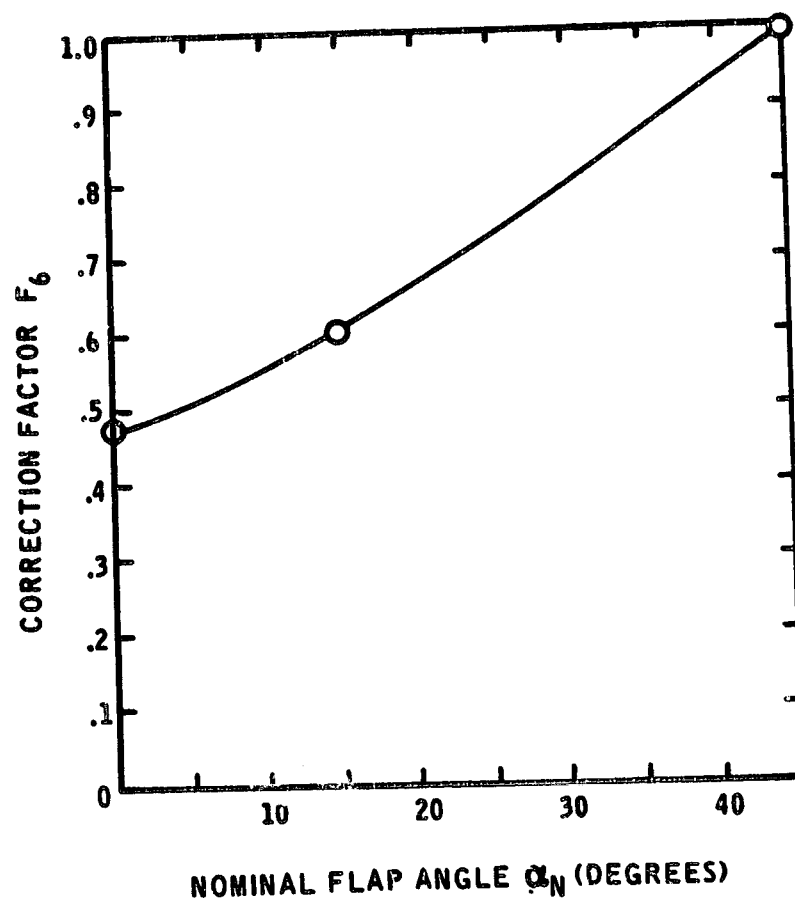
NOTE

$$X_N = (LH/D^2) / [(L_R/D_R)(H_R/D_R)]$$

$$L_R/D_R = 7.1, H_R/D_R = 1.5$$

b)  $\psi = 170^\circ$  AND  $180^\circ$

FIGURE 46.-CONCLUDED



NOTE

ENGINE PLACEMENT EFFECT =  $F_5(X_N, \Psi) F_6(\alpha_N)$

SEE FIGURE 406 FOR  $F_5(X_N, \Psi)$

FIGURE 47.—FLAP ANGLE CORRECTION TO ENGINE PLACEMENT EFFECT



- $T_{SR}$  = reference static temperature (absolute units) from figure 41  
 $\rho$  = density of the jet  
 $\rho_R$  = reference density = 16.02 KG/M<sup>3</sup> (1 lbm/ft<sup>3</sup>)  
 $A$  = discharge area of nozzle  
 $A_R$  = reference area = 0.0929 M<sup>2</sup> (1 ft<sup>2</sup>)  
 $M_0$  = aircraft Mach number  
 $\xi$  = angle between direction of aircraft motion and sound propagation path  
 $\psi$  = directivity angle relative to engine inlet  
 $\beta_0$  = elevation angle (figs. 4 and 39)  
 $X_N$  = dimensionless engine location when  $\alpha_N = 45^\circ$   
 $\quad = (L/D)(H/D)/\text{fig. 10.65}$   
 $D$  = nozzle diameter. If the nozzle is not circular, use the hydraulic diameter,  $4A/\text{perimeter}$ .

The overall SPL for N identical blown-flap configurations is estimated by adding the multi-engine correction, equation (2B) in section 5.1.1.6, to the result from equation (26) above. The 1/3 octave band spectrum shape is shown in figure 48. Using this curve, the sound pressure level spectrum is defined as

$$SPL(f) \approx OASPL + F_7(f/f_0) \quad (27)$$

where

$F_7$  is an empirically derived curve (fig. 48)

$$\begin{aligned}
 f_0 &= \text{the characteristic Strouhal frequency in Hz} \\
 &\approx (V_F/D) \sqrt{0.5(1 + \sin^2 \alpha_N)/(1 - M_0 \cos \xi)}.
 \end{aligned}$$

• SPL(f) - 1/3 OCTAVE BAND SOUND PRESSURE LEVEL AT CENTER FREQUENCY f - (HZ)

• OASPL - OVERALL SOUND PRESSURE LEVEL

• f<sub>0</sub> - CHARACTERISTIC FREQUENCY - WZ

$$= \frac{V_f}{D} \sqrt{\frac{1 + \sin^2 \alpha_N}{2}} \left( 1 - M_0 \cos \xi \right)$$

WHERE:

• V<sub>f</sub> - IMPINGEMENT VELOCITY

• D - HYDRAULIC DIAMETER OF NOZZLE

• α<sub>N</sub> - NOMINAL FLAP ANGLE

• M<sub>0</sub> - AIRPLANE MACH NUMBER

• ξ - ANGLE BETWEEN DIRECTION OF AIRCRAFT  
MOTION AND PROPAGATION PATH

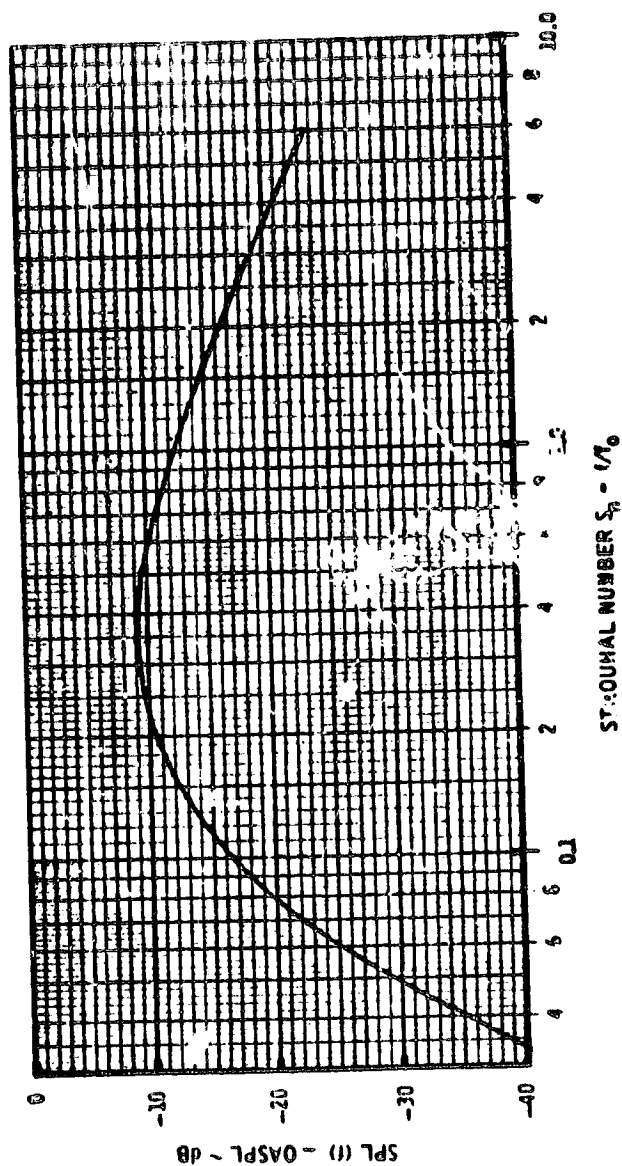


FIGURE 48. - 1/3 OCTAVE BAND SPECTRUM SHAPE

The factor,  $\sqrt{0.5 (1 + \sin^2 \alpha_N)}$ , results from the change in the hydraulic diameter of the flow projection on the flap(s) as the flap angle,  $\alpha_N$ , is varied. This expression assumes that the impingement area is an ellipse for the discharge from a circular nozzle. In reality, the impingement area is a hyperbolic section, and the resulting formula is considerably more complicated. However, the scatter in the data (ref. 28), does not merit such refinement. The term,  $(1 - M_O \cos \xi)$ , represents the Doppler shift for an aircraft in flight.

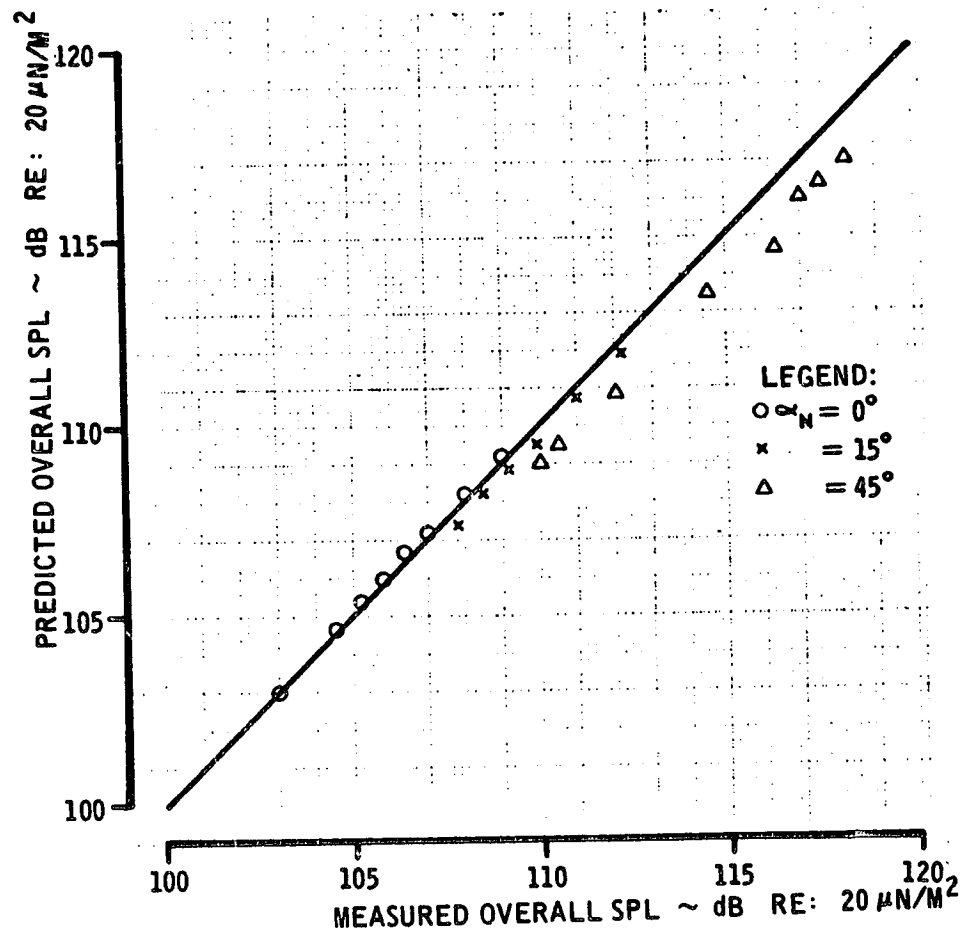
A few concluding remarks about this procedure are:

- a) The data analysis would be simplified if the reference coordinate system was relative to the flap(s) instead of the centerline of the nozzle. This would permit the same data to be represented by fewer curves.
- b) Additional hot flow tests are required to verify the methods used to extrapolate the test (cold flow) data (ref. 28) to that applying to real engines.
- c) For cold flow models, it is expected that the procedure presented above will predict the OASPL within  $\pm 3$  dB provided the jet Mach number is less than one.
- d) A comparison of predicted values with a set of test data taken from reference 28 is shown in figures 49 and 50.

### 5.2.3 Core and Turbine Noise

The goal of reducing subsonic aircraft noise has led to the consideration of engines with lower jet velocities when compared to turbojets. The SAE jet noise procedure (ref. 7) when applied to these newer engines results in lower levels than that observed—even when efforts are made to eliminate the fan noise component. Recent jet model tests (ref. 20), in which care was taken to keep upstream noise to a minimum, have shown that a trend similar to that given by ref. 7 is valid at velocities less than 305 M/S (1000 fps). This observation became more apparent after appropriate modifications to the density correction exponent or the inclusion of a  $(\rho^2 T_S^{1.5})$  factor was used to collapse the model data (sec. 5.2.2).

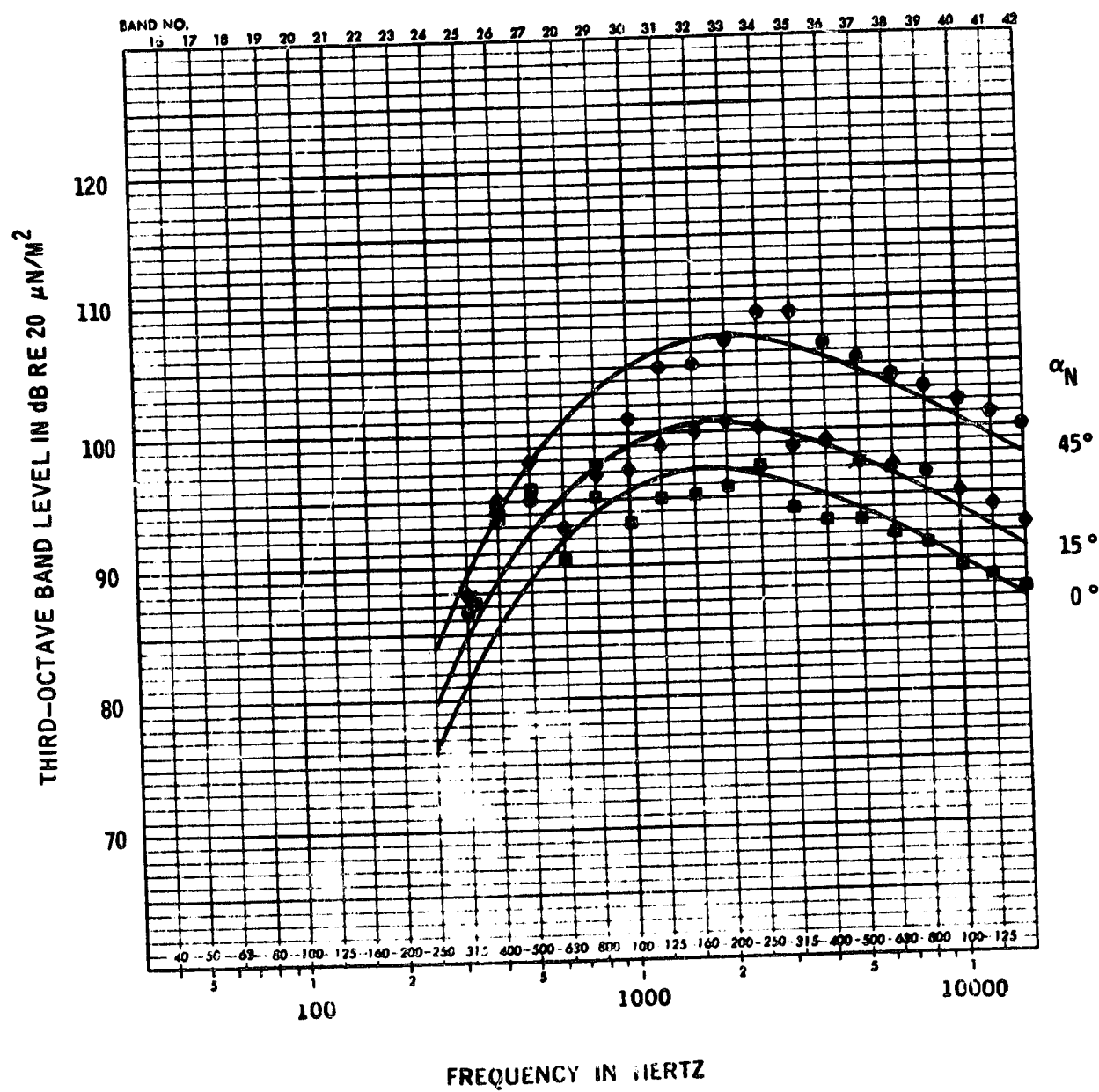
Full scale engine tests at low power settings, however, exhibit a significantly different trend at jet velocities below 305 M/S than observed from the jet model tests. Apparently there are additional noise sources which produce more low frequency noise than is predicted for jet noise. Also, discrete tones due to the last turbine stage have been identified. These sources are believed to be generated upstream from the nozzle exit and can be attributed to various items:



NOTES:

- 1) PRESSURE RATIO = 1.7, TOTAL TEMPERATURE = 283° K
- 2) MEASUREMENT RADIUS = 3.05 M
- 3) ELEVATION ANGLE  $\beta_0 = 90^\circ$
- 4)  $L/D = 7.1$ ,  $H/D = 1.5$

FIGURE 49.—PREDICTED VERSUS MEASURED OVERALL  
SPL FOR BLOWN-FLAP MODEL



#### LEGEND

— PREDICTED

MEASURED

●  $\alpha_N = 45^\circ$

◆  $\alpha_N = 15^\circ$

■  $\alpha_N = 0^\circ$

#### CONDITIONS

$P_T/P_{S0} = 1.7$

$\psi = 80^\circ$

$\beta_o = 90^\circ$

FIGURE 50.—SAMPLE FLAP IMPINGEMENT NOISE PREDICTION

- a) Combustion
- b) Static pressure fluctuations for flow through the turbine rotors
- c) Turbulent flow impinging on the turbine rotors and stators
- d) Turbulent flow along the inner surface of the engine and nozzle walls
- e) Separated flow on the tailpipe cone and/or turbine exit struts

Of the items mentioned, those associated with the turbine produce high frequency, broadband and tone noise. The low frequency broadband noise is probably due to combustion. For the purpose of noise prediction two components will be identified—(1) core noise for the low frequency and (2) turbine noise for the high frequency contributors.

The present noise prediction procedures for these components are based on data provided by various engine manufacturers, research institutes, and NASA. Most of the data is proprietary and thus little substantiating data can be presented at this time to justify the procedures. In fact, the procedures are not all that good; the tolerance is approximately  $\pm 7$  PNdB. A more detailed analysis of available engine data could result in a better core noise prediction procedure. Particular attention should be given to the progress made by various governmental contracts with industry, e.g., GE/FAA.

#### 5.2.3.1 Core Noise Prediction

The following prediction procedure for core noise has been developed from full scale engine acoustic measurements (primarily from high bypass ratio turbofans). The noise source is assumed to be a monopole. The strength of the source is related to the engine's combustor and turbine inlet and exit parameters. Theoretically, a monopole source has a uniform omni-directional radiation pattern, but far-field engine data indicates that the sound is attenuated in the inlet quadrant (see fig. 51). The reasons for this attenuation are probably due to a combination of effects: (1) the source is generated inside a duct, (2) convection, and (3) refraction. In mathematical terms, the overall sound pressure level for a single engine at the free-field, index condition is given by

$$\begin{aligned} \text{OASPL} = 10 \log_{10} & \left[ \left( \frac{\dot{m}_c}{\dot{m}_R} \right) \left( \frac{T_{TX}}{T_{SR}} \right)^2 \left( \frac{P_{TI}}{P_{TX}} \right)^3 (1 - M_0 \cos \xi)^{-2} \right] \\ & + F_1(\psi) + 76 + a + K \end{aligned} \quad (28)$$

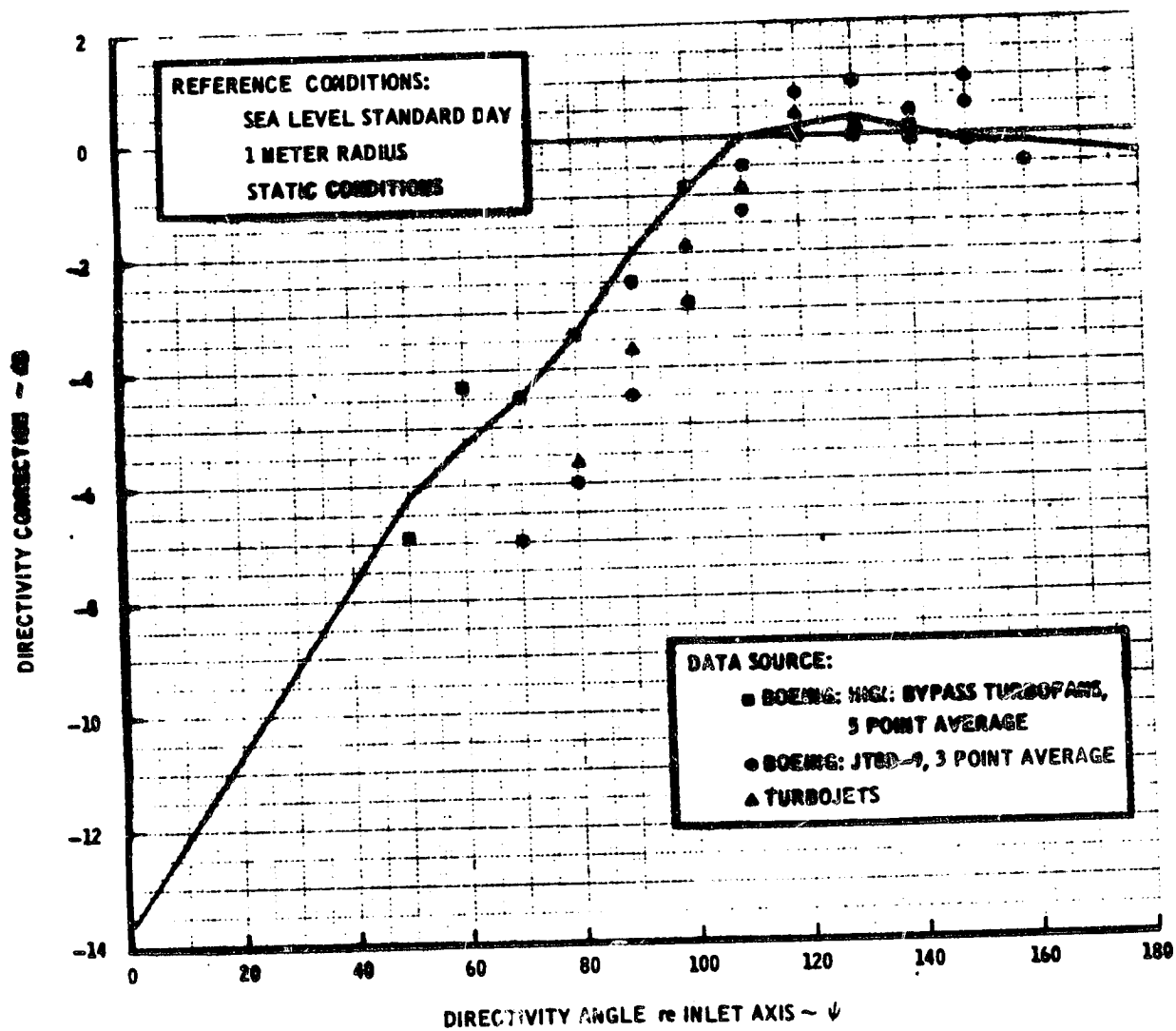


FIGURE 51.—CORE NOISE DIRECTIVITY PATTERN

where

$\dot{m}_c$  = combustor corrected mass flow

$$= \dot{m} \sqrt{T_{TX}/T_{SR}} / (P_{TC}/P_{SR})$$

$\dot{m}$  = primary mass flow

$\dot{m}_R$  = reference mass flow = 0.4536 KG/S (1 lbm/sec)

$T_{TX}$  = combustor exit total temperature (absolute units)

$T_{SR}$  = reference temperature = 288°K (518.7°R)

$P_{TI}$  = turbine inlet total pressure (absolute units)

$P_{TX}$  = turbine exit total pressure (absolute units)

$P_{TC}$  = combustor total pressure (absolute units)

$P_{SR}$  = reference pressure = 1 S. ATM. (2116 psfa)

$M_O$  = aircraft Mach number

$\xi$  = angle between direction of aircraft motion and sound propagation path

$\psi$  = directivity angle re inlet axis

$F_1$  = empirical curve (fig. 51)

$a$  = correction for the type of burner

= 0 for annular types

= +9 for can types, i.e., JT8D

$K$  = specific engine correction (see table 10)

The use of multiple engines is to be estimated by adding equation (2B) in section 5.1.1.6 to equation (28) above.



**TABLE 10.—SPECIFIC ENGINE CORRECTION**

<u>TYPE OF ENGINE</u>	<u>K</u>
CF6-6	-1
JT8D-9	0
JT8D-1	-3.5
JT9D-7	+2
RB.211-22B	+4
RB.211-22B (With Revised Strut Design)	+1
TF34-GE-2	-2
Paper Engine Studies	0

Very little data are available concerning the core noise spectrum shape. Essentially, no useful spectral information can be deduced from conventional engine measurements (without a significant amount of work) due to the ground reflections at low frequencies. Presently, the SAE flight Strouhal spectrum is used, since core noise has been confused with jet noise in the past and is assumed broadband in nature. The 1/3 octave sound pressure level spectrum is defined as

$$\text{SPL}(f) = \text{OASPL} + F_2(f / f_0) \quad (29)$$

where

$F_2$  is the flight Strouhal spectrum shape (fig. 20b)

$f_0$  = characteristic frequency in Hz

$$= b / \left[ \sqrt{\dot{m}_c} (1 - M_0 \cos \xi) \right]$$

$$b = 1246 \text{ Hz} - (\text{KG/sec})^{0.5} = 1850 \text{ Hz} - (\text{lbm/sec})^{0.5}$$

### 5.2.3.2 Turbine Noise Prediction

The turbine noise prediction procedure considers two noise components: broadband and discrete tone. Both components have been related to the relative tip velocity of the turbine's last stage, the primary mass flow, and local speed of sound at the turbine exit. The effects of stator/rotor spacing on the discrete tone levels is also considered.

It has been assumed that both components have spectra shapes that normalize with respect to the fundamental blade passage frequency of the last stage of the turbine. The predicted spectra are given in terms of 1/3 octave band levels (dB re 20  $\mu\text{N/M}^2$ ) at the free-field, index ( $R = 1 \text{ M}$ ) condition.

**Broadband component.** - The relation for the peak 1/3 octave band level at a radius of 45.7 M (150 ft) from the source is

$$L_0 \approx 10 \log_{10} \left[ \left( \frac{V_{TR} C_R}{V_R C_L} \right)^3 \left( \frac{\dot{m}}{\dot{m}_R} \right) (1 - M_0 \cos \xi)^{-4} \right] \quad (30)$$

$$+ F_1(\psi) - 10$$

where

$V_{TR}$  = Relative tip speed of last rotor of the turbine. If  $V_{TR}$  is unknown, use 0.7 times the tip speed.

$V_R$  = Reference velocity, 0.305 M/S (1 fps)

$\dot{m}$  = Primary mass flow

$\dot{m}_R$  = Reference mass flow, 0.4536 KG/S (1 lbm/sec)

$C_L$  = Speed of sound at the turbine exit. If  $C_L$  is unknown, use  
 $C_L \approx a \sqrt{T_{T7}}$  with  
 $a = 19.8 \text{ M/S per } (^{\circ}\text{K})^{0.5}$   
 $= 48.5 \text{ fps per } (^{\circ}\text{R})^{0.5}$

$T_{T7}$  = Turbine exit total temperature

$C_R$  = Reference speed of sound, 340.3 M/S (1116 fps)

$M_O$  = Aircraft Mach number

$\xi$  = Angle between direction of aircraft motion and sound propagation path

$\psi$  = Directivity angle re. inlet axis

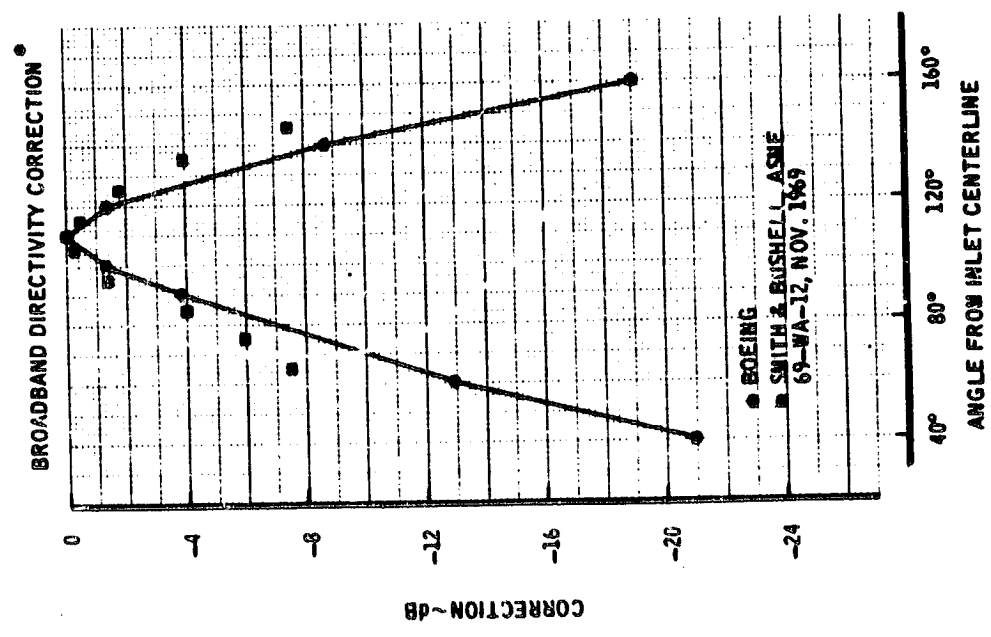
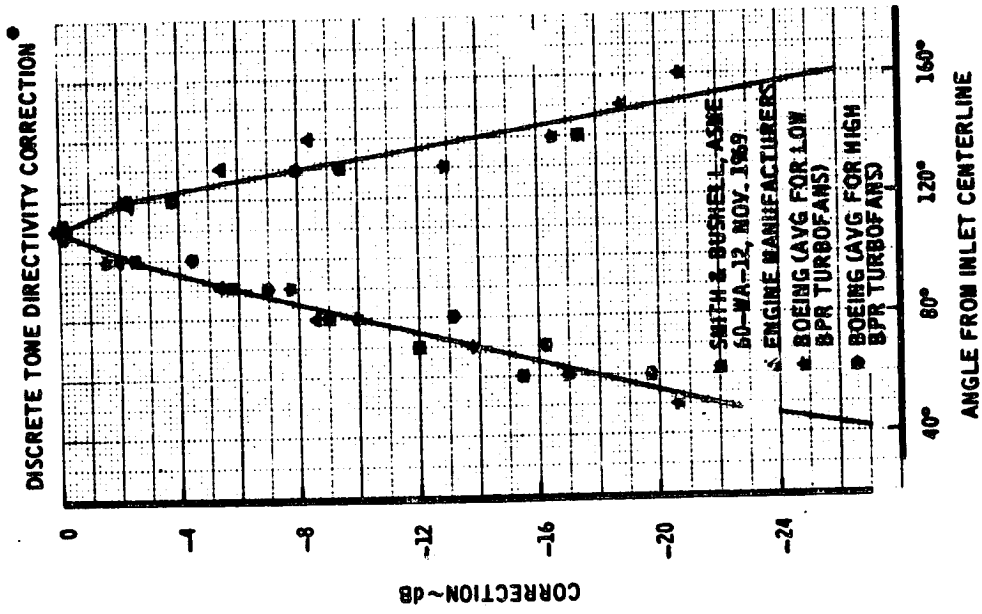
$F_1$  = Empirical curve shown in figure 52

Sample data and predicted results are shown in figure 53. The 1/3 octave band spectrum shape is shown in figure 54. The sound pressure level spectrum is defined as

$$\text{SPL}(f) \approx L_0 + F_2(f/f_0) \quad (31)$$

where

$f_0$  = fundamental blade passage frequency of the last rotor stage of the turbine  
 $= B \dot{\theta} / [60 (1 - M_O \cos \xi)]$



• DATA HAS BEEN AVERAGED AND ADJUSTED TO PEAK AT  $\psi = 110$

FIGURE 52. - TURBINE NOISE DIRECTIVITY CORRECTIONS

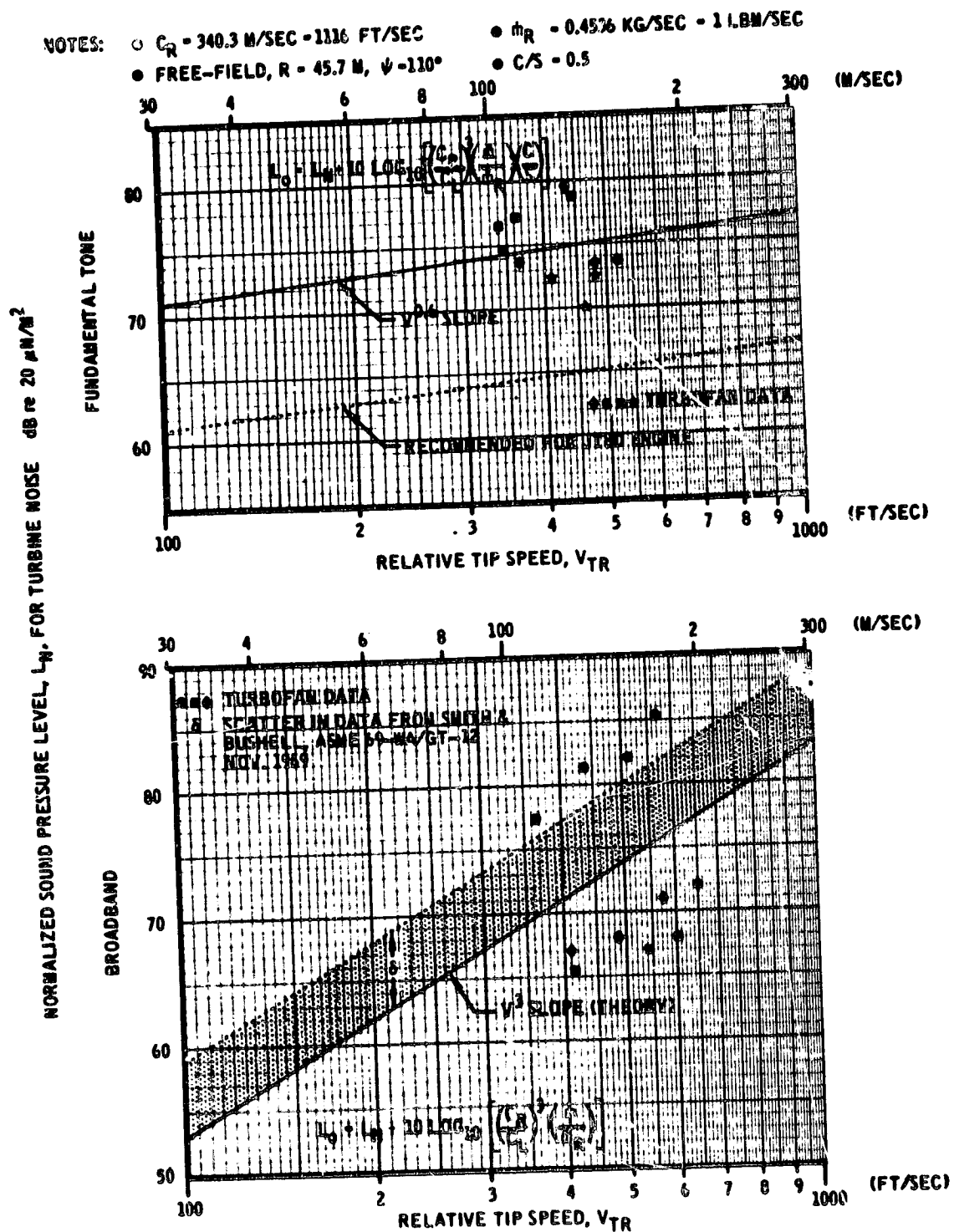


FIGURE 53.—CHARACTERISTIC TURBINE NOISE LEVELS VS RELATIVE TIP SPEED

$F_2$  = Function shown in figure 54

$B$  = Number blades for the last rotor stage of the turbine

$\dot{\theta}$  = Shaft speed in rpm

The use of multiple engines requires the correction, eq. (2B) in sec. 5.1.1.6, and the spectrum is extrapolated to a radius of one meter using

$$\left. \text{SPL}(f) \right|_{1 \text{ M}} = \left. \text{SPL}(f) \right|_{45.7 \text{ M}} + 33.2 + \Delta \text{dB}(f) \quad \text{Table 4} \quad (32)$$

*Discrete tone component.*—The discrete tone component of turbine noise is defined in a manner similar to that for broadband noise. The level of the fundamental tone at 45.7 M (150 ft) from the source is given by

$$L_o \approx 10 \log_{10} \left[ \left( \frac{V_{TR}}{V_R} \right)^{0.6} \left( \frac{C_R}{C_L} \right)^3 \left( \frac{\dot{m}}{\dot{m}_R} \right) \left( \frac{C}{S} \right) (1 - M_o \cos \xi)^{-4} \right] \quad (33)$$

$$+ F_1(\psi) + 56 + K$$

where

$C/S$  = stator/rotor spacing shown in figure 55

$K$  = correction for turbofans with a primary nozzle exit plane upstream from the secondary nozzle exit plane, i.e., the JT8D

$\approx -10$  dB for the JT8D

$\approx 0$  dB for dual exhaust systems with co-planar exits, or turbojets

The frequency of the fundamental tone corresponds to the blade passage frequency,  $f_o$ , above. The higher harmonics are assumed to fall off at a -10 dB slope as shown in figure 54. A review of available test data indicates that the second harmonic ranges from 8 to 20 dB below the fundamental. In some cases, the harmonics for the second to the last turbine stage were dominate. The lack of adequate information precluded further study of the phenomenon.

In the computer program, the tones are added to the broadband spectrum (eq. (31) above) before the corrections for the use of multiple engines and index ( $R = 1 \text{ M}$ ) conditions are applied. After the corrections are made, the resulting spectrum represents the turbine noise at the free-field, index condition.

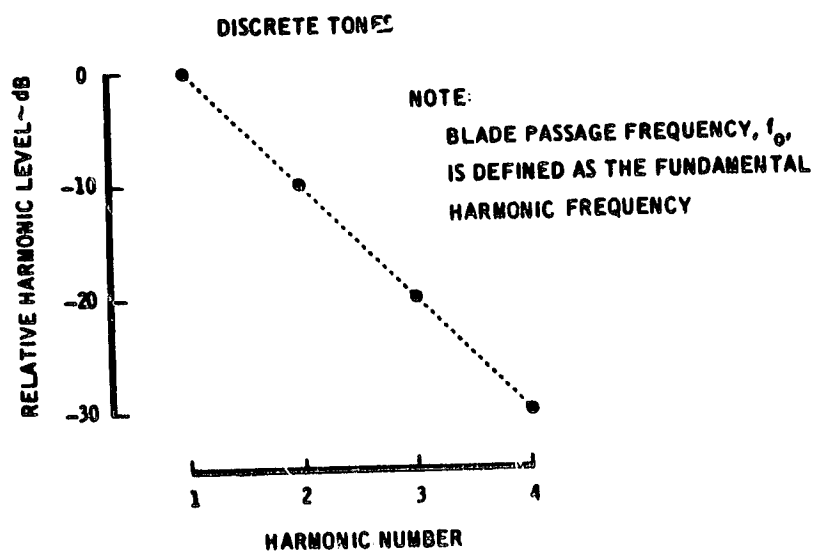
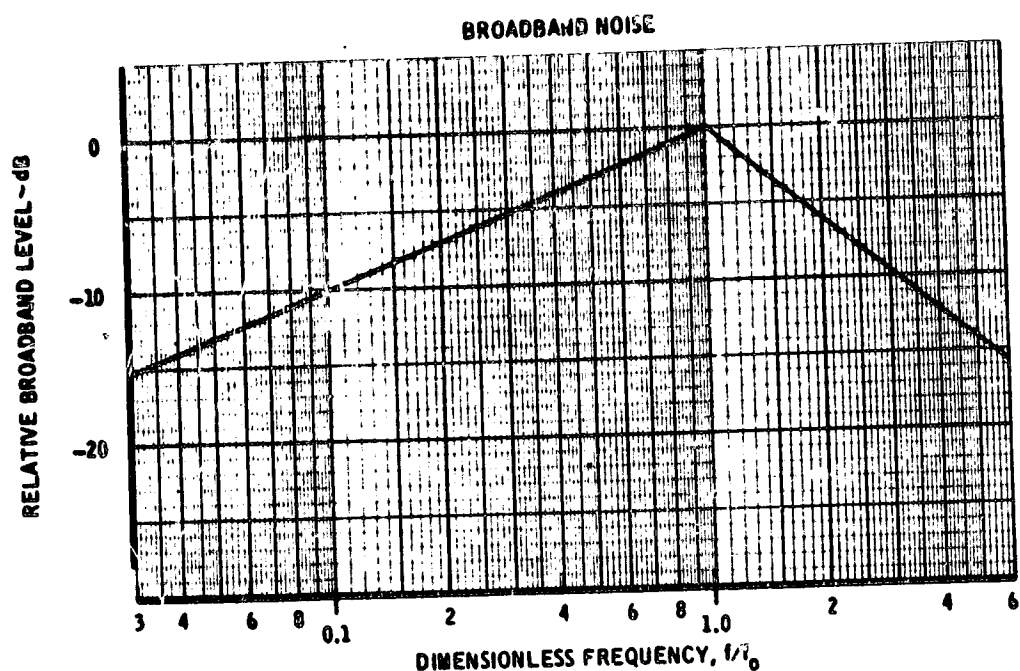
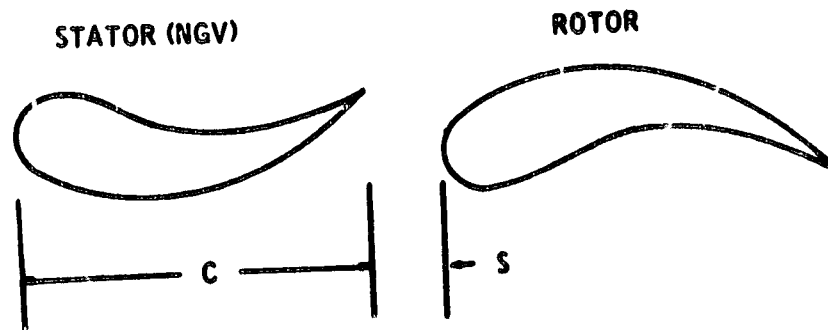


**FIGURE 54.—TURBINE NOISE SPECTRUM SHAPE**



STATOR ROTOR SPACING EQUALS  $C / S$

**FIGURE 55.—DEFINITION OF STATOR-ROTOR SPACING FOR TURBINES**



#### 5.2.4 Compressor or Fan Noise

This section deals with the prediction procedures for 1/3 octave band noise due to rotating compressor and fan blades. The procedures predict the noise spectra for the free-field, index conditions discussed in section 5.1.1.2. The methods given are applicable to turbojet compressors, single or multistage turbofans with or without inlet guide vanes, and lift fans for STOL aircraft. It is assumed that the inlets are the "fixed-inlet type," i.e., no blow-in-doors and the blade/vane number ratios for the fans or compressors are optimum for minimum noise.

The empirical noise prediction procedures discussed in this section were derived from JT9D and JT3D static engine tests. The data was analyzed in terms of the following noise components:

- a) Inlet fan or compressor noise emitted from the inlet duct
  - 1) Broadband noise
  - 2) Discrete tone noise
  - 3) Combination tone noise (buzz-saw)
- b) Fan discharge noise emitted from the fan discharge duct
  - 1) Broadband noise
  - 2) Discrete tone noise

The computer program predicts each of the subcomponent (broadband, discrete tone, and combination tone) noise for items a) and b) above and the spectrum levels are combined on an energy basis to form a single spectrum. For an engine with more than one fan stage, each stage is treated as an independent source and the sound energy produced by each stage is accumulated accordingly. No correction is made for blade row attenuation. Caution is to be applied in using this procedure for turbofans with more than two fan stages. In the case of a turbojet, the noise from the first compressor stage is assumed to be representative of the far-field noise.

##### 5.2.4.1 Background

This discussion touches briefly on the various ideas and philosophies that went into the development of the procedures. Of the items discussed, the first is the definition of the source noise associated with the rotating blades inside a duct with inlet and exit guide vanes. The second is a

description of some of the procedure-related corrections that are employed. Special applications and limitations are noted briefly.

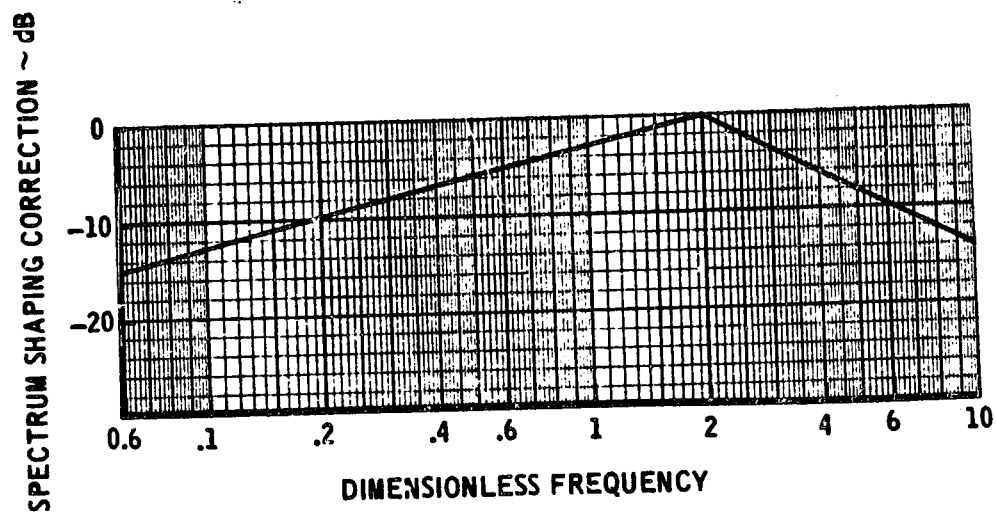
*Broadband noise.*—The term broadband noise is associated with “white” noise that is generated by unstable air flow past the rotors and stators of each fan stage. This noise is not strictly white noise because at a frequency of approximately twice the fundamental blade passage frequency, the spectral density levels have been observed to fall off at approximately 30 dB per decade. The corresponding 1/3 octave band spectrum shape is shown in figure 56a. The exact mechanisms which generate the noise are not well understood, but are thought to involve local variations in the static pressure field due to:

- 1) vortex shedding from the blades and vanes,
- 2) lift fluctuations resulting from approaching eddies in unstable flow, and
- 3) turbulent boundary layer(s)

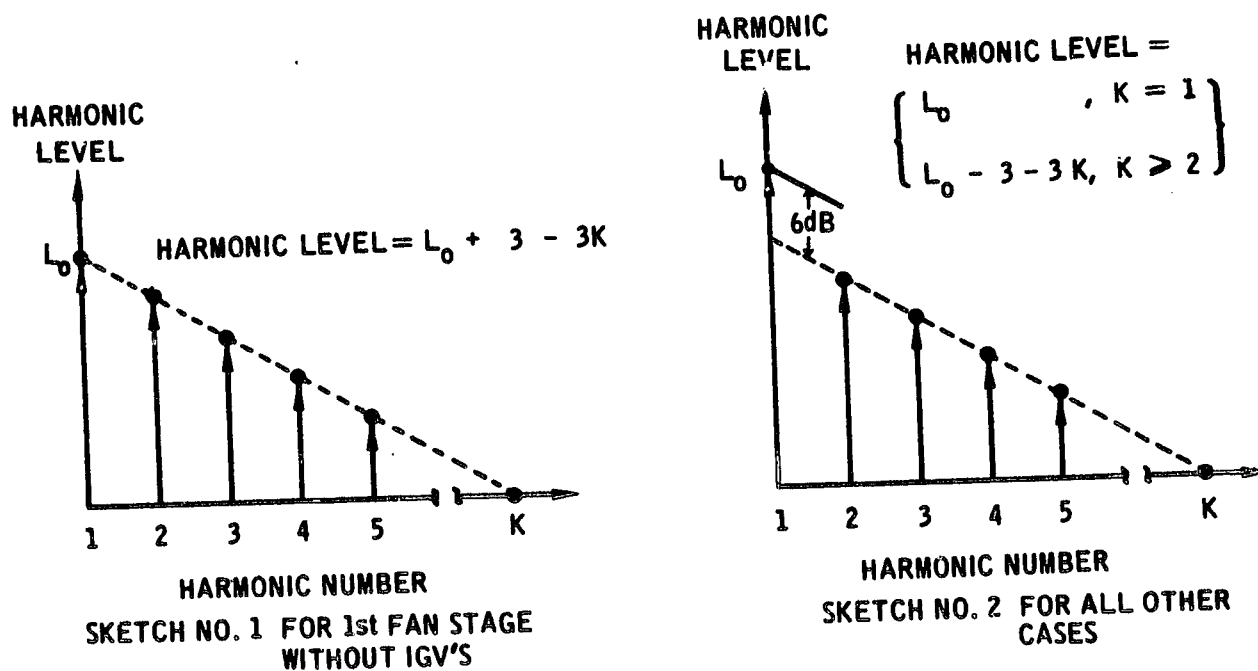
In this procedure, the broadband noise is separated into two components; one radiating upstream and out the inlet, and one radiating downstream and out the fan discharge nozzle. Engine size scaling is accomplished by normalizing the inlet component with respect to the rotor diameter and the discharge component with respect to the exit area of the fan discharge nozzle. This normalization approximates the more classical mass flow scaling as discussed in section 5.1.1.5. The validity of the approximation is due to the way the turbofan engines are designed, i.e., the inlet and discharge Mach numbers do not vary appreciably for different engines operating at the same fan pressure ratio. The normalized levels are then related to the rise in pressure across each fan stage as shown in figures 57a and 57b.

*Discrete tone noise.*—Discrete tones at integer multiples of the fundamental blade passage frequency are radiated from the fans and compressors of all jet engines when operated at either subsonic or supersonic tip speeds. A major source of the tones for fans with inlet guide vanes (IGV's) is the static pressure field developed as the blades chop through the wakes from the inlet guide vanes. For fans without IGV's, inlet flow turbulence produces the same effect, but the sound produced is of a lower level.

An additional source of nearly equal strength to the noise generated by the IGV-rotor interaction is the noise produced by rotor and exit-guide-vane (EGV) interaction. A significant parameter affecting the rotor-EGV interaction is the blade/vane number ratio. This effect is illustrated in section 5.2.4.4. In both cases, IGV-rotor or rotor-EGV interaction, the noise is generated by a static pressure field which can be related to lift fluctuations on the blades and vanes.

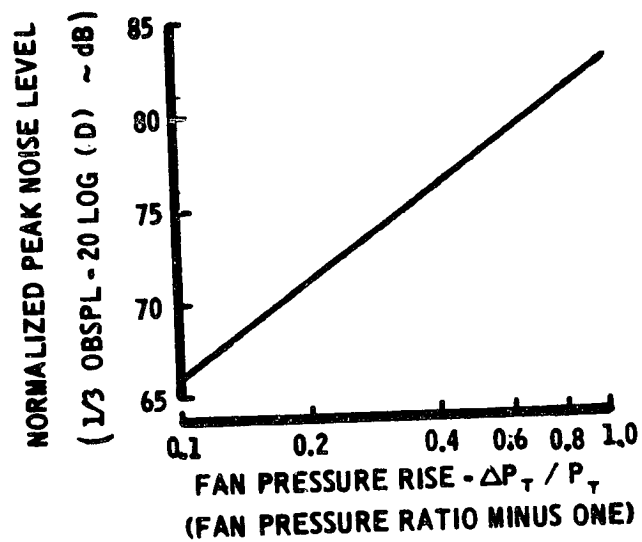


a) BROADBAND NOISE SPECTRUM SHAPE

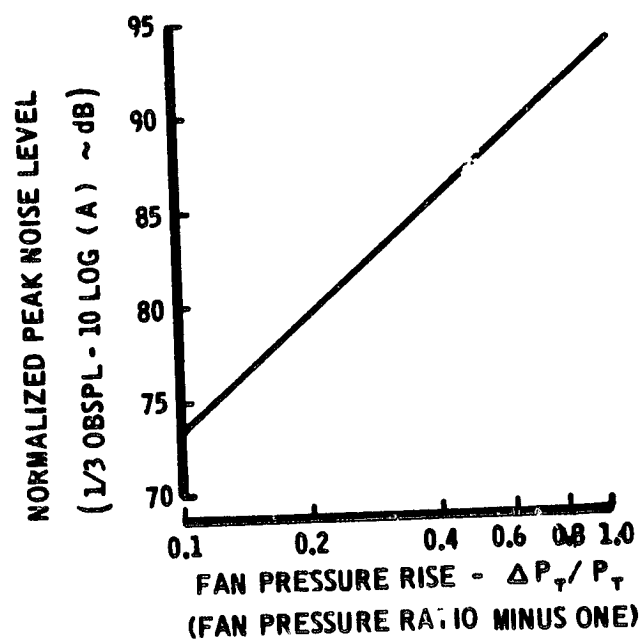


b) DISCRETE TONE-RELATIVE LEVEL VS HARMONIC NUMBER

FIGURE 56.-FAN NOISE SPECTRUM SHAPES



a) NOISE EMITTED FROM THE INLET DUCT



b) NOISE EMITTED FROM THE FAN DISCHARGE DUCT

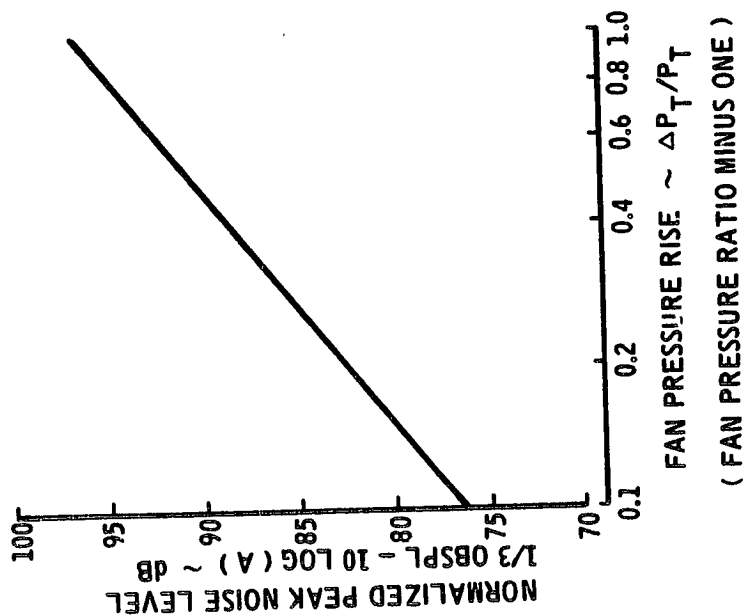
FIGURE 57.—BROADBAND FAN NOISE (PEAK ONE-THIRD OCTAVE BAND SOUND PRESSURE LEVEL)

In the prediction procedure, the discrete-tone noise is separated into two noise components in the same manner as that done for broadband noise. The normalized levels for these components are shown in figures 58a and 58b. For turbofans without IGV's for the first fan stage, e.g., the JT9D, there is an additional noise source radiating out the inlet as the relative tip Mach number exceeds unity. This noise is called combination tones and is discussed below. As the relative tip Mach number exceeds one, the harmonic tones at multiples of the fundamental blade passage frequency decrease with an increase in tip speed or fan pressure ratio. This phenomenon is thought to be the result of a non-linear transformation of acoustic energy from the discrete-tone noise to combination tones. It is treated as follows for noise prediction purposes. At low relative tip Mach numbers, the fundamental tone follows the solid line shown in figure 58b. This curve is used until the Mach number exceeds unity. After this point is reached, noise level decays for an increase in the Mach number or fan pressure ratio as shown by the dashed line in figure 58b. It should be remembered, that the intersection point of the solid curve and the dashed line vary with different engines. This point corresponds to the condition where the relative tip Mach number just exceeds unity—1.025 is used in the computer program. The effect just described applies only to the first fan stage without IGV's, otherwise the solid curve in figure 58b is used for all fan or compressor stages.

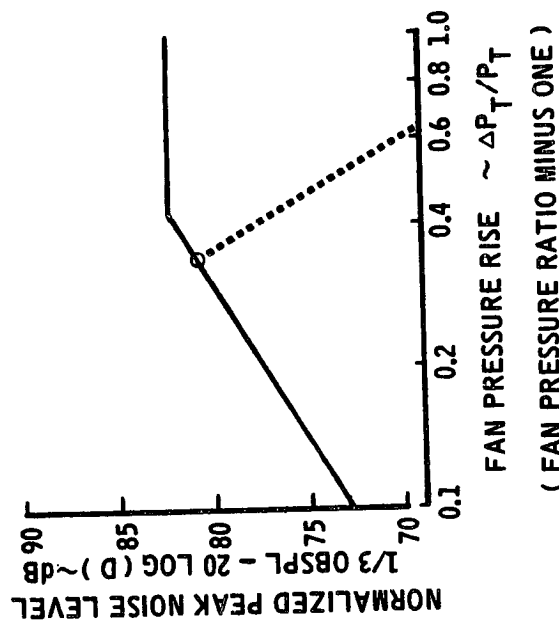
Both the inlet and discharge fundamental tones are assumed to have their peak level at the blade passage frequency. The relative levels for the higher harmonics are shown in figure 56b.

*Combination tone noise (buzz-saw).*—When the first rotor stage does not have IGV's, an additional source of fan noise becomes significant when the relative tip Mach number goes supersonic. At these high tip speeds, a shock forms on each rotor blade. These shocks move upstream and decay into a system of Mach waves which propagate out of the inlet duct. Theoretically, they would be observed in the far field as a series of tones at multiples of the blade passage frequency. Experience indicates that there is a redistribution of energy. Small differences within the manufacturing and assembly tolerances of rotor blades appear to affect the detailed shape of the shocks attached to each blade. Thus, the Mach wave system repeats itself with each revolution of the rotor, rather than with the passage of each blade. The resulting noise spectrum contains all harmonics of the shaft's rotational speed. This noise has been termed combination tone noise for the subjective response it produces.

A noise spectrum, consisting of a series of tones each with the same order of magnitude and separated by a fixed frequency, is referred to as a combination tone. It is a characteristic of the human auditory system to judge the pitch of this type of noise as though it were a tone at the separation frequency, although there may be little sound energy at that frequency. This type of noise is found in all fans and compressors which operate at supersonic tip speeds, but it may be masked by a louder tone at the blade-passage frequency or by jet noise. The presence of inlet-guide-vanes attenuates the Mach wave system; hence, the combination tone noise is



a) NOISE EMITTED FROM THE FAN DISCHARGE DUCT



b) NOISE EMITTED FROM THE INLET DUCT

FIGURE 58.—DISCRETE TONE FAN NOISE (PEAK ONE-THIRD OCTAVE BAND SOUND PRESSURE LEVEL)

insignificant compared to the other components as in the case of the older bypass engines. However, if one observes a 747 aircraft during takeoff, the noise emitted from the inlets of the JT9D engines is perceived to be similar to that produced by a buzz-saw.

In the prediction procedure, the calculation of combination tone noise includes the following simplifying assumptions:

- 1) Combination tone noise is emitted only from the fan inlet.
- 2) It will contribute to the total fan noise only if the relative tip Mach number is greater than one.
- 3) It will contribute to the total fan noise for fans without IGV's.
- 4) Combination tone noise can be predicted in terms of three separate spectrums based on peak noise levels centered at one-half, one-fourth, and one-eighth of the fundamental blade passage frequency of the first fan stage.

The three peak noise levels are shown in figure 59, plotted against the relative tip Mach number. The spectrum shapes corresponding to the three peak noise levels are shown in figure 60.

*Corrections.*—In the prediction procedures, various corrections are employed to account for changes in the engine configuration from that for the reference JT3D and JT9D engines. The corrections reflect the effects for varying such items as rotor-stator spacing, directivity angle, bypass-ratio, discharge duct length, flight effects, and the use of IGV's and multiple engines. Each of these corrections are discussed below.

- 1) **Rotor-Stator Spacing Correction**—This correction accounts for the noise generated due to the presence of stators in front and behind of the rotor. The correction is shown in figure 61 and is to be added to the peak noise levels described above in "Broadband Noise" and "Discrete Tone Noise." Figure 62 illustrates the definition of the rotor-stator spacing that refer to conditions at the rotor tip.
- 2) **Directivity Correction**—This correction accounts for the fact that the radiation pattern for the fan or compressor noise is not spherically symmetric about the source. The procedure uses simplified directivity patterns for the noise subcomponents (figs. 63 and 64). These directivity patterns show that the noise is maximum at  $\Psi = 60^\circ$  for the inlet components and at  $\Psi = 110^\circ$  for the fan discharge components. Engine test data has

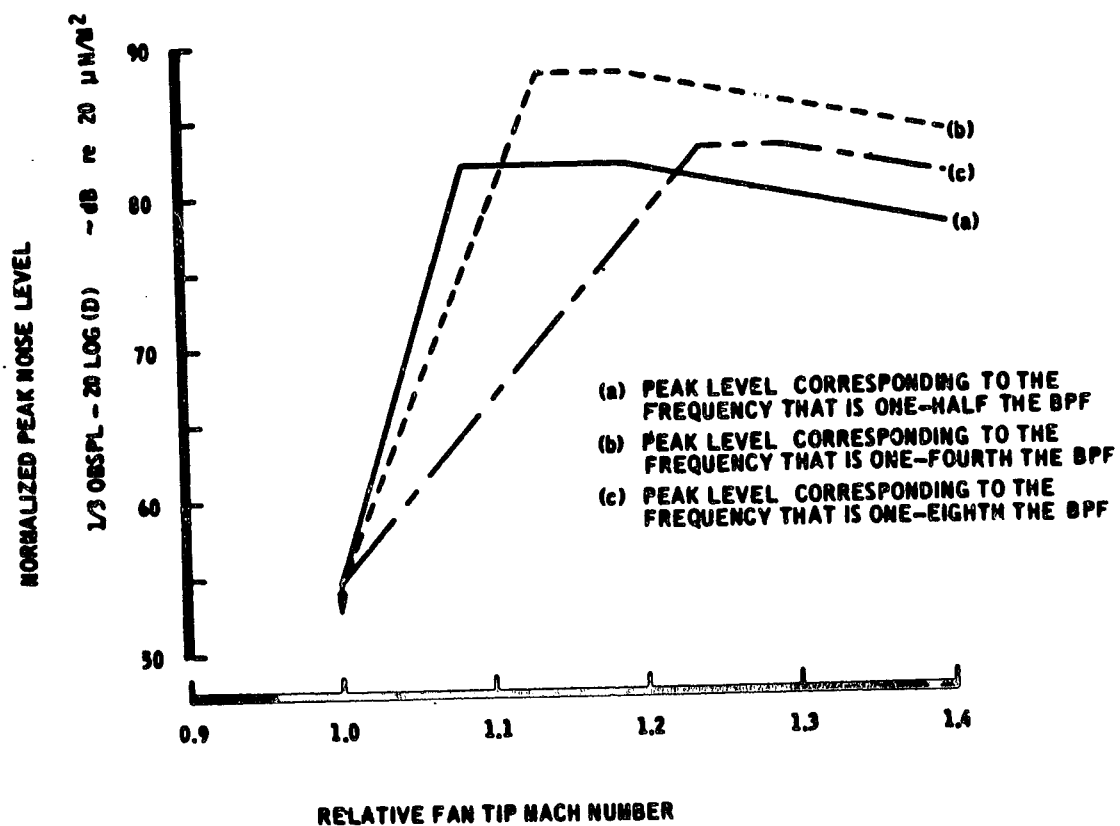


FIGURE 59.—INLET FAN COMBINATION TONE NOISE



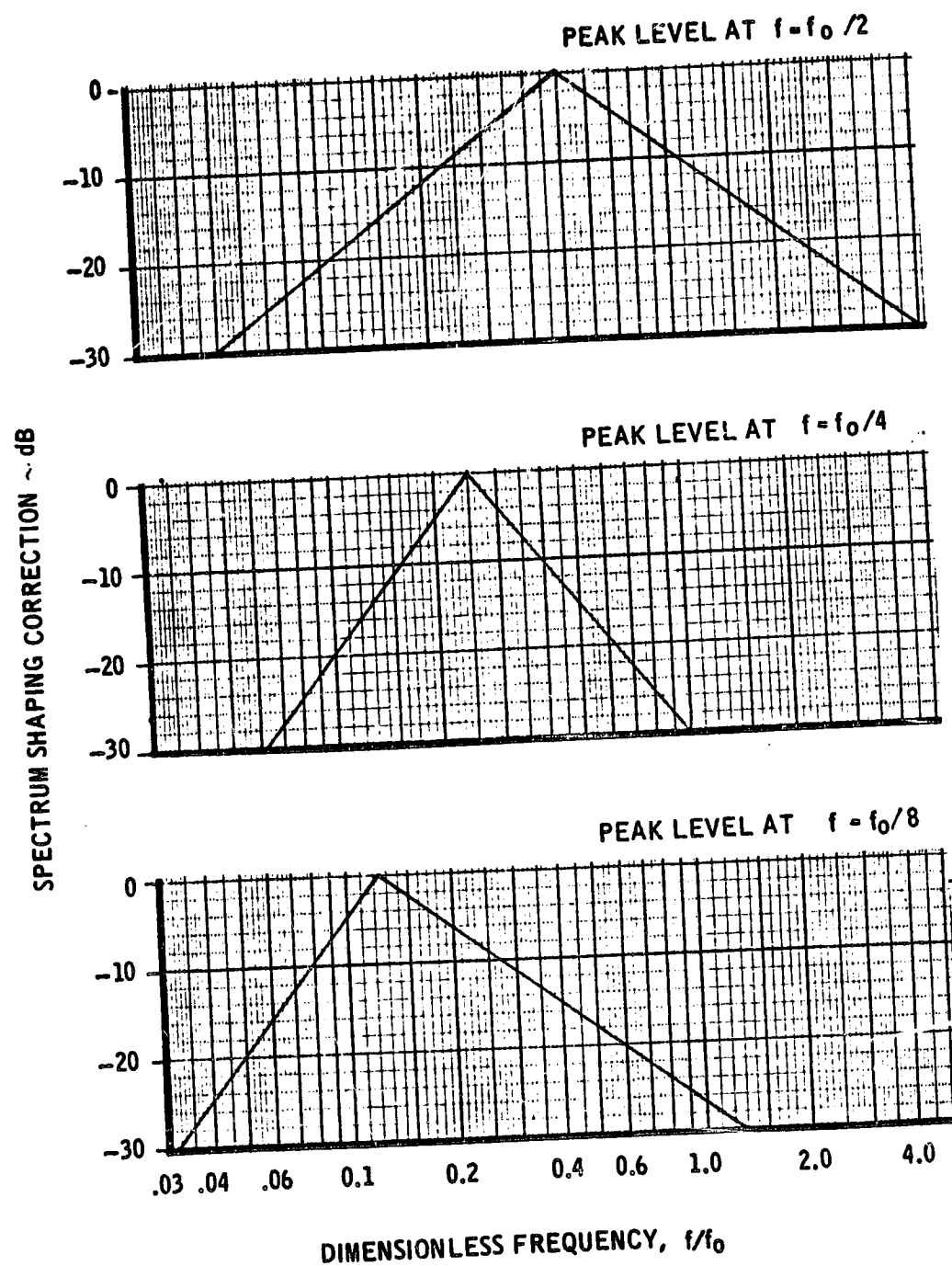


FIGURE 60.—COMBINATION TONE NOISE SPECTRUM SHAPES

# ROTOR-STATOR SPACING CORRECTION

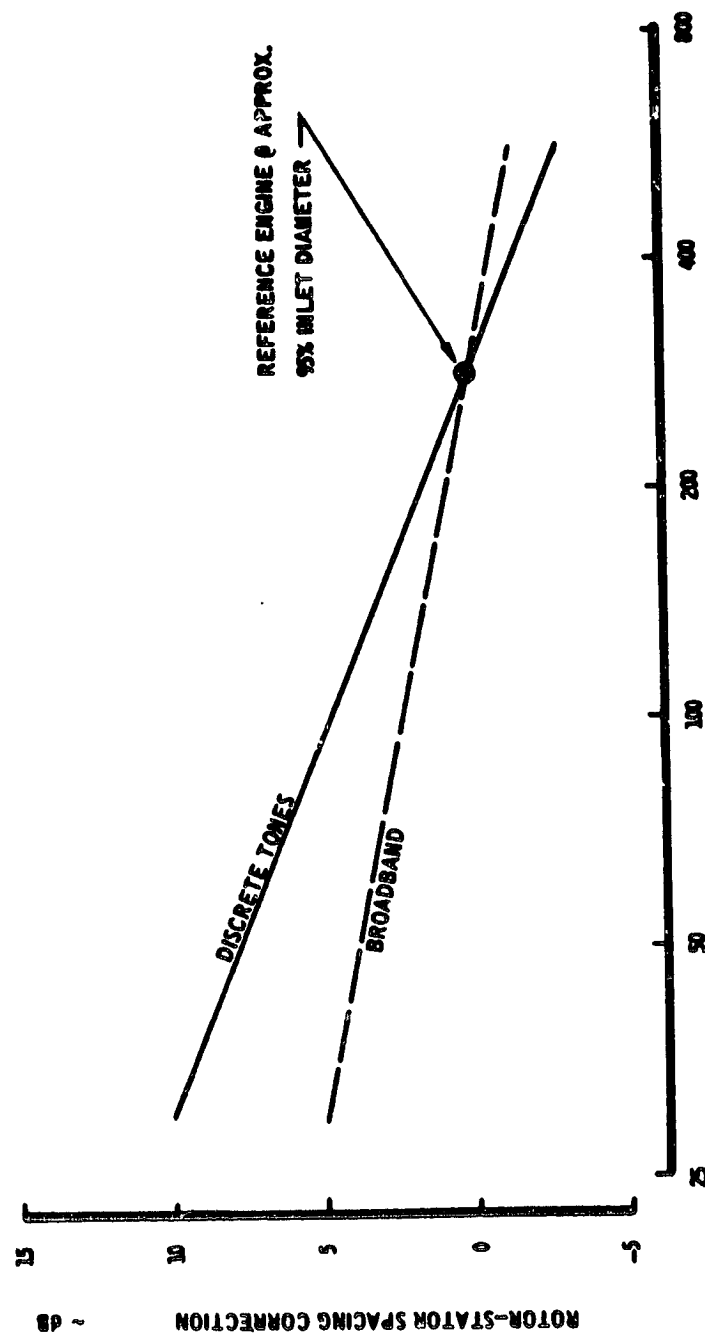
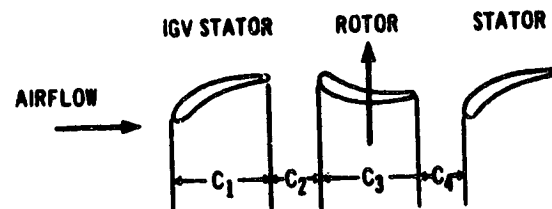


FIGURE 61.—ROTOR-STATOR SPACING, RSS (%)

# TURBOFANS WITH INLET GUIDE VANES (IGV)

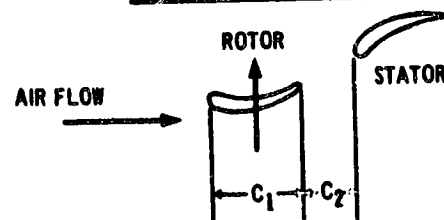


$$S_1 = C_2/C_1, S_2 = C_4/C_3$$

$$RSS = \text{MINIMUM OF } (S_1, S_2) \times 100$$

WHERE RSS IS THE MINIMUM ROTOR/STATOR  
SPACING IN PERCENT

# FIRST STAGE OF TURBOFANS WITHOUT IGV'S



$$RSS = C_2/C_1 \times 100$$

WHERE RSS IS THE ROTOR/STATOR SPACING  
IN PERCENT

**FIGURE 62.—ROTOR-STATOR SPACING**

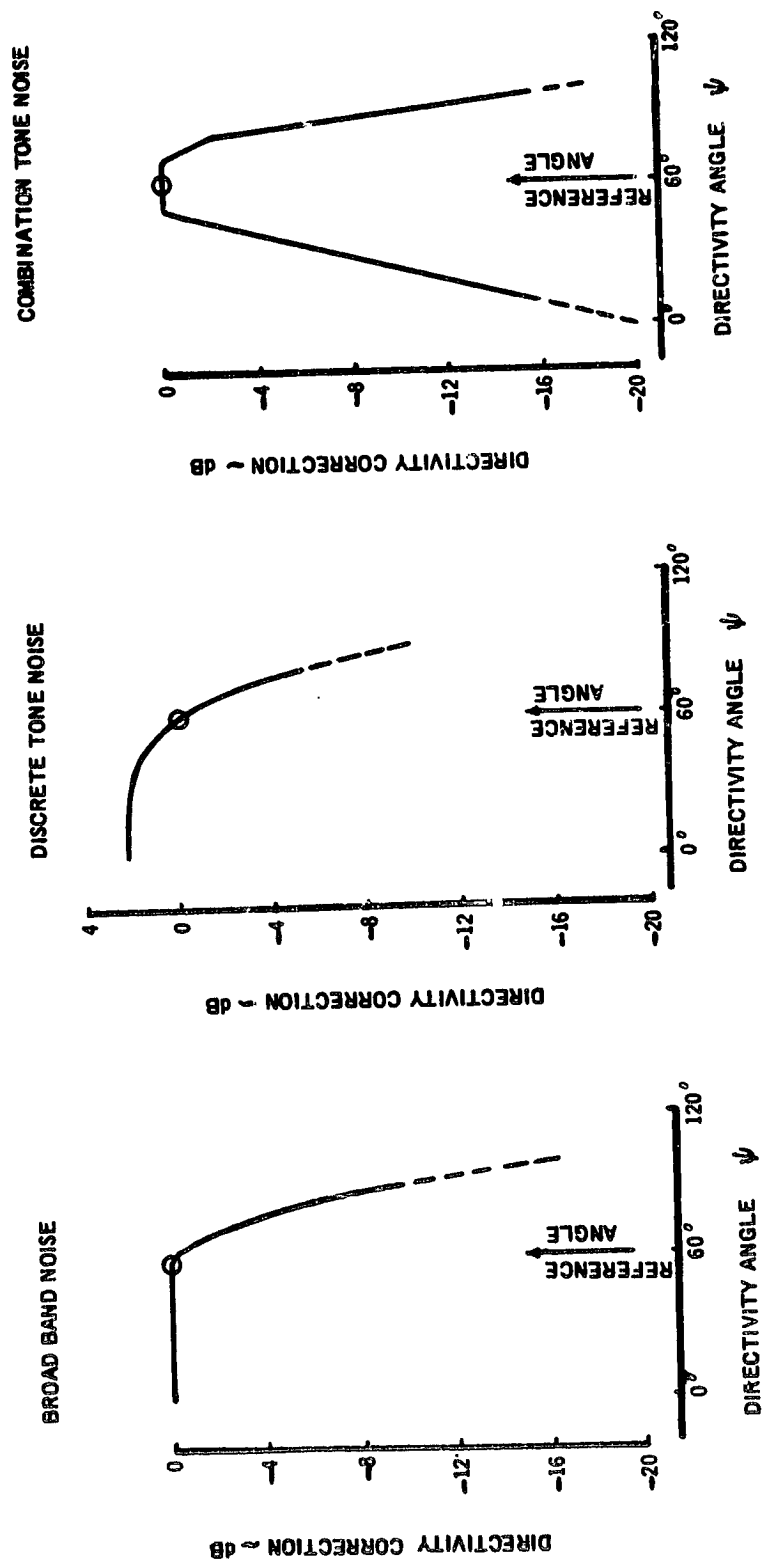


FIGURE 63.—INLET COMPRESSOR AND FAN NOISE DIRECTIVITY CORRECTIONS

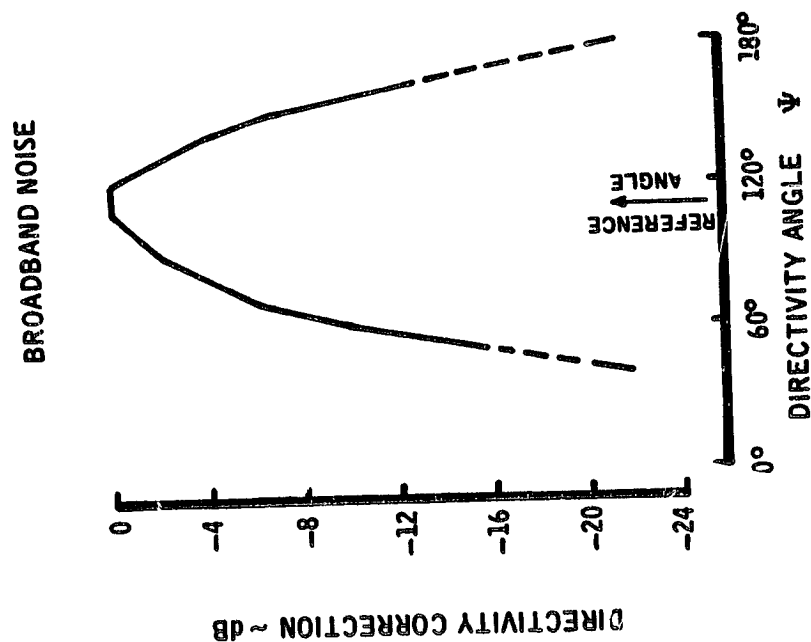
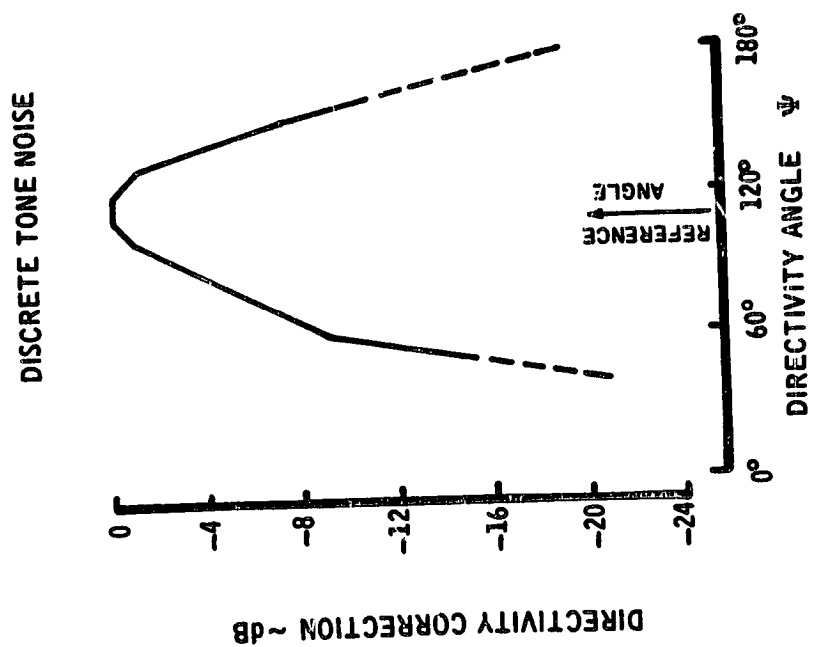


FIGURE 64.—DISCHARGE DIRECTIVITY CHARACTERISTICS

shown a variation in directivity angle for the maximum noise—namely 50° to 70° and 90° to 120° for the inlet and discharge components. Since community noise estimates are based on passby conditions, the error in EPNdB incurred by using this simplified approach is small.

- 3) **Guide Vane Correction**—The presence of inlet-guide-vanes for the first fan stage, or exit guide-vanes of a preceding stage, alters the observed discrete tone components for the fan stage being considered. The broadband component radiating out the discharge duct is also affected. The change in noise is accounted for as follows:
  - a) For the inlet fan noise—subtract 6 dB from all discrete tones except the fundamental tone at the blade passage frequency. Combination tones (buzz-saw) are not considered to be significant in the far field and hence are not calculated.
  - b) For the fan discharge noise—add 6 dB to the fundamental tone and 3 dB to the broadband component.
- 4) **Bypass Ratio and Duct Length Correction**—This correction approximates for the change in the fan discharge noise that would be observed in the far-field if the bypass ratio and duct length were varied. At the present time, the physics for this effect are not completely understood, but are thought to be due to a change in the transmission coefficient at the end of the discharge duct, i.e., the duct acts as a short-wave-guide. The correction is defined as follows, i.e., let

$$\text{let } \Delta L = \left\{ \begin{array}{ll} -7.8 & \text{for BPR} \leq 0.5 \\ 6 \log_{10}(\text{BPR} / 10) & \text{for } 0.5 < \text{BPR} < 10 \\ 0 & \text{for BPR} \geq 10 \end{array} \right\}$$

Update  $\Delta L$  for the change in duct length, i.e., let

$$\Delta L = (\Delta L) C$$

The constant,  $C$  equals 0, 1/6, 1/3, 1 respectively for short fan ducts, 3/4 length fan ducts, long fan ducts with coplanar primary/secondary nozzle exits, and long fan ducts with a retracted primary nozzle, i.e., the JT8D engine.  $\Delta L$  is added to the discrete tone levels and  $\Delta L/2$  is added to the broadband levels of the discharge fan noise.

- 5) **Flight Effect Correction**—This is an optional correction consisting of two parts. The first part is the Doppler-shift which is well known and requires no explanation. The second part includes a theoretical level correction assuming a dipole source. The result of this level correction gives a slight increase in noise level in the forward quadrant and a slight decrease in level for the aft quadrant.

An additional flight effect applies for a lift fan mounted in the wing of an aircraft. This effect is due to the flow distortion that results from flow separation at the inlet lip and the work distribution difference on the fan rotor. Since this effect is peculiar to the lift-fan configuration, it will be discussed further in section 5.2.4.4.

- 6) **Multiple Engines Corrections**—To account for multiple sources, two corrections are employed—one applies to the inlet fan noise components and the second applies to the discharge fan noise components. Equations (2A) and (2B) in section 3.1.1.6 are applied respectively for the inlet and discharge fan components.
- 7) **Index Spectra Correction**—To remove atmospheric effects from the predicted spectra, the spectra are extrapolated inward to a radius of one meter. The fan noise prediction procedures are based on data originally measured at a radius of 45.7 M (150 ft). The correction for spherical divergence is +33.2 dB and the atmospheric absorption correction is given in table 4.

*Results.*—Before the actual prediction procedures for compressor or fan noise are presented, it seems appropriate to show a comparison of the results that have been obtained with measured engine data. Figures 65 and 66 show the comparison. It is expected that the observed far-field noise can be predicted within  $\pm 3$  PNdB for engines similar to those in current usage.

#### 5.2.4.2 Inlet Fan and Compressor Noise Prediction

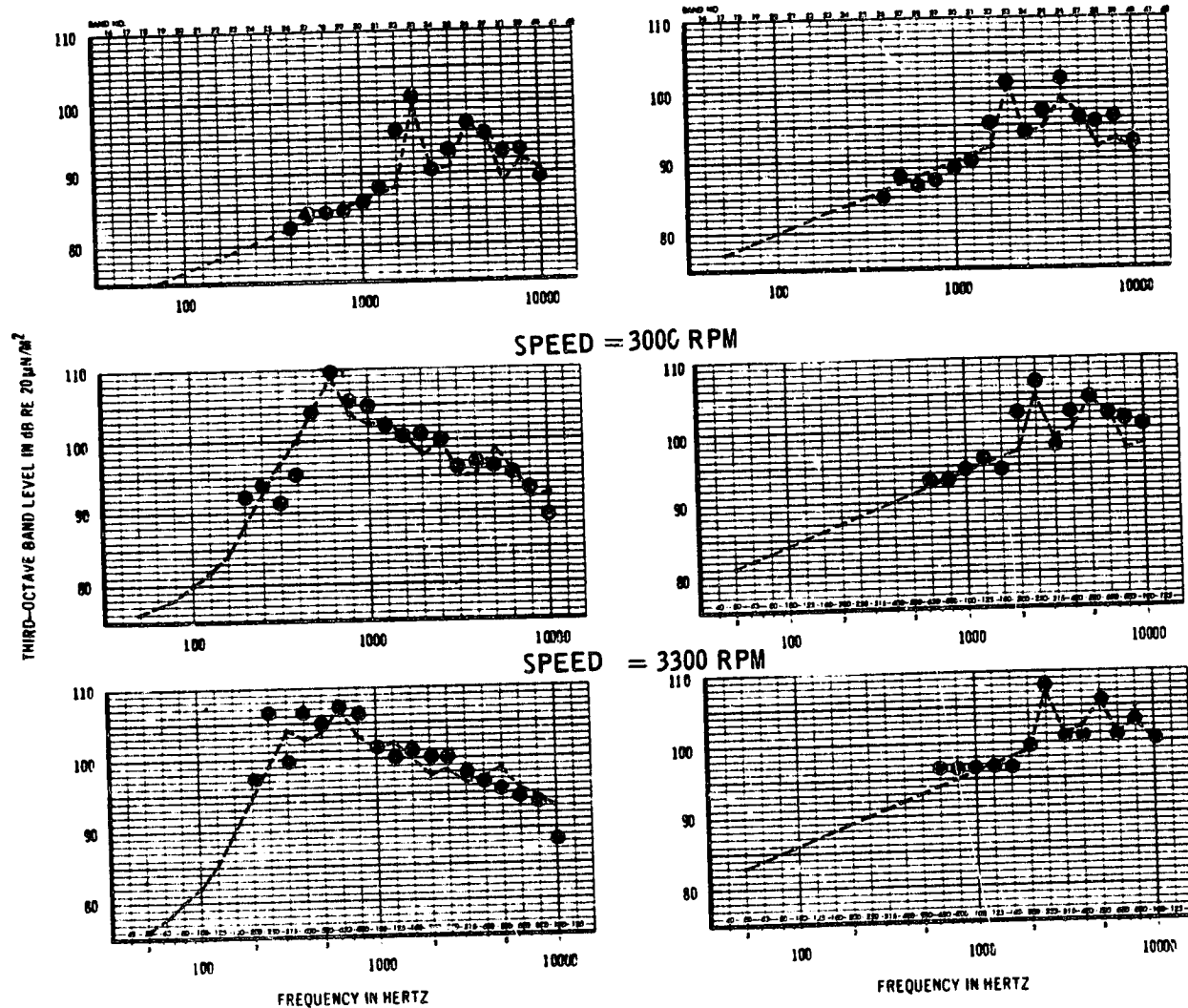
This section deals with the prediction of the three noise components radiating out the inlet for conventional turbofan and turbojet engines. The noise from the compressor of a turbojet engine is predicted as though it was a single-stage fan. The noise from the turbofan engine is predicted as the energy sum of that produced by each fan stage. The procedure is based on data from single and double stage fans. Hence, care should be exercised in using these procedures for fans with more than two stages because blade row attenuation is not considered.

*Broadband component prediction.*—The characteristic peak 1/3 octave band sound pressure level of a single fan stage is defined by

INLET FAN COMPONENT  $\psi = 60^\circ$

DISCHARGE FAN COMPONENT  $\psi = 110^\circ$

SPEED = 2400 RPM



LEGEND: - - - - - PREDICTED  
● MEASURED AVERAGE

FIGURE 65.—PEAK FAN NOISE FOR JT9D ENGINE ON A RADIUS OF 45.7 METERS





$$L_0 = F_1(\text{FPR} - 1) + F_2(\text{RSS}) + F_3(\psi) + 10 \log_{10} \left[ \left( \frac{D}{D_R} \right)^2 (1 - M_0 \cos \xi)^{-4} \right] \quad (34)$$

where

$F_1, F_2, F_3$  represent the appropriate curves in figures 57a, 61, and 63, respectively

$\text{FPR} =$  Fan pressure ratio, i.e., total pressure ratio across the fan stage being considered

$\text{RSS} =$  Rotor-Stator spacing in %, see figure 62

$\psi =$  Directivity angle re. inlet axis

$D =$  Fan diameter

$D_R =$  Reference diameter = 0.305 M (1 ft)

$(1 - M_0 \cos \xi) =$  Doppler-shift factor

The result,  $L_0$ , is a free-field level in dB re.  $20 \mu \text{ N/M}^2$  at a radius of 45.7 M from the source at standard day conditions ( $15^\circ \text{C}$ , 70% relative humidity). The sound pressure level spectrum is obtained from figure 56a, i.e.,

$$\text{SPL}(f) = L_0 + F_4(f / f_0) \quad (35)$$

where

$f_0 =$  the fundamental blade passage frequency in Hz  
 $= B \dot{\theta} / [60 (1 - M_0 \cos \xi)]$

$B =$  the number of fan blades on the stage being considered

$\dot{\theta} =$  the wheel speed in rpm

*Discrete tone component prediction.*—The characteristic peak level in dB re  $20\mu\text{N}/\text{M}^2$  for the fundamental tone of a single fan stage is given by

$$L_o = F_1(\text{FPR} - 1) + F_2(\text{RSS}) + F_3(\psi) + 10 \log_{10} \left[ \left( \frac{D}{D_R} \right)^2 (1 - M_o \cos \xi)^{-4} \right] \quad (36)$$

where  $F_1$ ,  $F_2$ ,  $F_3$  represent the appropriate curves in figure 58b, 61, and 63, respectively. The solid-line curve in figure 58b is to be used for all fan stages with the exception of the 1st stage for a turbofan engine *without* inlet-guide-vanes and operating at a fan pressure ratio greater than critical. The calculation for this case is

$$F_1(\text{FPR} - 1) = F_1(\text{FPR}_o - 1) \Big|_{\text{solid line}} - 30.4 \log_{10} \left( \frac{\text{FPR} - 1}{\text{FPR}_o - 1} \right)$$

where  $\text{FPR}_o$  equals the critical fan pressure ratio when the relative tip Mach number just exceeds unity. The typical result of the calculation for the JT9D engine is shown as the dashed-line in figure 58b. The characteristic level,  $L_o$  from equation (36), is at free-field, standard day conditions and 45.7 M from the source.

The next step is the accumulation of the harmonic levels to form the acoustic spectrum. The relative harmonic levels are shown in figure 56b. The tones are added on an energy basis to the broadband spectrum. The calculation steps for accumulating the harmonic levels are outlined below. The steps contain the logic for calculating only those harmonics that are necessary to form the 1/3 octave band spectrum instead of the "brute-force" approach of calculating many harmonic tones and then determining which tones are contained in each pass band. The indicator IGV in the logic denotes if inlet-guide-vanes are present for the first stage, i.e.,  $\text{IGV} \neq 0$ . The symbols  $f_o$ ,  $f_l$  denote the fundamental blade passage frequency and the cutoff frequencies for the filters, respectively. Also, the equals sign has been generalized to denote that the results of the right replaces the quantity to the left of the equals sign.

*Fortran instructions.*—

$$a_o = 0.1 (L_o - 3.)$$

$$\text{IF (IGV .EQ. 0) } a_o = a_o + 0.6$$

$$N_1 = 1. + f_1 / f_o$$

$$DO\ 3\ I = 1, 24$$

$$P_I = 10. ** (0.1 * SPL_I)$$

$$N_2 = f_{I+1} / f_o$$

IF  $((N_2 - N_1) .LT. 0)$  GO TO 3

$$DO\ 2\ K = N_1, N_2$$

IF  $(K .EQ. 1)$  GO TO 1

$$P_I = P_I + 10. ** (a_o - 0.3 * K)$$

GO TO 2

$$1\ P_I = P_I + 10. ** (0.1 * L_o)$$

2 CONTINUE

$$SPL_I = 10. * ALOG10(P_I)$$

$$3\ N_1 = N_2 + 1$$

The results of the above calculation are twenty-four 1/3 octave band sound pressure levels for the inlet fan spectrum which includes the broadband and discrete-tone components.

*Combination-tone component prediction.*—Combination tone noise is calculated only for the first fan stage for turbofans without inlet-guide-vanes. It is assumed that only this stage contributes to buzz-saw noise observed in the acoustic far-field. Further, this noise is assumed to exist only when the relative tip Mach number is greater than one.

The characteristic peak (1/3) octave band sound pressure levels in dB re  $20 \mu N/M^2$  at center frequencies equal to 1/2, 1/4, and 1/8 of the fundamental blade passage frequency  $f_o$  are given by

$$\left. \begin{aligned} L_1 &= a_0 + F_5(M_{TR}) & \text{for } f &= f_0/2 \\ L_2 &= a_0 + F_5(M_{TR}) & \text{for } f &= f_0/4 \\ L_3 &= a_0 + F_5(M_{TR}) & \text{for } f &= f_0/8 \end{aligned} \right\} \quad (37)$$

where

$F_5$  are the appropriate curves in figure 59

$M_{TR}$  = relative tip Mach number

$$a_0 = F_3(\Psi) + 10 \log_{10} \left[ \left( \frac{D}{D_R} \right)^2 (1 - M_0 \cos \xi)^4 \right]$$

$F_3$  = the directivity correction shown in figure 63

The levels ( $L_1$ ,  $L_2$ ,  $L_3$ ) are at free-field, standard day conditions at a radius of 45.7 M from the source.

The sound pressure level spectrum for this component is approximated by

$$SPL(f) = 10 \log_{10} \left\{ \sum_{K=1}^3 10^{0.1[L_K + G_K(f/f_0)]} \right\} \quad (38)$$

where  $G_K$  represents the spectrum shape curves shown in figure 60 for  $K = 1, 2, 3$ .

#### 5.2.4.3 Discharge Fan Noise Prediction

Two components are accumulated to provide the total fan noise radiating from the fan discharge duct. These components are broadband and discrete tone noise. The noise produced by more than one fan stage is estimated by predicting the noise for each stage and the results are summed on an energy basis. The compressor noise contribution emitting from the engine discharge does not appear significant in the far-field; hence, it can be ignored. The reasons are (1) it is masked by more dominant sources, i.e., fan, jet, core and turbine components and (2) it is attenuated in its propagation through the higher compressor stages, the combustor, and turbine stages.

**Broadband component prediction.**—The characteristic peak 1/3 octave band sound pressure level of a single fan stage is defined as follows:

$$L_0 = F_1(\text{FPR} - 1) + F_2(\text{RSS}) + F_3(\psi) + C \\ + 10 \log_{10} \left[ \left( \frac{A}{A_R} \right) (1 - M_0 \cos \xi)^{-4} \right] + \frac{\Delta L}{2} \quad (39)$$

where

$F_1, F_2, F_3$  represent the appropriate curves in figures 57b, 61, and 64, respectively.

FPR	=	Fan pressure ratio, i.e., total pressure ratio across the fan stage being considered.
RSS	=	Rotor-Stator spacing in %, see figure 62.
$\psi$	=	Directivity angle re inlet axis.
A	=	Fan discharge nozzle area.
$A_R$	=	Reference area = 0.0929 M <sup>2</sup> (1 ft <sup>2</sup> )
$(1 - M_0 \cos \xi)$	=	Doppler-shift factor.
C	=	3 dB for fan stages with inlet-guide-vanes. 0 dB for the 1st fan stage without IGV's.
$\Delta L$	=	Bypass-ratio and duct length correction discussed in section 5.2.4.1.

The result,  $L_0$ , is a free-field level in dB re 20  $\mu\text{N/M}^2$  at a radius of 45.7 M from the source at standard day conditons (15°C, 70% relative humidity). The sound pressure level spectrum is obtained in the same manner as described for the inlet broadband component.

**Discrete-tone component prediction.**—The characteristic peak level in dB re 20  $\mu\text{N/M}^2$  for the fundamental tone of a single fan stage is given by

$$L_o = F_1(FPR - 1) + F_2(RSS) + F_3(\psi) + C$$

$$+ 10 \log_{10} \left[ \left( \frac{A}{A_R} \right) (1 - M_o \cos \xi)^{-4} \right] + \Delta L$$
(40)

where

$F_1, F_2, F_3$  represent the appropriate curves in figures 58a, 61, and 64, respectively.

$C$  = 6 dB for fan stages with inlet-guide vanes.  
 = 0 dB for the first fan stage without IGV's.

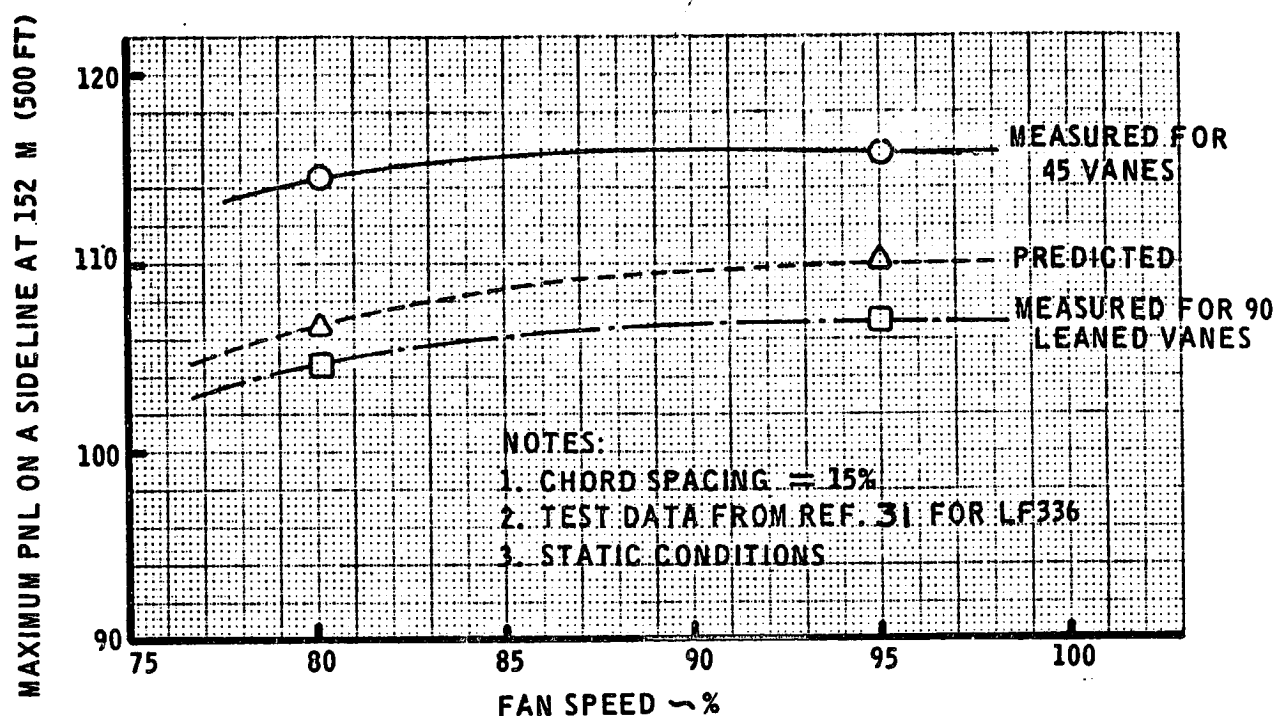
The characteristic level,  $L_o$  from equation (40), is at free-field standard day conditions and 45.7 M from the source.

The next step is the accumulation of the harmonic levels to form the acoustic spectrum. The procedure for adding the tones to the broadband component is the same as that described for the inlet discrete-tone component with the exception that we have a different characteristic level,  $L_o$ .

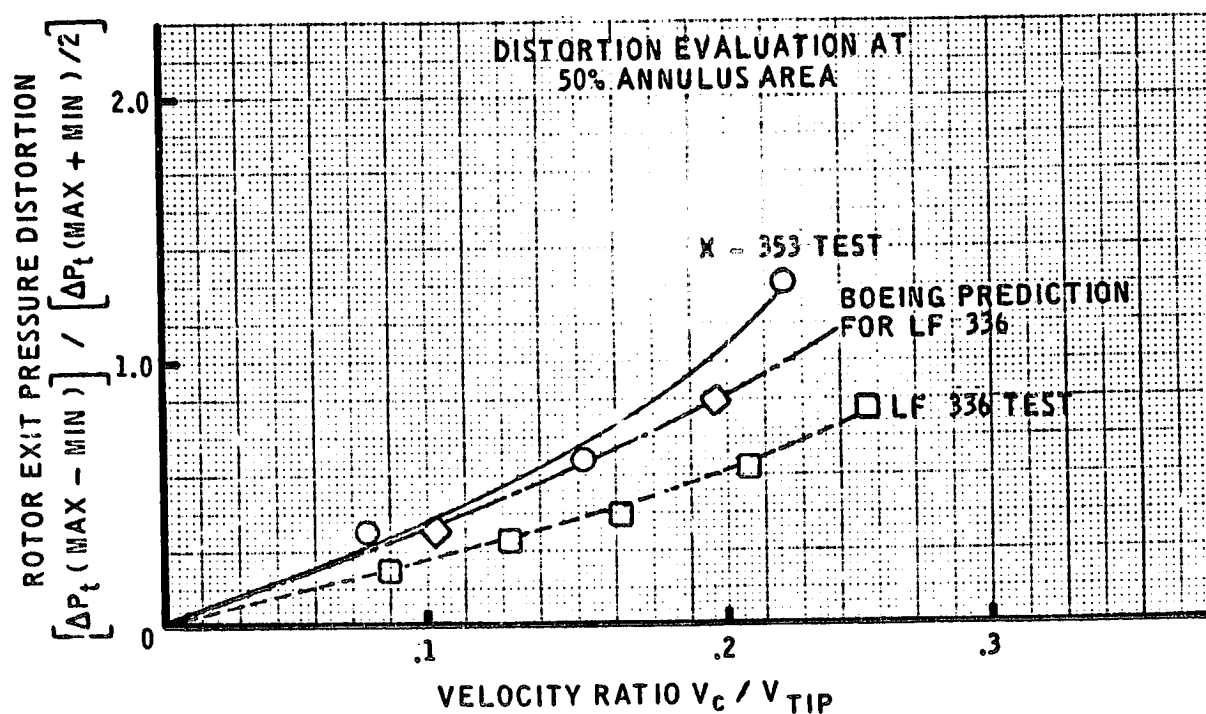
#### 5.2.4.4 Lift Fan Noise Prediction

The lift fan noise prediction procedure has been developed based on the fan noise prediction procedure, described in previous sections 5.2.4.2 and 5.2.4.3, and a forward velocity correction utilizing existing experimental data (ref. 30). The static noise level of an existing lift fan (ref. 31) was compared to the predicted noise by the method outlined in the previous two sections and good agreement was found (fig. 67a). It is assumed that the predicted results correspond to a fan design with an optimum blade/vane number ratio; however the effects of varying the number of exit guide vanes or "leaning" vanes, are not considered in the prediction.

The noise sources for lift fan propulsion systems are similar to that of conventional engines. The fan itself constitutes the major noise source. In addition to the fan noise, noise due to the jet and turbine are also generated by the drive system. The noise of each of these components can be evaluated by the methods described in sections 5.2.2 and 5.2.3. The total noise is the energy sum of the individual components. For lift fans that are driven by a tip turbine, the maximum design tip Mach number of the fan will generally be less than one, mainly because of the turbine stress limit. This limits the fan pressure ratio to below 1.3, which results in low jet velocities and jet noise. Therefore, the jet noise seldom contributes significantly to the perceived noise level for the lift fan



a) COMPARISON OF PREDICTED AND MEASURED LIFT FAN NOISE FOR STATIC OPERATION



b) LIFT FAN ROTOR EXIT DISTORTION TEST VERSUS PREDICTION

FIGURE 67.-LIFT FAN PREDICTIONS



configuration. The noise due to the tip turbine also is of secondary importance due to the large number of turbine blades, i.e., the fundamental blade passage frequency for the turbine usually lies above the audio frequency range.

The effect of forward motion requires consideration of the flow distortion effect on noise generation. This flow distortion results mainly from two sources. Flow separation is possible at the inlet lip due to the small radius of curvature required by wing installations. The second and the more severe distortion results from a non-uniform loading distribution existing on the fan rotor. Figure 68 shows a typical takeoff flight path for a lift fan installation in two modes of operation. Mode 1 represents vertical takeoff or the zero crossflow velocity case similar to static operation, and Mode 2 represents the operation with crossflow imposed on the fan.

The complete vector diagram for the "upwind" side of the fan is shown. On this side, the crossflow loads up the rotor and increases the fan pressure ratio; but on the "downwind" side, the opposite happens. The difference in work that results can be stated as follows:

$$\Delta W \sim \frac{1}{g_c} (U_2 V_2 - U_1 V_1)$$

let

$$U = \text{rotational speed} = U_1 = U_2$$

$$\Delta V = \text{change in fan exit velocity} = V_2 - V_1$$

Therefore

$$\Delta W \sim \frac{U}{g_c} \Delta V$$

Upwind:

$$\Delta W \sim \frac{U}{g_c} (\Delta V + V_c)$$

Downwind:

$$\Delta W \sim \frac{U}{g_c} (\Delta V - V_c)$$

The above difference in work assumes that no flow entrainment takes place due to the inlet walls before the air enters the fan. This assumption is reasonable for shallow inlets such as a

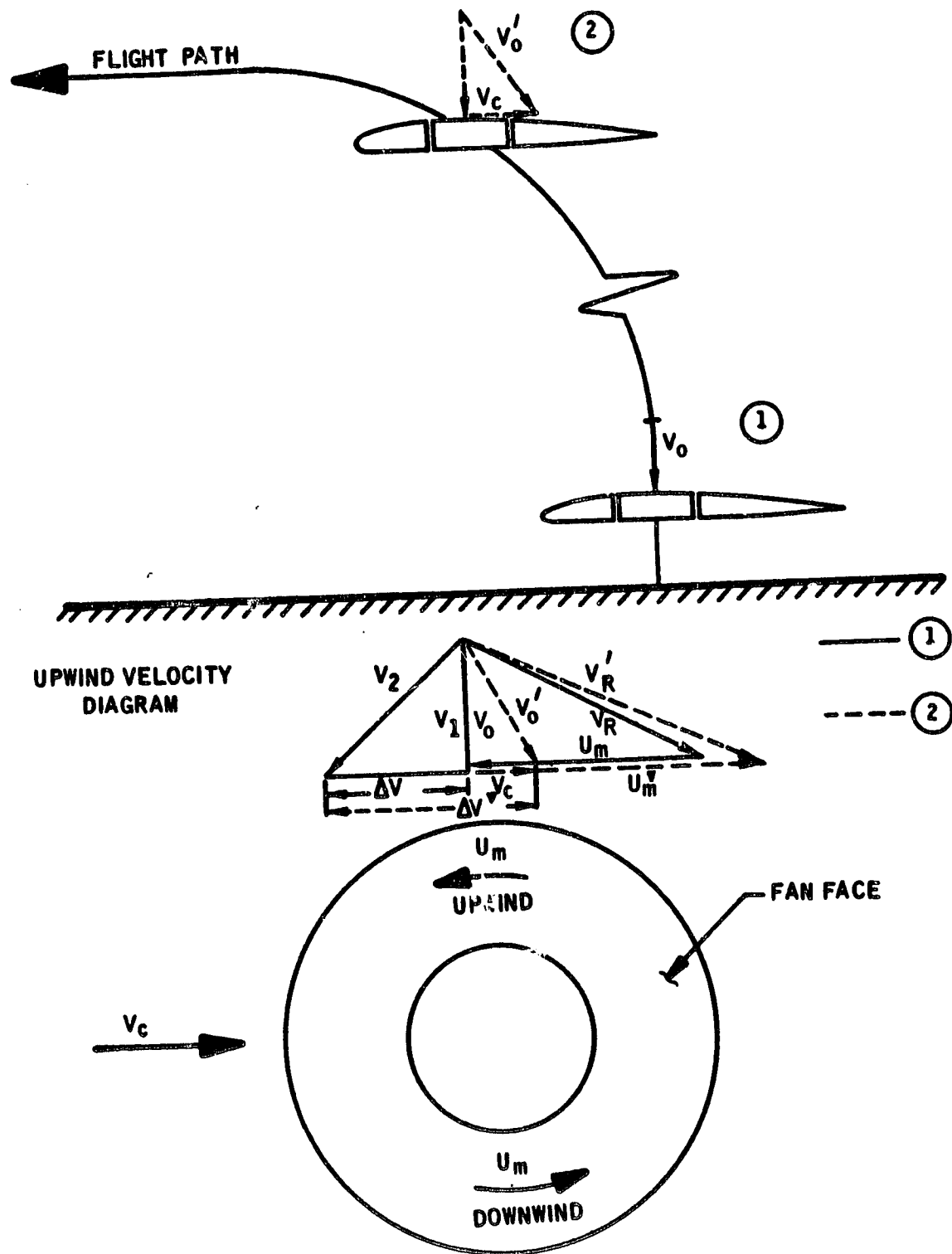


FIGURE 68.—EFFECT OF CROSSFLOW ON LIFT FAN PERFORMANCE

"fan-in-wing" propulsion system. A lift-cruise fan would have a longer inlet, and in this case, nearly complete entrainment of the air would take place before flow incidence on the fan face. Therefore, the distortion effects on noise generation could be significantly less than that cited above.

The distortion for the two lift fans, for which experimental data was available in reference 31, have been calculated. Figure 67b compares the measured and calculated distortion for the X-535 and LF366 configurations. The calculated trend agrees well with the experimental data. This indicates that the ratio of forward velocity to tip speed is indeed a good correlation parameter for distortion effects.

The distortion effects on noise have been reported in reference 31 based on actual lift fan noise tests. A review of other literature and related data has indicated that the state-of-the-art in predicting the effect of distortion is best represented by the data presented in reference 31.

The corresponding correction, to be added to the discrete fan tones, is shown in figure 69 as a function of the velocity ratio  $V_C/V_{TIP}$ .

Concluding, the basic fan noise procedure described in sections 5.2.4.2 and 5.2.4.3 is adequate to predict the noise for a lift fan at static conditions. It has been shown that forward velocity is the major parameter producing distortion in lift fans. Therefore, the increase in discrete-tone noise can be reasonably represented as a function of  $V_C/V_{TIP}$ . Experimental data is currently the most reliable source for representing the change in noise due to distortion.

### 5.2.5 Propeller, Helicopter, and Tilt Rotor Noise

Two prediction procedures have been developed for these noise components. One is empirical and applies to propeller aircraft. The other has a theoretical basis and applies to helicopters and tilt rotor aircraft. In the development of the latter procedure, it was found that it could also be applied for propeller noise prediction because the acoustic theory for propellers is essentially the same as that for rotors.

Both procedures consider two subcomponents for the observed far-field noise. The subcomponents are (1) discrete-tone, rotational noise and (2) broadband vortex noise. In each procedure the vortex noise is predicted by empirical equations because the more refined integration and boundary-value problem approaches are computationally expensive and they require more information than is readily available. These refined approaches are important for propeller/rotor design; but the increase in accuracy for *absolute* levels is not that impressive. The two procedures described here differ in only one respect. The rotational noise is predicted empirically in one and theoretically in the other.

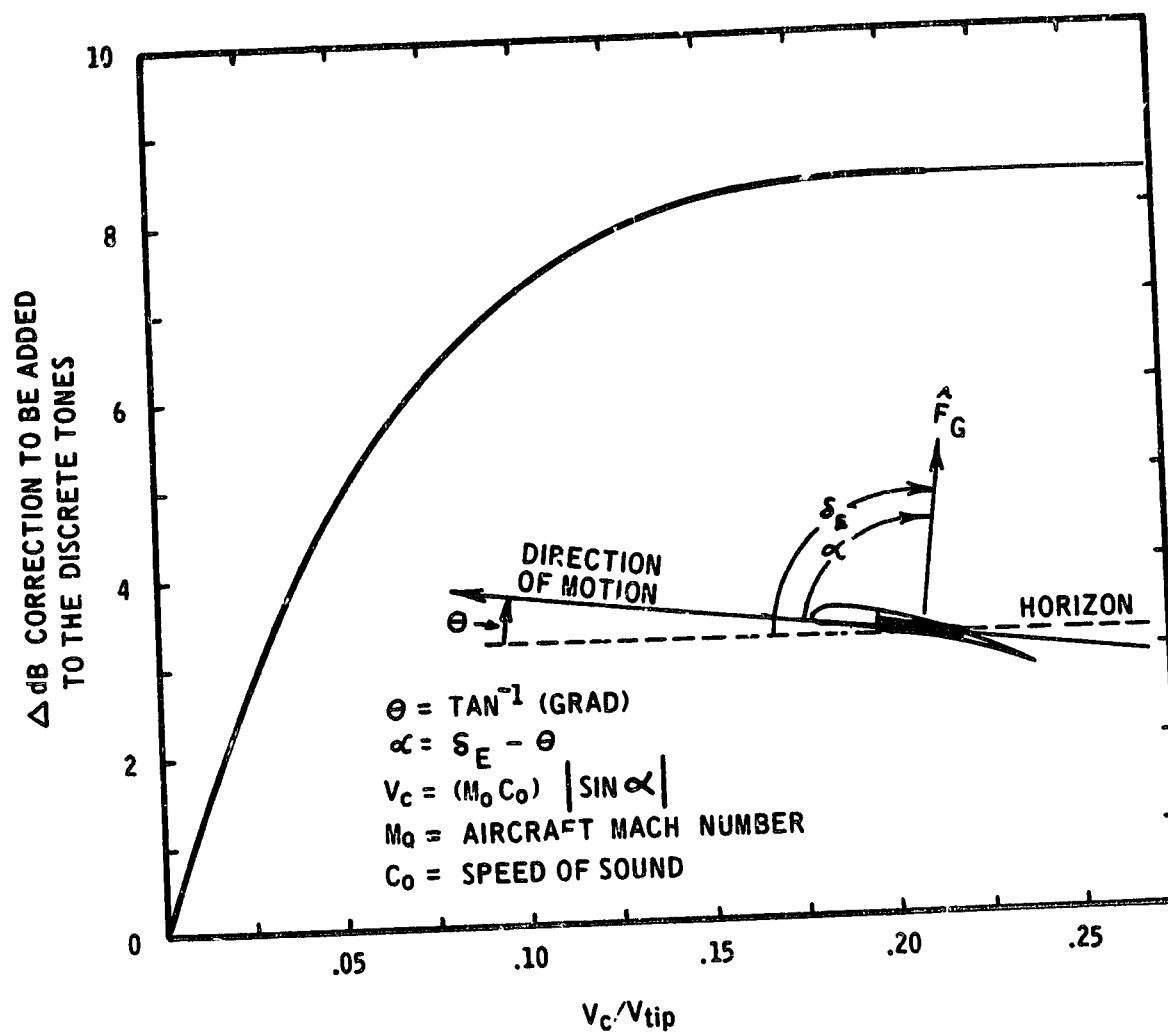


FIGURE 69.—CORRECTION FOR CROSSFLOW ON LIFT FAN NOISE

An error analysis has been made comparing the two procedures with data given in references 37 and 38. The acoustic data was measured inside a hanger at approximately 3.9 M from the center of the propeller. Since the propeller diameter was 1.5 M, it was not known if the measured noise represented far-field levels. A correction of -1.1 dB for ground interference was added to the data to obtain nominal free-field conditions. In theory the ground reflection anomaly varies between  $\pm 4$  dB for the test conditions with the first destructive interference occurring between 50 and 70 Hz.

The data analysis is too lengthy to present here, but it is worth noting the results that were obtained for a four-bladed H.S. 212-14 propeller. Based on a sample of 90 spectra, the 90% confidence band is  $\begin{pmatrix} +7.0 \\ -5.8 \end{pmatrix}$  PNdB and  $\begin{pmatrix} +5.4 \\ -3.7 \end{pmatrix}$  PNdB for the rotor and propeller prediction procedures, respectively. Hence, one can conclude that the accuracy of each procedure is roughly equal. At the present time, one procedure can not be recommended in preference to the other. More data and study are required. Some sample predictions are shown in figures 70 and 71.

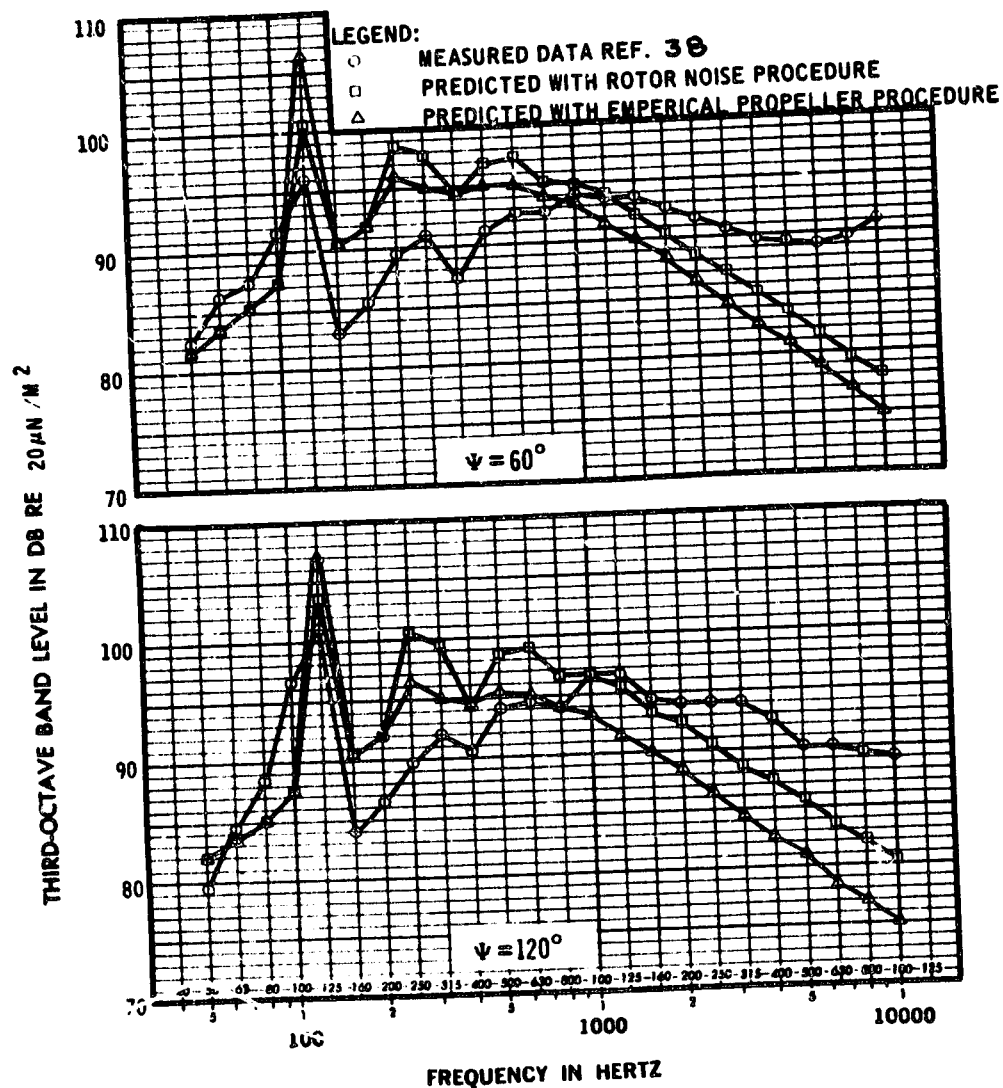
#### 5.2.5.1 Propeller Noise Prediction

A simplified prediction procedure for estimating propeller noise has been developed. The procedure considers two noise components that are generated by a rotating propeller. These components are (1) broadband vortex noise and (2) discrete-tone, rotational noise. The vortex noise is caused by the shedding of vortices, similar to the Karman vortex street, from the trailing edge of a propeller blade. Rotational noise is developed from the harmonic loads that exist on the blades due to the static pressure field developed by the propeller. A third type of noise, "blade-slap" is mentioned in references 33 through 35; but it is rarely present for conventional propeller aircraft operating at subsonic tip speeds.

The procedure defined for vortex noise is based on a combination of the empirical approaches given in references 33 through 38. Reference 32 gives a simplified, empirical procedure for predicting the rotational noise component. That used here is identical to that provided in reference 32 with the exception that the Doppler shift and level change is included per references 33 and 36.

*Vortex noise.*—The equation for the overall sound pressure level,  $L_O$ , in dB re  $20 \mu\text{N/M}^2$  at a distance of 152.4 M is given by reference 35 as

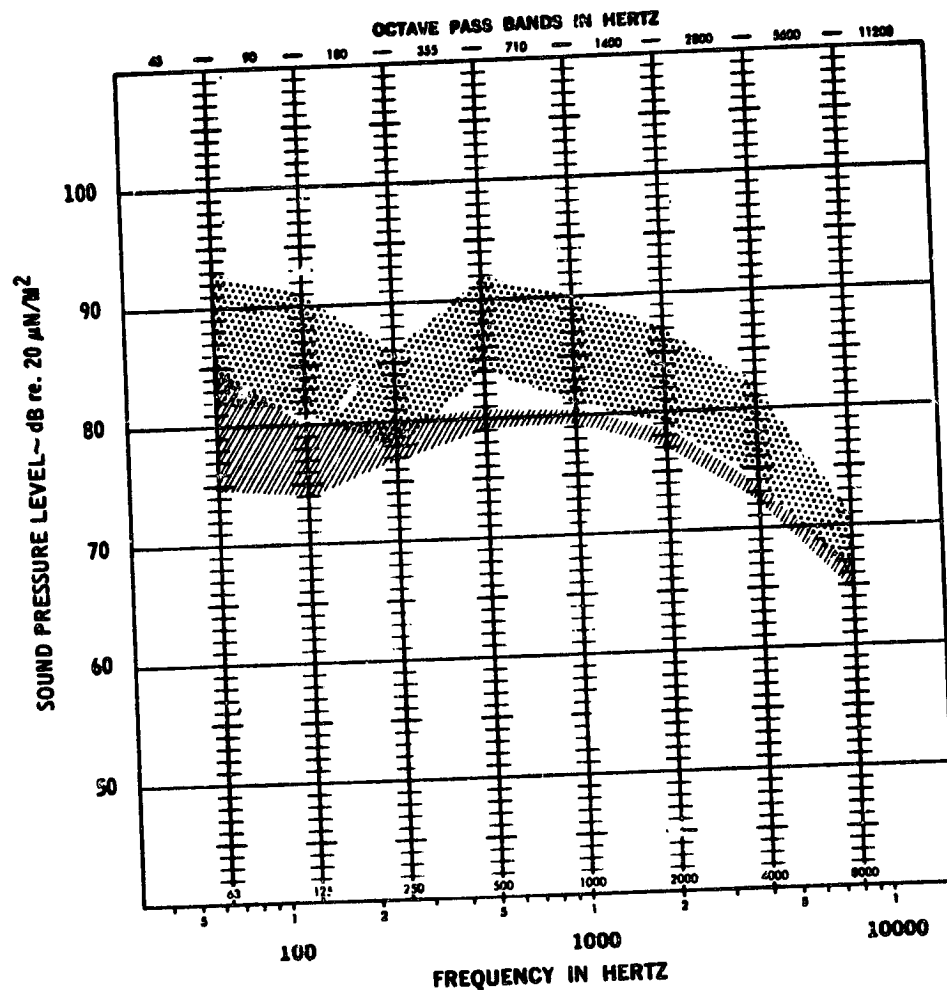
$$L_O = 20 \log_{10} \left[ \frac{V_{TE} T}{(V_R T_R)} \right] + 10 \log_{10} \left[ \frac{A_R}{A_B} \left( \frac{0.1 + \cos^2 \psi}{0.1 + \cos^2 70^\circ} \right) (1 - M_0 \cos^2 \psi)^{-1} \right] - 43$$



CONDITIONS:

- FREE-FIELD, INDEX (R = 1 M)
- TIP MACH NO. = 0.4, SHAFT SPEED = 1720 R/M
- FOUR 5 FT. DIA BLADES, BLADE ANGLE =  $16^\circ$  AT 0.75 SPAN
- THRUST = 324 LBF, TORQUE = 147 FT-LBF, SHAFT POWER = 48.1 HP

FIGURE 70.—MEASURED DATA (H.S.212-14 PROPELLER) VERSUS PREDICTIONS

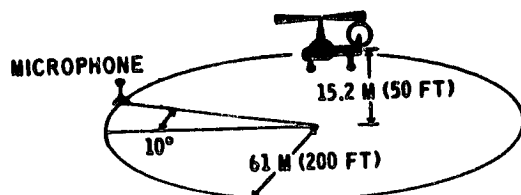


**LEGEND:**



**MEASURED**  
**PREDICTED**

DATA SCATTER FOR GROUND MEASUREMENTS MADE AT  
VARIOUS ANGULAR POSITIONS ON THE 61 METER POLAR ARC



**TEST CONDITIONS:**

ISA CONDITION

HOVER

AIRCRAFT WEIGHT = 20,000 N (4,500 LBF)

BOELKOW-105 HELICOPTER

**FIGURE 71.—SAMPLE HELICOPTER PREDICTION**

where

$V_{TE}$  = effective helical tip speed

$$\approx C_o \sqrt{M_T^2 + (M_o \cos \alpha)^2}$$

$V_R$  = reference velocity = 0.305 M/S (1 fps)

$M_T$  = tip Mach number

$M_o$  = aircraft Mach number

$\alpha$  = angle between propeller axis and direction of aircraft motion

$C_o$  = ambient speed of sound

$T$  = thrust developed by propeller

$T_R$  = reference thrust = 4.45 N (1 lbf)

$A_B$  = total blade area on one side of the propeller

$A_R$  = reference area = 0.0929 M<sup>2</sup> (1 ft<sup>2</sup>)

$\Psi$  = directivity angle re inlet axis of propeller

$\xi$  = angle between flight path and sound propagation path

However, both references 33 and 35 point out that this formula pertains to propellers with 5 or 6 blades and a correction of +5 dB should be added for conventional propellers of 2 to 4 blades. Also corrections for atmospheric absorption and ground reflection appear not to have been included in references 33, 35, and 38. It is desired to have the overall at free-field index conditions (R = 1 M). Hence, the constant -43 dB in the above equation is adjusted as follows.

-43.0                      from original equation

+42.7                      spherical divergence between  $R_1 = 152.4$  M and  $R_2 = 1$  M

+3.0                      estimate of atmospheric absorption at 152.4 M



+5.0	number of blade correction
-3.0	correction to free-field condition
<hr/> +5.7	Total

The resulting equation for the overall SPL of a single propeller at free-field index, conditions is

$$L_0 = 20 \log_{10} [V_{TE} T / (V_R T_R)] + 10 \log_{10} \left[ \frac{A_R}{A_B} \left( \frac{0.1 + \cos^2 \psi}{0.1 + \cos^2 70^\circ} \right) (1 - M_0 \cos \xi)^{-1} \right] + 5.7 \quad (41)$$

The characteristic Strouhal frequency  $f_0$  is given by reference 37 as

$$f_0 = 0.28 V / [(t \cos \delta + l \sin \delta) (1 - M_0 \cos \xi)]$$

where  $(V, t, l, \delta)$  are the effective helical velocity, blade thickness, chord length, and angle of attack respectively at 0.7 span. The basic spectrum shape, SS, which includes frequency modulation effects of blade rotation is given by the formula:

$$\begin{aligned} SS &= 10 \log_{10} \left[ \int_{S_1}^{S_2} g(x) dx \right] \\ &= \frac{1}{2} \log_e \left\{ \frac{[1 + (a S_2)^2] [1 + (b S_1)^2]}{[1 + (b S_2)^2] [1 + (a S_1)^2]} \right\} \end{aligned} \quad (42)$$

where

$$S_1 = f_1 / f_0$$

$$S_2 = f_2 / f_0$$

$$f_1, f_2 = \text{lower and upper cutoff frequencies for the pass band being considered}$$

$g(x)$  = the normalized, power spectral density function

$$= \frac{x}{c} \left[ \frac{a^2}{(1 + a^2 x^2)} - \frac{b^2}{(1 + b^2 x^2)} \right]$$

$a$  =  $1 + M_{TE}$

$b$  =  $1 - M_{TE}$

$c$  =  $\log_e(a/b)$

$M_{TE}$  = effective helical tip Mach number.

The spectrum shape formula has a singularity at  $M_{TE}$  equal to one and thus the procedure fails as the effective tip speed goes supersonic. The vortex noise prediction procedure is limited to values of  $M_{TE}$  less than one. In practical applications this range is reduced further to:  $0 < M_{TE} \leq 0.93$ . The sound pressure level spectrum is defined by adding the spectrum shape result for a series of pass bands to the overall sound pressure level,  $L_O$ .

$$SPL(f) = L_O + SS \quad (43)$$

*Rotational noise.*—The characteristic level in dB re  $20 \mu N/M^2$  at 152.4 M for the rotational noise is given by reference 32 as

$$L_O = 10 \log_{10} \left[ \left( \frac{W}{W_R} \right)^{1.55} \left( \frac{D}{D_R} \right)^{-2.265} \right] + 38 M_{TE} - 2.2 B + F_1(\psi) + 100.$$

where

$W$  = shaft power

$W_R$  = reference power = 745.7 KW (1000 Hp)

$D$  = propeller diameter

$D_R$  = reference diameter = 0.305 M (1 ft)

$B$  = number of blades

$F_1$  = directivity correction (fig. 72)

The expression above is a curve-fit to the empirical figures given in reference 32. It is assumed that this level is representative of measured ground test data at 152.4 M from the source. The lowest frequency for destructive interference due to ground reflection would be between 2 and 5 KHz—well above the first ten harmonics in the rotational noise spectrum. This implies that the characteristic level  $L_0$  is 6 dB above free-field conditions. References 33 and 36 report that a Doppler-shift and level change occurs for a propeller in translational motion. Thus to meet the requirement here, the following formula results for the characteristic level at the free-field, index condition.

$$L_0 = 10 \log_{10} \left[ \left( \frac{W}{W_R} \right)^{1.55} \left( \frac{D}{D_R} \right)^{-2.265} (1 - M_0 \cos \xi)^{-4} \right] + 38 M_{TE} - 2.2 B + F_1(\psi) + 137.7 \quad (44)$$

where the term  $(1 - M_0 \cos \xi)$  is the Doppler factor. This last expression assumes that the air absorption present is negligible due to the fundamental frequency for the propeller tones being typically less than 250 Hz.

The levels of the harmonic tones are determined through use of figure 73 for the function  $F_2$  used in the equation below.

$$L_k = L_0 + F_2(M_{TE}, K), \quad K = 1, 2, 3, \dots \text{etc.} \quad (45)$$

The fundamental frequency for the first harmonic is defined as

$$f_0 = B \dot{\theta} / [60 (1 - M_0 \cos \xi)] \quad (46)$$

where  $\dot{\theta}$  is the shaft speed in rpm. The discrete tones are added to the broadband spectrum in a manner similar to that described for the fan noise procedures (sec. 5.2.4).

#### 5.2.5.2 Rotor Noise Prediction

A simplified prediction procedure for estimating rotor/propeller noise has been developed. The procedure considers two noise components that are generated by rotating blades. These components

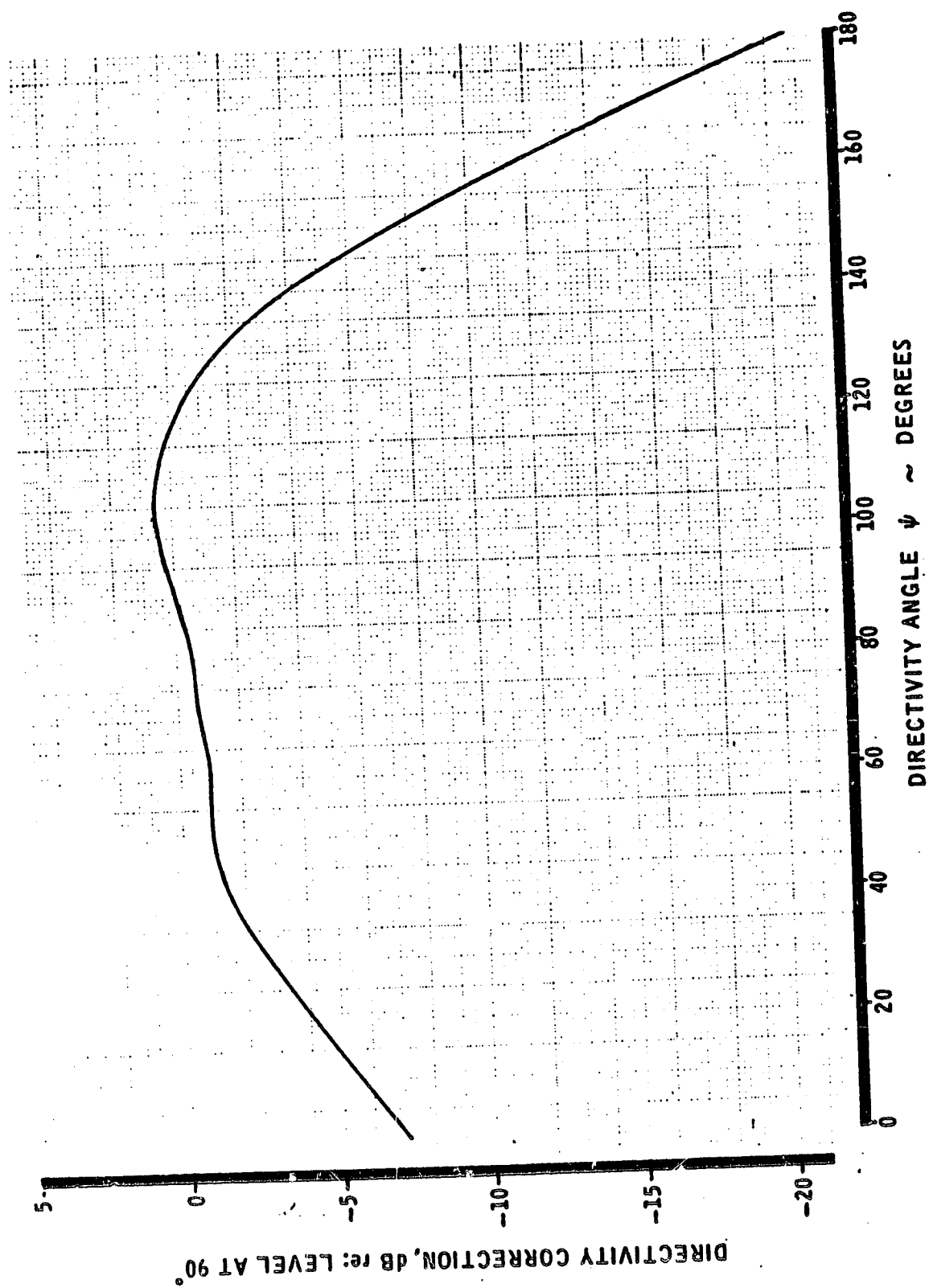


FIGURE 72.—DIRECTIVITY CORRECTION,  $F_1(\psi)$  FOR PROPELLER ROTATIONAL NOISE

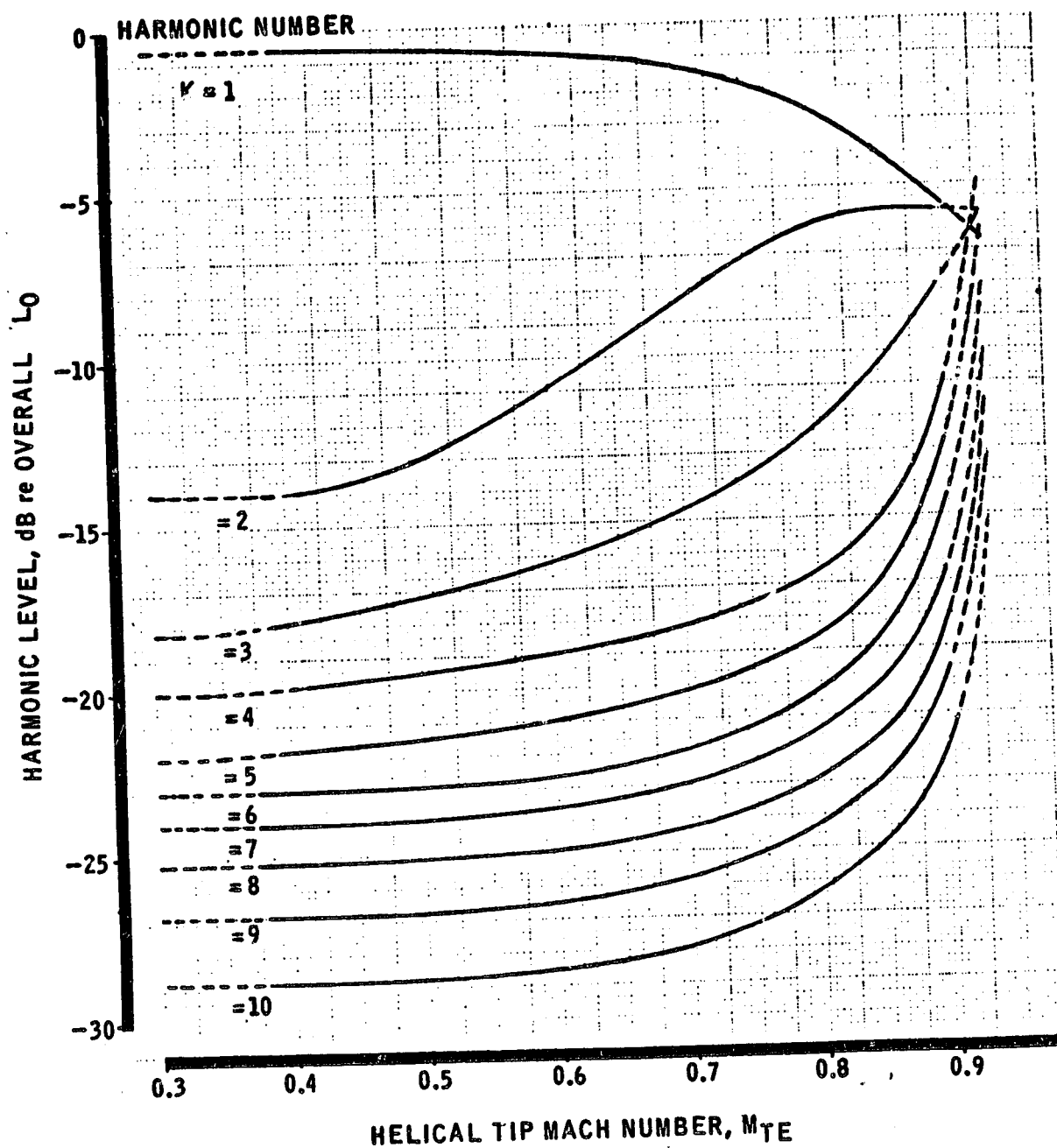


FIGURE 73.—RELATIVE HARMONIC LEVELS  $F_2(M_{TE}, K)$   
FOR PROPELLER ROTATIONAL NOISE

are (1) discrete-tone, rotational noise and (2) broadband, vortex noise. Rotational noise is developed from the harmonic loads that exist on the blades and that for vortex noise is due to the shedding of vortices from the trailing edge of the blades. Other noise sources are mentioned in the references, but they are usually neglected. The reasons are discussed at the end of this section.

*Vortex noise.*—The previous section 5.2.5.1 provides a simplified, empirical procedure for estimating this component. The method used here is identical to that described in that section. An error analysis was made on some of the data given in references 37 and 38. The results indicate that the empirical method provides reasonable predictions for community noise estimates and it is "cheap" in comparison to refined integration and boundary-value problem approaches. Also, they require more information than is readily available, e.g., the complete blade geometry, etc.

*Rotational noise.*—The procedure for rotational noise is based on a theoretical math model (ref. 33) that is simplified by a "loading-law" concept (refs. 35, 37, and 38). For the purpose of noise calculations, the harmonic loads are considered random in phase and applied at a single point on a blade. The position of this equivalent point load is based on a centroid calculation for the mean-square pressure distribution on the blades. Experimental data (refs. 35, 37, and 38) have shown that the load harmonics can be estimated from a simple formula. This formula contains only three empirical parameters which can be determined from acoustic data.

Reference 35 gives data which show that the harmonic loads are different for a rotor with translational motion. Hence, the loading-law parameters will have to be obtained from wind tunnel tests in order to predict the rotational noise for flight conditions. From what little data that is available, the discrete-tones for flight could be significantly less than that from a static aircraft (ref. 37).

One may ask, "Why don't you assume some form of a time-varying pressure distribution on a blade; compute the Fourier series; and use the coefficients thus obtained for the loading harmonics?" The answer is—it was tried and wasn't successful! (ref. 33). Furthermore, it is rather computationally expensive and each rotor design requires a different pressure distribution. On-the-other-hand, the loading-law concept simplifies a rather formidable mathematical problem and provides realistic noise estimates. At the same time, it lumps together many effects that are difficult to predict into only three empirical parameters. Some of the effects are blade flapping, flight, vortex interaction, and changes in blade design. Of the various means available to measure the harmonic loads, the acoustic method (refs. 37 and 38) seems to be the best. This is because other techniques (ref. 33) are presently unable to determine the harmonic loads to the high-order required for noise prediction.

Rotational noise for helicopters and tilt rotors is composed of discrete-tones that occur at harmonic multiples of the fundamental blade passage frequency,  $f_o$ .

$$f_o = B \dot{\theta} / (60 \text{ SF}) \text{ in Hz}$$

$$B = \text{Number of rotor blades}$$

$$\dot{\theta} = \text{Rotational speed in rpm}$$

$$\text{SF} = \text{Doppler-shift factor } (1 - M_o \cos \xi)$$

$$M_o = \text{Aircraft Mach number}$$

$$\xi = \text{Angle between flight path and line to the observer at "retarded time"—the time the sound is generated, not the time when the sound is heard.}$$

The harmonic levels, dB re  $20 \mu\text{N}/\text{M}^2$ , for the rotational noise are given by

$$\begin{aligned} L_N &= 10 \log_{10} \left| \frac{C_N}{\sqrt{2} p_o} \right|^2 \\ &= 124.57 + 10 \log_{10} \left| \frac{C_N}{p_R} \right|^2 \end{aligned}$$

with

$$p_o = 20 \mu\text{N}/\text{M}^2 = 4.177 \times 10^{-7} \text{ psf}$$

$$p_R = 47.88 \text{ N}/\text{M}^2 = 1 \text{ psf}$$

Reference 33 provides a theoretical approach for estimating the far-field, acoustic pressure produced by harmonic loads on a rotor. The result, equation (34) in reference 33, gives an expression for the discrete tone phasor,  $C_N$ , above in terms of these loads.

$$C_N = C_{TN} + C_{DN} + C_{RN} \quad (47)$$

with

$$C_{TN} = \sum_{\lambda=-\infty}^{\infty} i^{-(n-\lambda)} \left( \frac{i n \Omega x}{2 \pi c_0 r_1^2} \right) A_{T\lambda} J_{n-\lambda} \left( \frac{n M y}{r_1} \right)$$

= Thrust component

$$C_{DN} = - \sum_{\lambda=-\infty}^{\infty} i^{-(n-\lambda)} \left( \frac{i(n-\lambda)}{2 \pi r_1 R} \right) A_{D\lambda} J_{n-\lambda} \left( \frac{n M y}{r_1} \right)$$

= Drag or torque component

$$C_{RH} = \sum_{\lambda=-\infty}^{\infty} i^{-(n-\lambda)} \left( \frac{n \Omega y}{2 \pi c_0 r_1^2} \right) A_{R\lambda} J'_{n-\lambda} \left( \frac{n M y}{r_1} \right)$$

= Radial component

where

$n$  = NB

$r_1$  = r SF

$r$  = Distance from observer to rotor hub at retarded time

$M$  = Rotational Mach number of a point on the rotor

=  $\Omega R / c_0$

$\Omega$  = Rotational speed (rad/sec)

$R$  = Radius of a point on the rotor

$c_0$  = Local speed of sound



$$\frac{x}{r} = \cos \psi$$

$$\frac{y}{r} = \sin \psi$$

$\psi$  = Directivity angle between the rotor inlet axis and a line to the observer at retarded time

$i$  = Imaginary number,  $\sqrt{-1}$

and  $(A_{T\lambda}, A_{D\lambda}, A_{R\lambda})$  represent the complex Fourier coefficients for the harmonic loads appearing on a rotor blade, i.e.,

$$A_{\lambda} = \frac{\Omega}{2\pi} \int_{-\pi/\Omega}^{\pi/\Omega} f(\tau) \exp(-i\lambda\Omega\tau) d\tau$$

$$f(\tau) = \sum_{\lambda=-\infty}^{\infty} A_{\lambda} \exp(i\lambda\Omega\tau)$$

However, reference 35 points out that an "effective" helical Mach number,  $M_E$ , is to be used in lieu of  $M$  above to account for motion relative to a stationary observer.

$$M_E^2 \approx M^2 + (M_O \cos \alpha)^2$$

In this expression,  $\alpha$  is the angle between the rotor axis and the direction of the aircraft's motion. Combining terms into equation (47) gives

$$C_{TN} \approx \frac{i n M_E \cos \psi}{2 \pi R r S F^2} \sum_{\lambda=-\infty}^{\infty} i^{-(n-\lambda)} A_{T\lambda} J_{n-\lambda} \left( \frac{n M_E \sin \psi}{S F} \right)$$

$$C_{DN} \approx \frac{-i n M_E}{2 \pi R r S F^2} \sum_{\lambda=-\infty}^{\infty} i^{-(n-\lambda)} A_{D\lambda} \left[ \frac{S F}{M_E} \left( \frac{n-\lambda}{n} \right) \right] J_{n-\lambda} \left( \frac{n M_E \sin \psi}{S F} \right)$$

$$C_{R'i} \approx \frac{n M_E \sin \psi}{2 \pi R r S F^2} \sum_{\lambda=-\infty}^{\infty} i^{-(n-\lambda)} A_{R\lambda} J'_{n-\lambda} \left( \frac{n M_E \sin \psi}{S F} \right)$$

Changing the order of summation from  $(-\infty, \infty)$  to  $(1, \infty)$  and noting that  $A_{-\lambda} = A_{\lambda}^*$ , complex conjugate, yields

$$C_N = C_{TN} + C_{DN} + C_{RN} \quad (48)$$

$$\begin{aligned} \text{with } C_{TN} &\approx \frac{i M_E \cos \psi}{2 \pi R r S F^2} \left\{ i^{-n} A_{T0} J_n \right. \\ &\quad \left. + \sum_{\lambda=1}^{\infty} i^{-(n-\lambda)} \left[ A_{T\lambda} J_{n-\lambda} + (-1)^{\lambda} A_{T\lambda}^* J_{n+\lambda} \right] \right\} \\ C_{DN} &\approx \frac{-i n M_E}{2 \pi R r S F^2} \left\{ i^{-n} A_{D0} \left( \frac{S F}{M_E} \right) J_n \right. \\ &\quad \left. + \sum_{\lambda=1}^{\infty} i^{-(n-\lambda)} \left[ \left\{ \frac{S F}{M_E} \left( \frac{n-\lambda}{n} \right) \right\} A_{D\lambda} J_{n-\lambda} + (-1)^{\lambda} \left\{ \frac{S F}{M_E} \left( \frac{n+\lambda}{n} \right) \right\} A_{D\lambda}^* J_{n+\lambda} \right] \right\} \\ C_{RN} &\approx \frac{n M_E \sin \psi}{2 \pi R r S F^2} \left\{ i^{-n} A_{R0} J'_n \right. \\ &\quad \left. + \sum_{\lambda=1}^{\infty} i^{-(n-\lambda)} \left[ A_{R\lambda} J'_{n-\lambda} + (-1)^{\lambda} A_{R\lambda}^* J'_{n+\lambda} \right] \right\} \end{aligned}$$

where the argument in the Bessel functions above is  $(n M_E \sin \psi / S F)$  and the following identities are to be used in evaluating the negative order Bessel functions and their derivatives.

$$J'_{n-\lambda} = 0.5 \left[ J_{n-\lambda-1} + J_{n-\lambda+1} \right]$$

$$J'_{n+\lambda} = 0.5 \left[ J_{n+\lambda-1} + J_{n+\lambda+1} \right]$$

$$J_{n-\lambda} = (-1)^{n-\lambda} J_{|n-\lambda|}$$

*Loading laws.*—Up to this point, it has been assumed that the harmonic loads ( $A_{T\lambda}$ ,  $A_{D\lambda}$ ,  $A_{R\lambda}$ ) are known; in reality they are not. References 33, 35, and 36 argue that the harmonic loads are to be considered random in phase with respect to harmonic order,  $\lambda$ , and position,  $R$ , across the rotor. For the purpose of noise calculations, an equivalent load is assumed to be applied somewhere between 0.5 and 0.8 span. The position is based on a centroid calculation for the mean-square-pressure distribution on a blade.

This point load concept permits a simplification of equation (48), i.e., the values of  $M_E$  and  $R$  at the centroid can be used, to relate noise to the steady forces on a rotor. The harmonic loads are in turn related to the steady force by the following approximate loading law.

$$2 |A_{\lambda}| / A_0 = g(\lambda) \quad (49)$$

where

$$g(\lambda) \approx c |\lambda|^{-(m+0.5)}$$

and  $m$  and  $c$  are determined by physical argument and/or experiment.

These loading laws imply that an effective phase for the Fourier coefficients,  $A_{\lambda}$ , is  $45^\circ$  for  $\lambda > 0$ . Also, the summation in equation (48) with respect to  $\lambda$  is to be done on an R-M-S basis after the algebraic sum of the load components. Free-field, acoustic measurements on the inlet axis of the rotor, theoretically, provide an estimate for  $|A_{T\lambda}|$  with ( $r > 10 \max[c_0/(Nf_0), R_T]$  and  $\lambda = NB$ ).

$$\text{That is: } |A_{T\lambda}|^2 \approx 8 \left( \frac{\pi R r S F^2 p_0}{\lambda M_E} \right)^2 10^{-1} L_N$$

Similarly, measurements in the plane of the rotor can provide an estimate of  $|A_{D\lambda}|^2$  if the radial forces are small in comparison to the drag forces due to torque—i.e.,

$$|A_{R\lambda}| \ll |A_{D\lambda}|$$

See references 37 and 38 for further details.

References 33 and 37 say that  $c \approx 1$  and  $m \approx 2$  for hovering helicopters. Thus

$$g(\lambda) \approx |\lambda|^{-2.5} \quad (50A)$$

On the other hand, reference 35 gives a physical argument and data (fig. 74) which show that equation (49) applies with  $c \approx 1$  and the exponent term,  $m$ , determined by a formula which includes effects of rotor orientation and aircraft speed. Therefore for helicopters and tilt rotors:

$$g(\lambda) \approx |\lambda|^{-(m+0.5)} \quad (50B)$$

where

$$m \approx 0.0485 \left[ \frac{16 \pi (V_o \cos \alpha + v)}{\sigma S \Omega R_T} \right] + 1.3$$

$$\approx 1.3 + 0.4876 [V_I S_o / (S \sigma V_T)]$$

$V_o$  = Aircraft velocity

$v$  = Induced velocity of the air

$$\approx 0.5 \left\{ -(V_o \cos \alpha) + [(V_o \cos \alpha)^2 + (2 g_c T) / (\rho_o R_T^2)]^{.5} \right\}$$

$V_I$  = Normal inflow velocity

$$\approx 0.5 \left\{ (V_o \cos \alpha) + [(V_o \cos \alpha)^2 + a \frac{T_{so} T}{P_{so} D_T^2}]^{.5} \right\}$$

$V_T$  = Tip speed

$T$  = Total gross thrust for rotor

$\rho_o$  = Density of the air

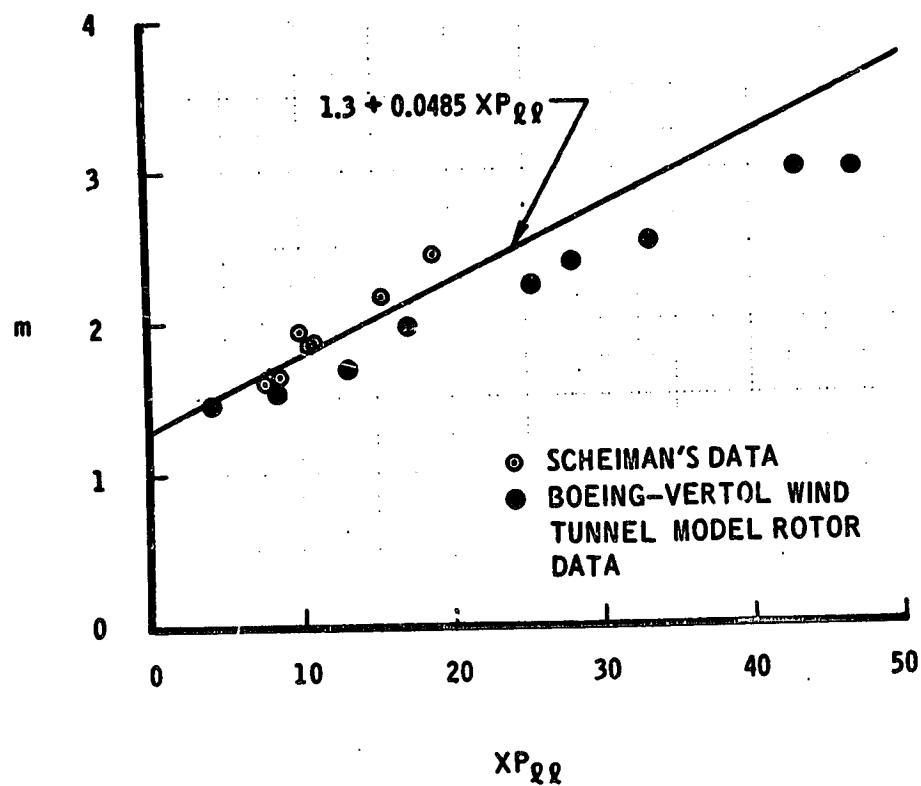
$$= P_{so} / (R_c T_{so})$$

$P_{so}$  = Static pressure of ambient air (absolute units)

$T_{so}$  = Static temperature of ambient air (absolute units)

$R_T$  = Tip radius

$D_T$  = Tip diameter



$$XP_{RL} = \frac{16\pi(V_0 \cos \alpha + v)}{\sigma S \Omega R_T}$$

FIGURE 74.—LOADING LAW PARAMETER "m" FOR HELICOPTERS AND TILT ROTORS

$\sigma$  = Blade area/disc area

$S$  = Lift-curve slope of one rotor blade

$S_0$  = Reference lift-curve slope  $\approx 5$  for data in figure 74

$a$  =  $730.97 (M/S)^2$  per  $(^\circ K)$

$$= 7.2141 \times 10^{-3} \frac{ATM}{N/M^2} (M/S)^2 \text{ per } (^\circ K)$$

$$= 4371.03 (fps)^2 \text{ per } (^\circ R)$$

$$g_c = 1.0 \frac{KG-M}{N-sec^2} = 32.17405 \frac{lbm-ft}{lbf-sec^2}$$

$$R_c = 287.05 \frac{N-M}{KG-^\circ K} = 2.833 \times 10^{-3} \frac{ATM-M^3}{KG-^\circ K}$$

$$= 53.35045 \frac{ft-lbf}{lbm-^\circ R}$$

For low-speed,  $M_T < 0.3$ , propeller noise estimates, reference 37 gives the empirical loading law

$$g(\lambda) \approx 0.86 |\lambda|^{-1.43} \quad (50C)$$

and reference 36 says; for the same tip speed range

$$g(\lambda) \approx 0.04 [\lambda^2 (1 + |\lambda/36|^3)]^{-0.5}$$

There seems to be a typographical error here, because this formula doesn't match the empirical data in reference 37. The correct formula should be

$$\begin{aligned} g(\lambda) &\approx 1.22 \left[ |\lambda|^3 \left\{ 1 + (\lambda/36)^2 \right\} \right]^{-0.5} \\ &\approx 44.0 |\lambda|^{-2.5} / \left[ 1 + (36/\lambda)^2 \right]^{0.5} \end{aligned} \quad (50D)$$

Although the two equations, (50C) and (50D), appear quite different, they match the same data (fig. 75a) and have one thing in common when compared to the equations for helicopters—the propeller harmonic loads are typically higher.

More recent data (ref. 38) at the propeller conditions,  $0.5 < M_T < 0.7$ , yield yet another loading law

$$g(\lambda) \approx 24.4 |\lambda|^{-2.5} / [1 + (30/\lambda)^2]^{0.5} \quad (50E)$$

This formula is derived from the data given in reference 38. The spread in the data between that for the thrust and torque harmonics is probably due to—the equivalent point loads for thrust and drag act at different centroids. Thus, the use of a single point load for calculating the harmonic tones results in a tolerance of about  $\pm 8.0$  dB. A plot of equation (50E) is shown in figure 75b. In view of the data and formulae presented, one would expect that the general form of the loading law is

$$g(\lambda) \approx c \left[ |\lambda|^{2m+1} \left\{ 1 + (\lambda_c/\lambda)^2 \right\} \right]^{-0.5} \quad (51)$$

with the parameters  $(c, m, \lambda_c)$  determined by experiment. In actual practice, the form of equation (49) should suffice for determining the sound harmonics of orders;  $1 < N < 30/B$ . For more accurate estimation of sound harmonics outside this range, equation (51) should be used.

*Simplification.*—In order to put equation (48) in more useable form, the following notation is used.

$$A_{TO} = T/B$$

$$A_{DO} = h_D A_{TO}$$

$$A_{RO} = h_R A_{TO}$$

$$|A_{T\lambda}| = 0.5 A_{TO} g(\lambda) \quad \text{for } |\lambda| > 0$$

$$|A_{D\lambda}| = h_D |A_{T\lambda}| \quad \text{for } |\lambda| > 0$$

$$|A_{R\lambda}| = h_R |A_{T\lambda}| \quad \text{for } |\lambda| > 0$$





with the function  $g(\lambda)$  given by one of the various loading laws, equations (49), (50A) through (50E), and (51). Assuming random phase, as was done in references 33 and 35, we put

$$A_\lambda \approx \frac{|A_\lambda|}{\sqrt{2}} (1 + i), \quad \lambda > 0$$

for each load component. Insertion into the random phase form of equation 48 yields

$$|C_N|^2 \approx \left( \frac{N M_E T}{4 \pi R r S F^2} \right)^2 \left[ 2 (\alpha_{n0}^2 + \beta_{n0}^2) + \sum_{\lambda=1}^{\infty} g^2(\lambda) (\alpha_{n\lambda}^2 + \beta_{n\lambda}^2) \right] \quad (52)$$

where

$$\alpha_{n\lambda} = \left[ h_R \sin \psi J'_{n-\lambda} \right] + \left[ \cos \psi - h_D \left( \frac{SF}{M_E} \right) \left( \frac{n+\lambda}{n} \right) \right] (-1)^\lambda J_{n+\lambda}$$

$$\beta_{n\lambda} = \left[ \cos \psi - h_D \left( \frac{SF}{M_E} \right) \left( \frac{n-\lambda}{n} \right) \right] J_{n-\lambda} - \left[ h_R \sin \psi (-1)^\lambda J'_{n+\lambda} \right]$$

$(n M_E \sin \psi / SF)$  = argument in the Bessel functions

$n$  =  $N B$

$M_E$  = Helical Mach number at radius  $R$

$R$  = Radial centroid for equivalent point load.

Equation (52) above provides an estimate of the far-field discrete tones at a distance,  $r$ , from the rotor hub. This estimate also corresponds to free-field conditions.

In the application of equation (52), limitations must be employed to computerize the procedure. Obviously, the summation with respect to  $\lambda$  must be truncated when the terms cease to add to the noise. References 33, 37, and 38 show that the effective range for  $\lambda$  is

$$n (1 - q) \leq \lambda \leq n (1 + q)$$

with

$$q = \left| M_E \sin \psi / SF \right|$$

and the terms containing  $J_{n+\lambda}$  and  $J'_{n+\lambda}$  can be neglected.

It also can be shown that the radial load components can be neglected in equation 52 because their amplitude is much less than that due to thrust or torque. This results in a less complex equation

$$|C_N|^2 \approx \left( \frac{N M_E T}{4 \pi R r SF^2} \right)^2 \left[ 4 \left\{ \cos \Psi - h_D \left( \frac{SF}{M_E} \right) \right\}^2 J_n^2(nq) + \sum_{\lambda=K_1}^{K_2} g^2(\lambda) J_{n-\lambda}^2(nq) \left\{ \cos \Psi - h_D \left( \frac{SF}{M_E} \right) \left( \frac{n-\lambda}{n} \right) \right\}^2 \right] \quad (53)$$

where

$$K_1 = \text{Max}[n(1-q)-0.5, 1] \text{ (integer result)}$$

$$K_2 = n(1+q)+0.5 \quad \text{(integer result)}$$

$$q = \left| M_E \sin \Psi / SF \right|$$

$$n = NB$$

$$M_E = \text{Helical Mach number at radius } R$$

$$R = \text{Radial centroid for equivalent point load}$$

$$g(\lambda) = \text{Represents the loading-law function, equations (49) through (51)}$$

$$T = \text{Total thrust for rotor}$$

$$h_D = \text{Drag/thrust ratio}$$

$$h_D = (Q/R)/T \text{ where } Q \text{ is the total torque on the rotor}$$

$$r = \text{Distance from rotor hub at retarded time}$$

$$\Psi = \text{Directivity angle re. rotor inlet axis at retarded time}$$

$$SF = \text{Doppler-shift factor, } 1 - M_O \cos \xi$$

The use of equation (53) to calculate *all* the sound harmonics required in the audio frequency range would be quite expensive—even on high-speed computers. Reference 33 has shown that the resulting values of  $L_N$  vary in a smooth fashion when plotted against  $\log(N)$ . Suppose that a data curve as shown in figure 76 can be developed through use of equation (53) for a selected set of values for  $N$ . Then by means of interpolation/extrapolation with respect to  $\log(N)$ , *all* the necessary sound harmonic levels,  $L_N$ , can be obtained at a tremendous saving in computer storage and time.

Additional limitations must be employed in order to reduce computer storage and time. The practical limitations for rotors and propellers are

$$2 \leq B \leq 6$$

$$0 < \frac{M_E}{SF} < 1$$

As was mentioned previously, the values of  $N$  will be limited to

$$1 \leq N \leq 21$$

Also, symmetry implies that the values for  $\sin \Psi$  are contained in

$$0 \leq \sin \Psi \leq 1$$

Thus the maximum range for  $\lambda$  in equation (53) is given by

$$1 \leq \lambda \leq 2n$$

where  $n = NB$  and the orders of the Bessel functions,  $J_K$ , which could have to be calculated and stored are

$$0 \leq K \leq n$$

Inserting the possible values give

$$0 \leq K \leq 42 \quad \text{for } B = 2$$

$$0 \leq K \leq 63 \quad \text{for } B = 3$$

....

$$0 \leq K \leq 126 \quad \text{for } B = 6$$

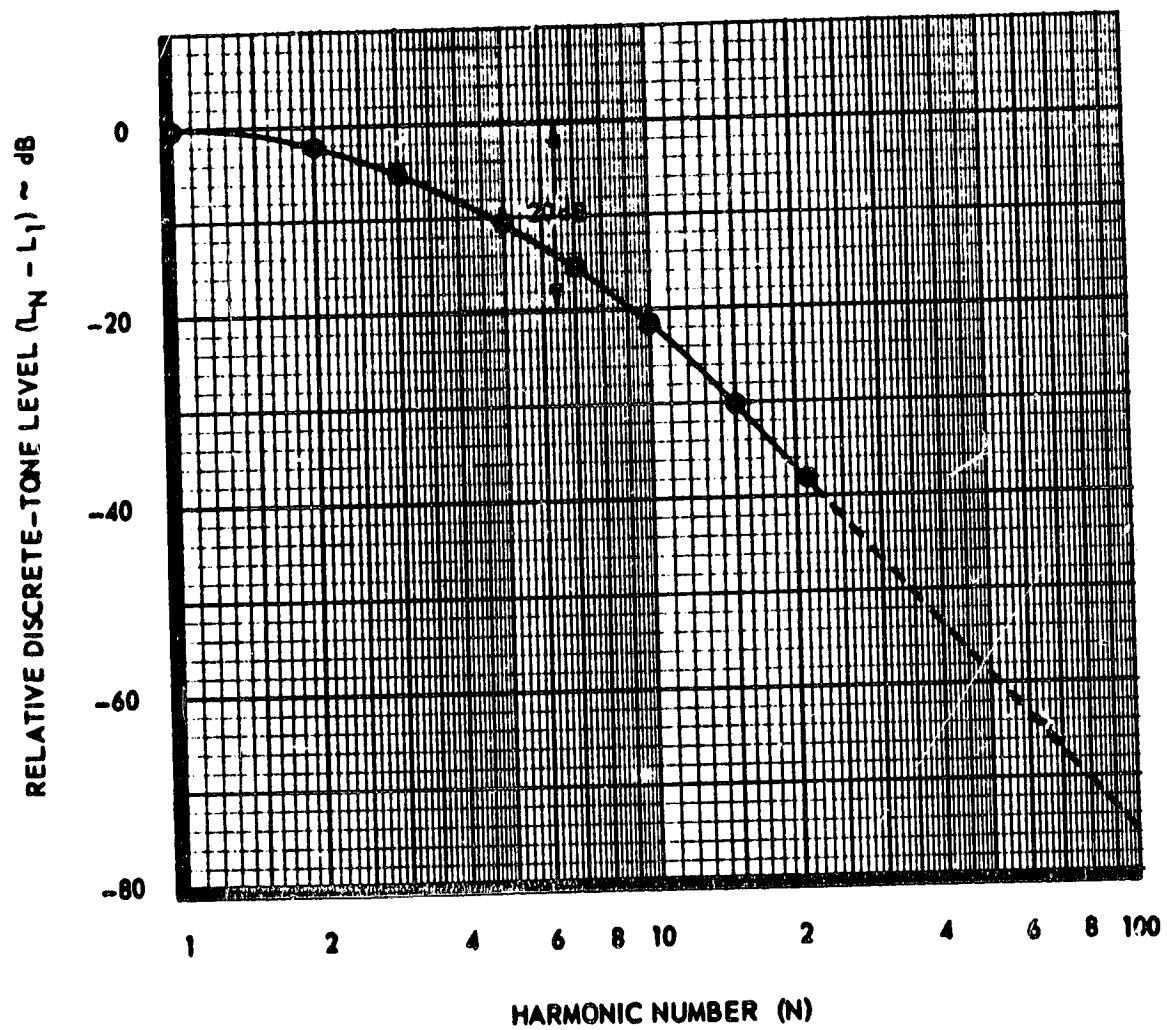


FIGURE 76.—TYPICAL DISCRETE-TONE LEVELS VERSUS HARMONIC NUMBER

or in general,

$$0 \leq K \leq N B$$

with  $N$  being the harmonic number for the discrete-tone occurring at the frequency,  $N f_0$ .

*Other harmonic noise sources.*—There are three other noise sources present for rotating propellers, and/or rotors. These sources are (1) "thickness-noise" (dipole character), (2) Reynolds stress noise (quadrupole character), and (3) blade-slap. In practice, these noise sources are usually neglected. The reasons are discussed below.

In addition to the thrust and drag loading noise already discussed, another dipole source is present (refs. 36 through 38). This source has been given the term "thickness noise" due to its strength being proportional to the blade volume and the local blade acceleration (ref. 36). For rotors operating at constant speed ( $\dot{\theta}$  and  $M_0$  constant), the only acceleration present is that in the radial direction. (Note that the blades are considered rigid.) Thus this source corresponds to the radial loads that appear on the blades. In order to evaluate this source, knowledge of the complete blade geometry is required to perform the necessary integration over the blades. Both Hamilton Standard reports (refs. 37 and 38) have included this source in their calculations. They report that this source can dominate over the loading noise due to thrust and drag if the propeller is lightly loaded or if the blades are rather thick. Reference 36 argues that this source will only be significant, relative to the thrust and drag terms, for very thick blades at low loading conditions. Although these three reports agree in concept; the emphasis of reference 36 differs. This latter emphasis leads to the assumption: "The thickness-noise contribution to the discrete-tone levels produced by propellers/rotors can be neglected, if the blades are not thick and/or lightly loaded."

The relative magnitude of the quadrupole sources when compared to that for dipole sources is given by reference 36 as

$$\left( \frac{C_N}{\text{Quadrupole}} \right) / \left( \frac{C_N}{\text{Dipole}} \right) \sim n M \left( \frac{t}{R} \right) \cos \xi$$

This relation shows that the dipole (force) noise components dominate in most practical applications. However, as  $M \cos \xi$  approaches unity and  $n$  gets greater than 100, the quadrupole sources become dominant. "In assessing these results, it is of course important to remember that these results apply only to the specific case examined. . . . Despite these limitations, it may be concluded that for quiet propellers operating at tip speeds of less than about  $M = 0.5$ , the quadrupole noise should not be expected to make significant contributions to the harmonic noise

for  $n < 200$ , even on the propeller axis" (ref. 36). For further details see pages 1, 9, 68 of reference 36.

Under the various helicopter operations (for instance, during low-power descent), the rotor produces a loud impulsive noise. The energy for this noise consists of harmonic tones that occur at multiples of the fundamental blade-passage frequency, but the distribution does not fall-off rapidly with increasing harmonic number—hence, the impulsive character. This noise has been given the term "blade-slap." Whenever this "impulsive" noise occurs, it is particularly severe, but it also has a highly directional radiation pattern. Thus blade-slap is not always heard, even though it may exist (ref. 33).

This phenomena occurs at precisely those conditions when a vortex wake can be expected to pass very close to the rotor. Blade-slap can also occur when the rotors are operated at high speed. Then, it is associated with transonic flow over the rotor blades. Thus, there are two possible sources of blade-slap—vortex interaction and/or transonic flow. These phenomena can be predicted. "However, it seem inappropriate to consider blade-slap as a separate phenomenon. The helicopter rotor is always undergoing some form of vortex interaction, and blade-slap is simply a severe form. Perhaps it is more realistic to suppose that, at least from the acoustic point of view, the helicopter is always flying under some degree of blade-slap" (ref. 33).

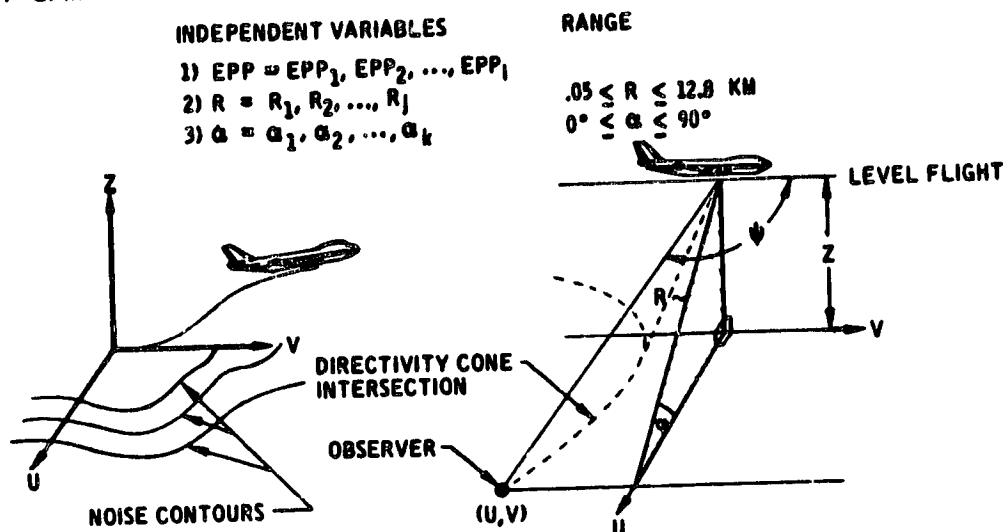
The loading-law, equation (50<sup>B</sup>), includes some of these vortex interaction effects and its use is recommended. Hopefully, this equation approximates the low-degree, blade-slap mentioned above. No additional effort was made, however, to try and predict the special severe case.

### 5.3 NOISE CONTOUR ESTIMATION

A noise contour is the locus of points on the ground in which the noise is at a constant acoustic level. The calculation of a noise contour requires the establishment of the relationship between the aircraft's noise performance and the aero/propulsion parameters during takeoff and landing. The following optimized method is presented which will fit within the computer time and storage constraints of the Ames flight simulator.

The relationships mentioned above are established when data points are given for noise level (NL), engine performance (EPP), range at closest point of approach (R), and elevation angle ( $\alpha$ ), for an aircraft during level flight (see fig. 15 and table 11). This data can then be formed into tabular functions: NL versus (EPP,  $\log R, \alpha$ ), or  $\log R$  versus ( $\alpha$ , EPP) for each noise contour. When the airplane coordinates and EPP are given, interpolation using these functions at the geometry shown in figure 77 provides two points (one for each side of the flight track) on the ground for a specific

TABLE 11.—SAMPLE NOISE DATA GRID FOR NOISE CONTOUR COMPUTER PROGRAM



NOISE DATA GRID: 54 OBSERVER POSITIONS, 22 ALTITUDES									
VARIABLE	DISTANCES (KM)								
R	.05	.1	.2	.4	.8	1.6	3.2	6.4	12.8
$\alpha = 0^\circ \quad \sin \alpha = 0$									
U =	.05	.1	.2	.4	.8	1.6	3.2	6.4	12.8
Z =	0	0	0	0	0	0	0	0	0
$\alpha = 7.18^\circ \quad \sin \alpha = .125$									
U =	.0496	.0992	.198	.397	.794	1.59	3.17	6.35	12.7
Z =	.00625	.0125	.025	.05	.1	.2	.4	.8	1.6
$\alpha = 14.46^\circ \quad \sin \alpha = .25$									
U =	.0484	.0968	.194	.387	.774	1.55	3.10	6.20	12.4
Z =	.0125	.025	.05	.1	.2	.4	.8	1.6	3.2
$\alpha = 30^\circ \quad \sin \alpha = .5$									
U =	.0433	.0866	.173	.346	.693	1.38	2.77	5.54	11.1
Z =	.025	.05	.1	.2	.4	.8	1.6	3.2	6.4
$\alpha = 45^\circ \quad \sin \alpha = .707107$									
U =	.0354	.0707	.141	.283	.566	1.13	2.26	4.52	9.05
Z =	.0354	.0707	.141	.283	.566	1.13	2.26	4.52	9.05
$\alpha = 90^\circ \quad \sin \alpha = 1.0$									
U =	0	0	0	0	0	0	0	0	0
Z =	.05	.1	.2	.4	.8	1.6	3.2	6.4	12.8

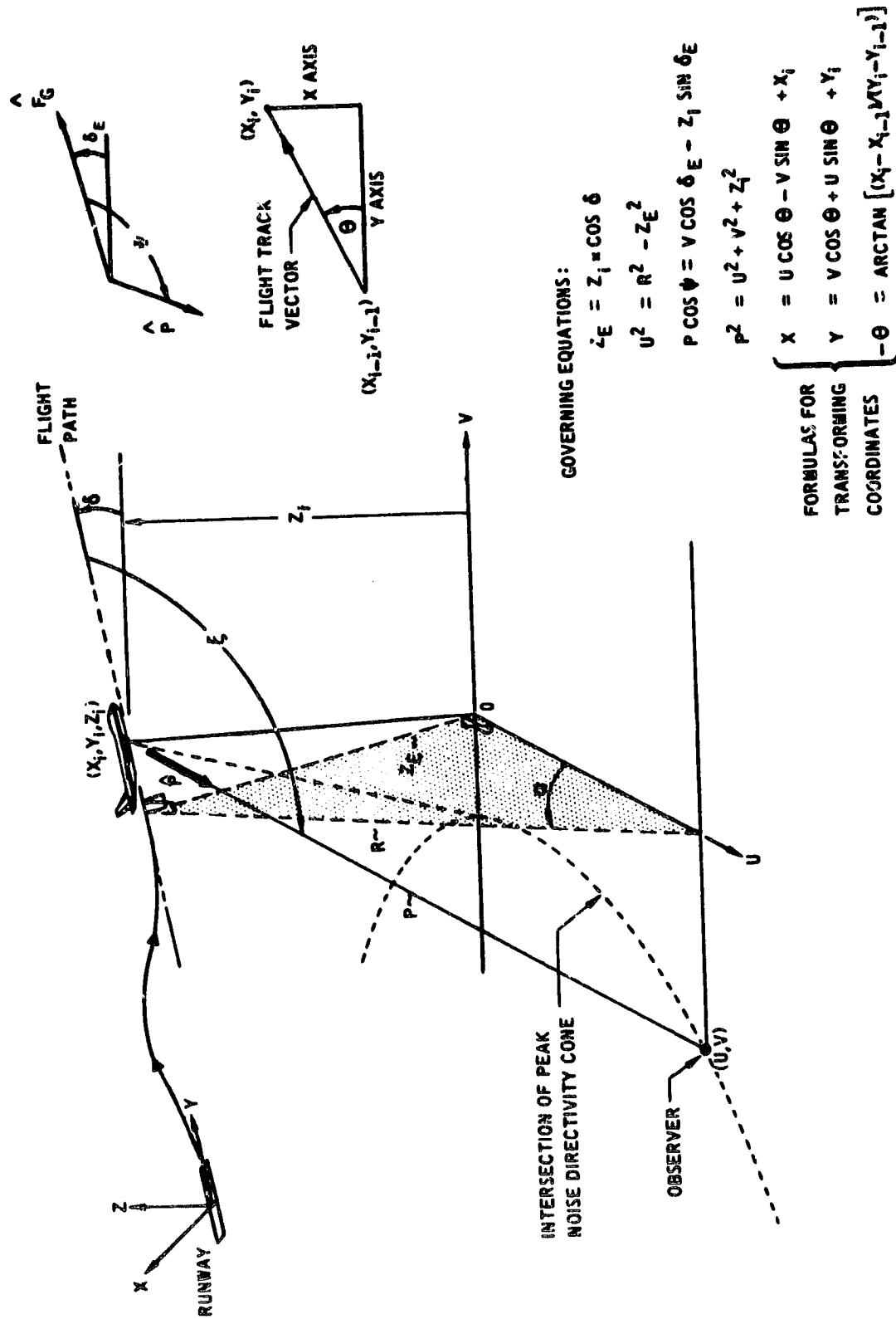


FIGURE 77.—NOISE CONTOUR GEOMETRICAL RELATIONSHIPS



noise level. If a series of these points are calculated during an aircraft's takeoff or landing, a noise contour is determined. The area enclosed by this contour can be calculated.

Although there exist more refined methods for calculating noise contours, they require rather lengthy calculations, and result in increased computer time and storage. This makes them undesirable candidates for flight simulator use. The approach presented here has the advantage of minimizing computations and reducing storage requirements. Despite the fact that this method uses approximations, when sufficient data points are provided by measurement or by prediction, the procedure provides reasonably accurate noise contours.

### 5.3.1 Acoustic Data

The acoustic data required for noise contour estimation consists of a directivity angle for peak noise radiation and a tabulated function of three variables—noise level versus EPP, R, and  $\alpha$  (see fig. 15). It is of particular importance, when constructing this function, that the data is for level flight and that it is sampled in the manner indicated in table 11; i.e., in equal steps of  $\log R$  for angular increments of  $\sin \alpha = 0, 0.125, 0.25, 0.5, 0.707107, \text{ and } 1.0$ . The noise contour computer program has been optimized for data given in this form and provides the greatest accuracy for a minimum amount of data. Also the noise levels are to be strictly monotonic; decreasing noise with respect to increasing values of  $\log R$ . If this constraint is not adhered to, the whole procedure fails. This constraint poses no restriction to observed aircraft noise or to that provided by the noise source estimation procedure.

### 5.3.2 Aero/Propulsion Data

The aero-propulsion data required for noise contour estimation consists of a series of points along the aircraft's takeoff or landing flight path which define the airplane position ( $x, y, z$ ), the orientation angle ( $\delta_E$ ) for the reference axis of the dominant noise source and the engine performance (EPP). During the Phase A portion of the contract, the key engine performance parameter was engine pressure ratio (EPR) due to its relationship to other jet engine cycle parameters, i.e., there is one-to-one correspondence between EPR and all other engine cycle parameters and this correspondence is constant with altitude for a fixed aircraft velocity. Since the noise produced by jet engines is directly related to the engine cycle, it will also follow this correspondence with EPR at a reference off-axis distance. However, jet engines are not the only powerplants considered in the Phase B effort. The choice of what the engine performance parameter represents is left up to the user.

### 5.3.3 Noise Contour Calculation

The noise contour calculation can be broken down into four basic steps. The first is the formation of the acoustic data functions:

$$NL = f_1(EPP, \log R, \alpha)$$

and

$$\log R = f_2(\alpha, EPP)$$

for each noise contour from the given data points ( $NL_k, EPP_k, R_k, \alpha_k$ ). This step is done only once. Thereafter, the calculation requires interpolation for  $\log R$  at a desired contour noise level (CNL) and geometry shown in figure 77. The next steps are the geometric solutions for the contour points (U, V) in a moving reference frame and finally, the transformation of contour coordinates (U, V) to the fixed (X, Y, Z) coordinate system (see fig. 77). The details are outlined below.

a) Formation of the acoustic data functions,  $f_1$  and  $f_2$ :

Data points ( $NL_k, EPP_k, R_k, \alpha_k$ ) are assumed to be given from the use of the noise source estimation computer program or from measurements (table 11). Sort the given data with respect to increasing values of  $EPP_k, R_k, \alpha_k$  as these variables will be treated as independent for the function  $f_1$ . Next, determine the distinct values for the given arrays ( $EPP_k, R_k, \alpha_k$ ) and use the results for the independent variable data arrays specifying where noise levels are defined.

NOTE: The three-dimensional function  $NL = f_1(EPP, \log R, \alpha)$  is now formed.

Specifying the desired contour noise levels ( $CNL_j$ ) permits the transformation of the function  $f_1$  to a function  $\log R = f_2(\alpha, EPP)$  for each  $CNL_j$ . This is done by one-dimensional interpolation on  $f_1$  at  $NL = CNL_j$  for  $j = 1, 2$ , etc.

NOTE: The transformation assumes that the function  $f_1$  is monotonic: decreasing with respect to increasing values of  $\log R$ .

b) Calculation of  $\log R$  for a specific contour  $CNL_j$ :

At each point along the aircraft's flight path the following data is required.

$z_i$  aircraft height above the ground

$\delta_i$  climb angle, i.e., computed as the arc tangent of the climb gradient

$\delta_{Ei}$  Orientation angle of the dominant noise source reference axis—usually the angle between the gross thrust vector and the horizon

$EPP_i$  engine performance parameter

Calculation:

$$\begin{aligned} \text{let } Z_E &= \text{aircraft-to-ground distance perpendicular to the flight path} \\ &= z_i \cos \delta_i \end{aligned}$$

Iterate the calculations below until  $|\alpha - \alpha_0| \leq \epsilon |\alpha|$ . In this iteration,  $\alpha_0$  is set initially to the value  $45^\circ$  for each noise contour and is updated at each aircraft position along the flight path. The value,  $\epsilon$ , is a tolerance constant for the iteration; a reasonable value is  $1.2 \times 10^{-3}$ .

$$\log R = \text{interpolation on } f_2 \text{ at } (\alpha_0, EPP_i)$$

$$\alpha = \arcsin (Z_E/R)$$

Test  $\alpha$  for convergence with  $\alpha_0$  and update  $\alpha_0$  if another iteration is required.

In the computer program, a test for contour closure is made just before the calculation of  $\alpha$  above. Closure occurs when  $R < Z_E$ . The action taken is to set  $\alpha = 0.5 (\alpha_0 + 90^\circ)$ . This is done to avoid premature closure estimates that have occurred during rapid cutback operations. If closure has indeed occurred, the program contains a "trap" and sets a corresponding error code.

c) Calculation of contour points (U, V):

$$U^2 = R^2 - Z_E^2$$

$$V = \text{Solution of } \begin{cases} P \cos \psi = V \cos \delta_{Ei} - z_i \sin \delta_{Ei} \\ P^2 = U^2 + V^2 + z_i^2 \end{cases}$$

where

$R$  = range at CPA calculated for the noise contour in step (b).

$\psi$  = directivity angle for peak passby noise propagation relative to the dominant noise source reference axis.

NOTE: Singularities can exist when  $\delta_{Ei} = \pm 90^\circ$ , and/or the directivity cone does not intersect the ground at sideline distances  $\pm U$ . Helicopters, tilt rotor aircraft, etc. require special consideration. The singularities can be avoided by letting

$$\delta_{Ei} = \delta_i \text{ and } \Psi = 90^\circ.$$

d) Coordinate transformations:

$$\text{let } dx = x_i - x_{i-1}$$

$$dy = y_i - y_{i-1}$$

$$ds_i^2 = dx^2 + dy^2$$

$$\sin \theta = -dx/ds_i$$

$$\cos \theta = dy/ds_i$$

$$x = U \cos \theta - V \sin \theta + x_i$$

$$y = V \cos \theta + U \sin \theta + y_i$$

where

$(x_{i-1}, y_{i-1}), (x_i, y_i)$  = Aircraft coordinates for the previous and present position along the flight path.

$(U, V)$  = Contour points in moving reference frame calculated in (c).

#### 5.3.4 Area Calculation

The area enclosed by each noise contour is calculated after the points,  $(U, V)$ , are determined for aircraft positions  $(x_i, y_i, z_i)$ ,  $i = 1, 2$ , etc. The procedure is as follows:

$$A_j = \sum_i \Delta A_{ij}$$

for each contour  $CNL_j$  where (from section 5.2.3)

$$\Delta A_{ij} = (U_i + U_{i-1})(V_i - V_{i-1} + ds_i)$$

NOTE: The formula assumes negligible error due to changes in the flight track vector from iteration (i-1) to (i).

### 5.3.5 Noise Estimate on Sideline

Multiple sideline noise estimates are included with the noise contour computer program. The observer locations for these noise numbers are on the sidelines in the (U, V, Z) coordinate system, as shown in figure 77. The sideline distances can be specified by the user; the default values are 1.0 m, 152.4 m (500 feet), 463.3 m. If any or all of the values need to be changed, they may be as a user input.

Calculation:

$$\text{let } R_i^2 = SD^2 + Z_E^2$$

$$\alpha_i = \arccos(SD/R_i)$$

where SD is a set of sideline distances.

A three-dimensional interpolation on  $f_1$  at  $(EPP_i, \log R_i, \alpha_i)$  yields the specified noise estimates.

Boeing Commercial Airplane Company  
P.O. Box 3707  
Seattle, Washington, July 1973

## APPENDIX A THEORETICAL GROUND REFLECTION PREDICTION PROCEDURE

### BACKGROUND (PLANE WAVES)

An acoustic wave in the vicinity of a reflecting surface can be treated as the sum of a direct and reflected wave. The difference in path length for the two signals introduces terms for spherical divergence, phase delay, and absorption (ground and the air). This latter term for air absorption is negligible when compared to the others and will therefore be ignored. When the phase delay approaches odd multiples of  $180^\circ$ , destructive interference results. At even multiples of  $180^\circ$ , constructive interference occurs. This interference complicates the analysis of acoustic data unless efforts are made to eliminate the anomalies it produces in noise spectra. If ground reflection cannot be eliminated, perhaps its effect can be estimated, and measured data can be corrected to free-field or vice-versa. The following is an analysis directed at solving this problem.

Figure A1 shows the geometry of the reflection problem. The receiver (microphone or ear of the observer) receives signals from a direct path and from a reflected path. The distance for the reflected path is  $(P + \Delta P)$ , which can be readily computed from equations (6A) or (6B) in section 5.1.2. Similarly, the angle of incidence,  $\nu_0$ , (which is the same as  $\beta_1$  in section 5.1.2) can be obtained from equation 7. The angle of refraction,  $\nu_1$ , is given by the acoustic equivalent of Snell's law.

$$K_0 \cos \nu_0 = K_1 \cos \nu_1$$

where

$$K_0 = 2\pi f / C_0 \text{ (wave number in air)}$$

$$K_1 \sim 2\pi f / C_1 \text{ (wave number in ground)}$$

In general,  $K_1$  is complex (non-uniform wave), but it can be shown that a *uniform acoustic plane* wave cannot attenuate in the Y-direction for both media (air and ground) when air absorption is neglected.

Further, the imaginary part of  $K_1$  affects only the transmitted signal and not the reflected signal. For this reason, only the real part of  $K_1$  will be considered in what follows. Spherical propagation will be treated later.

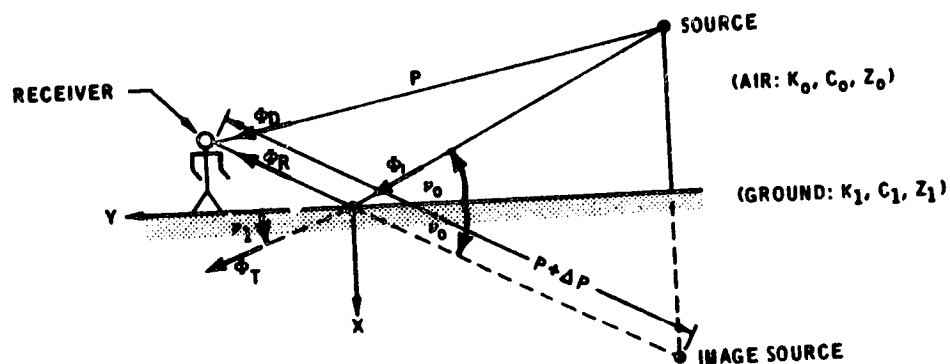


FIGURE A1.—REFLECTION GEOMETRY

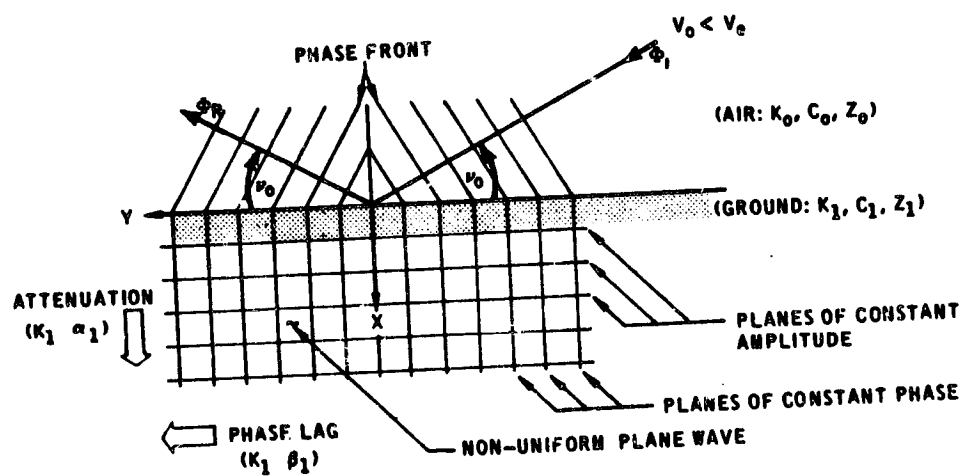


FIGURE A2.—ANGLE OF INCIDENCE LESS THAN CRITICAL

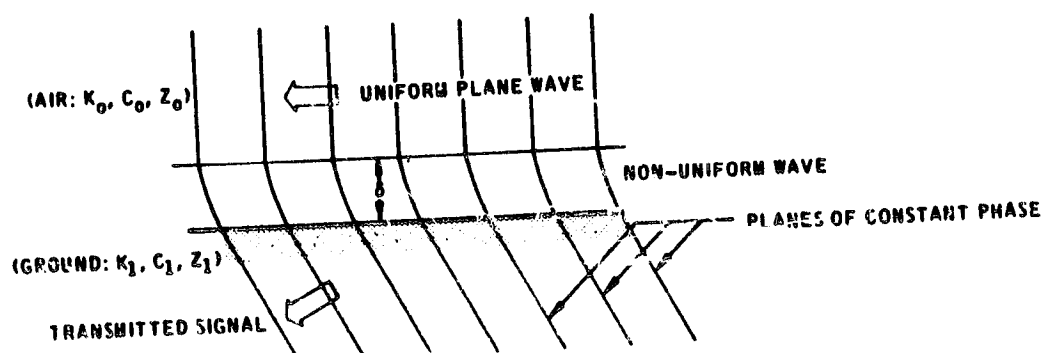


FIGURE A3.—PROPAGATION NEAR A DISSIPATIVE MEDIUM

Therefore,

$$K_1 / K_0 \sim C_0 / C_1$$

where  $C_0$  and  $C_1$  are speeds of sound in the air and ground respectively.

Continuing with the solution for  $\sin \nu_1$ , yields

$$\sin^2 \nu_1 \approx 1 - (K_0/K_1)^2 \cos^2 \nu_0$$

If  $K_0/K_1$  is greater than unity, as is most likely the case for the ground, there is a critical angle,  $\nu_c$ , in which  $\sin^2 \nu_1$  can become negative. That is,

$$\sin \nu_1 = \begin{cases} \alpha_1 & \text{FOR } \nu_0 \geq \nu_c \\ \pm i \alpha_1 & \text{FOR } \nu_0 < \nu_c \end{cases} \quad (\text{A1})$$

where

$$\nu_c = \cos^{-1} (K_1 / K_0)$$

$$\alpha_1 = |1 - (K_0 / K_1)^2 \cos^2 \nu_0|^{0.5}$$

The choice of sign when  $\sin \nu_1$  is imaginary depends upon the convention used to denote phase delay in the velocity potentials ( $\phi$ ) and impedance ( $Z_1$ ), and in the boundary condition—the transmitted signal ( $\phi_T$ ) should vanish as  $X$  approaches infinity.

The convention used here is

$$\begin{aligned} \phi_I &= \text{incident signal} \\ &= \phi_0 \exp[-i K_0 (X \sin \nu_0 + Y \cos \nu_0)] \\ \phi_R &= \text{reflected signal} \\ &= \phi_0 \Gamma \exp[-i K_0 (-X \sin \nu_0 + Y \cos \nu_0)] \\ \phi_T &= \text{transmitted signal} \\ &= \phi_0 \Gamma \exp[-i K_1 (X \sin \nu_1 + Y \cos \nu_1)] \\ \Gamma &= \text{plane-wave reflection coefficient} \\ &= \frac{(Z_1/Z_0) - (\sin \nu_1 / \sin \nu_0)}{(Z_1/Z_0) + (\sin \nu_1 / \sin \nu_0)} \end{aligned} \quad (\text{A2})$$



$$\begin{aligned}
T &= \text{plane-wave transmission coefficient} \\
&= 1 + \Gamma = \frac{2(Z_1/Z_0)}{(Z_1/Z_0) + (\sin \nu_1 / \sin \nu_0)}
\end{aligned}$$

when  $\nu_0$  is less than  $\nu_c$ , we see that  $\phi_T$  will vanish as  $X$  approaches infinity, if and only if;

$$\sin \nu_1 = -i \alpha_1 \text{ and } \cos \nu_1 = \beta_1 = (K_0/K_1) \cos \nu_0$$

where  $(\alpha_1, \beta_1)$  are *positive real* numbers.

That is:

$$\begin{aligned}
\phi_T &= \phi_0 T \exp[-i K_1 (-i \alpha_1 X + \beta_1 Y)] \\
&= \phi_0 T \exp(-K_1 \alpha_1 X) \exp(-i K_1 \beta_1 Y) \\
\lim_{X \rightarrow \infty} \phi_T &= \lim_{X \rightarrow \infty} \exp(-K_1 \alpha_1 X) [\phi_0 T \exp(-i K_1 \beta_1 Y)] \\
&= 0
\end{aligned}$$

These relationships where  $\phi_T$  represents a *non-uniform*, plane wave are shown in figure A2. It is worth noting that there is *no* flow of *real* acoustic power in the  $X$  direction, but there is *real* power flow in the  $Y$  direction for both media (air and ground). Note that  $K_1$  is considered real, i.e., a lossless medium. If  $Z_1/Z_0$  is a positive real number, then the reflection coefficient  $\Gamma$  is  $\exp(i \theta)$ ; and the reflected signal  $\phi_R$  is equal in magnitude to the incident signal  $\phi_I$ , but suffers a phase shift given by

$$\theta = 2 \tan^{-1}[\alpha_1 Z_0 / (Z_1 \sin \nu_0)]$$

This explains how the reflection coefficient can have a phase term different than zero when the ground impedance is real—an apparent contradiction of physics; though not really so, when the critical angle is included in the analysis.

The composite signal of the direct and reflected sound is then given by the velocity potential solution for plane waves as

$$\begin{aligned}
\phi_C &= \phi_D + \phi_R = \phi_D (1 + \phi_R / \phi_D) \\
&= \phi_D [1 + \Gamma \exp(-i K_0 \Delta P)] \quad (A3)
\end{aligned}$$

where  $\phi_D$  is the signal for the direct path and  $\Gamma$  is the reflection coefficient given in equation (A2).

For acoustically hard surfaces like water or concrete,  $|Z_1/Z_0|$  may be as large as  $3 \times 10^3$ , so that the reflection coefficient is approximately unity, except for very small angles of  $\nu_0$ . When  $\nu_0$  approaches zero (grazing incidence), the  $\Gamma$  approaches minus one regardless of the impedance values. Since the difference in path length,  $\Delta P$ , also approaches zero under these conditions, the erroneous conclusion given by equation (A3) is that the observed signal,  $\phi_C$ , vanishes. The contradiction is solved by noting that uniform acoustic plane waves just do not exist. A more detailed analysis in references <sup>15</sup> and <sup>16</sup> shows that the wave fronts are bent in the vicinity of the ground for a "dissipative" reflecting plane (see figure A3).

Since we are interested in the reflected signal, not the transmitted signal, further analysis of this boundary layer phenomenon can serve only academic interest. Its presentation was to point out one reason why equation (A3) fails for propagation at grazing incidence. Another approach follows which considers acoustic waves with spherical propagation. It does not have this singularity.

### SPHERICAL PROPAGATION

Rudnick (ref. 16) showed that equation (A3) can be replaced by

$$\phi_C = \phi_D \left\{ 1 + \Gamma' \exp(-i K_0 \Delta P) \right\} \quad (A4)$$

where

$\Gamma'$  = effective reflection coefficient for spherical propagation

$$= [\Gamma + (1 - \Gamma) F(W)] / (1 + \frac{\Delta P}{P})$$

$\Gamma$  = plane-wave reflection coefficient

$F(W)$  = the "boundary loss factor"

$$\begin{aligned} &= 1 + i 2 \sqrt{W} \exp(-W) \int_{-i\sqrt{W}}^{\infty} \exp(-Z^2) dZ \\ &= 1 - \sqrt{\pi} \int_0^{\infty} Z \exp(Z^2) \operatorname{Erfc}(Z) dZ \text{ with } Z = -i \sqrt{W} \\ W &= [i 2 K_0 P \sin^2 \nu_1] / \left[ \frac{Z_1}{Z_0} (1 - \Gamma) \cos \nu_0 \right]^2 \end{aligned}$$

Equation (A4) applies to a point source, homogeneous media (air and ground) and a smooth/infinite/reflecting plane with complex acoustic wave impedance. When the observer gets sufficiently far away from the sound source,  $\Delta P/P$  approaches zero. If the angle of incidence,  $\nu_0$ , approaches  $90^\circ$  under these conditions, then equation (A4) become identical to equation (A3). In this case, the plane wave approximation is as good as that for spherical propagation. However, aircraft/observer geometry cannot be restricted to just this case and equation (A4) is a better formulation for describing the ground reflection phenomenon and it has therefore been incorporated into the extrapolation methods used in the computer program.

For the purpose of evaluating the "boundary loss factor," the following expansions are given.

When  $|W|$  is less than ten, then

$$F(W) = 1 - \exp(-W) \left[ 2W \sum_{K=0}^{\infty} \frac{W^K}{(2K+1) K!} - i \sqrt{\pi W} \right] \quad (A5.1)$$

When  $|W|$  is greater than or equal to ten, then

$$F(W) \approx g(W) / [W + g(W)]$$

$$\text{with } g(W) = -[0.5 + \frac{0.5}{W - 2.5 - 3}] \quad (A5.2)$$

$$\frac{W - 4.5 - 7.5}{W - 6.5 - 10.803}$$

$$\frac{W - 4.269}{W - 4.269}]$$

Due to truncation error by the computer (not enough significant digits), equation (A5.1) is not computationally stable for values of  $|W|$  greater than ten, although, in theory, the series converges for all  $W$ . Equation (A5.2) is stable for values of  $|W|$  greater than 10. It was formed by transforming the Taylor series of  $\text{Erfc}(Z)$  into Gaussian continued fraction (ref. 19) and truncating after five terms. The maximum absolute error of this approximation is  $(1.1 \times 10^{-9})$ .

## BANDWIDTH EFFECTS

So far the analysis has considered only a simple harmonic source. What acoustical engineers are really interested in is how ground reflection affects Sound Pressure Level Spectra (SPLS), as measured with finite bandwidth equipment. Since detection equipment sums the signals with

frequencies contained in the bandwidth of the filters, it is necessary to integrate equation (A4) to determine the bandwidth effect.

$$\Delta \text{SPL} = 10 \log_{10} \left[ \frac{1}{f_U - f_L} \int_{f_L}^{f_U} \left( \frac{\phi_c}{\phi_D} \right) \left( \frac{\phi_c}{\phi_D} \right)^* df \right]$$

where (\*) denotes complex conjugate and  $(f_L, f_U)$  denote the cutoff frequencies for the filters.

If the values for  $Z_1/Z_0$  and  $K_1/K_0$  do not vary erratically over the frequency limits of integration, this integral can be approximated by

$$\Delta \text{SPL} \approx 10 \log_{10} \left[ 1 + A^2 + 2 A \cos(S_2 - \theta) \frac{\sin(S_1)}{S_1} \right] \quad (\text{A6})$$

where

$$A = |\Gamma'| \quad \text{and} \quad \theta = \arg(\Gamma')$$

$$S_1 = \pi \Delta P (f_U - f_L) / C_0$$

$$S_2 = \pi \Delta P (f_U + f_L) / C_0$$

and the values for  $\Gamma'$  are evaluated at the geometric-mean-frequencies for the filters.

## OTHER EFFECTS

There are other effects which affect noise measurements in the vicinity of a reflecting ground plane: wind and temperature gradients; noise source distribution; and scattering of the sound by an acoustically rough ground plane, etc. These other effects have not been adequately quantified at this time for incorporation into mathematical terms.

PRECEDING PAGE BLANK NOT FILMED

**APPENDIX B**  
**THEORETICAL EJECTOR PERFORMANCE**

# COORDINATION SHEET

TO

W. C. Storey

NO RFP-6-8462-30-59

ITEM NO

CC

J. R. Anderson W. R. Johnson  
W. K. Bauermeister R. B. Tate

DATE October 7, 1971

MODEL 727

GROUP INDEX 727 Retrofit Feasibility Program

SUBJECT Theoretical Ejector Performance Parameters  
Utilizing Simulated JT8D-9 Engine Conditions

In order to make certain ejector design decisions, the flow properties at the entrance and exit of the ejector shroud were requested verbally by Acoustics Staff personnel. Presented here are these flow properties as determined by a Propulsion Research-developed ejector computer program for mixed-to-primary area ratios ( $A_M/A_P$ ) of 1.6, 1.8, 2.0, and 2.2. The P&WA JT8D-9 turbofan engine conditions were simulated and are tabulated along with the ejector geometry and loss inputs. Figure 1 through 32 present the ejector performance parameter versus airspeed for lines of constant EPR. The following table is an index to the figures:

Performance Parameter	$A_M/A_P$			
	1.6	1.8	2.0	2.2
$Q$	Fig. 1	Fig. 9	Fig. 17	Fig. 25
$M_E$	Fig. 2	Fig. 10	Fig. 18	Fig. 26
$M_P$	Fig. 3	Fig. 11	Fig. 19	Fig. 27
$M_S$	Fig. 4	Fig. 12	Fig. 20	Fig. 28
$W_S/W_P$	Fig. 5	Fig. 13	Fig. 21	Fig. 29
$T_{TE}/T_{T\infty}$	Fig. 6	Fig. 14	Fig. 22	Fig. 30
$P_S/P_{\infty}$	Fig. 7	Fig. 15	Fig. 23	Fig. 31
$P_P/P_{\infty}$	Fig. 8	Fig. 16	Fig. 24	Fig. 32

Where:

$A_M/A_P$	=	Ejector Mixing to Primary Area Ratio
$Q$	=	Ejector Net Thrust Ratio ( $F_{net}/F_{np}$ )
$M_E$	=	Ejector Exit Mach No. at Station $\textcircled{E}$
$M_P$	=	Primary Flow Mach No. at Station $\textcircled{1}$
$M_S$	=	Secondary Flow Mach No. at Station $\textcircled{1}$
$W_S/W_P$	=	Secondary Airflow to Primary Airflow Ratio
$T_{TE}/T_{T\infty}$	=	Ejector Exit Total Temperature Ratio
$P_S/P_{\infty}$	=	Secondary Static Pressure Ratio at Station $\textcircled{1}$
$P_P/P_{\infty}$	=	Primary Static Pressure Ratio at Station $\textcircled{1}$

These curves are to provide trend data only and are not to be utilized for estimating the performance of a specific ejector-suppressor configuration. It should be noted that the primary flow Mach Number at Station ① is not the fully expanded Mach Number.

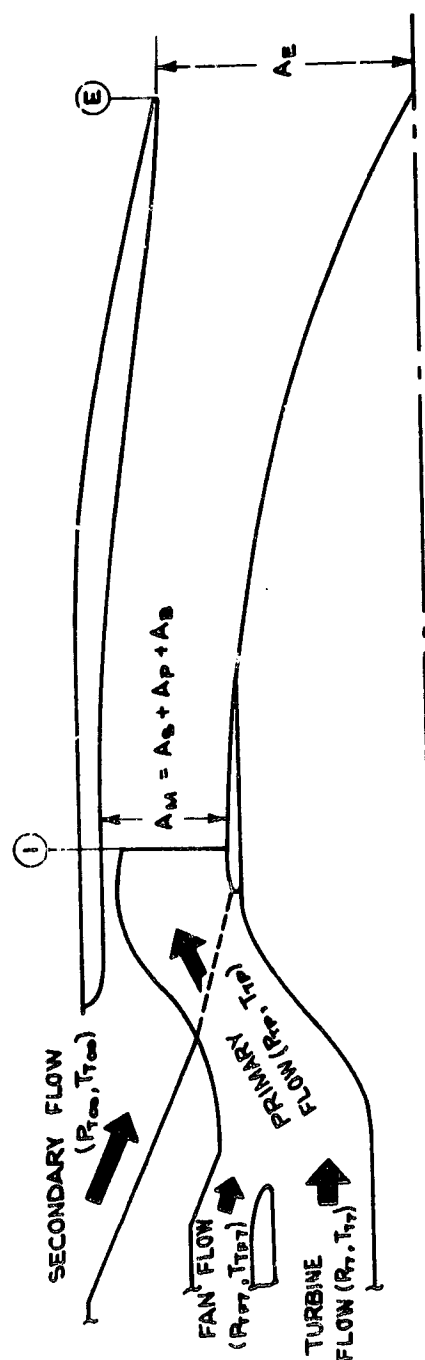
Unfortunately, this ejector program assumes complete mixing and does not provide the ejector flow properties between the entrance and exit of the shroud. A mixing program is being formulated by the Propulsion Research group to provide flow properties as a function of axial displacement. The mixing program will probably be ready for checkout in December 1971.

Prepared by W. J. Haugan 10/7/71  
W. J. Haugan

Approved by   
E. Tjonneland

Attachment: Table I, Figures 1-32

TABLE I  
EJECTOR PROGRAM INPUTS



SIMULATED JT8D-9 TURBOFAN ENGINE PARAMETERS		
EPR	$P_{TP}/P_{T\infty}$	$T_{TP}/T_{T\infty}$
$a(P_{T7}/P_{T2})$		
2.0	1.948	1.944
1.95	1.906	1.906
1.9	1.864	1.875
1.8	1.778	1.817
1.7	1.691	1.763
1.5	1.510	1.655
1.3	1.313	1.523

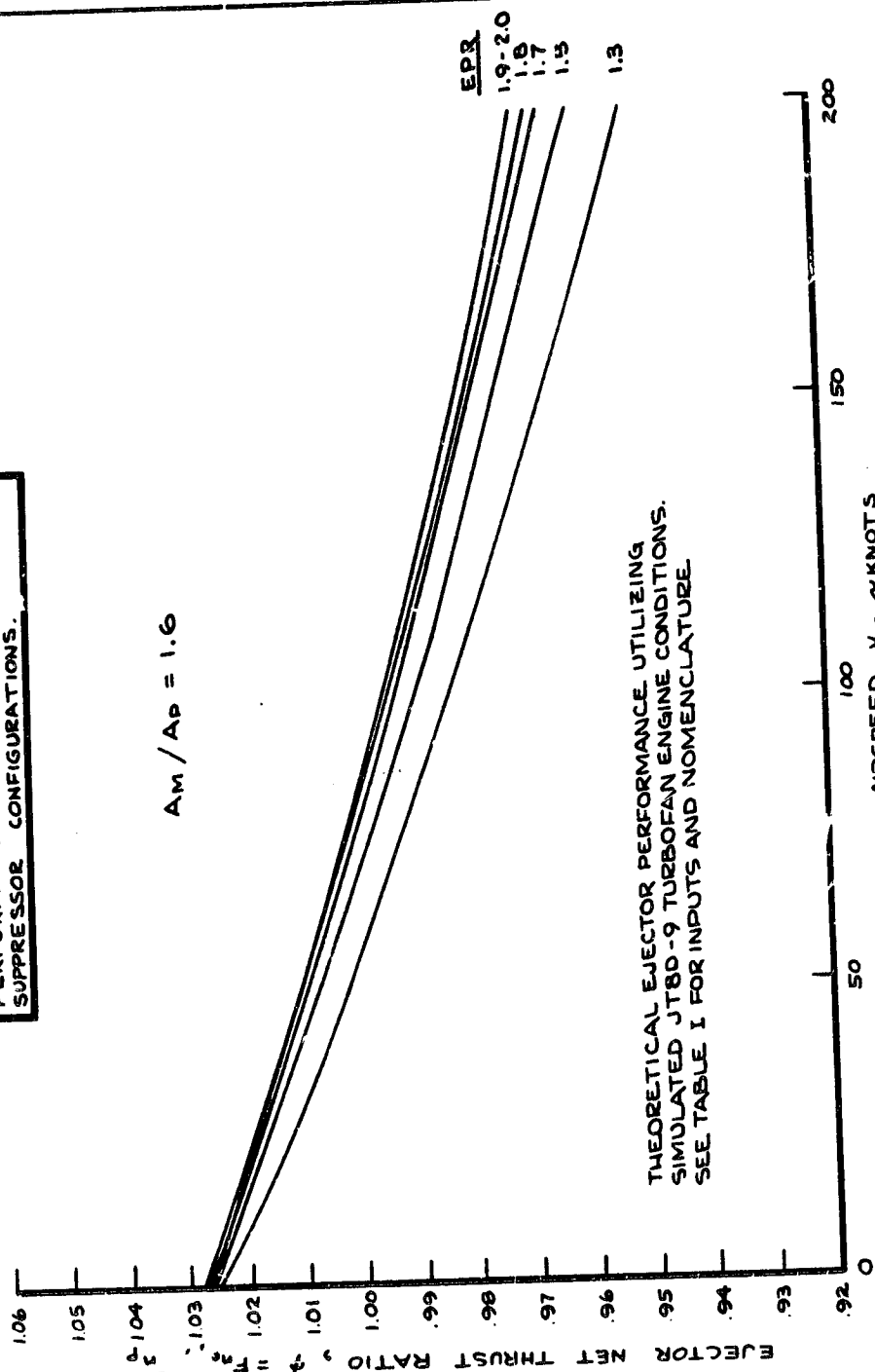
\* ENGINE INLET RECOVERY 8100%

EJECTOR INPUTS	
$A_M/A_1$	= 1.6; 1.8; 2.0; 2.2
$A_E/A_M$	= 1.0
$A_B/A_1$	= 0.05
SECONDARY INLET LOSS, $\frac{\Delta P_T}{q_S}$	= 0.2
FRICTION COEFFICIENT, $C_f$	= 0.0045
EJECTOR LENGTH-DIAMETER RATIO, $L/D$	= 2.5



DO NOT USE FOR ESTIMATING THE  
PERFORMANCE OF SPECIFIC EJECTOR  
SUPPRESSOR CONFIGURATIONS.

$$A_m / A_p = 1.6$$



THEORETICAL EJECTOR PERFORMANCE UTILIZING  
SIMULATED JT8D-9 TURBOFAN ENGINE CONDITIONS.  
SEE TABLE I FOR INPUTS AND NOMENCLATURE.

CALC					
CHECK					
APR					
APR					

EJECTOR NET THRUST RATIO VS.  
AIRSPEED FOR  $A_m / A_p = 1.6$   
EJECTOR (JT8D-9 ENG. SIM.)

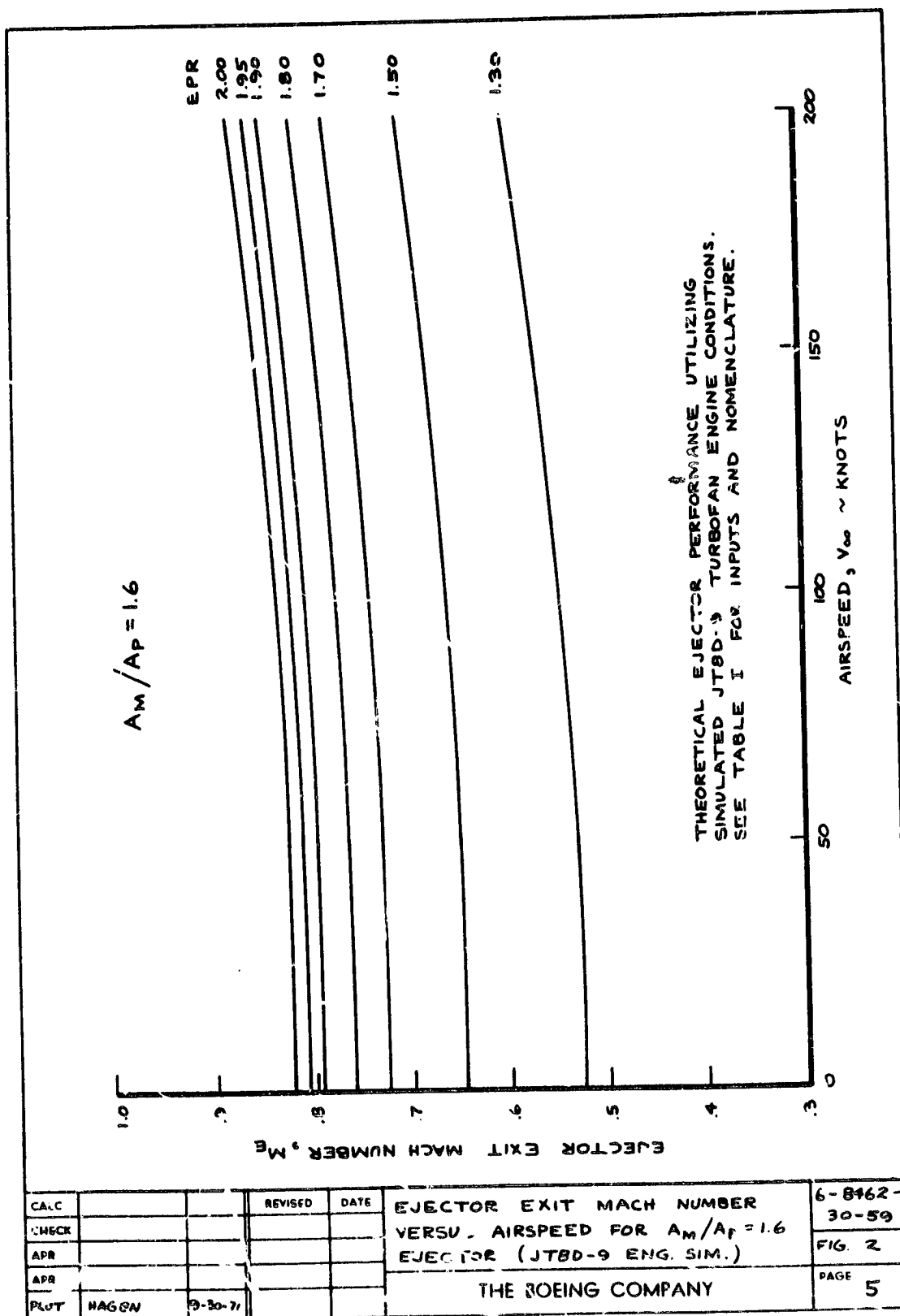
THE BOEING COMPANY

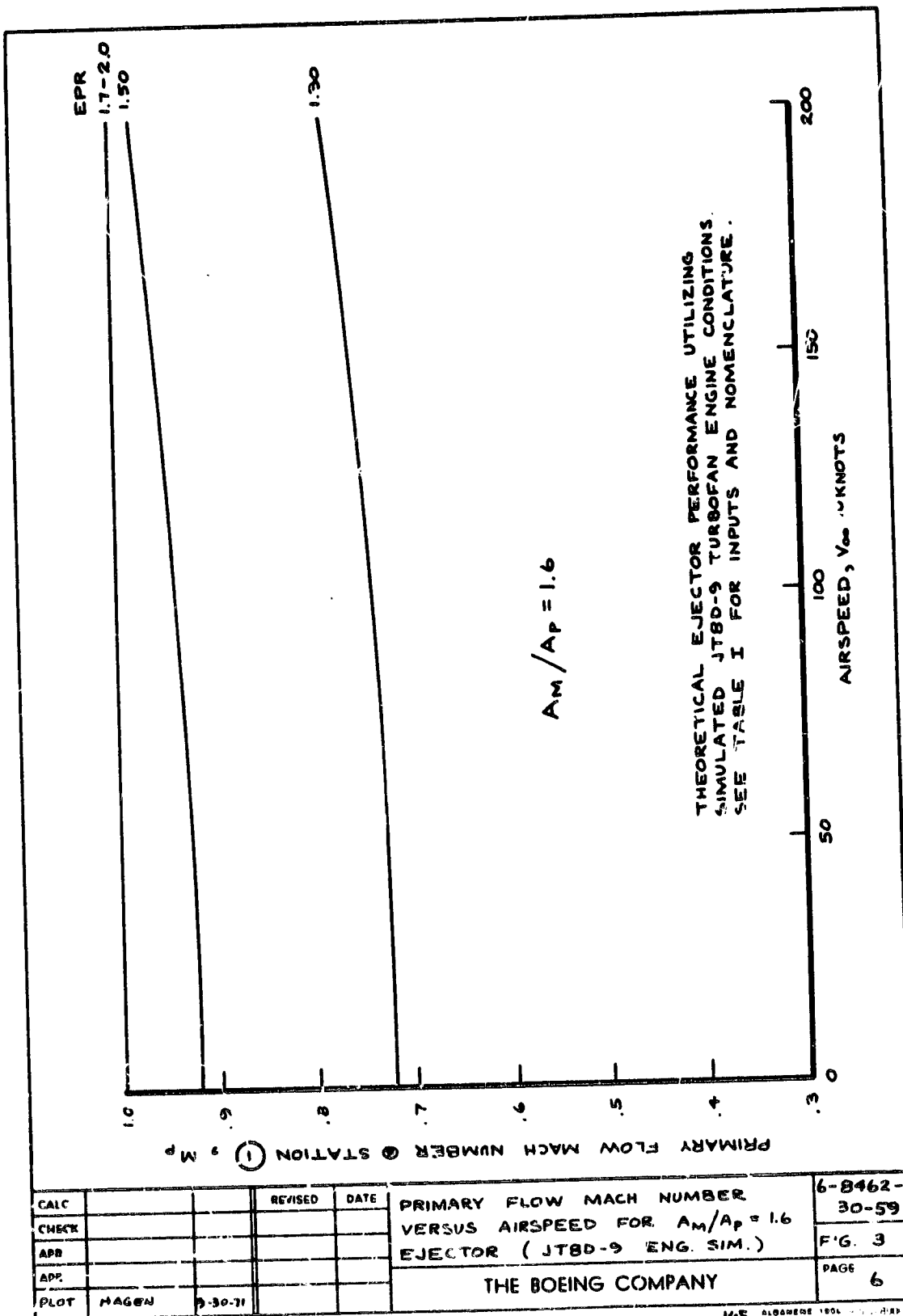
6-8462-  
30-59

FIG. 1

PAGE 4

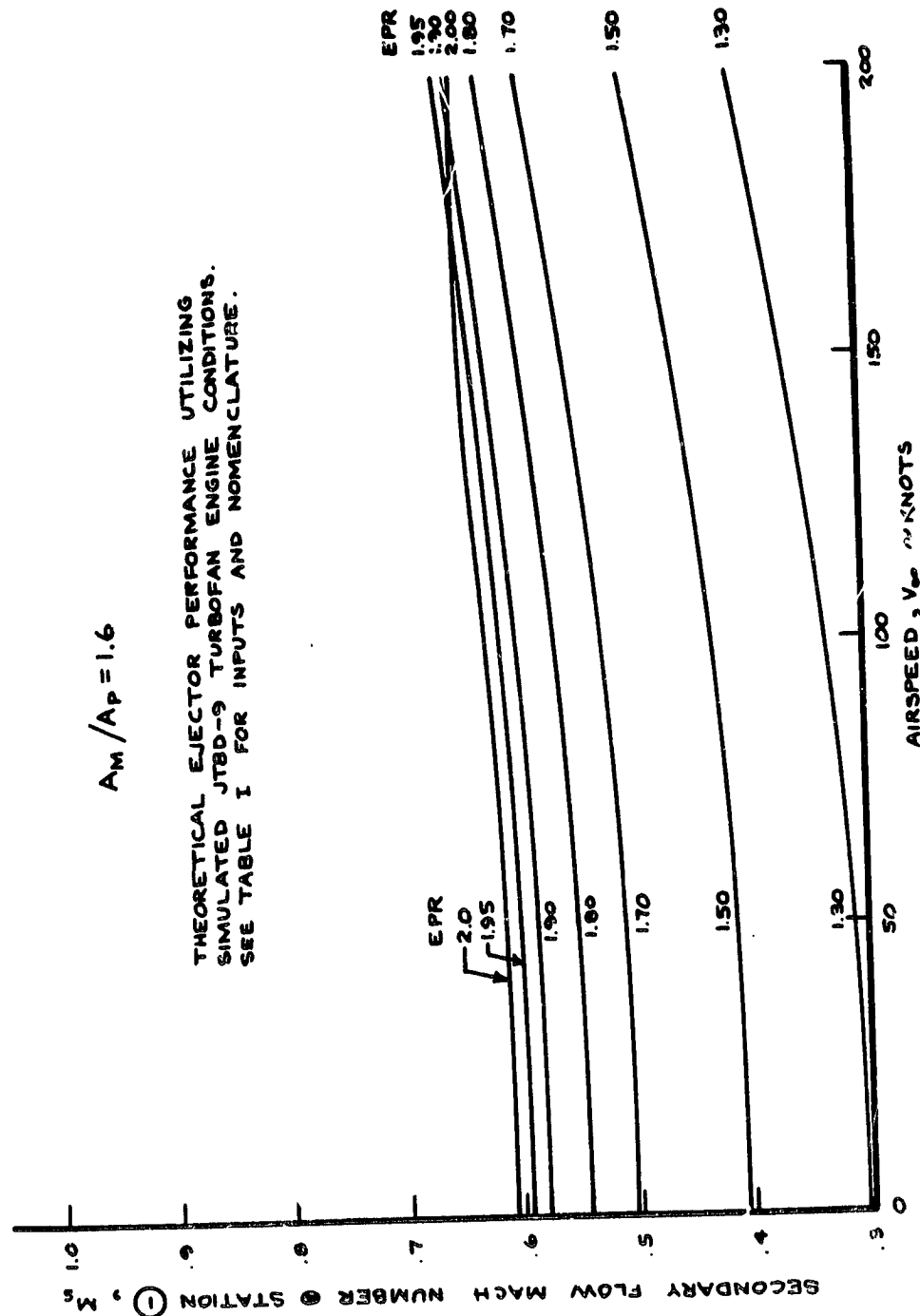
100% 100% 100% 100% 100% 100%





$$A_M/A_P = 1.6$$

THEORETICAL EJECTOR PERFORMANCE UTILIZING  
SIMULATED JTBD-9 TURBOFAN ENGINE CONDITIONS.  
SEE TABLE 1 FOR INPUTS AND NOMENCLATURE.



CALC			REVISED	DATE	SECONDARY FLOW MACH NUMBER VERSUS AIRSPEED FOR $A_M/A_P = 1.6$ EJECTOR (JTBD-9 ENG. SIM.)	6-8162-
CHECK						30-59
APR						FIG. 4
APR						PAGE 7
PLOT	HAGEN	8-30-71			THE BOEING COMPANY	

NOTED: 100%  
100% 100%

THEORETICAL EJECTOR PERFORMANCE UTILIZING  
SIMULATED JTBD-9 TURBOFAN ENGINE CONDITIONS.  
SEE TABLE I FOR INPUTS AND NOMENCLATURE.

$A_M/A_P = 1.6$

SECONDARY AIRFLOW TO PRIMARY AIRFLOW RATIO,  $W_s/W_p$

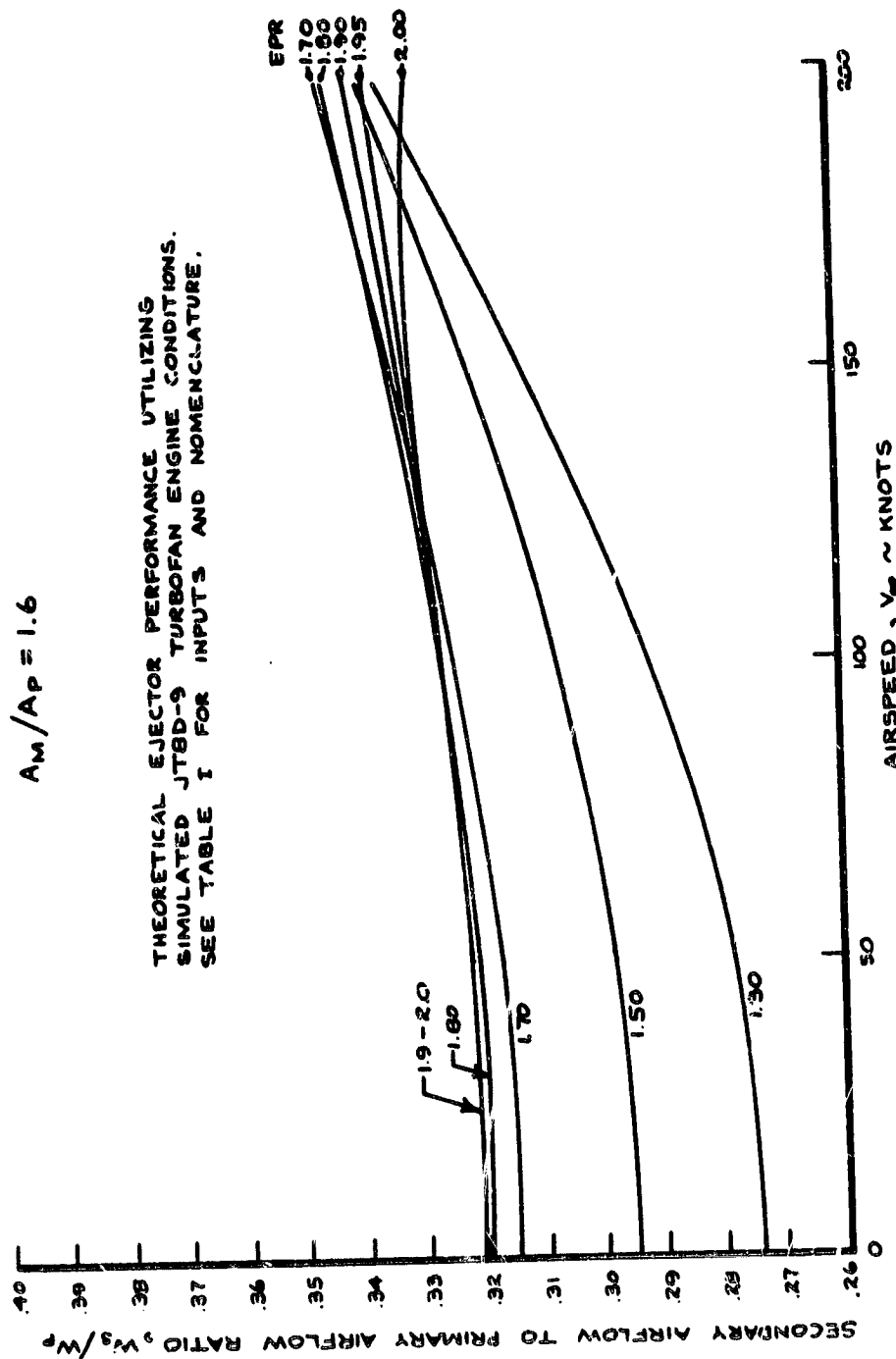
AIRSPEED,  $V_\infty$  ~ KNOTS

EPR

1.70  
1.80  
1.90  
1.95  
2.00

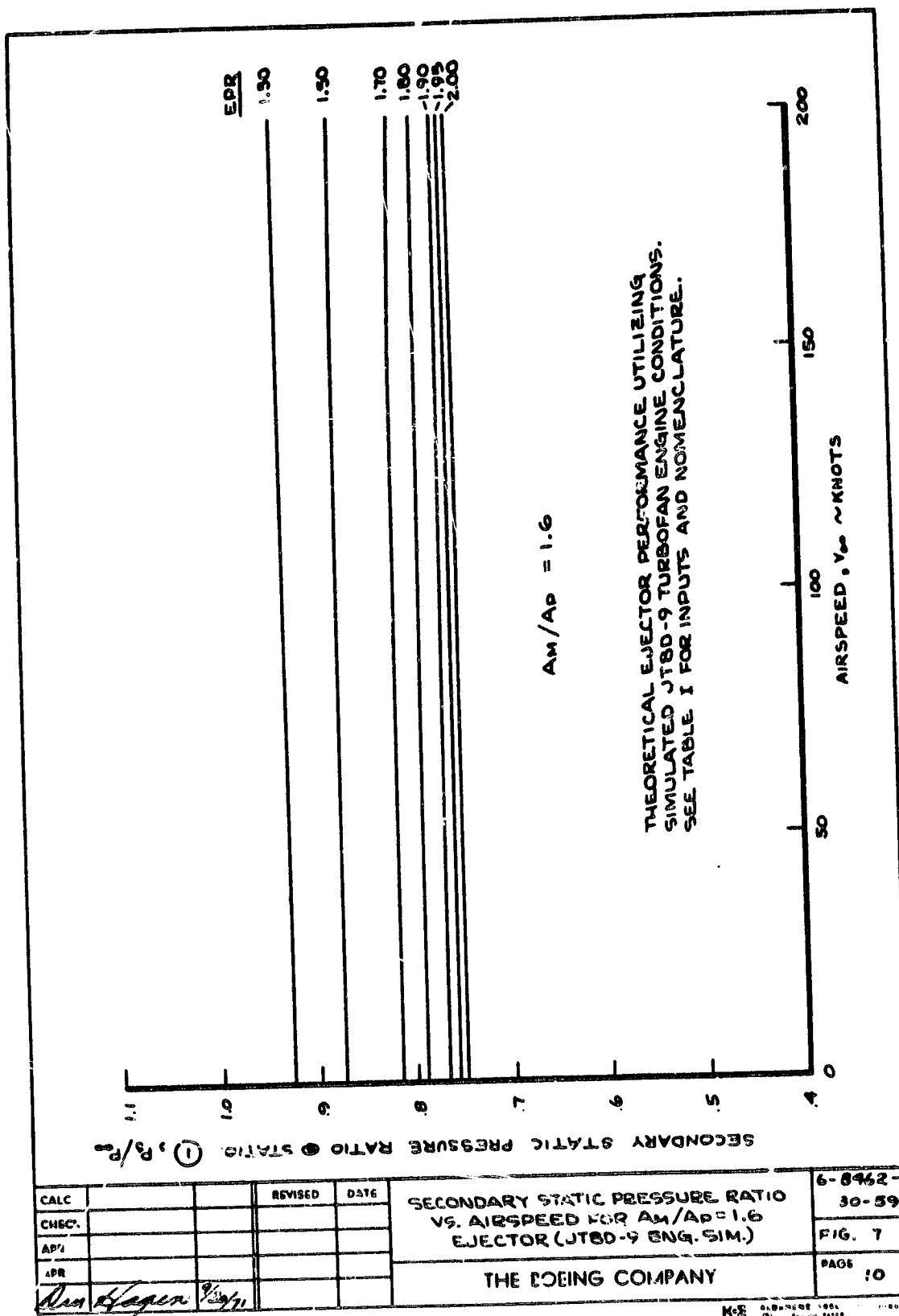
1.9-2.0  
1.80  
1.70  
1.50  
1.30

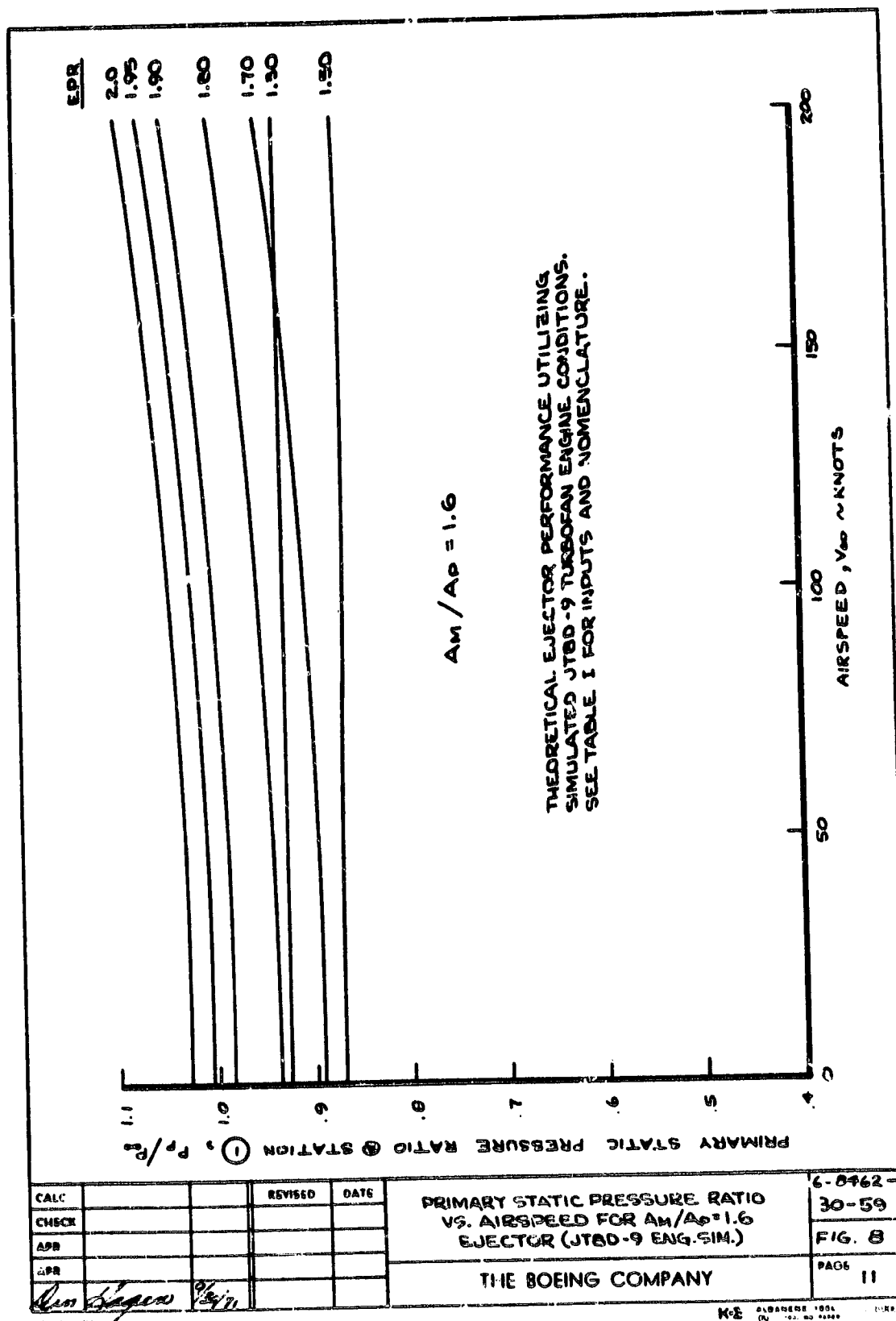
THEORETICAL EJECTOR PERFORMANCE UTILIZING  
SIMULATED JTBD-9 TURBOFAN ENGINE CONDITIONS.  
SEE TABLE I FOR INPUTS AND NOMENCLATURE.



CALC			REVISED	DATE	SEC. AIRFLOW - PRI. AIRFLOW RATIO VERSUS AIRSPEED FOR $A_m/A_p = 1.6$ EJECTOR (JT8D-9 ENG. S/M.)  THE BOEING COMPANY	5-8762- 30-59
CHECK						FIG 5
APP						PAGE
APP						8
PLOT	HALSEN	9-30-71				



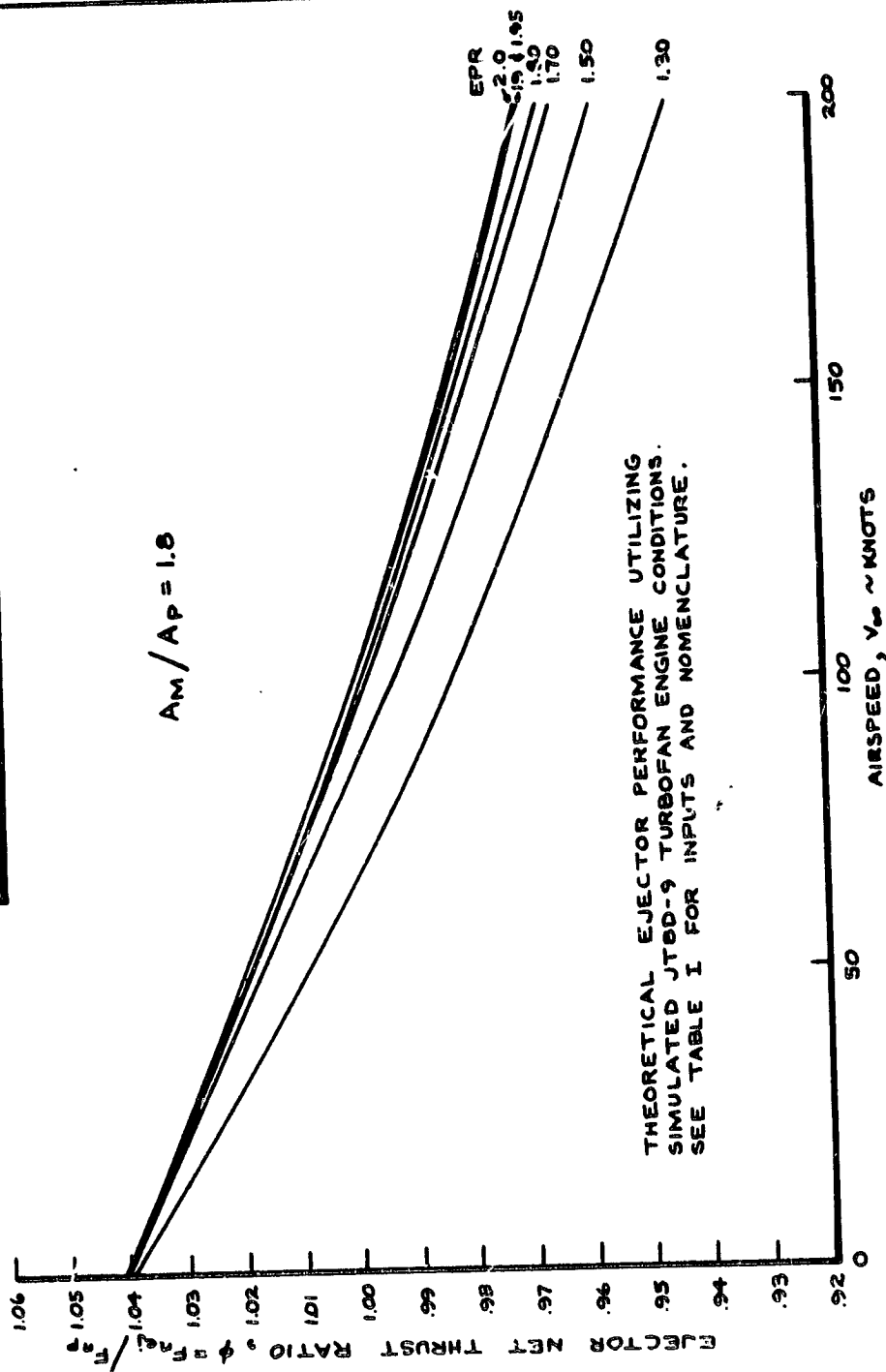






DO NOT USE FOR ESTIMATING THE  
PERFORMANCE OF SPECIFIC EJECTOR  
SUPPRESSOR CONFIGURATIONS.

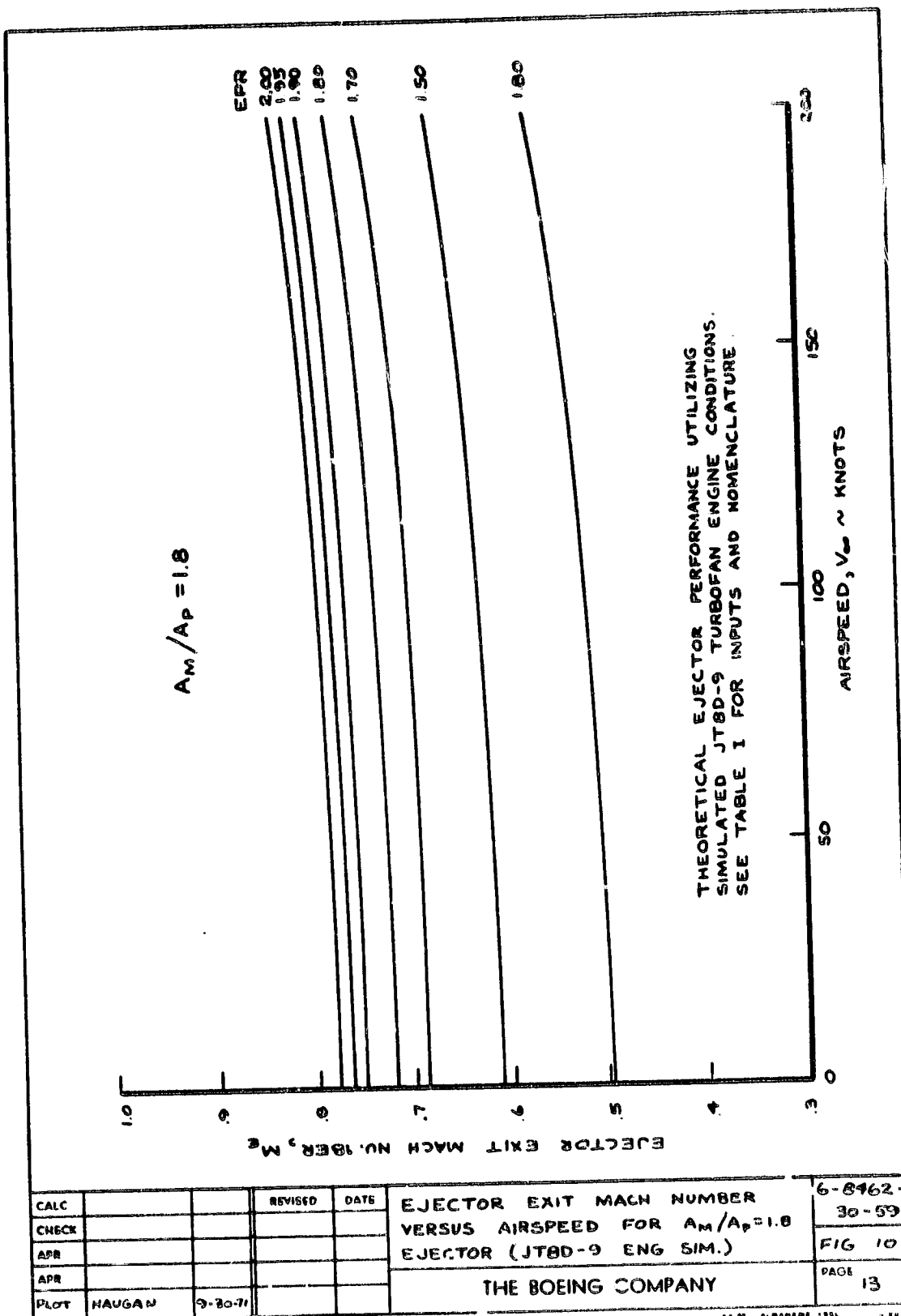
$$A_M / A_P = 1.8$$

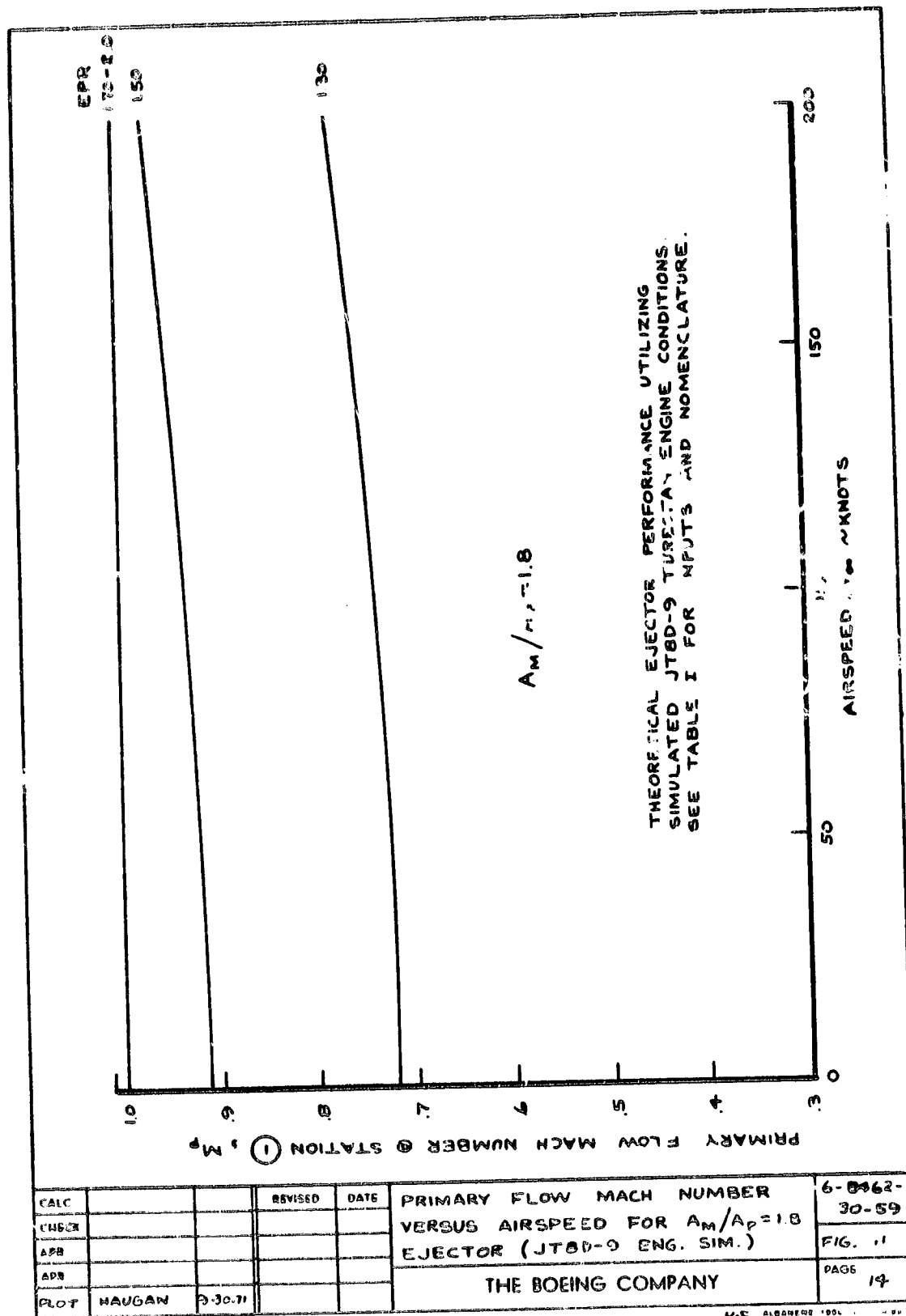


THEORETICAL EJECTOR PERFORMANCE UTILIZING  
SIMULATED JT8D-9 TURBOFAN ENGINE CONDITIONS.  
SEE TABLE I FOR INPUTS AND NOMENCLATURE.

C/ALC			REVISED	DATE	EJECTOR NET THRUST RATIO VERSUS AIRSPEED FOR $A_M/A_P = 1.8$ EJECTOR (JT8D-9 ENG. SIM.)	6-8462-
CHECK						80-59
APR						FIG. 9
APR						PAGE 12
PLOT	HAUGAN	9-29-71			THE BOEING COMPANY	

HE PLANNED 1981  
1981 00 0000

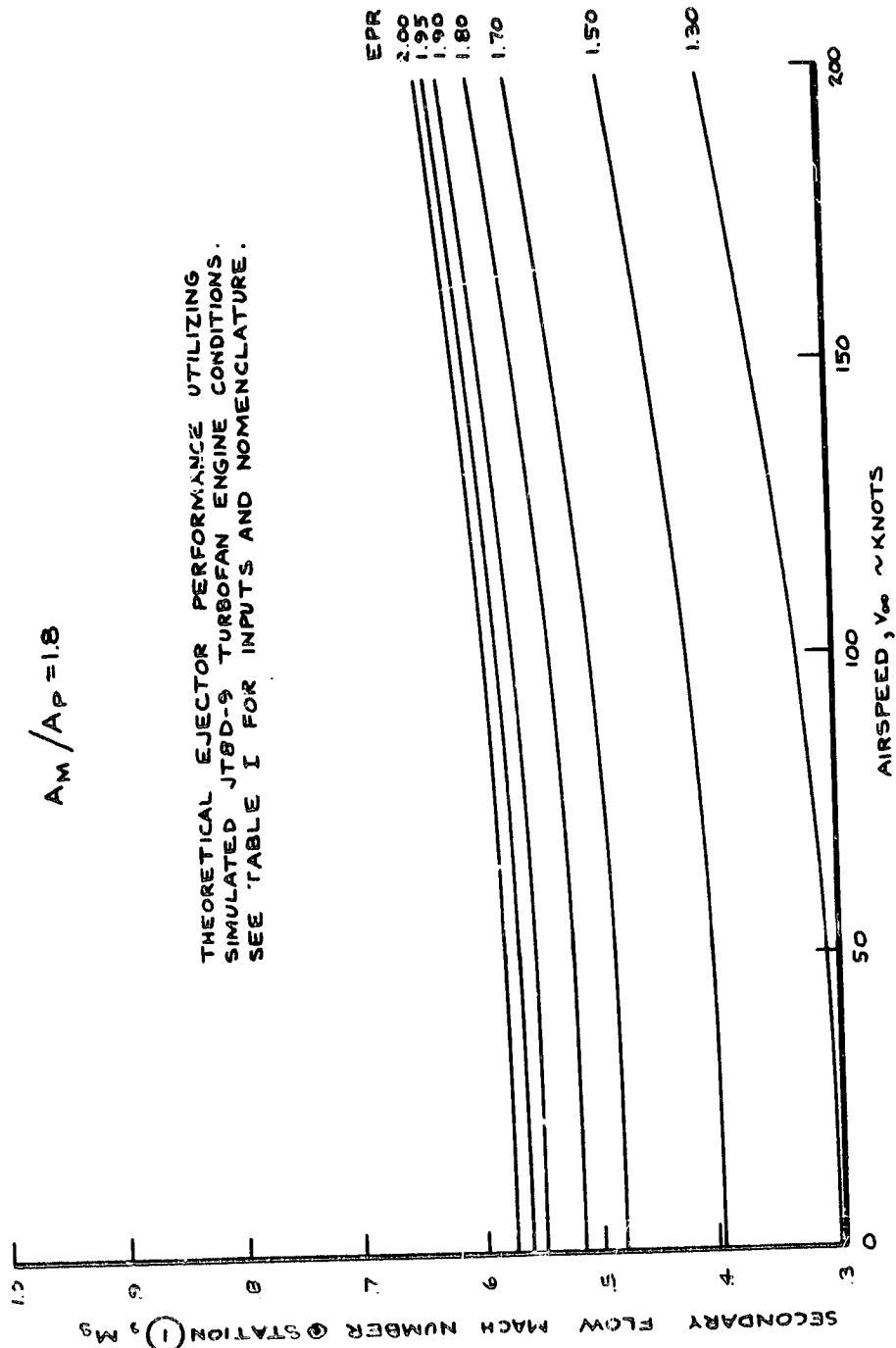




ALBANY 100L  
1000 00 PAPER

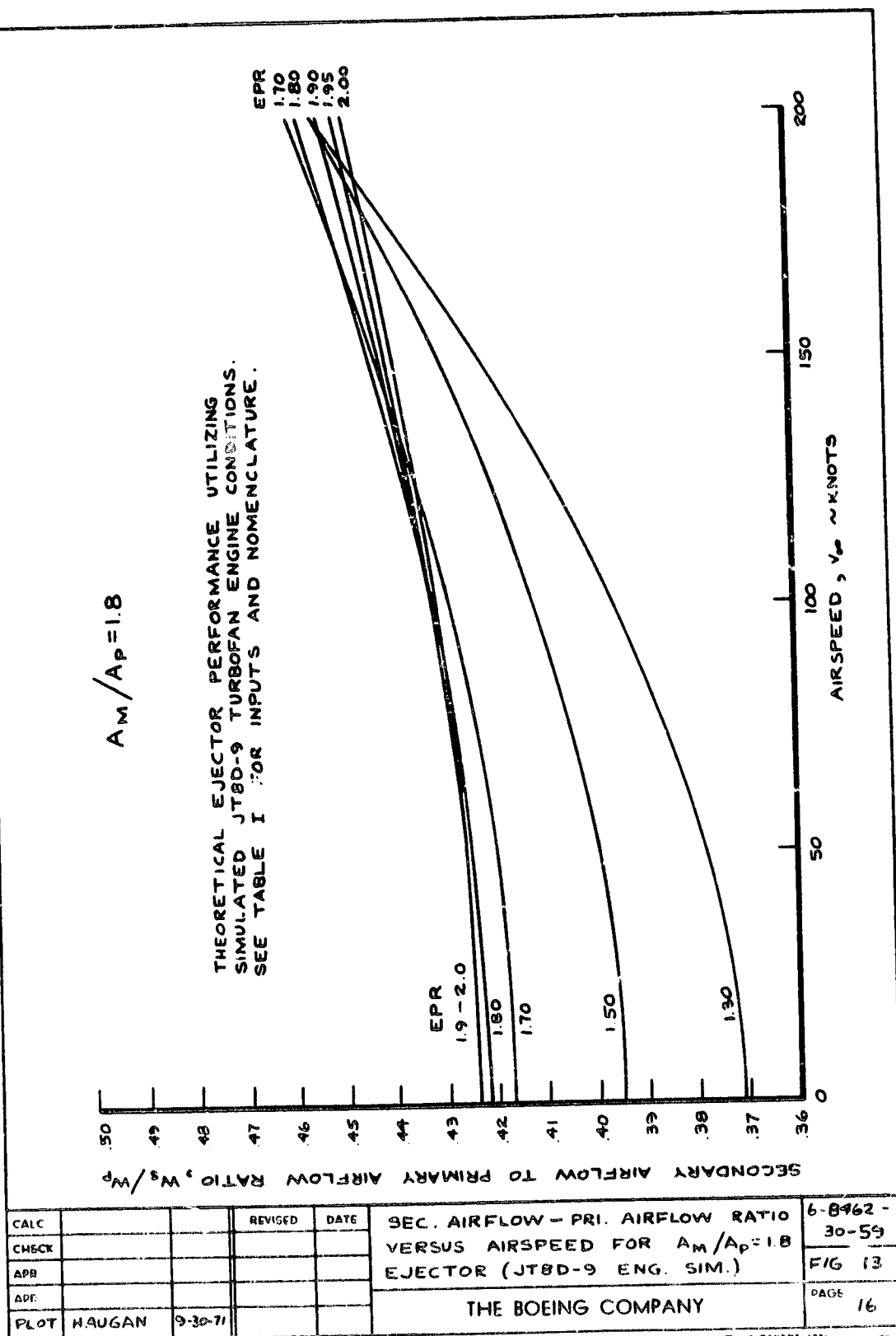
$$A_m / A_p = 1.8$$

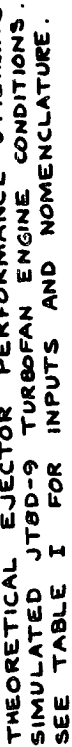
THEORETICAL EJECTOR PERFORMANCE UTILIZING  
SIMULATED JT8D-9 TURBOFAN ENGINE CONDITIONS.  
SEE TABLE I FOR INPUTS AND NOMENCLATURE.

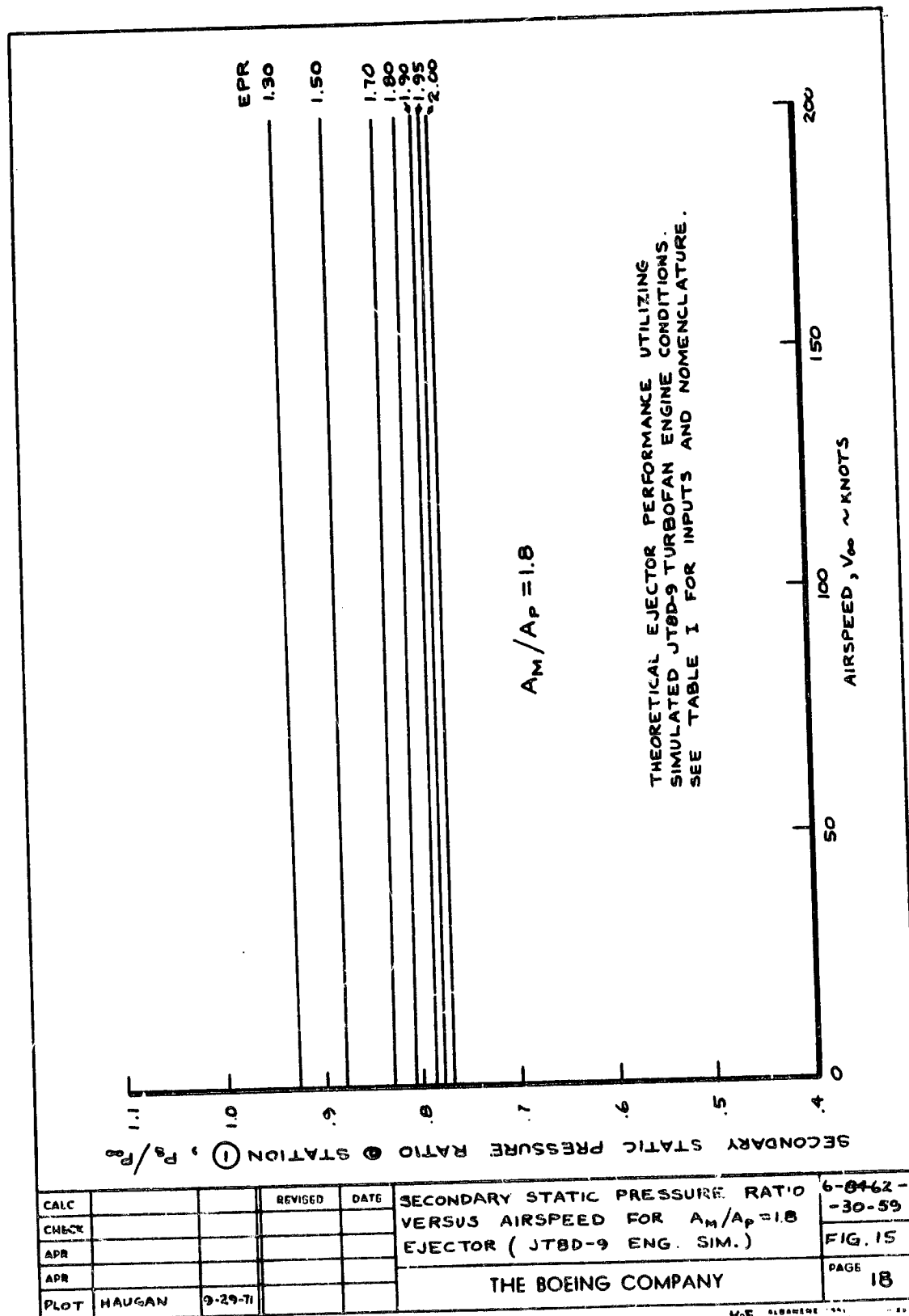


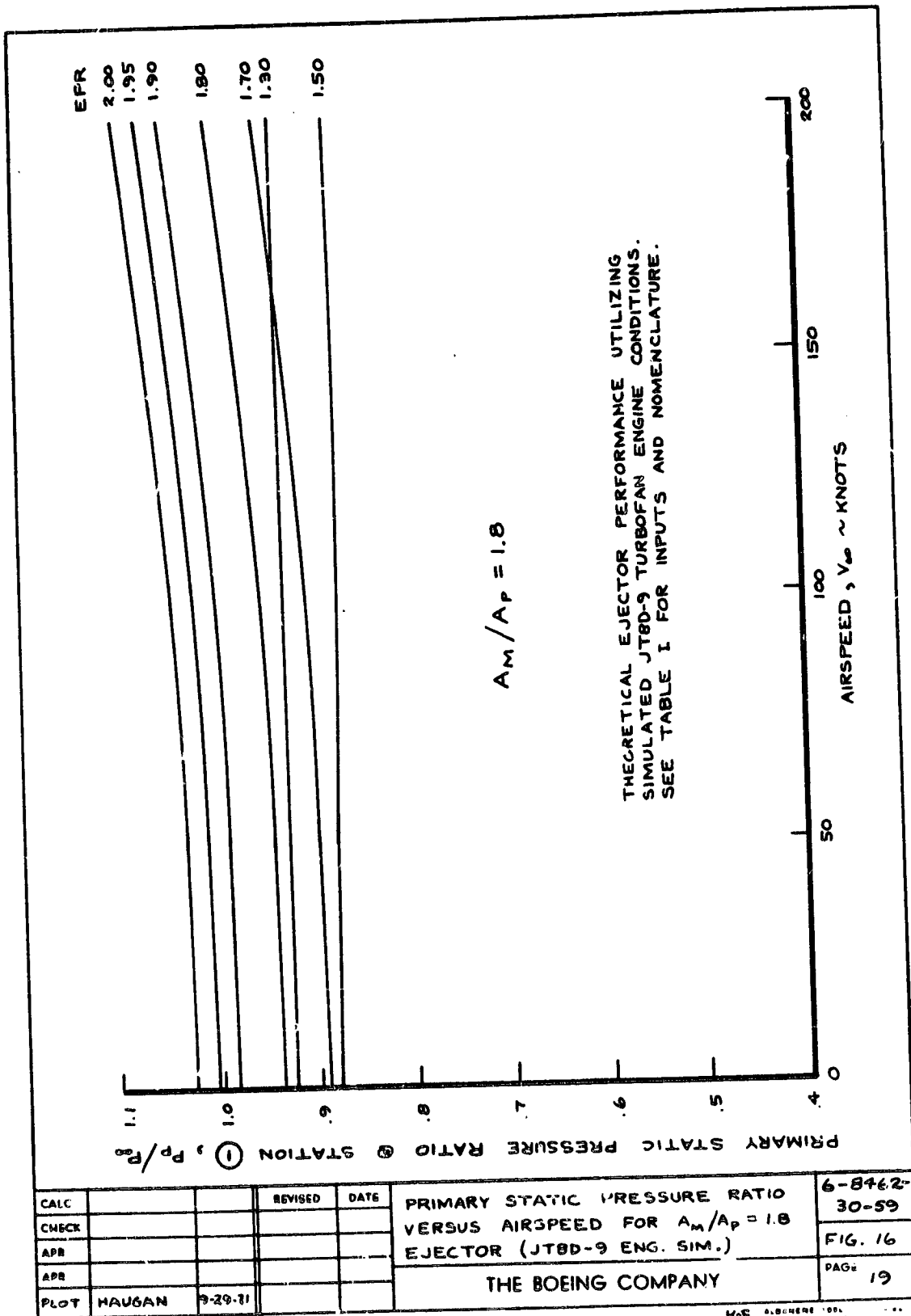
CAIC			REVISED	DATE	SECONDARY FLOW MACH NUMBER VERSUS AIRSPEED FOR $A_m/A_p = 1.8$ EJECTOR (JT8D-9 ENG. SIM.)	6-3462-
CHECK						30-59
APR						FIG. 12
FOR						PAGE
PLOT	NAUGAN	7-30-71			THE BOEING COMPANY	15

K-E ALBANY 1051





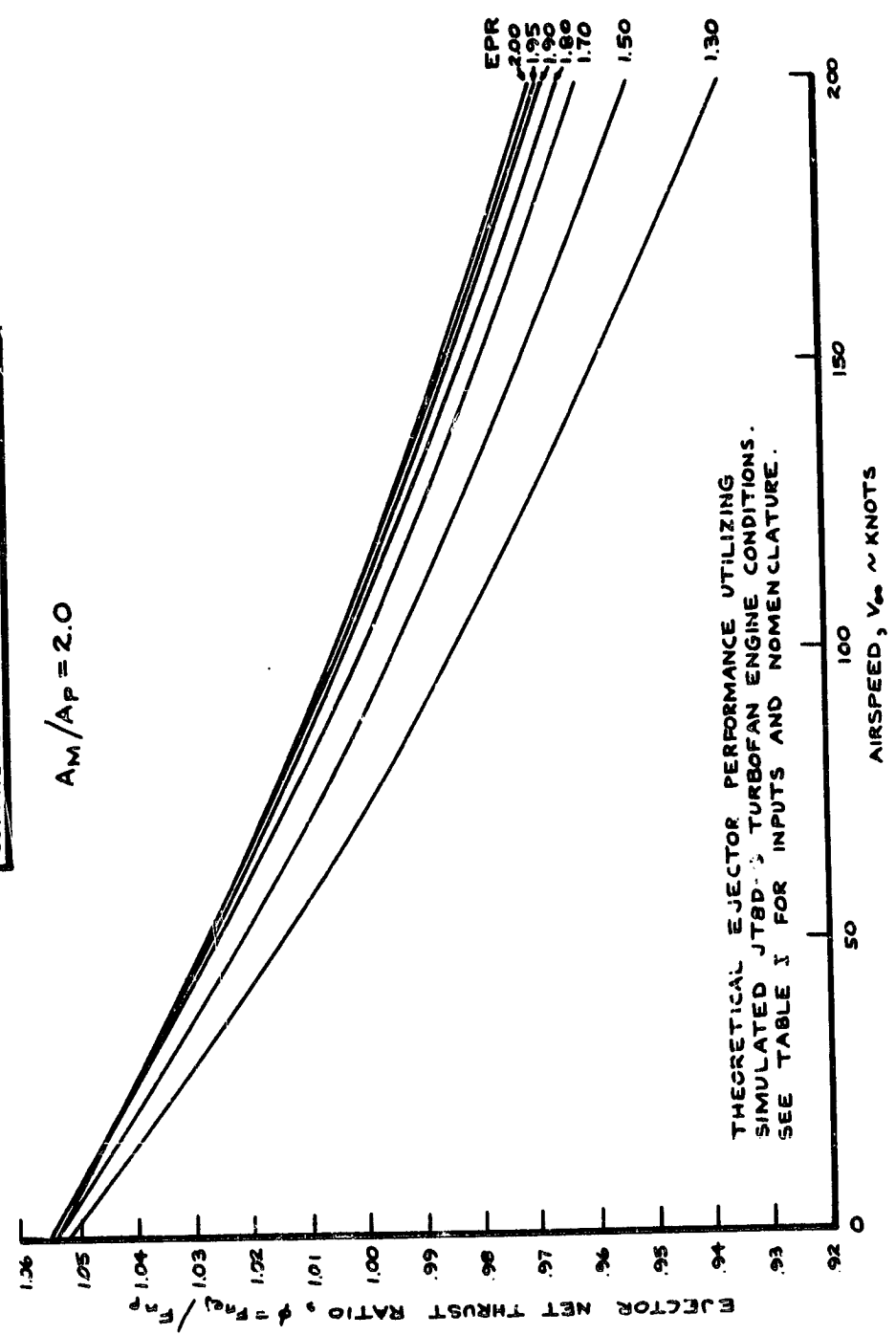






DO NOT USE FOR ESTIMATING THE  
PERFORMANCE OF SPECIFIC EJECTOR  
SUPERPRESSOR CONFIGURATIONS.

$$A_M/A_P = 2.0$$

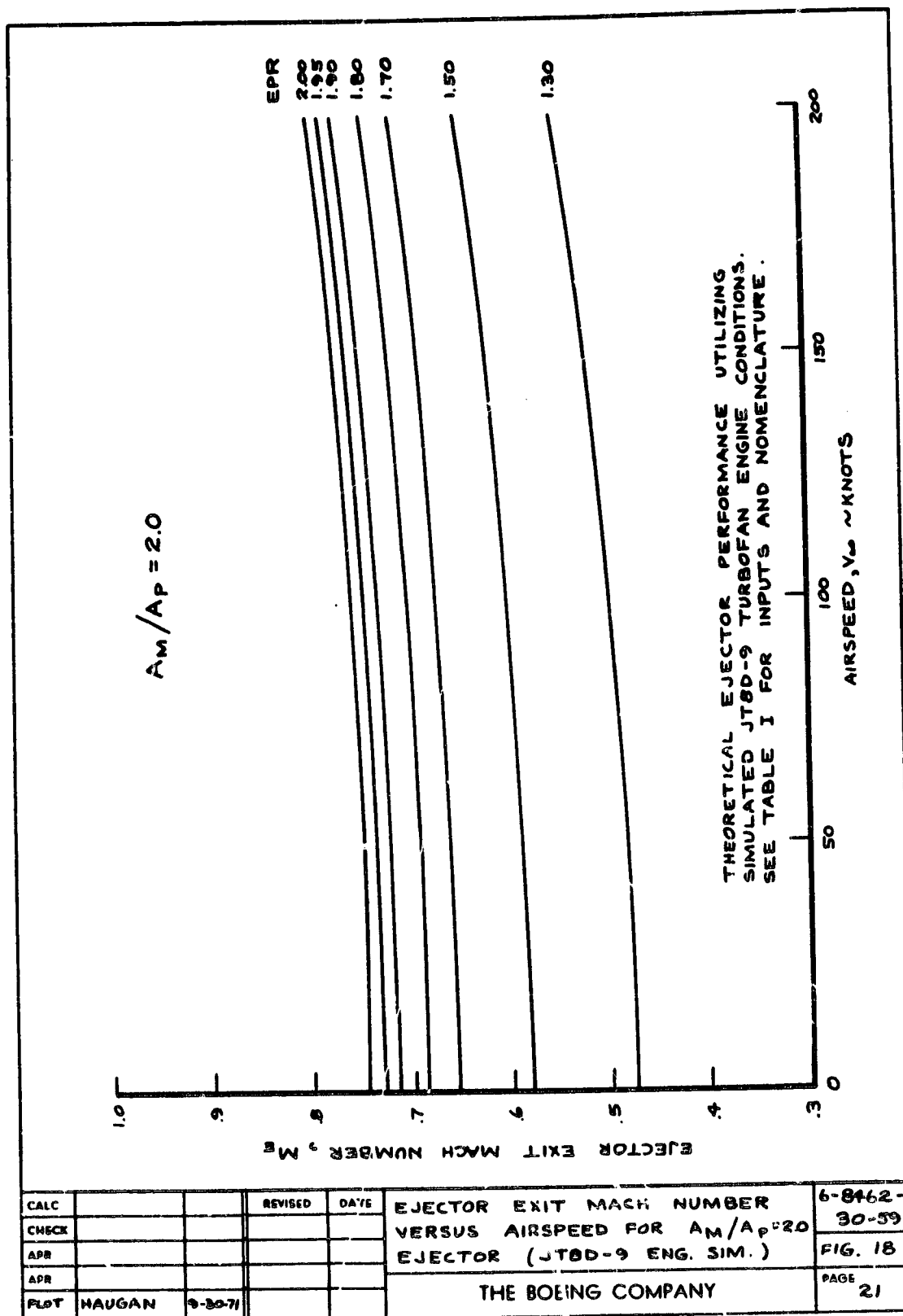


THEORETICAL EJECTOR PERFORMANCE UTILIZING  
SIMULATED JT8D-9 TURBOFAN ENGINE CONDITIONS.  
SEE TABLE I FOR INPUTS AND NOMENCLATURE.

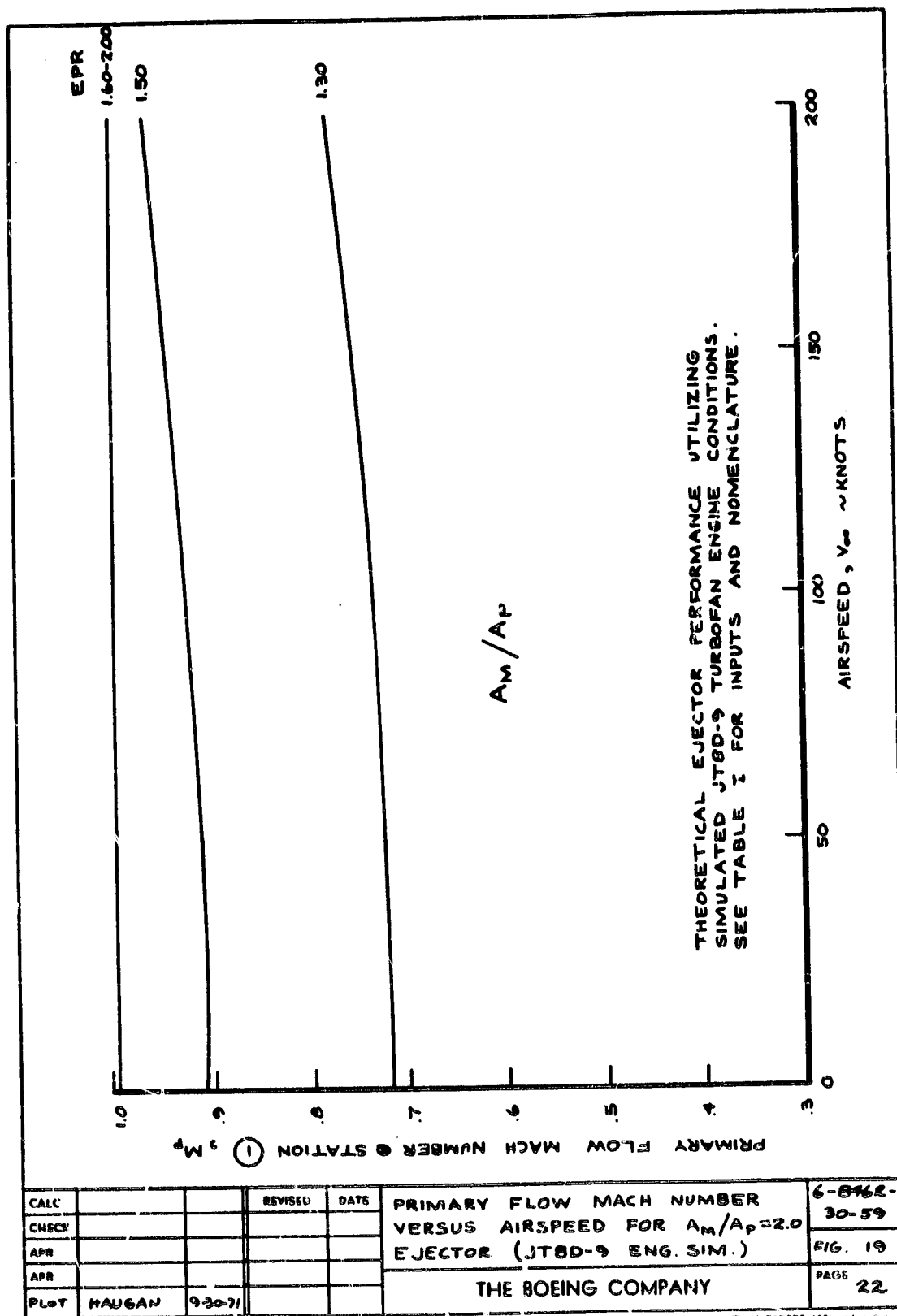
CALC			REVISED	DATE	EJECTOR NET THRUST RATIO VERSUS AIRSPEED FOR $A_m/A_p=2.0$ EJECTOR (JT8D-9 ENG. SIM.)	6-8462 - 30-59
CHECK						FIG. 17
APR						PAGE
APR						20
PLDT	HAUGAN	9-30-71				THE BOEING COMPANY

MOE A. DANIEL 100L 11-11-71

M-E ALBANY 1981 11-88  
100% CO. PAPER



K-E ALBANY 1001

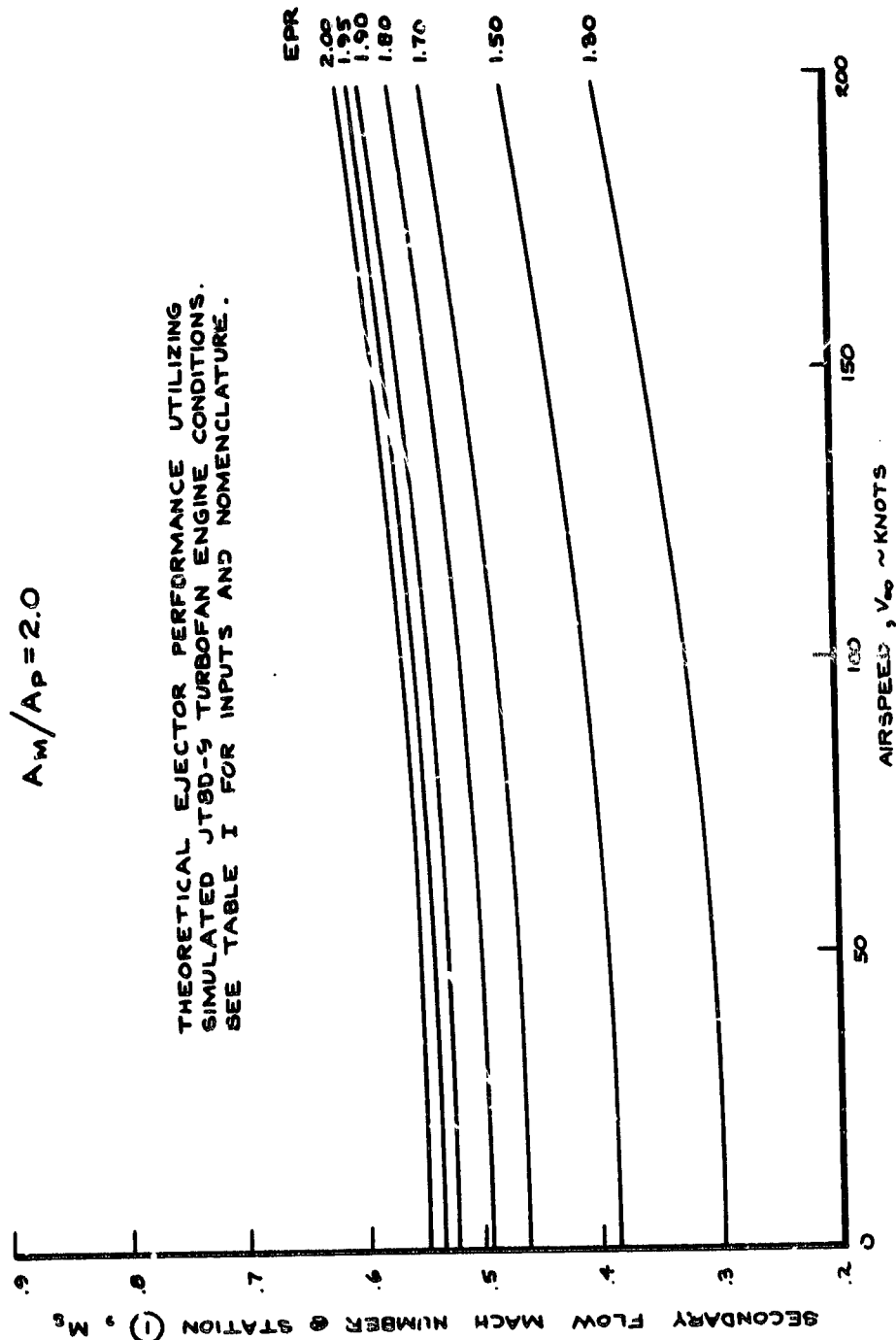


CALC			REVISED	DATE	PRIMARY FLOW MACH NUMBER VERSUS AIRSPEED FOR $A_m/A_p = 2.0$ EJECTOR (JT8D-9 ENG. SIM.)	6-8762- 30-59
CHECK						FIG. 19
APR						PAGE 22
PLT	HAUGAN	9-30-71			THE BOEING COMPANY	

K-E ALBONERT 1001, 4.5, 7, 8, 9, 10, 11, 12, 13, 14, 15, 16, 17, 18, 19, 20, 21, 22, 23, 24, 25, 26, 27, 28, 29, 30, 31, 32, 33, 34, 35, 36, 37, 38, 39, 40, 41, 42, 43, 44, 45, 46, 47, 48, 49, 50, 51, 52, 53, 54, 55, 56, 57, 58, 59, 60, 61, 62, 63, 64, 65, 66, 67, 68, 69, 70, 71, 72, 73, 74, 75, 76, 77, 78, 79, 80, 81, 82, 83, 84, 85, 86, 87, 88, 89, 90, 91, 92, 93, 94, 95, 96, 97, 98, 99, 100, 101, 102, 103, 104, 105, 106, 107, 108, 109, 110, 111, 112, 113, 114, 115, 116, 117, 118, 119, 120, 121, 122, 123, 124, 125, 126, 127, 128, 129, 130, 131, 132, 133, 134, 135, 136, 137, 138, 139, 140, 141, 142, 143, 144, 145, 146, 147, 148, 149, 150, 151, 152, 153, 154, 155, 156, 157, 158, 159, 160, 161, 162, 163, 164, 165, 166, 167, 168, 169, 170, 171, 172, 173, 174, 175, 176, 177, 178, 179, 180, 181, 182, 183, 184, 185, 186, 187, 188, 189, 190, 191, 192, 193, 194, 195, 196, 197, 198, 199, 200, 201, 202, 203, 204, 205, 206, 207, 208, 209, 210, 211, 212, 213, 214, 215, 216, 217, 218, 219, 220, 221, 222, 223, 224, 225, 226, 227, 228, 229, 230, 231, 232, 233, 234, 235, 236, 237, 238, 239, 240, 241, 242, 243, 244, 245, 246, 247, 248, 249, 250, 251, 252, 253, 254, 255, 256, 257, 258, 259, 260, 261, 262, 263, 264, 265, 266, 267, 268, 269, 270, 271, 272, 273, 274, 275, 276, 277, 278, 279, 280, 281, 282, 283, 284, 285, 286, 287, 288, 289, 290, 291, 292, 293, 294, 295, 296, 297, 298, 299, 300, 301, 302, 303, 304, 305, 306, 307, 308, 309, 310, 311, 312, 313, 314, 315, 316, 317, 318, 319, 320, 321, 322, 323, 324, 325, 326, 327, 328, 329, 330, 331, 332, 333, 334, 335, 336, 337, 338, 339, 340, 341, 342, 343, 344, 345, 346, 347, 348, 349, 350, 351, 352, 353, 354, 355, 356, 357, 358, 359, 360, 361, 362, 363, 364, 365, 366, 367, 368, 369, 370, 371, 372, 373, 374, 375, 376, 377, 378, 379, 380, 381, 382, 383, 384, 385, 386, 387, 388, 389, 390, 391, 392, 393, 394, 395, 396, 397, 398, 399, 400, 401, 402, 403, 404, 405, 406, 407, 408, 409, 410, 411, 412, 413, 414, 415, 416, 417, 418, 419, 420, 421, 422, 423, 424, 425, 426, 427, 428, 429, 430, 431, 432, 433, 434, 435, 436, 437, 438, 439, 440, 441, 442, 443, 444, 445, 446, 447, 448, 449, 450, 451, 452, 453, 454, 455, 456, 457, 458, 459, 460, 461, 462, 463, 464, 465, 466, 467, 468, 469, 470, 471, 472, 473, 474, 475, 476, 477, 478, 479, 480, 481, 482, 483, 484, 485, 486, 487, 488, 489, 490, 491, 492, 493, 494, 495, 496, 497, 498, 499, 500, 501, 502, 503, 504, 505, 506, 507, 508, 509, 510, 511, 512, 513, 514, 515, 516, 517, 518, 519, 520, 521, 522, 523, 524, 525, 526, 527, 528, 529, 530, 531, 532, 533, 534, 535, 536, 537, 538, 539, 540, 541, 542, 543, 544, 545, 546, 547, 548, 549, 550, 551, 552, 553, 554, 555, 556, 557, 558, 559, 560, 561, 562, 563, 564, 565, 566, 567, 568, 569, 570, 571, 572, 573, 574, 575, 576, 577, 578, 579, 580, 581, 582, 583, 584, 585, 586, 587, 588, 589, 590, 591, 592, 593, 594, 595, 596, 597, 598, 599, 600, 601, 602, 603, 604, 605, 606, 607, 608, 609, 610, 611, 612, 613, 614, 615, 616, 617, 618, 619, 620, 621, 622, 623, 624, 625, 626, 627, 628, 629, 630, 631, 632, 633, 634, 635, 636, 637, 638, 639, 640, 641, 642, 643, 644, 645, 646, 647, 648, 649, 650, 651, 652, 653, 654, 655, 656, 657, 658, 659, 660, 661, 662, 663, 664, 665, 666, 667, 668, 669, 670, 671, 672, 673, 674, 675, 676, 677, 678, 679, 680, 681, 682, 683, 684, 685, 686, 687, 688, 689, 690, 691, 692, 693, 694, 695, 696, 697, 698, 699, 700, 701, 702, 703, 704, 705, 706, 707, 708, 709, 710, 711, 712, 713, 714, 715, 716, 717, 718, 719, 720, 721, 722, 723, 724, 725, 726, 727, 728, 729, 730, 731, 732, 733, 734, 735, 736, 737, 738, 739, 740, 741, 742, 743, 744, 745, 746, 747, 748, 749, 750, 751, 752, 753, 754, 755, 756, 757, 758, 759, 760, 761, 762, 763, 764, 765, 766, 767, 768, 769, 770, 771, 772, 773, 774, 775, 776, 777, 778, 779, 780, 781, 782, 783, 784, 785, 786, 787, 788, 789, 790, 791, 792, 793, 794, 795, 796, 797, 798, 799, 800, 801, 802, 803, 804, 805, 806, 807, 808, 809, 810, 811, 812, 813, 814, 815, 816, 817, 818, 819, 820, 821, 822, 823, 824, 825, 826, 827, 828, 829, 830, 831, 832, 833, 834, 835, 836, 837, 838, 839, 840, 841, 842, 843, 844, 845, 846, 847, 848, 849, 850, 851, 852, 853, 854, 855, 856, 857, 858, 859, 860, 861, 862, 863, 864, 865, 866, 867, 868, 869, 870, 871, 872, 873, 874, 875, 876, 877, 878, 879, 880, 881, 882, 883, 884, 885, 886, 887, 888, 889, 890, 891, 892, 893, 894, 895, 896, 897, 898, 899, 900, 901, 902, 903, 904, 905, 906, 907, 908, 909, 910, 911, 912, 913, 914, 915, 916, 917, 918, 919, 920, 921, 922, 923, 924, 925, 926, 927, 928, 929, 930, 931, 932, 933, 934, 935, 936, 937, 938, 939, 940, 941, 942, 943, 944, 945, 946, 947, 948, 949, 950, 951, 952, 953, 954, 955, 956, 957, 958, 959, 960, 961, 962, 963, 964, 965, 966, 967, 968, 969, 970, 971, 972, 973, 974, 975, 976, 977, 978, 979, 980, 981, 982, 983, 984, 985, 986, 987, 988, 989, 990, 991, 992, 993, 994, 995, 996, 997, 998, 999, 1000, 1001, 1002, 1003, 1004, 1005, 1006, 1007, 1008, 1009, 1010, 1011, 1012, 1013, 1014, 1015, 1016, 1017, 1018, 1019, 1020, 1021, 1022, 1023, 1024, 1025, 1026, 1027, 1028, 1029, 1030, 1031, 1032, 1033, 1034, 1035, 1036, 1037, 1038, 1039, 1040, 1041, 1042, 1043, 1044, 1045, 1046, 1047, 1048, 1049, 1050, 1051, 1052, 1053, 1054, 1055, 1056, 1057, 1058, 1059, 1060, 1061, 1062, 1063, 1064, 1065, 1066, 1067, 1068, 1069, 1070, 1071, 1072, 1073, 1074, 1075, 1076, 1077, 1078, 1079, 1080, 1081, 1082, 1083, 1084, 1085, 1086, 1087, 1088, 1089, 1090, 1091, 1092, 1093, 1094, 1095, 1096, 1097, 1098, 1099, 1100, 1101, 1102, 1103, 1104, 1105, 1106, 1107, 1108, 1109, 1110, 1111, 1112, 1113, 1114, 1115, 1116, 1117, 1118, 1119, 1120, 1121, 1122, 1123, 1124, 1125, 1126, 1127, 1128, 1129, 1130, 1131, 1132, 1133, 1134, 1135, 1136, 1137, 1138, 1139, 1140, 1141, 1142, 1143, 1144, 1145, 1146, 1147, 1148, 1149, 1150, 1151, 1152, 1153, 1154, 1155, 1156, 1157, 1158, 1159, 1160, 1161, 1162, 1163, 1164, 1165, 1166, 1167, 1168, 1169, 1170, 1171, 1172, 1173, 1174, 1175, 1176, 1177, 1178, 1179, 1180, 1181, 1182, 1183, 1184, 1185, 1186, 1187, 1188, 1189, 1190, 1191, 1192, 1193, 1194, 1195, 1196, 1197, 1198, 1199, 1200, 1201, 1202, 1203, 1204, 1205, 1206, 1207, 1208, 1209, 1210, 1211, 1212, 1213, 1214, 1215, 1216, 1217, 1218, 1219, 1220, 1221, 1222, 1223, 1224, 1225, 1226, 1227, 1228, 1229, 1230, 1231, 1232, 1233, 1234, 1235, 1236, 1237, 1238, 1239, 1240, 1241, 1242, 1243, 1244, 1245, 1246, 1247, 1248, 1249, 1250, 1251, 1252, 1253, 1254, 1255, 1256, 1257, 1258, 1259, 1260, 1261, 1262, 1263, 1264, 1265, 1266, 1267, 1268, 1269, 1270, 1271, 1272, 1273, 1274, 1275, 1276, 1277, 1278, 1279, 1280, 1281, 1282, 1283, 1284, 1285, 1286, 1287, 1288, 1289, 1290, 1291, 1292, 1293, 1294, 1295, 1296, 1297, 1298, 1299, 1300, 1301, 1302, 1303, 1304, 1305, 1306, 1307, 1308, 1309, 1310, 1311, 1312, 1313, 1314, 1315, 1316, 1317, 1318, 1319, 1320, 1321, 1322, 1323, 1324, 1325, 1326, 1327, 1328, 1329, 1330, 1331, 1332, 1333, 1334, 1335, 1336, 1337, 1338, 1339, 1340, 1341, 1342, 1343, 1344, 1345, 1346, 1347, 1348, 1349, 1350, 1351, 1352, 1353, 1354, 1355, 1356, 1357, 1358, 1359, 1360, 1361, 1362, 1363, 1364, 1365, 1366, 1367, 1368, 1369, 1370, 1371, 1372, 1373, 1374, 1375, 1376, 1377, 1378, 1379, 1380, 1381, 1382, 1383, 1384, 1385, 1386, 1387, 1388, 1389, 1390, 1391, 1392, 1393, 1394, 1395, 1396, 1397, 1398, 1399, 1400, 1401, 1402, 1403, 1404, 1405, 1406, 1407, 1408, 1409, 1410, 1411, 1412, 1413, 1414, 1415, 1416, 1417, 1418, 1419, 1420, 1421, 1422, 1423, 1424, 1425, 1426, 1427, 1428, 1429, 1430, 1431, 1432, 1433, 1434, 1435, 1436, 1437, 1438, 1439, 1440, 1441, 1442, 1443, 1444, 1445, 1446, 1447, 1448, 1449, 1450, 1451, 1452, 1453, 1454, 1455, 1456, 1457, 1458, 1459, 1460, 1461, 1462, 1463, 1464, 1465, 1466, 1467, 1468, 1469, 1470, 1471, 1472, 1473, 1474, 1475, 1476, 1477, 1478, 1479, 1480, 1481, 1482, 1483, 1484, 1485, 1486, 1487, 1488, 1489, 1490, 1491, 1492, 1493, 1494, 1495, 1496, 1497, 1498, 1499, 1500, 1501, 1502, 1503, 1504, 1505, 1506, 1507, 1508, 1509, 1510, 1511, 1512, 1513, 1514, 1515, 1516, 1517, 1518, 1519, 1520, 1521, 1522, 1523, 1524, 1525, 1526, 1527, 1528, 1529, 1530, 1531, 1532, 1533, 1534, 1535, 1536, 1537, 1538, 1539, 1540, 1541, 1542, 1543, 1544, 1545, 1546, 1547, 1548, 1549, 1550, 1551, 1552, 1553, 1554, 1555, 1556, 1557, 1558, 1559, 1560, 1561, 1562, 1563, 1564, 1565, 1566, 1567, 1568, 1569, 1570, 1571, 1572, 1573, 1574, 1575, 1576, 1577, 1578, 1579, 1580, 1581, 1582, 1583, 1584, 1585, 1586, 1587, 1588, 1589, 1590, 1591, 1592, 1593, 1594, 1595, 1596, 1597, 1598, 1599, 1600, 1601, 1602, 1603, 1604, 1605, 1606, 1607, 1608, 1609, 1610, 1611, 1612, 1613, 1614, 1615, 1616, 1617, 1618, 1619, 1620, 1621, 1622, 1623, 1624, 1625, 1626, 1627, 1628, 1629, 1630, 1631, 1632, 1633, 1634, 1635, 1636, 1637, 1638, 1639, 1640, 1641, 1642, 1643, 1644, 1645, 1646, 1647, 1648, 1649, 1650, 1651, 1652, 1653, 1654, 1655, 1656, 1657, 1658, 1659, 1660, 1661, 1662, 1663, 1664, 1665, 1666, 1667, 1668, 1669, 1670, 1671, 1672, 1673, 1674, 1675, 1676, 1677, 1678, 1679, 1680, 1681, 1682, 1683, 1684, 1685, 1686, 1687, 1688, 1689, 1690, 1691, 1692, 1693, 1694, 1695, 1696, 1697, 1698, 1699, 1700, 1701, 1702, 1703, 1704, 1705, 1706, 1707, 1708, 1709, 1710, 1711, 1712, 1713, 1714, 1715, 1716, 1717, 1718, 1719, 1720, 1721, 1722, 1723, 1724, 1725, 1726, 1727, 1728, 1729, 1730, 1731, 1732, 1733, 1734, 1735, 1736, 1737, 1738, 1739, 1740, 1741, 1742, 1743, 1744, 1745, 1746, 1747, 1748, 1749, 1750, 1751, 1752, 1753, 1754, 1755, 1756, 1757, 1758, 1759, 1760, 1761, 1762, 1763, 1764, 1765, 1766, 1767, 1768, 1769, 1770, 1771, 1772, 1773, 1774, 1775, 1776, 1777, 1778, 1779, 1780, 1781, 1782, 1783, 1784, 1785, 1786, 1787, 1788, 1789, 1790, 1791, 1792, 1793, 1794, 1795, 1796, 1797, 1798, 1799, 1800, 1801, 1802, 1803, 1804, 1805, 1806, 1807, 1808, 1809, 1810, 1811, 1812, 1813, 1814, 1815, 1816, 1817, 1818, 1819, 1820, 1821, 1822, 1823, 1824, 1825, 1826, 1827, 1828, 1829, 1830, 1831, 1832, 1833, 1834, 1835, 1836, 1837, 1838, 1839, 1840, 1841, 1842, 1843, 1844, 1845, 1846, 1847, 1848, 1849, 1850, 1851, 1852, 1853, 1854, 1855, 1856, 1857, 1858, 1859, 1860, 1861, 1862, 1863, 1864, 1865, 1866, 1867, 1868, 1869, 1870, 1871, 1872, 1873, 1874, 1875, 1876, 1877, 1878, 1879, 1880, 1881, 1882, 1883, 1884, 1885, 1886, 1887, 1888, 1889, 1890, 1891, 1892, 1893, 1894, 1895, 1896, 1897, 1898, 1899, 1900, 1901, 1902, 1903, 1904, 1905, 1906, 1907, 1908, 1909, 1910, 1911, 1912, 1913, 1914, 1915, 1916, 1917, 1918, 1919, 1920, 1921, 1922, 1923, 1924, 1925, 1926, 1927, 1928, 1929, 1930, 1931, 1932, 1933, 1934, 1935, 1936, 1937, 1938, 1939, 1940, 1941, 1942, 1943, 1944, 1945, 1946, 1947, 1948, 1949, 1950, 1951, 1952, 1953, 1954, 1955, 1956, 1957, 1958, 1959, 1960, 1961, 1962, 1963, 1964, 1965, 1966, 1967, 1968, 1969, 1970, 1971, 1972, 1973, 1974, 1975, 1976, 1977, 1978, 1979, 1980, 1981, 1982, 1983, 1984, 1985, 1986, 1987, 1988, 1989, 1990, 1991, 1992, 1993, 1994, 1995, 1996, 1997, 1998, 1999, 2000, 2001, 2002, 2003, 2004, 2005, 2006, 2007, 2008, 2009, 2010, 2011, 2012, 2013, 2014, 2015, 2016, 2017, 2018, 2019, 2020, 2021, 2022, 2023, 2024, 2025, 2026, 2027, 2028, 2029, 2030, 2031, 2032, 2033, 2034, 2035, 2036, 2037, 2038, 2039, 2040, 2041, 2042, 2043, 2044, 2045, 2046, 2047, 2048, 2049, 2050, 2051, 2052, 2053, 2054, 2055, 2056, 2057, 2058, 2059, 2060, 2061, 2062, 2063, 2064, 2065, 2066, 2067, 2068, 2069, 2070, 2071, 2072, 2073, 2074, 2075, 2076, 2077, 2078, 2079, 2080, 2081, 2082, 2083, 2084, 2085, 2086, 2087, 2088, 2089, 2090, 2091, 2092, 2093, 2094, 2095, 2096, 2097, 2098, 2099,

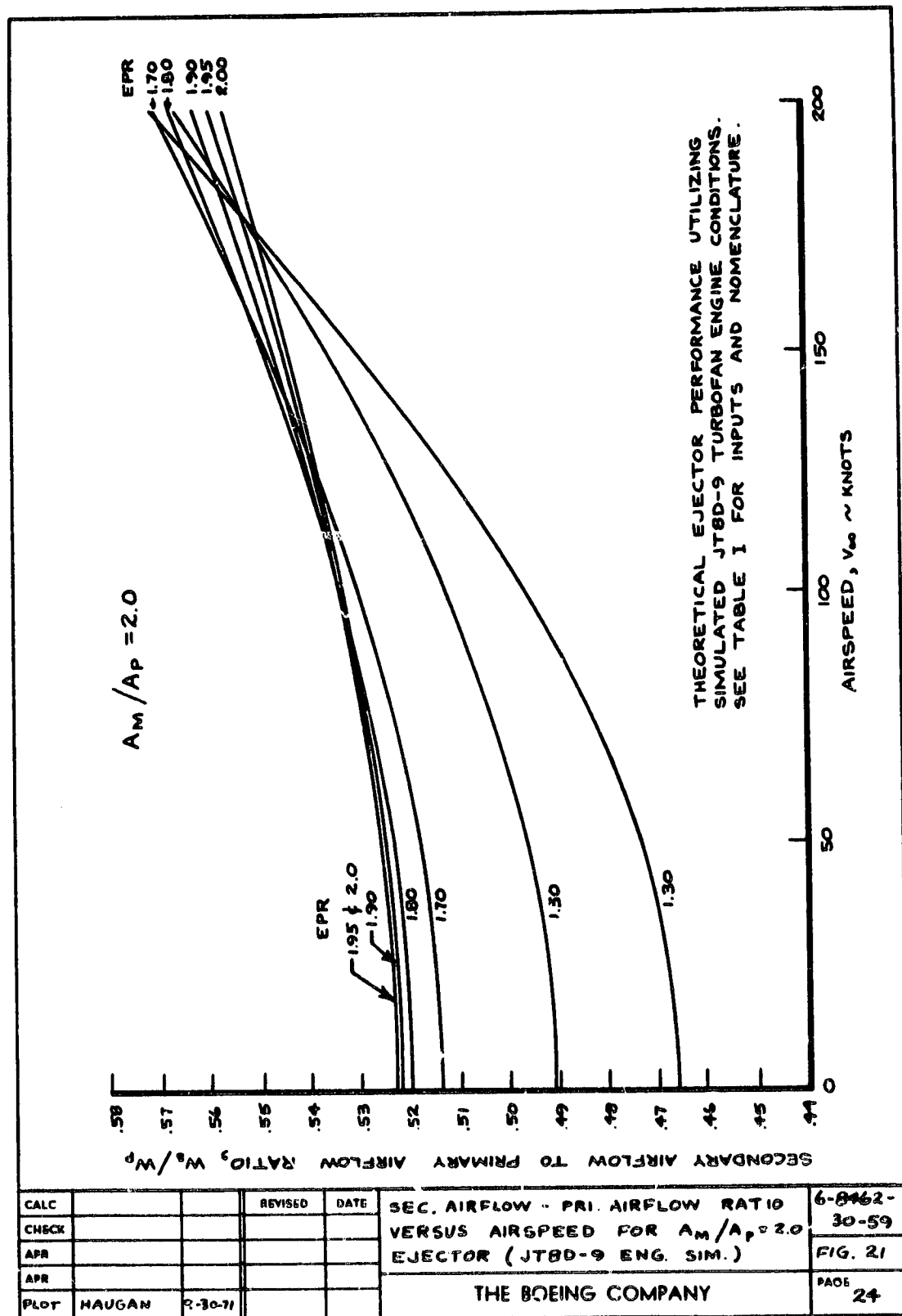
$$A_M/A_P = 2.0$$

THEORETICAL EJECTOR PERFORMANCE UTILIZING  
SIMULATED JT8D-9 TURBOFAN ENGINE CONDITIONS.  
SEE TABLE I FOR INPUTS AND NOMENCLATURE.



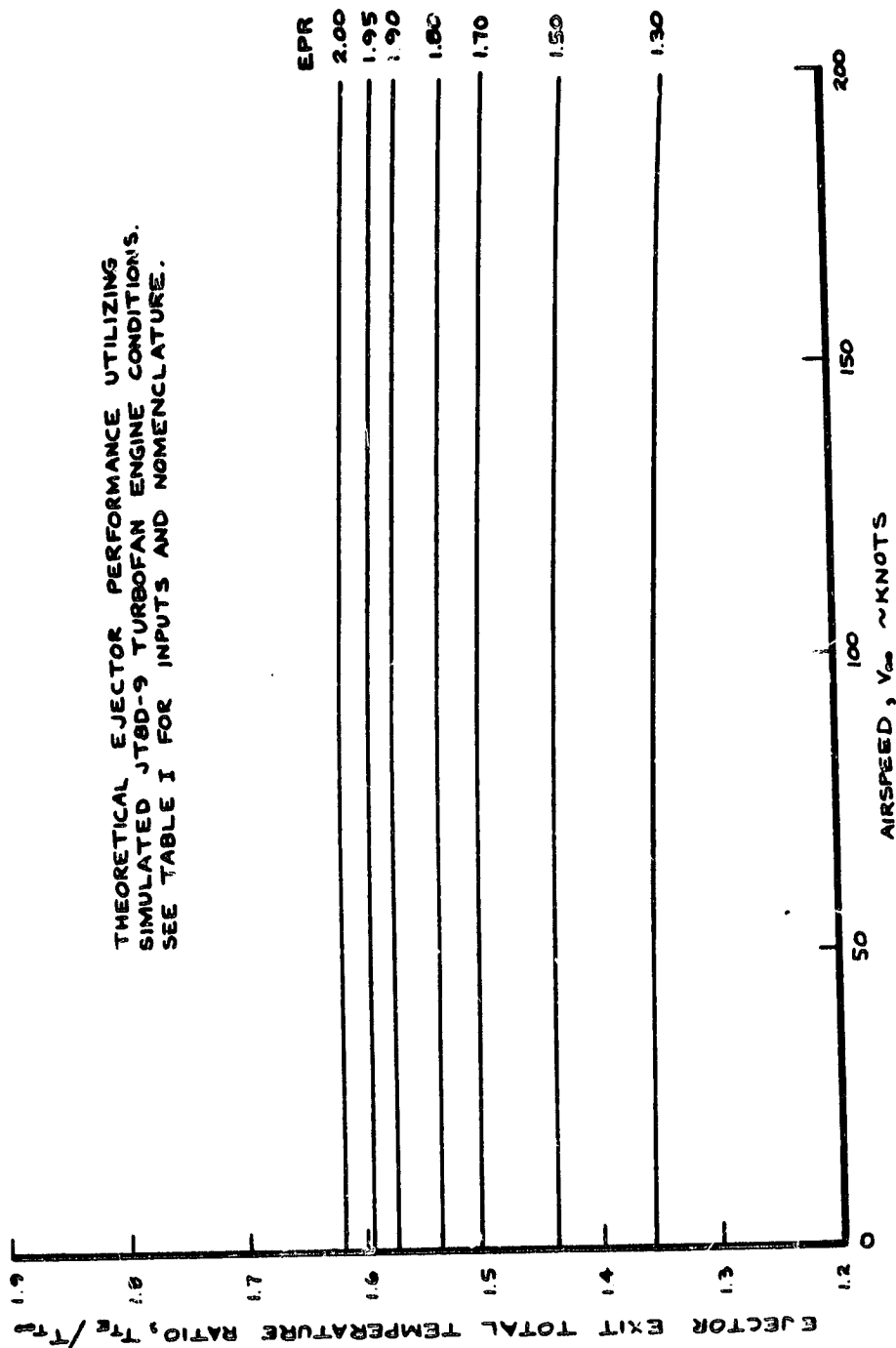
CALC			REVISED	DATE	SECONDARY FLOW MACH NUMBER VERSUS AIRSPEED FOR $A_M/A_P = 2.0$ EJECTOR (JT8D-9 ENG. SIM.)	6-8462-
CHECK						30-59
APR						FIG. 20
APR						PAGE
PLOT	HAUGAN	9-30-71			THE BOEING COMPANY	23

NOTES: 1. ALUMINUM 7001 - 60% H14  
2. 1/8" X 1/8" X 1/8" TYPICAL



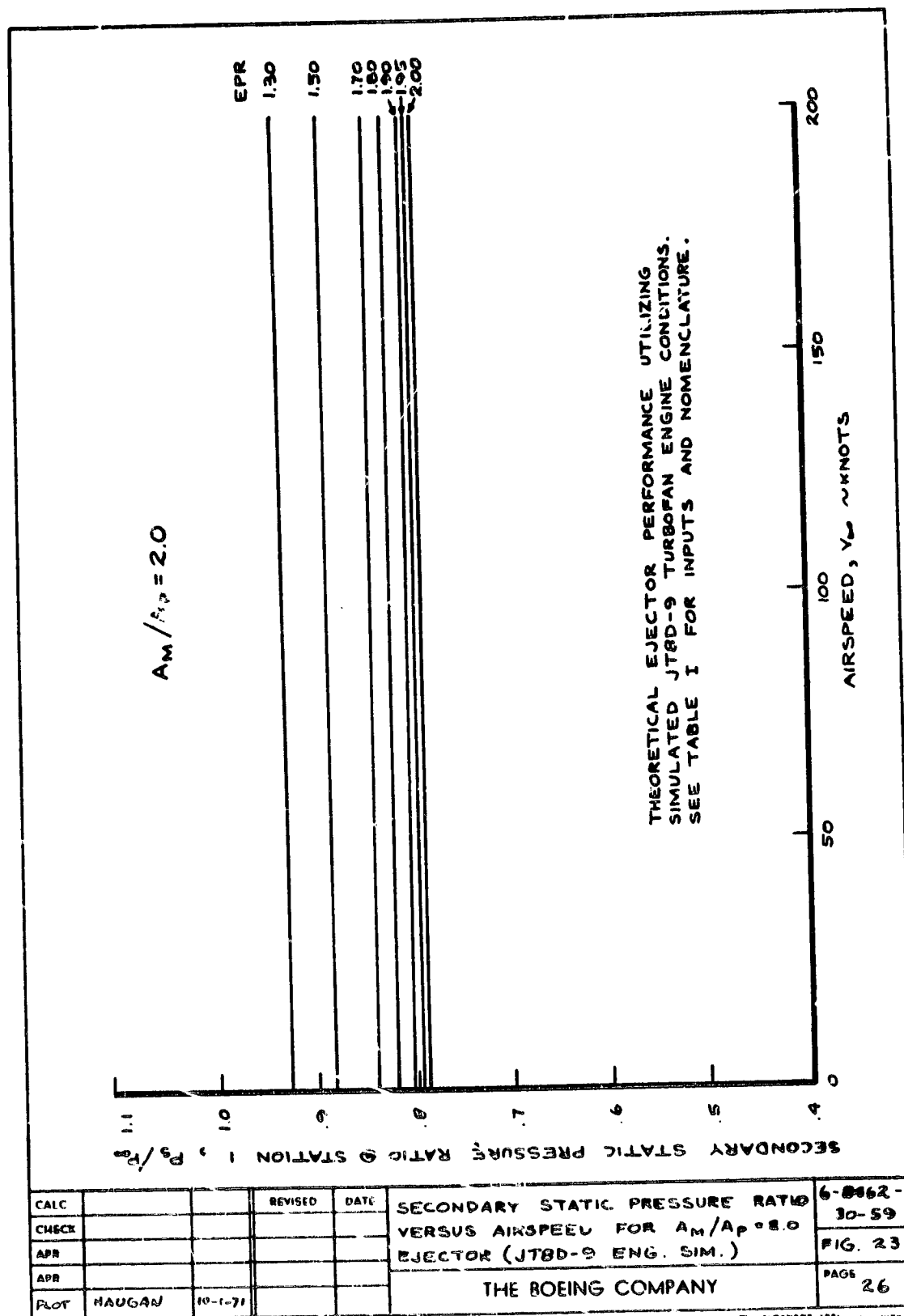
$$A_m/A_p = 2.0$$

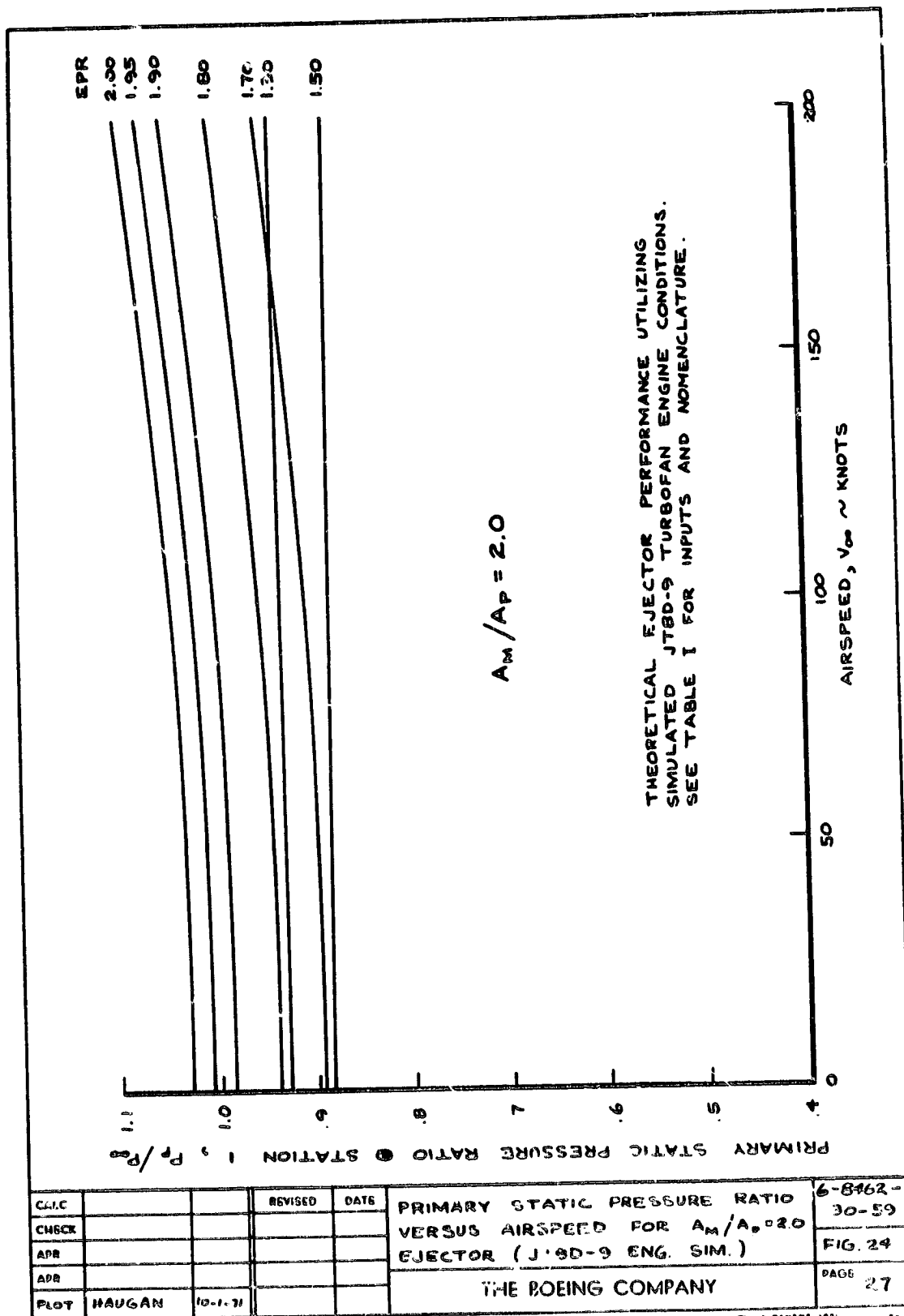
THEORETICAL EJECTOR PERFORMANCE UTILIZING  
SIMULATED JT8D-9 TURBOFAN ENGINE CONDITIONS.  
SEE TABLE I FOR INPUTS AND NOMENCLATURE.



CALC			REVISED	DATE	EJECTOR EXIT TOTAL TEMP RATIO VERSUS AIRSPEED FOR $A_m/A_p = 2.0$ EJECTOR (JT8D-9 ENG. SIM.)	6-8462- 30-59
CHECK						FIG. 22
APR						PAGE
APR						25
PLOT	HAUSAN	10-1-71			THE BOEING COMPANY	

W-E 4-000000 001

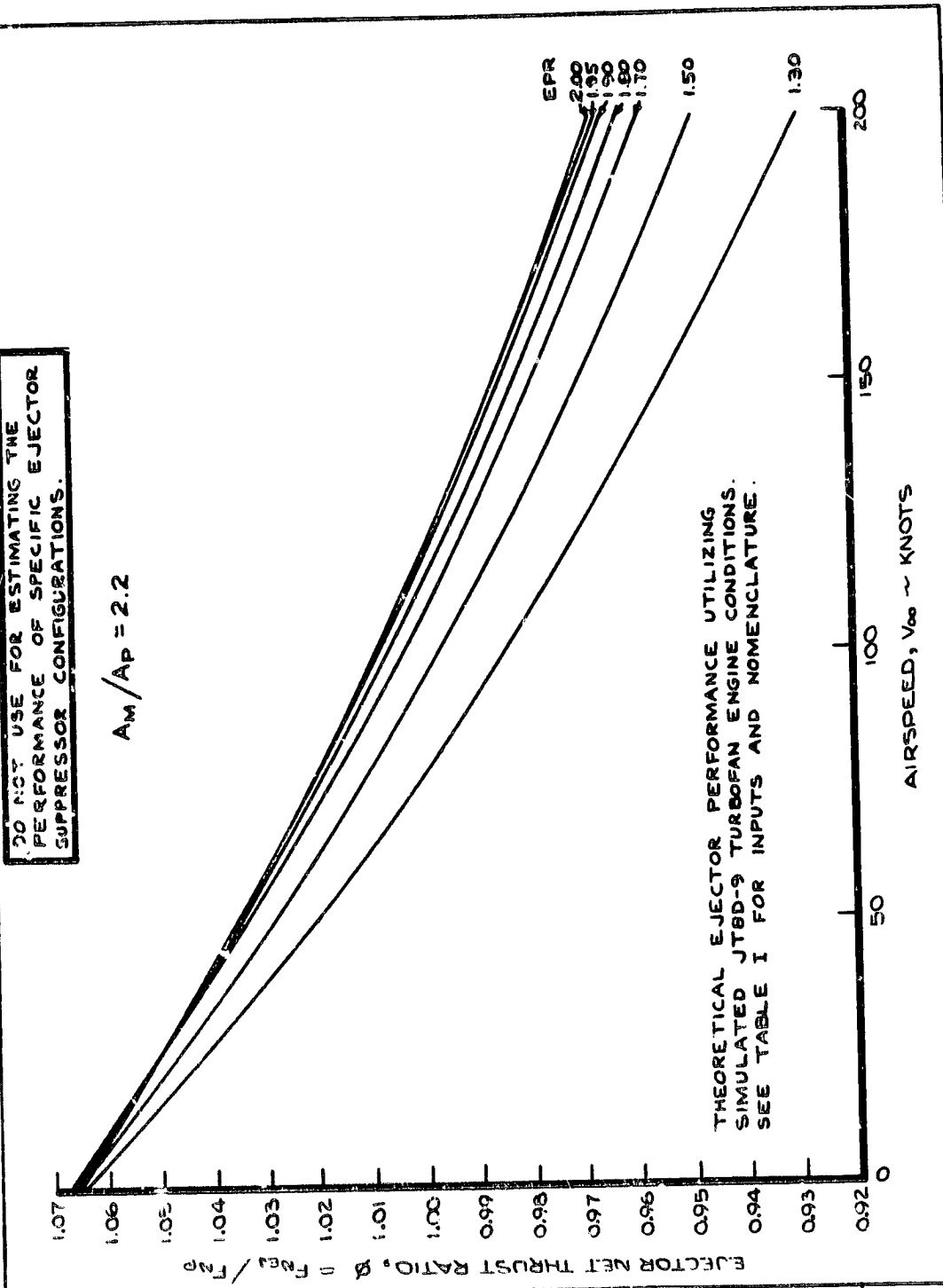






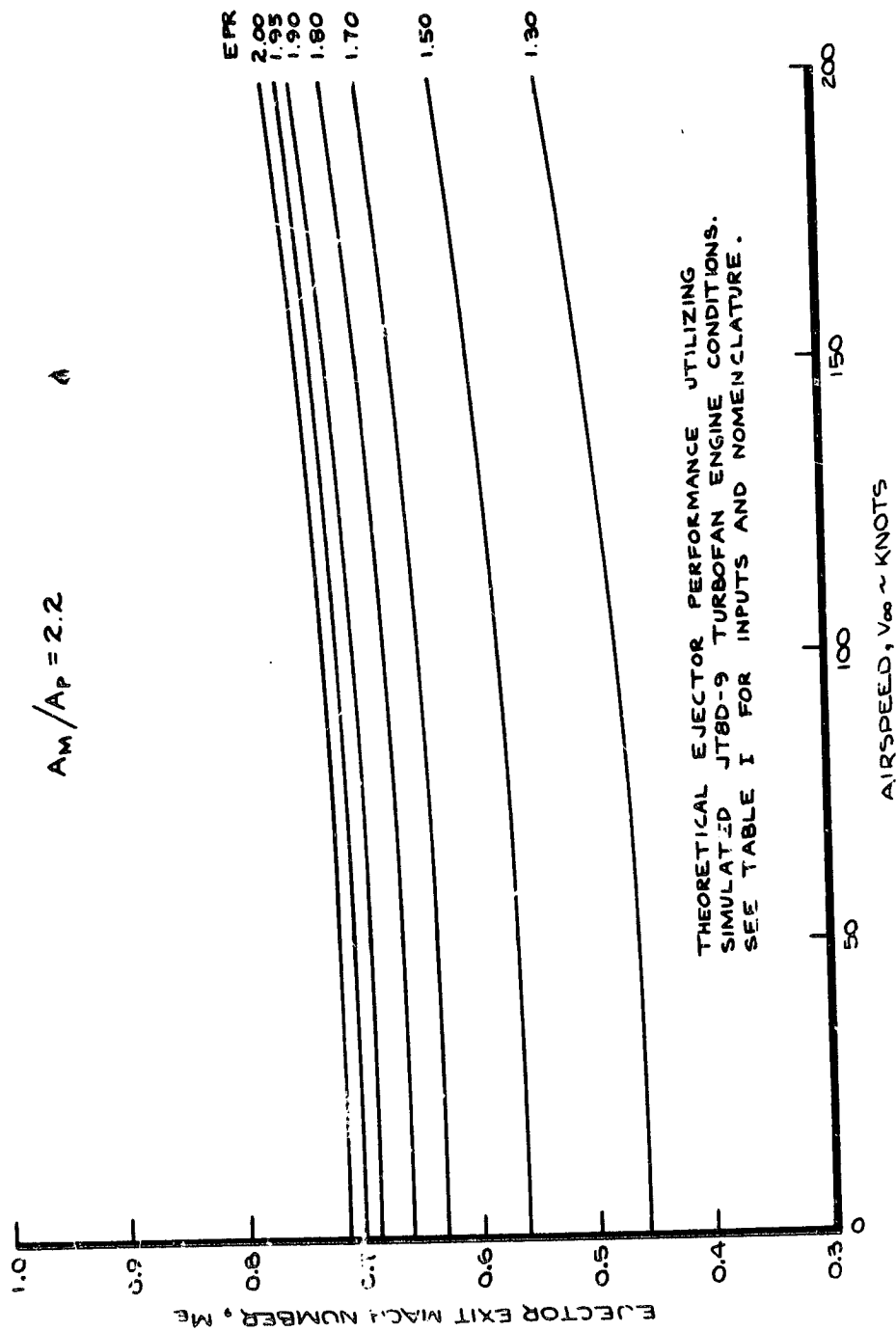
DO NOT USE FOR ESTIMATING THE  
PERFORMANCE OF SPECIFIC EJECTOR  
SUPPRESSOR CONFIGURATIONS.

$$A_m/A_p = 2.2$$



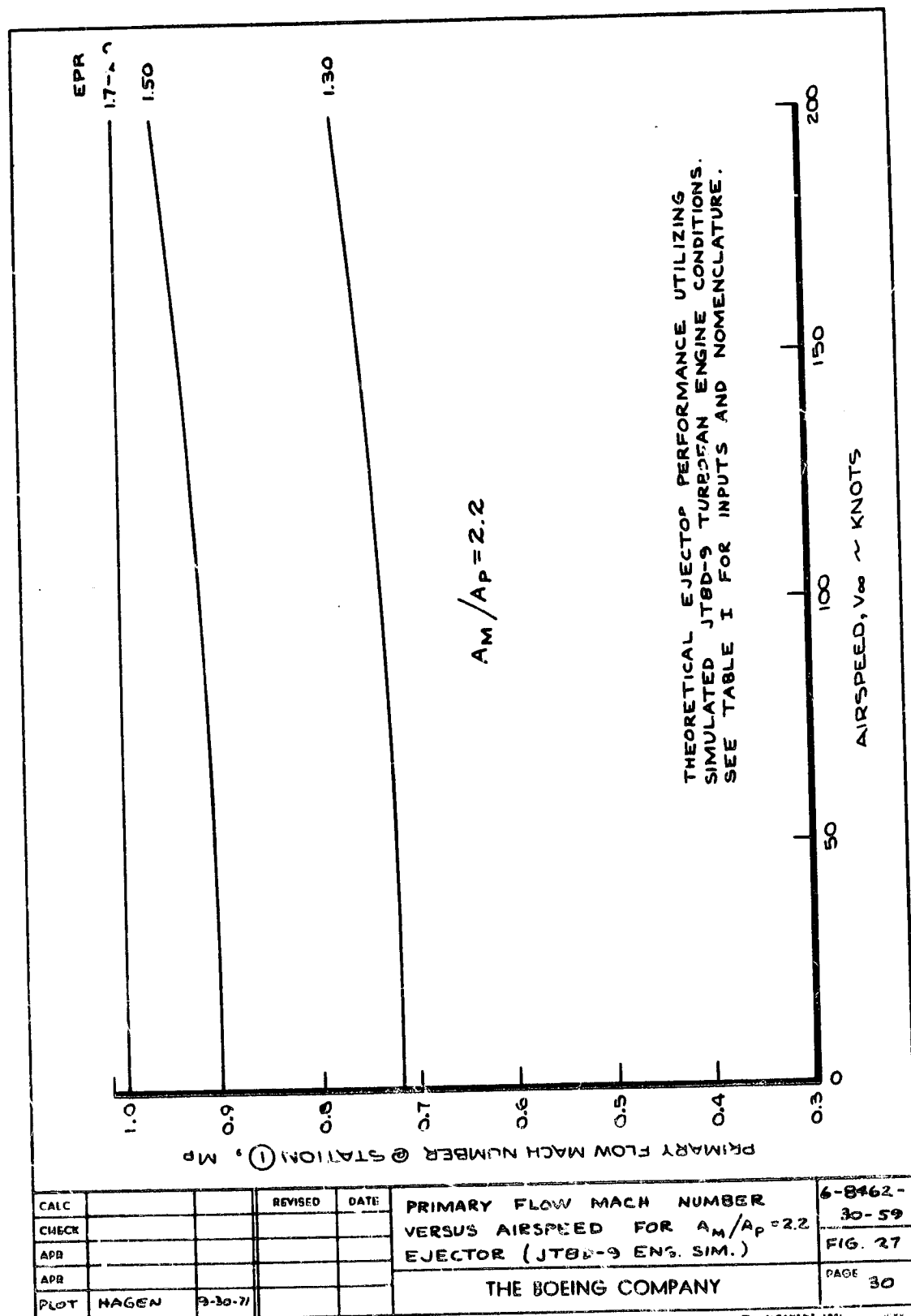
FILE			REVISED	DATE	EJECTOR NET THRUST RATIO VERSUS AIRSPEED FOR $A_m/A_p = 2.2$ EJECTOR (JT8D-9 ENG. SIM.)	6-8462-
CHECK						30-59
APP						FIG. 25
APB						PAGE
PLT	RAGON	9-10-77			THE JOEING COMPANY	28

NOT REPRODUCED BY THE JOEING COMPANY



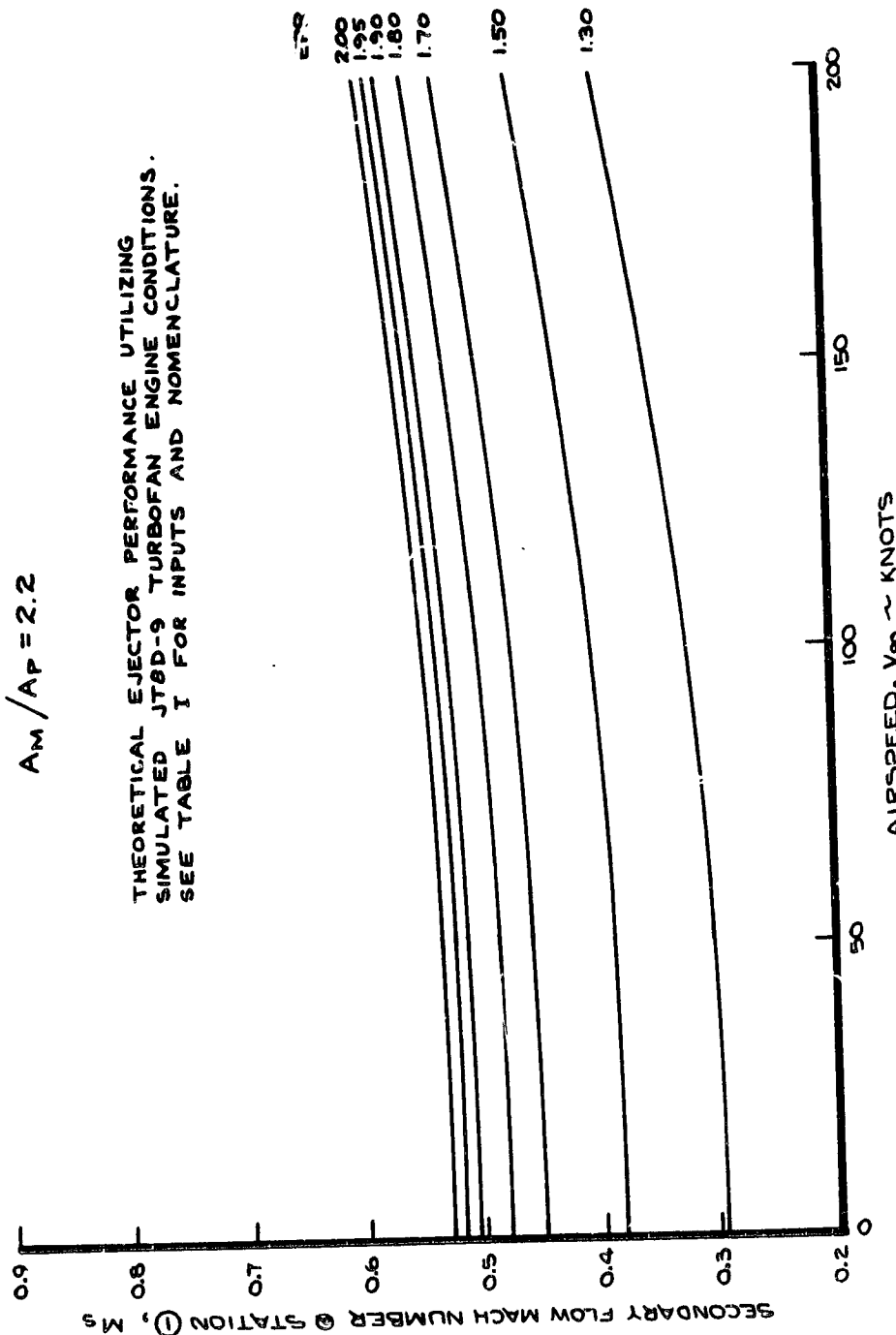
CALC			REVISED	DATE	EJECTOR EXIT MACH NUMBER VERSUS AIRSPEED FOR $A_m/A_p = 2.2$ EJECTOR (JT8D-9 ENG. SIM.)	6-8462-
CHECK						30-59
APR						FIG. 26
APR						PAGE 29
PLOT	HAGEN	30-71			THE BOEING COMPANY	

H-E ALUMINUM TOOL  
BY THE BOEING COMPANY



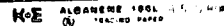
$$A_M / A_P = 2.2$$

THEORETICAL EJECTOR PERFORMANCE UTILIZING  
SIMULATED JT8D-9 TURBOFAN ENGINE CONDITIONS.  
SEE TABLE I FOR INPUTS AND NOMENCLATURE.



CALC			REVISED	DATE	SECONDARY FLOW MACH NUMBER VERSUS AIRSPEED FOR $A_M / A_P = 2.2$ EJECTOR (JT8D-9 ENG. SIM.)	6-13462- 30-59
CHECK						FIG. 28
APR						PAGE 31
APR						
PLT	HAGEN	9-20-71			THE BOEING COMPANY	

K-E ALUMINUM 100%  
CAL. CO. PAPER



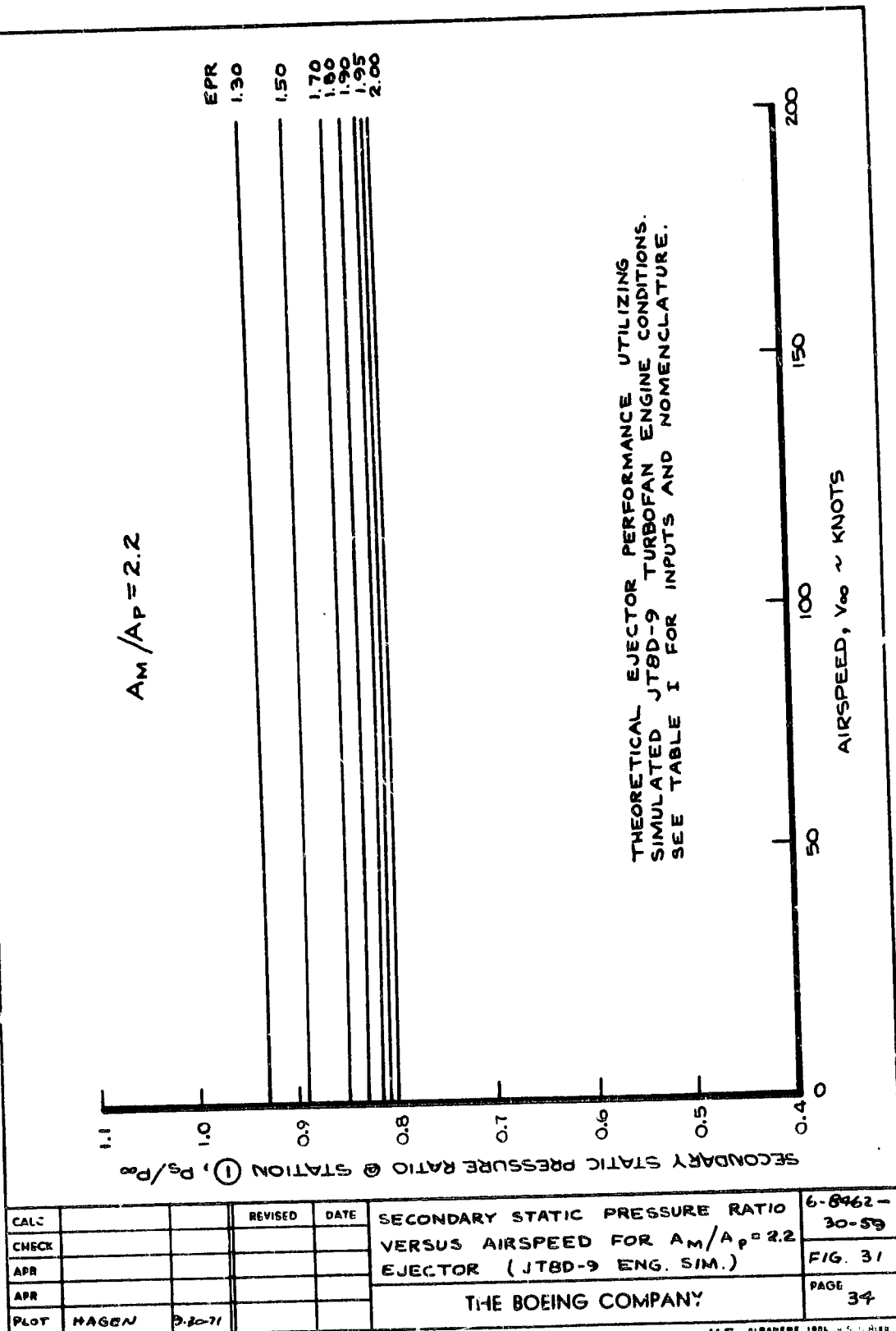
$A_M/A_P = 2.2$

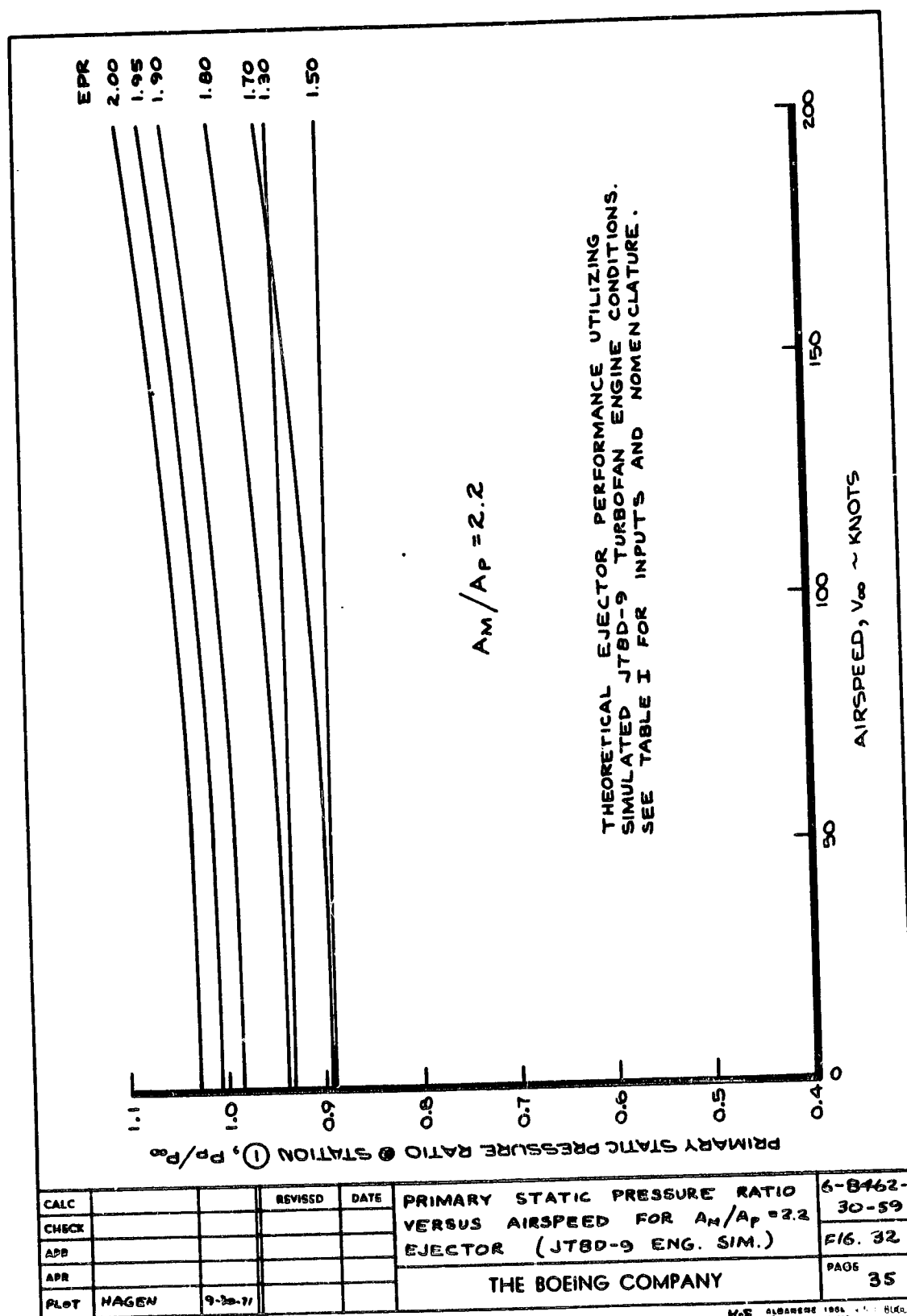
THEORETICAL EJECTOR PERFORMANCE UTILIZING  
 SIMULATED JT8D-9 TURBOFAN ENGINE CONDITIONS.  
 SEE TABLE I FOR INPUTS AND NOMENCLATURE.

The graph plots the Ejector Exit Total Temperature Ratio ( $T_{te}/T_0$ ) on the y-axis against Airspeed ( $V_\infty$ ) in knots on the x-axis. The y-axis ranges from 1.2 to 1.9 with major ticks every 0.1. The x-axis ranges from 0 to 200 knots with major ticks at 0, 50, 100, 150, and 200. Seven horizontal lines are drawn at different EPR values: 2.00, 1.95, 1.90, 1.80, 1.70, 1.50, and 1.30. The temperature ratio is constant for each EPR value across the entire airspeed range.

EPR	$T_{te}/T_0$
2.00	1.60
1.95	1.57
1.90	1.54
1.80	1.50
1.70	1.46
1.50	1.38
1.30	1.32

CALC			REVISED	DATE	EJECTOR EXIT TOTAL TEMP. RATIO VERSUS AIRSPEED FOR $A_m/A_p = 2.2$ EJECTOR (JT8D-9 ENG. SIM.)	6-8762- 30-59
CHECK						F16. 30
APR						
APR						
DOT	HAGEN	9-30-71			THE BOEING COMPANY	PAGE 33







## REFERENCES

1. K. C. Crowley, et al, "Aircraft Noise Source and Contour Computer Programs—User's Guide," NASA CR114650, July 1973.
2. DOT/FAA, "Federal Aviation Regulations," Vol. III—Part 36, Appendix B, December 1969.
3. J. F. McBride/N. A. Peart, "Development of Aircraft Engine Noise Source and Noise Footprint Computer Programs," Boeing Document D6-40122, 24 March 1972.
4. D. G. Dunn, et al, "Jet Engine Noise Source and Noise Footprint Computer Programs," NASA CR114517, October 1972.
5. Standard Values of Atmospheric Absorption as a Function of Temperature of Humidity for Use in Evaluating Aircraft Flyover Noise. Aerospace Recommended Practice No. 866, Society of Automotive Engineers, 31 August 1964.
6. Subcommittee Report of SAE Comm. A-21 on Atmospheric Absorption, Society of Automotive Engineers, July 1969.
7. Jet Noise Prediction, Aerospace Information Report No. 876, Society of Automotive Engineers, 10 July 1965.
8. Method for Calculating the Attenuation of Aircraft Ground to Ground Noise Propagation During Takeoff and Landing, Aerospace Information Report No. 923, Society of Automotive Engineers, 15 August 1966.
9. Definitions and Procedures for Computing the Perceived Noise Level of Aircraft Noise, Aerospace Recommended Practice No. 865A, Society of Automotive Engineers, 15 August 1965.
10. W. R. Johnson/M. B. McKaig, "Calculation of Shielding Effect of Multiple Noise Sources," Boeing Document D6-25260, 9 June 1970. (Proprietary)
11. J. M. Campbell, et al, "Design Integration and Noise Studies for Jet STOL Aircraft; Final Report, Vol. III—Static Test Program," NASA CR11473, May 1972.
12. P. M. Morse and K. U. Ingard, *Theoretical Acoustics*, McGraw Hill Book Co., 1968.

13. S. P. Pao and M. V. Lowson, "Spectral Techniques in Jet Noise Theory," Wyle Labs Report WR68-21, April 1969.
14. Walton L. Howes, "Ground Reflection Of Jet Noise," NASA TR-R-35, 1959.
15. P. B. Oncley, "Propagation of Jet Engine Noise Near a Porous Surface," Journal of Sound and Vibration, Vol. 13, C1970, pp. 27-35.
16. I. Rudnick, "Propagation of an Acoustic Wave Along a Boundary," Journal of Acoustical Society of America, Vol. 19, C1947, p. 348.
17. U. Ingard, "On the Reflection of a Spherical Sound Wave from an Infinite Plane," Journal of Acoustical Society of America, Vol. 23, C1951, p. 329.
18. R. B. Adler/L. J. Chu/R. M. Fano, *Electromagnetic Energy Transmission and Radiation*, John Wiley and Sons, Inc., C1960, pp. 351-369, 442-448.
19. H. S. Wall, *Analytic Theory of Continued Fractions*, D. Van Nostrand Co., Inc., Princeton, N. J., C1948, p. 196.
20. W. Bhat/C. Jaek, "A Study of the Effect of Density Variations on Clean Jet Noise," Boeing Document D6-40604, 21 September 1972. (Proprietary)
21. R. J. Koenig/P. R. Schorr, "Procedures for Estimating the Magnitude and Directivity Patterns of Jet Noise," Boeing Document D6-25490, 26 March 1971 (Proprietary)
22. G. W. Bielak, "Coaxial Flow Jet Noise," Boeing/Aeritalia Document D6E-10041-1, 18 April 1972 (Proprietary)
23. E. J. Richards/D. J. Mead, *Noise and Acoustic Fatigue in Aeronautics*, Chapter 11, John Wiley and Sons, Ltd., New York, 1968.
24. J. C. Laurence/J. M. Benninghoff, "Turbulence Measurements in Multiple Interfacing Air Jets," NACA TN 4029.
25. J. R. Anderson/H. G. Ridley/J. W. Smith, "727 Noise Retrofit Feasibility—Vol. II: Upper Goal Design, Fabrication, and Ground Testing," FAA-RD-72-40, II, November 1972.

26. The Boeing Company, "Design Integration and Noise Studies for Jet STOL Aircraft Task VIIA, Augmentor Wing Cruise Blowing Valveless System, Vol. II-Design Exploration," NASA CR-114570, April 1973.
27. J. M. Campbell/D. L. Harkonen/J. V. O'Keefe, "Design Integration and Noise Studies for Jet STOL Aircraft: Task VIIC, Augmentor Wing Cruise Blowing Valveless System, Vol. I-Static Testing of Augmentor Noise and Performance," NASA CR-114622, March 1973.
28. W. A. Oisen/R. G. Dorsch/J. H. Miles, "Noise Produced by a Small-Scale Externally Blown Flap," NASA TD-6636, 7 December 1971.
29. Grumman/Boeing, "Phase I Final Report for Quiet Experimental STOL Transport Research Airplane," Vol. 1 Summary, NASA PRD612-1, 15 June 1972.
30. D. L. Stimpert, "Effect of VTOL Aircraft Flight Speed on Lift Fan Noise Generation," General Electrical Company, TM No. 72-151, 15 May 1972.
31. S. B. Kazin/L. J. Volk, "LF336 Lift Fan Modification and Acoustic Test Program," NASA CR-1934, December 1971.
32. Rose Worobel/M. G. Mayo (Hamilton Standard), "Advanced General Aviation Propeller Study," NASA CR114289, April 1971.
33. M. V. Lowson/J. B. Ollerhead, "Studies of Helicopter Rotor Noise," USAAVLABS TR 68-60, January 1969.
34. J. B. Ollerhead/R. B. Taylor, "Description of a Helicopter Rotor Noise Computer Program," USAAVLABS TR 68-61, January 1969.
35. F. H. Schmitz/W. Z. Stepniewski/J. Gibbs/E. Hinterkeuser, "A Comparison of Optimal and Noise-Abatement Trajectories of a Tilt-Rotor Aircraft," NASA CR-2034, May 1972.
36. D. Brown/J. B. Ollerhead, "Propeller Noise at Low Tip Speeds," AFAPL-TR-71-55, September 1971.
37. F. W. Barry/B. Magliozzi (Hamilton Standard), "Noise Detectability Prediction Method for Low Speed Propellers," AFAPL-TR-71-37, June 1971.
38. T. G. Granger/B. Magliozzi (Hamilton Standard), "Advanced V/STOL Propeller Technology- Far Field Investigation," AFFDL-TR-71-88, Vol. XII, March 1972.

39. John Laufer, et al, "Acoustic Modeling of the Jet Noise Abatement Problem," Interagency Symposium on University Research in Transportation Noise, Proceedings Vol. 1, Stanford University, Stanford, California, March 28-30, 1973.
40. G. R. MacGregor, "The Location of Acoustic Sources in Jet Flows by Means of the Wall Isolation Technique," Boeing Document D6-40116, February 15, 1972 (Proprietary)
41. W. V. Morgan/L. C. Sutherland/K. J. Young, "The Use of Acoustic Scale Models for Investigating Near Field Noise of Jet and Rocket Engines," WADD Technical Report 61-178, 1961.